

Analytical Procedure for Flexible Airfield Pavement Rutting
Incorporating Environmental Location and Groundwater Table Effects

by

Ramadan A.Salim

A Thesis Presented in Partial Fulfillment
of the Requirements for the Degree
Master of Science

Approved November 2011 by the
Graduate Supervisory Committee:

Claudia Zapata, Co-Chair
Matthew Witczak, Co-Chair
Kamil Kaloush

ARIZONA STATE UNIVERSITY

December 2011

ABSTRACT

The structural design of pavements in both highways and airfields becomes complex when one considers environmental effects and ground water table variation. Environmental effects have been incorporated on the new Mechanistic-Empirical Pavement Design Guide (MEPDG) but little has been done to incorporate environmental effects on airfield design.

This work presents a developed code produced from this research study called ZAPRAM, which is a mechanistically based pavement model based upon Limiting Strain Criteria in airfield HMA pavement design procedures. ZAPRAM is capable of pavement and airfield design analyses considering environmental effects. The program has been coded in Visual Basic and implemented in an event-driven, user-friendly educational computer program, which runs in Excel environment.

Several studies were conducted in order to insure the validity of the analysis as well as the efficiency of the software. The first study yielded the minimum threshold number of computational points the user should use at a specific depth within the pavement system. The second study was completed to verify the correction factor for the Odemark's transformed thickness equation. Default correction factors were included in the code base on a large comparative study between Odemark's and MLET. A third study was conducted to provide a comparison of flexible airfield pavement design thicknesses derived from three widely accepted design procedures used in practice today: the Asphalt Institute, Shell Oil, and the revised Corps of Engineering rutting failure criteria to calculate the thickness requirements necessary for a range of design input variables. The results of the comparative study showed that there is a significant difference between the

pavement thicknesses obtained from the three design procedures, with the greatest deviation found between the Shell Oil approach and the other two criteria.

Finally, a comprehensive sensitivity study of environmental site factors and the groundwater table depth upon flexible airfield pavement design and performance was completed. The study used the newly revised USACE failure criteria for subgrade shear deformation. The methodology utilized the same analytical methodology to achieve real time environmental effects upon unbound layer modulus, as that used in the new AASHTO MEPDG. The results of this effort showed, for the first time, the quantitative impact of the significant effects of the climatic conditions at the design site, coupled with the importance of the depth of the groundwater table, on the predicted design thicknesses. Significant cost savings appear to be quite reasonable by utilizing principles of unsaturated soil mechanics into the new airfield pavement design procedure found in program ZAPRAM.

DEDICATION

This thesis is dedicated to my father Mr. Abdalla Salim, my mother, my sisters, and my brothers for their prayers, love, and support. Furthermore, I would like to dedicate this work to Libyan martyrs who sacrificed for the freedom of the country.

ACKNOWLEDGMENTS

I would like to extend my sincerest appreciation and gratitude for my advisor, Dr. Claudia Zapata, for her constant encouragement, technical guidance throughout the Master Program. I thank Dr. Matthew W. Witzak for the intensive technical discussions and suggestions during this research work. I would like to acknowledge the help of Waleed Zeiada and Daniel Rosenbalm during my studies. Special thanks are due to Dr. Kamil Kaloush for his useful opinions and discussions during this research work.

I am grateful to all my friends and colleagues of the Advanced Pavement Group, Department of Civil and Environmental Engineering at Arizona State University.

Finally, I am forever indebted to all my family members for their constant encouragement and support in every moment of my life.

TABLE OF CONTENTS

| | Page |
|---|------|
| LIST OF TABLES..... | viii |
| LIST OF FIGURES..... | xiii |
| CHAPTER | |
| 1 INTRODUCTION..... | 1 |
| 1.1 Introduction..... | 1 |
| 1.2 Scope of Work..... | 3 |
| 1.3 Research Objectives..... | 4 |
| 1.4 Organization..... | 5 |
| 2 LITERATURE REVIEW..... | 7 |
| 2.1 Introduction:..... | 7 |
| 2.2 ZAPMEDACA Software..... | 8 |
| 2.3 ZAPMEDACA Software Modules..... | 8 |
| 3 ENHANCEMENT OF ZAPMEDACA SOFTWARE..... | 29 |
| 3.1 ZAPRAM Software..... | 29 |
| 3.2 ZAPRAM Software Modules..... | 30 |
| 4 EVALUATION OF OPTIMAL DIFFERENTIAL AREAS IN NUMERICAL INTEGRATION PROCESS..... | 72 |
| 4.1 Introduction..... | 72 |
| 4.2 Selected Aircraft:..... | 73 |
| 4.3 Pavement System Utilized:..... | 75 |
| 4.4 Plan Study:..... | 75 |
| 4.5 The Study for Deep Depth ($Z=150.00$ in)..... | 76 |
| 4.6 The Study for Mid Depth ($Z=79.57$ in)..... | 87 |

| CHAPTER | Page |
|---|-------|
| 4.7 The Study for Shallow Depth (Z=20.00 in). | 93 |
| 4.8 Impact of the Computed Depth on Number of Computational Points..... | 99 |
| 4.9 Conclusions of the Study:..... | 105 |
| 5 STRESS AND STRAIN ANALYSIS IN ZAPRAM..... | 108 |
| 5.1 Introduction..... | 108 |
| 5.2 Corroborate the Validity of the Program | 108 |
| 5.3 The Correction Factor “F”:..... | 121 |
| 5.4 Conclusion | 165 |
| 6 COMPARISON OF AIRFIELD FLEXIBLE PAVEMENT DESIGN THICKNESS BASED UPON DIFFERING AGENCY LIMITING SUBGRADE STRAIN CRITERIA | 166 |
| 6.1 Introduction..... | 166 |
| 6.2 Objective..... | 166 |
| 6.3 Experimental Factorial..... | 167 |
| 6.4 Results and Analysis | 169 |
| 6.5 Influence of Design Factors..... | 171 |
| 6.6 Comparison of Criteria..... | 173 |
| 6.7 Statistical Summary of Agency Pavement Design | 175 |
| 6.8 Conclusions..... | 178 |
| 7 IMPACT OF ENVIRONMENTAL SITE LOCATION AND GROUNDWATER TABLE DEPTH ON THE THICKNESS OF FLEXIBLE AIRFIELD PAVEMENTS | 180 |
| 7.1 Introduction..... | 180 |
| 7.2 Objective..... | |

| CHAPTER | Page |
|---|------|
| 7.3 Background of Environmental Effects | 182 |
| 7.4 Experimental Matrix | 183 |
| 7.5 Pavement Structure | 186 |
| 7.6 Subgrade Soil Modulus Variations..... | 186 |
| 7.7 Results and Analysis | 188 |
| 7.8 Discussion of Results | 191 |
| 7.9 Summary and Conclusions | 195 |
| 8 SUMMARY AND CONCLUSIONS..... | 197 |
| 8.1 Summary..... | 197 |
| 8.2 Conclusions..... | 199 |
| 9 RECOMMENDATIONS AND FUTURE STUDIES | 207 |
| REFERENCES..... | 212 |
| APPENDIX | |
| A USER'S OPERATIONAL GUIDE..... | 215 |
| A.1 Introduction..... | 216 |
| A.2 Main Screen: | 218 |
| A.3 Load Configuration Module: | 219 |
| A.4 Pavement Structure Module | 226 |
| A.5 Traffic Analysis | 228 |
| A.6 Environmental Effects Module..... | 233 |
| A.7 Stress Analysis Module..... | 235 |
| A.8 Design Rutting Criteria | 238 |

LIST OF TABLES

| Table | Page |
|---|------|
| 2-1 Mean Possible Duration of Sunlight – Northern Hemisphere (Day-Length Correction Factor in Units of 30 Days of 12 Hours) | 14 |
| 2-2 Mean Possible Duration of Sunlight – Southern Hemisphere (Day-Length Correction Factor in Units of 30 Days of 12 Hours) | 15 |
| 2-3 Constants for TMI-P200 Model for Base Coarse-grained Materials | 16 |
| 2-4 Regression Constants for TMI-P200/wPI Model for Subbase/Subgrade Materials ... | 17 |
| 3-1 Listing of all the Specific Aircraft Types that Include d in the Library | 31 |
| 3-2 The Currently Available Cities that are Included in the City Library | 36 |
| 3-3 Input Type Gear Arrangement | 37 |
| 3-4 The Coordinate of Point of Interest for Single Tire Aircraft | 38 |
| 3-5 The Coordinate of Point of Interest for Dual Tire Aircraft | 39 |
| 3-6 The Coordinate of Point of Interest for Single Tandem Aircraft | 39 |
| 3-7 The Coordinate of Point of Interest for Dual Tandem Aircraft | 40 |
| 3-8 The Coordinate of Point of Interest for Tri-Tandem Aircraft | 41 |
| 3-9 The Coordinate of Point of Interest for C5A Aircraft | 43 |
| 3-10 The Coordinate of Point of Interest for Twin-Twin Aircraft | 45 |
| 3-11 The Coordinate of Point of Interest for A-380 Aircraft | 46 |
| 3-12 The Coordinate of Point of Interest for B-747 Aircraft | 48 |
| 3-13 Shell Oil Limiting Vertical Strain Criteria (Airfields) | 54 |
| 3-14 The Limiting Vertical Strain Criteria Summary (MS-11) Airfield | 56 |
| 3-15 Limiting Vertical Strain Criteria (MS-11 Airfield) | 58 |
| 3-16 Vertical Subgrade Strain Computations by Moduli | 60 |
| 3-17 USACE-WES Limiting Vertical Strain Criteria (β -Airfield) | 62 |

| Table | Page |
|---|------|
| 4-1 Properties of Layer Materials in Pavement Structure | 75 |
| 4-2 Analysis for Circular Tire Imprint Shape (Z=150 in) | 77 |
| 4-3 Analysis for Elliptical Tire Imprint Shape (Z=150 in)..... | 80 |
| 4-4 Analysis for Elliptical Tire Imprint Shape (Z=150 in) - $360/d\phi$ is Integer | 83 |
| 4-5 Analysis for Elliptical Tire Imprint Shape (Z=150 in) - $360/d\phi$ Is Integer and Even . | 85 |
| 4-6 Analysis for Circular Tire Imprint Shape (Z=79.57 in) | 88 |
| 4-7 Analysis for Elliptical Tire Imprint Shape (Z=79.57 in)..... | 91 |
| 4-8 Analysis for Circular Tire Imprint Shape (Z=20 in) | 94 |
| 4-9 Analysis for Elliptical Tire Imprint Shape (Z=20 in)..... | 97 |
| 4-10 Analysis for Circular Tire Imprint Shape | 100 |
| 4-11 Analysis for Elliptical Tire Imprint Shape | 103 |
| 5-1 JULEA (1 Layer) and ZAPRAM Comparison for Boeing B737-600 | 113 |
| 5-2 JULEA (1 Layer) and ZAPRAM Comparison for Airbus INDUSTRIE A300-C4 .. | 113 |
| 5-3 JULEA (3 Layers) and ZAPRAM Comparison for Boeing B737-600 | 118 |
| 5-4 JULEA (3 Layers) and ZAPRAM Comparison for Airbus INDUSTRIE A300-C4. | 118 |
| 5-5 JULEA (3 Layers) and ZAPRAM comparison for the 1st pavement system with different correction factors. | 122 |
| 5-6 JULEA (3 Layers) and ZAPRAM comparison for the 2nd pavement system with different correction factors. | 122 |
| 5-7 JULEA (3 Layers) and ZAPRAM comparison for the 3rd pavement system with different correction factors. | 123 |
| 5-8 JULEA (3 Layers) and ZAPRAM comparison for the 4th pavement system with different correction factors. | 123 |

| Table | Page |
|--|------|
| 5-9 JULEA (3 Layers) and ZAPRAM comparison for the 5th pavement system with different correction factors. | 124 |
| 5-10 JULEA (3 Layers) and ZAPRAM comparison for the 6th pavement system with different correction factors. | 124 |
| 5-11 JULEA (3 Layers) and ZAPRAM comparison for the 7th pavement system with different correction factors. | 125 |
| 5-12 JULEA (3 Layers) and ZAPRAM comparison for the 8th pavement system with different correction factors. | 125 |
| 5-13 JULEA (3 Layers) and ZAPRAM comparison for the 1st pavement system with different correction factors. | 126 |
| 5-14 JULEA (3 Layers) and ZAPRAM comparison for the 2nd pavement system with different correction factors. | 126 |
| 5-15 JULEA (3 Layers) and ZAPRAM comparison for the 3rd pavement system with different correction factors. | 127 |
| 5-16 JULEA (3 Layers) and ZAPRAM comparison for the 4th pavement system with different correction factors. | 127 |
| 5-17 JULEA (3 Layers) and ZAPRAM comparison for the 5th pavement system with different correction factors. | 128 |
| 5-18 JULEA (3 Layers) and ZAPRAM comparison for the 6th pavement system with different correction factors. | 128 |
| 5-19 JULEA (3 Layers) and ZAPRAM comparison for the 7th pavement system with different correction factors. | 129 |
| 5-20 JULEA (3 Layers) and ZAPRAM comparison for the 8th pavement system with different correction factors. | 129 |

| Table | Page |
|--|------|
| 5-21 The Best Section for f_1 , f_2 Value up to the Smallest σ_z , Percentage Diff, % for B737-600 | 130 |
| 5-22 The Best Section for f_1 , f_2 Value up to the Smallest ϵ_z , Percentage Diff, % for B737-600 | 131 |
| 5-23 The Best Section for f_1 , f_2 Value up to the Smallest σ_z , Percentage Diff, % for A300-C4 | 132 |
| 5-24 The Best Section for f_1 , f_2 Value up to the Smallest ϵ_z , Percentage Diff, % with A300-C4 | 133 |
| 5-25 Squared Error for the Strain for Every Set of Correction Factors for Different Pavement Systems with Boeing B737-600..... | 136 |
| 5-26 Squared Error for the Stress and Strain for every Set of Correction Factors for Different Pavement Systems with A600 | 138 |
| 5-27 Strain and Stress Value from Both Programs with Changes of h_1 | 140 |
| 5-28 Steps of Best Correction Factor Calculation | 141 |
| 5-29 f_2 Estimations for Vertical Stress and Vertical Strain Value | 142 |
| 5-30 JULEA (3 Layers) and ZAPRAM Comparison for Truck | 144 |
| 5-31 JULEA (3 Layers) and ZAPRAM Comparison for Heavy Load..... | 145 |
| 5-32 Strain and Stress Value from Both Programs with Changes of h_1 | 151 |
| 5-33 Steps of Best Correction Factor Calculation | 153 |
| 5-34 All the f_2 Estimations from 24 Systems Due to Vertical Stress and Strain (18KSAL) | 154 |
| 5-35 All the f_2 Estimations from 24 Systems Due to Vertical Stress and Strain (100kip Tire)..... | 155 |
| 5-36 The Sets of Data Used to Determine the Correction Factors..... | 157 |

| Table | Page |
|---|------|
| 5-37 The Correction Factors for the Cases 1, 2 and 3 | 159 |
| 5-38 The Correction Factors for the Case IV | 159 |
| 5-39 heT Measured and Predicted Value for Four Cases | 161 |
| 6-1 Pavement Structure and Input Data | 168 |
| 6-2 Design Pavement Structure Required (Granular Base Thickness: 12 inches) | 169 |
| 7-1 Input Parameters Used for the Pavement Structure | 185 |
| 7-2 Environmental Stages of the Subgrade MR Values | 187 |
| 7-3 Thickness of Subbase (in) for the Selected Aircraft | 190 |

LIST OF FIGURES

| Figure | Page |
|--|------|
| 2-1 Curve Used for Estimated the Suction of Base Material [kpa]..... | 17 |
| 2-2 Curve Used for Estimated the Suction [kpa] at $w_{pi} = 50$ | 18 |
| 2-3 Suction Profile Using γ_w | 19 |
| 2-4 Transformations Used in Odemark's Method. | 25 |
| 2-5 Stress in the Soil Due to Point Load at Surface (Rectangular Coordinates)..... | 26 |
| 3-1 Type Gear Single Tire..... | 38 |
| 3-2 Type Gear Dual Tire. | 39 |
| 3-3 Type Gear Single Tandem..... | 40 |
| 3-4 Type Gear Dual Tandem. | 41 |
| 3-5 Type Gear Tri- Tandem. | 42 |
| 3-6 Type Gear for C5A. | 44 |
| 3-7 Type Gear for B-52..... | 44 |
| 3-8 Type Gear for A-380..... | 45 |
| 3-9 Type Gear for B-747..... | 47 |
| 3-10 Vertical Strain at the Top of the Subgrade (ϵ_{vsg})..... | 52 |
| 3-11 Relation between Allowable Repetitions and the Vertical Strain at the Top of the Subgrade (ϵ_{vsg})..... | 53 |
| 3-12 Allowable Number of Repetition as a Function of the Vertical Strain at the Top of the Subgrade (Shell Oil - Airfields). | 55 |
| 3-13 Allowable Number of Repetitions as a Function of the Vertical Strain at the Top of the Subgrade (MS-11 Airfield). | 57 |
| 3-14 Allowable Number of Repetitions as a Function of the Vertical Strain at the Top of the Subgrade (MS-11 Airfield). | 58 |

| Figure | Page |
|--|------|
| 3-15 Design Criteria based on the ϵ_{vsg} (USACE. Original MLET-Airfield). | 61 |
| 3-16 Allowable Number of Repetition as a Function of the ϵ_{vsg} (USACE-WES (β - Airfield))..... | 63 |
| 3-17 Allowable Number of Repetition as a Function of the Vertical Strain at the Top of the Subgrade (from the Previous Four Methods). | 63 |
| 3-18 Load Distribution for Aircraft with Dual Tire Gear..... | 65 |
| 3-19 The Maximum Strain at the Top of Subgrade. | 66 |
| 3-20 Determines the Largest Strain Along X_i | 66 |
| 3-21 Maximum Strain for All the Points Along X_i | 67 |
| 3-22 The Distribution N_f underneath the Selected Strip..... | 68 |
| 3-23 The Unit Damage Cussed to Specific Pavement by Certain Aircraft. | 69 |
| 3-24 Distribution of Wander Laterally of the Vehicle. | 70 |
| 3-25 The Unit Damage for Particular Aircraft Moving Laterally Long the Airfield Pavement. | 71 |
| 3-26 Total Damage Accumulated by the Aircraft..... | 71 |
| 4-1 The Airbus A-380. | 73 |
| 4-2 Tire Configuration of the A-380 Airbus. | 73 |
| 4-3 Tires Location for Airbus A380. | 74 |
| 4-4 The Pavement System that Was Used in Comparison. | 75 |
| 4-5 Time and Number of dA Analysis for Circular Tire Imprint Shape ($Z=150$ in). | 78 |
| 4-6 Vertical Stress and Number of dA Analysis for Circular Tire Imprint Shape ($Z=150$ in). | 78 |
| 4-7 Vertical Strain and Number of dA Analysis for Circular Tire Imprint Shape..... | 79 |

| Figure | Page |
|---|------|
| 4-8 Vertical Stress and Number of dA Analysis for Elliptical Tire Imprint Shape (Z=150 in)..... | 81 |
| 4-9 Vertical Strain and Number of da Analysis for Elliptical Tire Imprint Shape (Z=150 in). | 82 |
| 4-10 Vertical Stress and Number of dA Analysis for Elliptical Tire Imprint Shape | 84 |
| 4-11 Vertical Strain and Number of dA Analysis for Elliptical Tire Imprint Shape (Z=150 in). | 84 |
| 4-12 Time and Number of dA Analysis for Elliptical Tire Imprint Shape (Z=150 in). | 86 |
| 4-13 Vertical Stress and Number of dA Analysis for Elliptical Tire Imprint Shape (Z=150 in). | 86 |
| 4-14 Vertical Strain and Number of dA Analysis for Elliptical Tire Imprint Shape (Z=150 in). | 87 |
| 4-15 Time and Number of dA Analysis for Circular Tire Imprint Shape | 89 |
| 4-16 Vertical Stress and Number of dA Analysis for Circular Tire Imprint Shape (Z=79.57 in)..... | 89 |
| 4-17 Vertical Strain and Number of dA Analysis for Circular Tire Imprint Shape (Z=79.57 in)..... | 90 |
| 4-18 Time and Number of dA Analysis for Elliptical Tire Imprint Shape..... | 92 |
| 4-19 Vertical Strain and Number of dA Analysis for Elliptical Tire Imprint Shape (Z=79.57 in)..... | 92 |
| 4-20 Vertical Strain and Number of dA Analysis for Elliptical Tire Imprint Shape (Z=79.57 in)..... | 93 |
| 4-21 Time and Number of dA Analysis for Circular Tire Imprint Shape (Z=20 in). | 95 |

| Figure | Page |
|---|------|
| 4-22 Vertical Stress and Number of dA Analysis for Circular Tire Imprint Shape (Z=20.00 in)..... | 95 |
| 4-23 Vertical Strain and Number of dA Analysis for Circular Tire Imprint Shape..... | 96 |
| 4-24 Time and Number of dA Analysis for Elliptical Tire Imprint Shape (Z=20 in)..... | 98 |
| 4-25 Vertical Stress and Number of dA Analysis for Elliptical Tire Imprint Shape (Z=20.00 in)..... | 98 |
| 4-26 Vertical Strain and Number of dA Analysis for Elliptical Tire Imprint Shape (Z=20.00 in)..... | 99 |
| 4-27 Relationship between Stress Percentage Diff (%) and Number of Computational Points of Circular Tire Imprint Shape. | 101 |
| 4-28 Relationship between Strain Percentage Diff (%) and Number of Computational Points of Circular Tire Imprint Shape. | 102 |
| 4-29 Relationship between Stress Percentage Diff (%) and No of Computational Points of Elliptical Tire Imprint Shape. | 104 |
| 4-30 Relationship between Strain Percentage Diff (%) and no of Computational Points of Elliptical Tire Imprint Shape. | 104 |
| 5-1 Pavement System Used in the Stress Comparison..... | 109 |
| 5-2 The Pavement System with All the Option..... | 112 |
| 5-3 Calculated Stresses from JULEA (1 Layer) and ZAPRAM by Using Boeing B737- 600..... | 114 |
| 5-4 Calculated Strain From JULEA (1 Layer) and ZAPRAM by Using Boeing B737-600. | 115 |
| 5-5 Calculated Stresses from JULEA (1 Layer) and ZAPRAM by Using Airbus INDUSTRIE A300-C4..... | 115 |

| Figure | Page |
|---|------|
| 5-6 Calculated Strain from JULEA (1 Layer) and ZAPRAM by Using Airbus INDUSTRIE A300-C..... | 116 |
| 5-7 The Pavement System with All Options..... | 117 |
| 5-8 Calculated Stresses from JULEA (3 Layers) and ZAPRAM by Using Boeing B737- 600..... | 119 |
| 5-9 Calculated Strain from JULEA (3 Layers) and ZAPRAM by Using Boeing B737- 600..... | 119 |
| 5-10 Calculated Stresses from JULEA (3 Layers) and ZAPRAM by Using Airbus INDUSTRIE A300-C4..... | 120 |
| 5-11 Calculated Strain from JULEA (3 Layers) and ZAPRAM by Using Airbus INDUSTRIE A300-C..... | 120 |
| 5-12 The Best Section for f_1, f_2 Value up to the Smallest σ_z , Percentage Diff, % for B737- 600..... | 130 |
| 5-13 The Best Section for f_1, f_2 Value up to the Smallest ϵ_z , Percentage Diff, % for B737- 600..... | 131 |
| 5-14 The Best Section for f_1, f_2 Value up to the Smallest σ_z , Percentage Diff, % for A300-C4..... | 132 |
| 5-15 The Best Section for f_1, f_2 Value up to the Smallest ϵ_z , Percentage Diff, % with A300-C4..... | 133 |
| 5-16 Correction Factor for Different Combination of Different Pavement System with Boeing B737-600..... | 134 |
| 5-17 Correction Factor for Different Combination of Different Pavement System with Boeing B737-600..... | 134 |

| Figure | Page |
|---|------|
| 5-18 Correction Factor for Different Combination of Different Pavement System with A300-C4. | 135 |
| 5-19 Correction Factor for Different Combination of Different Pavement System with A300-C4. | 135 |
| 5-20 Squared Error Versus Correction Factor Set for Stress (B-737)..... | 137 |
| 5-21 Squared Error Versus Correction Factor Set for Strain (B-737)..... | 137 |
| 5-22 Squared Error Versus Correction Factor Set for Stress (A-300). | 138 |
| 5-23 Squared Error Versus Correction Factor Set for Strains (A-300). | 139 |
| 5-24 Estimate the Equivalent Depth that the Stresses Must Be Calculated. | 140 |
| 5-25 Calculated Stresses from JULEA (3 Layers) and ZAPRAM for Light Load. | 146 |
| 5-26 Calculated Strain from JULEA (3 Layers) and ZAPRAM for Light Load. | 146 |
| 5-27 Calculated Stresses from JULEA (3 Layers) and ZAPRAM for Heavy Load. | 147 |
| 5-28 Calculated Strain from JULEA (3 Layers) and ZAPRAM for Heavy Load. | 147 |
| 5-29 The Effect of CBR on Percent Error (Stress) – Truck. | 148 |
| 5-30 The Effect of CBR on Percent Error (Strain) – Truck. | 148 |
| 5-31 The Effect of h_1 on Percent Error (Stress). | 149 |
| 5-32 The Effect of h_1 on Percent Error (Strain). | 149 |
| 5-33 The Effect of h_2 on Percentage Error (Stress)..... | 150 |
| 5-34 The Effect of h_1 on Percent Error (Strain). | 150 |
| 5-35 Estimate the Equivalent Depth that the Stresses Must Be Calculated. | 152 |
| 5-36 h_{eT} Measured and Predicted Value for Case I. | 163 |
| 5-37 h_{eT} Measured and Predicted Value for Case II..... | 163 |
| 5-38 h_{eT} Measured and Predicted Value for Case III..... | 164 |
| 5-39 h_{eT} Measured and Predicted Value for Case IV. | 164 |

| Figure | Page |
|--|------|
| 6-1 Design Factors Influence upon the Sub-Base Thickness Considering 6 Inches of AC. | 171 |
| 6-2 Design Factors Influence upon the Sub-Base Thickness Considering 10 Inches of AC. | 172 |
| 6-3 Difference in Design Thickness Relative to the AI Criterion (6 Inches of AC). | 174 |
| 6-4 Statistical Summary of Agency Pavement Design (a) with 6 inches of AC, (b) with 10 Inches of AC. | 176 |
| 6-5 Typical Design Thickness ± 2 S Error Associated between Design Methods. | 177 |
| 7-1 Investigation Plan. | 184 |
| 7-2 Subgrade Soil Modulus Variations. | 188 |
| 7-3 Required Subbase Thickness (in) for Boeing B737-600. | 192 |
| 7-4 Required Subbase Thickness (in) for Airbus INDUSTRIE A300-C4. | 193 |
| 7-5 Required Subbase Thickness (in) for Boeing B747-400. | 194 |

NOMENCLATURE

a_f soil parameter for non-plastic soils which is primarily a function of the air entry value of the soil

AADT Annual Average Daily Traffic

A_c Tire Imprint Area

b_f soil parameter for non-plastic soils which is primarily a function of the rate of water extraction from the soil, once the air entry value has been exceeded

c_f soil parameter for non-plastic soils which is primarily a function of the residual water content

$C(h)$ correction factor which is a function of matric suction (Fredlund and Xing)

CBR California bearing ratio

D_e Directional Distribution Factor

DF damage factor

D_i day-length correction as a function of latitude

$\exp 2.718282\dots$

E_i modulus of layer i

E_n modulus of the lowest layer

f correction factor for the transformed thickness equation. (assumed to be equal to one in ZAPMEDACA but changed in ZAPRAM to allow more accurate estimation of the pavement response variable)

F_{env} Environmental Factor

G_s specific gravity of the solids

GWT ground water table

h_{ei} equivalent thickness for layer i

h_i actual thickness for layer i

h_i Monthly heat index

h_m matric suction $u_a - u_w$

h_{r_f} a soil parameter for non-plastic soils which is primarily a function of the suction at which residual water content occurs (Fredlund and Xing equation)

H_y Yearly heat index

H_y Yearly heat index [dimensionless]

L Lane Distribution Factor

LL Liquid limit

MET method of equivalent thicknesses

M_R resilient modulus of the subgrade

MSE mean squared error

n_f Frohlich number

N Design Life

N Number of effective (actual) strain repetitions

N_f Number of allowable strain repetitions to failure

N_i number of days in the month

P annual precipitation

p tire pressure

P Tire load

P_{200} percent passing No. 200 US sieve

PE_i Monthly evapotranspiration

PI plasticity index

P_{j_0} Passes of Vehicle at Base Year

P_{jt} Passes of Vehicle at End of Design Life

PL plastic limit

p_t Percentage of Trucks in the AADT

r_g Traffic Growth Rate

S degree of saturation

SWCC soil-water characteristic curve

t_i mean monthly temperature

T_f Truck Factor

TMI Thornthwaite Moisture Index

ua-uw matric suction

w gravimetric water content

w_{opt} optimum gravimetric moisture content

wPI weighted PI = Passing #200 \times PI

w_t Tire Width

γ_{dry} dry unit weight (bulk density)

γ_{water} unit weight of water (density of the water)

ϵ_x Strain in the x direction

ϵ_y Strain in the y direction

ϵ_z Strain in the z direction

ϵ_{vsg} Vertical strain at the top of subgrade

θ_{sat} soil porosity or saturated volumetric water content

θ_w volumetric water content

μ mean

σ standard deviation

σ_x Normal stress in the x direction

σ_y Normal stress in the y direction

σ_w Gear wander standard deviation

σ_z Normal stress in the z direction

τ_{xy} Shear stress in the xy plane

τ_{xz} Shear stress in the xz plane

τ_{yz} Shear stress in the yz plane

ν Poisson's ratio of the soil

ψ total suction

CHAPTER 1 INTRODUCTION

1.1 Introduction

In the past, the majority of structural designs for highway and airfield pavements have been developed on the simplifying assumption that sooner or later, in the pavement lifespan, all unbound material layers would be exposed to saturated conditions. In essence, the use of this assumption negates the real possibility that true saturation will never be the "norm" in a wide variety of environmental locations and groundwater table (GWT) conditions. This is true as hotter, arid locations are encountered with deep water tables. Another reason for the simplifying assumption is the fact that the area of unsaturated soil mechanics, coupled with the site environmental properties, is not yet well understood by most of the practicing community. Furthermore, the variations of site soil properties have a significant impact on structural designs for highway and airfield pavements.

However, in the last decade, very significant advances in the area of unsaturated soil mechanics and the ability to model damage as a direct result of the environmental effects, soil properties and groundwater table location have been made in the pavement design community. The first comprehensive subsystem to incorporate these environmental elements into the pavement design process was developed as a part of the new AASHTO Mechanistic Empirical Pavement Design Guide (MEPDG) developed under NCHRP projects 1-37A and 1-40D. These efforts were intended to predict/simulate the changes in behavior and material response in all unbound materials in conjunction with environmental conditions over years of operation.

Arizona State University (ASU) played a significant role for the inclusions and implementation of the Enhanced Integrated Climatic Model (EICM) into the MEPDG

between 1999 and 2006. Since that time, a series of continuously enhanced, educational computer codes have been developed at ASU. The initial software, called ZAPMEDACA, incorporated unsaturated soil mechanics principles and environmental effects technology directly into structural pavement design software codes developed for flexible airfield pavements. A next generation program is already completed and is called ZAPRAM. This program was an enhancement of the original ZAPMEDACA program by the author. This thesis describes the enhancements that were incorporated to develop the present computer code. The most significant capability of the program is its ability to incorporate actual site environmental factors and ground water table depth to characterize real time effect of partly saturated to saturated conditions/response of all unbound layers.

Program ZAPMEDACA is an acronym for Dr. Claudia Zapata (main development leadership), Mena Souliman; Dan Rosenbalm, and Carlos Cary, ASU graduate students. This program is an educational software program developed by graduate students at Arizona State University (ASU) for the analysis of asphalt highway and airfield pavement structures. The main program uses a mechanistic analysis of pavement systems that presently use failure criteria based upon the well known limiting strain criteria. The program computes stress, strains, and displacements within the pavement structure from an enhanced application of Odemark's transformation theory of layered systems. Pavement responses are then computed by numerical integration of the Boussinesq solution. This allows the program to evaluate any multi-tire configuration of wheel loads. Each tire can be modeled by a circular, rectangular or elliptical wheel load and can be treated with either a uniform or non-uniform contact pressure.

The latest revision to the series of "ZAP" codes is called ZAPRAM. This software is an Excel-based computer code that primarily focuses upon flexible airfield pavements and, most importantly, the incorporation of the real time effects of site

environmental conditions and groundwater table depth upon airfield pavement performance. To the author's knowledge, this is the first program of its type that has been developed. The program is capable of running several different environmental scenarios to examine the sensitivity of these factors on the pavement response and pavement design requirements to develop a structure cross section that will resist excessive shear displacements, leading to permanent deformation or rutting of the pavement system.

1.2 Scope of Work

The scope of work for this research included the following work activities:

- Conduct a literature search.
- Gain an understanding of the ZAPMEDACA software modules. This stage reviewed the methods that have been used to estimate the environmental effects and to calculate the stress and strain analysis.
- Enhancement of the ZAPMEDACA software. This work activity was the most important one and required the majority of time utilized for the total study. In general this task consisted of improvement the existing program modules, development of new modules and the creation of a new enhanced version of ZAPMEDACA called ZAPRAM.
- Development of a computational study to ascertain the optimized number of differential load areas necessary to obtain accurate pavement response comparisons by the numerical integration approach.
- Conduct a study to corroborate that the production of stresses/strain with the transformed section approach by Odemark and numerical integration yielded accurate comparisons to other well known multilayer pavement region solutions.

- Conduct a series of sensitivity/analysis studies which focused upon quantifying the significance of the Environmental location and Ground Water Table depth upon the design thickness of the pavement to accommodate repetitive shear in the unbound layer.
- Create a user's guide manual which provides detailed assistance for individuals using the program.
- Develop a final report of all activities associated with the development of ZAPRAM.

1.3 Research Objectives

The major objective of this study was to create an improved computer code of ZAPMEDACA that will provide an enhanced range of solutions of asphalt airfield pavement sections.

- One major objective of this investigation was to provide a quantitative assessment of the potential differences in pavement design thickness resulting from the site specific environmental properties (moisture -temperature) and the groundwater table depth.
- Another main objective of this thesis was to develop a comparison study of flexible airfield pavement design thicknesses, derived from a variety of accepted limiting strain failure criteria used in practice today throughout the world.
- The final goal of this study was to present the effect and sensitivity of several key soil properties in pavement design thickness that were computed for a matrix of Environmental locations and ground water table depths. These factors provided a better understanding of their importance to the pavement design methodology.

Beside these major objectives, there are several other tasks contained in this thesis. They are:

- An in-depth description of the ZAPMEDACA program is presented. Explanation of the environmental impact and material properties equations used in the ZAPMEDACA solution are provided in this thesis.
- Illustrate the capability of the ZAPRAM program for analyzing performance for a wide variety of mechanistic design approaches. This part specifically focuses upon the prediction of pavement designs to guard against excessive shear deformations (rutting).
- One objective contained in this study is the evaluation of accuracy of the vertical stresses and strain calculated along with the time in which the program should carry out the analysis to insure the number of differential loading areas the user should use for a given depth.

1.4 Organization

This thesis has been divided into nine chapters. Chapter 1 includes the introduction, objectives of the study and scope of work.

Chapter 2 summarizes the literature review, and a description of the ZAPMEDACA software modules. This chapter reviews the methods that have been used to predict the environmental effects as well as the computational methodology used to calculate the stress and strain regions.

Chapter 3 describes the enhancement of the ZAPMEDACA software that was accomplished in this thesis. Some general concepts about the vertical subgrade strain criteria calculation are also presented in this chapter. This chapter concludes with the

introduction of the ZAPRAM program, describing the specific enhancements made by the program.

Chapter 4 contains the specifics of the evaluation of the time and space study for different tire imprint shapes as well as a special study that clarifies the impact of the computed depth on the minimum number of computational points required for an accurate numerical integration method.

Chapter 5 is intended to substantiate the validity of the program for the stress and strain analysis. In essence, the chapter demonstrates the relative accuracy of pavement response parameters predicted from the Odemark transformed section analysis and the numerical integration approach compared to the classical multi-layered Elastic response solution.

Chapter 6 described the comparison of airfield flexible pavement design thickness based upon several differing agency limiting subgrade strain criteria.

Chapter 7 documents the impact of environmental site location and groundwater table depth on the thickness of flexible airfield pavements.

Finally, Chapter 8 contains the summary and conclusions of this research, including the implication for engineering practice.

Future recommendations for further enhancing the current ZAPRAM program are presented in Chapter 9.

It is to be noted that the User's Guide is included as an appendix to assist the user with the code implementation.

CHAPTER 2 LITERATURE REVIEW

2.1 Introduction:

ZAPMEDACA is an educational pavement engineering software program developed by graduate students at Arizona State University (ASU) for the analysis of asphalt highway and airfield pavement structures. The basic intention of this educational process of the ZAP program code is to allow a new set of students in each future semester to enhance the prior program. The program computes stress, strains, and displacements within a given pavement structure from an enhanced application of Odemark's transformation theory of layered systems (1). Pavement responses are then computed by numerical integration of the Boussinesq solution (2). This allows the program to evaluate any multi-tire configuration of wheel loads. Each tire can be modeled by a circular, rectangular or elliptical wheel load and can be treated with either a uniform or non-uniform contact pressure.

The most important capability of the program is its ability to incorporate actual site environmental factors and ground water table depth to characterize the real time effect of partly saturated to saturated conditions/response of all unbound layers. The program used in ZAPMEDACA to account for the environmental impact upon material properties is identical to the process introduced in the AASHTO MEPDG by Dr. Claudia Zapata.

Program ZAPMEDACA is an acronym for Dr. Claudia Zapata (main development leadership), Mena Souliman; Dan Rosenbalm, and Carlos Cary, ASU graduate students. The next generation program has been completed and is called ZAPRAM. This program is an enhancement of ZAPMEDACA by Ramadan Salim, ASU graduate student. The specific enhancements of ZAPRAM are presented in this thesis.

ZAPRAM primarily concentrates on the incorporation of a series of analytical enhancement applications for airfield pavement design. The main program uses a mechanistic analysis of pavement systems that presently uses failure criteria based upon the well known limiting strain criteria. Thus ZAPRAM is presently capable of analyzing pavement systems designed to minimize permanent deformation (rutting) of the aircraft-pavement system.

2.2 ZAPMEDACA Software

The concept adopted in the ZAPMEDACA pavement analysis procedure is based upon the numerical integration of Boussinesq response equations applied to an Odemark's transformed pavement section (2). This approach has been repeatedly verified over the years, by a wide range of researchers, to provide **generally** accurate estimates of stress, strain and displacement compared to the solution by more mathematically rigorous multi-layered Elastic theory solutions.

One of the most current important capabilities, of ZAPMEDACA, is to assess the environmental effects on pavement design. The program will allow the solution for several different environmental scenarios. These "environmental scenarios" are represented by the influence of site temperature moisture conditions, for a given ground water table depth. ZAPMEDACA allows the user to examine the sensitivity of these factors on the pavement response. As a result, a greater understanding of the environmental effects on the entire pavement structure will be achieved.

2.3 ZAPMEDACA Software Modules

The design inputs in ZAPMEDACA are divided into four main categories: load configuration, pavement structure and material properties, environmental effects and

pavement response computations. The main outputs of the program are the damage (rutting) at any given depth and lateral location across the taxiway/runway caused by the vehicle or aircraft on the specific pavement cross section being analyzed at a particular environmental site. The following is a brief description regarding the inputs and outputs.

2.3.1 Load Configuration

The Load Configuration module is the first interface in which the user will work with. Most of the data in this module are associated with input information. The following are required input parameters in the load configuration module:

- Number of tires in gear to be analyzed
- Tire spacing's (location in x-y coordinates)
- Load per tire (lb)
- Tire pressure (psi)
- Pressure distribution. This can be either “uniform” or “ non uniform”. If the user selects non uniform, a pop out message will ask the user to input the wall stiffening ratio.
- Tire imprint shape (circular, rectangular, elliptical)
- Distance from centerline of aircraft fuselage to geometric center of main gear, X_j (ft)
- Lateral Aircraft Wander Standard Deviation, sw (ft)
- USACE Traffic Lane Width, T , (ft)
- Number of Longitudinal Segments in Tire Imprint (if rectangular or elliptical)
- Number of Transverse Segments in Tire Imprint (if rectangular or elliptical)
- Number of Radial Segments in Tire Imprint (if circular or elliptical)
- Number of Angular Segments in Tire Imprint (if circular or elliptical)

- Tire Loading Points Cartesian Coordinates (locations in x-y coordinate)

The program uses these inputs within other modules to perform the necessary damage calculations. Within the load configuration module, several computations are performed that are required for the solution. They are:

- Tire Imprint Area, A_c (in²): the tire imprint area is calculated by the following equation:

$$A_c = \frac{P}{p} \quad (2-1)$$

Where:

A_c : Tire Imprint Area (in²)

P: Tire load (lb)

p : The tire pressure (psi)

- Tire Width, w_t (in): the width of a circular tire will be equal to the diameter of the tire. If a rectangular or elliptical tire imprint is selected the following equation is used to calculate w_t (3):

$$w_t = 0.6 \sqrt{\frac{P}{0.5228p}} \quad (2-2)$$

Where:

w_t : Tire Width, w_t (in)

P: The load (lb)

p: The tire pressure (psi)

2.3.2 Pavement Structure and Material Properties

In this module, the program requires the number of specific material layers in the entire pavement structure and the depth of the ground water table. This depth is defined from the top of the pavement surface. This is followed by inputting specific data for each layer thickness, material type (asphalt, granular base, granular subbase, or subgrade), and

Poisson's ratio. For the asphalt layer, the user *must* input the critical effective asphalt mix modulus that is unique to each critical strain criteria (design agency methodology). This is discussed further in later sections of this thesis.

For all unbound layers, the user can input strength/response properties such as CBR, R-value or the resilient modulus. Empirical equations correlating CBR or R values to the resilient modulus values are used in the program. The user is also asked to input the percentage passing the No.200 sieve, plasticity index, specific gravity of solids, optimum moisture content, and maximum dry density. The following are the specific required input parameters used in the pavement structure module:

- 1- Number of Layers
- 2- Ground Water Table Depth, (ft)
- 3- Material Type Identification
- 4- Layer of Thickness (in)
- 5- Modulus at Optimum Conditions, E (psi)
 - CBR (%)
 - R value
 - AASHTO Layer Coefficient, ai
 - Soil Classification (AASHTO or USCS)
- 6- Passing Sieve #200 (%), P200
- 7- Plasticity Index , PI
- 8- Specific Gravity of Solids, Gs
- 9- Optimum Moisture Content, w_{opt} (%):
- 10- Maximum Dry Density, $\gamma_d \max$ (pcf):

2.3.3 *Environmental Effects*

The concept of the environmental effects utilized in ZAPMEDACA has been based upon the fundamental concepts used in the MEPDG and developed under NCHRP 1-40D and NCHRP 1-37A (4, 5, 6, and 7). These technical reports define the fundamental methodology by which the Enhanced Integrated Climatic Model (EICM) module was incorporated by ASU researchers to predict real time variation in moisture content (degree of saturation) for all unbound pavement layers due to environmental conditions and soil properties.

A brief explanation of the most important steps and variables used to estimate the environmental effects for unsaturated soils are presented. For a given in-situ condition and time, an environmental factor is computed and used to adjust the resilient modulus of the unbound material to real time conditions. The models input and output parameters used in the AASHTO MEPDG are presented in the following paragraphs.

2.3.3.1 *Thornthwaite Moisture Index, TMI*

The Thornthwaite Moisture Index was found to be the most significant parameter for predicting suction under pavements (8). In 1948, Thornthwaite introduced the TMI as an index that classified the climate of a given location (9). To estimate this index, the following parameters need to be computed:

- Monthly heat index [dimensionless]:

$$h_i = (0.2t_i)^{1.514} \quad (2-3)$$

where:

t_i = mean monthly temperature [$^{\circ}$ C]

- Yearly heat index[dimensionless]:

$$H_y = \sum h_i \quad (2-4)$$

- Monthly evapotranspiration [cm]:

$$PE_i^* = 1.6 \left(\frac{10t_i}{H_y} \right)^a \quad (2-5)$$

where:

$$a = 6.75 \times 10^{-7} H_y^3 - 7.71 \times 10^{-5} H_y^2 + 0.017921 H_y + 0.49239$$

t_i = mean monthly temperature [°C]

H_y = Yearly heat index [dimensionless]

- Monthly evapotranspiration corrected by length of a day[cm]:

$$PE_i = PE_i^* \left(\frac{D_i N_i}{30} \right) \quad (2-6)$$

where:

D_i = day-length correction as a function of latitude, (obtained from TABLE 2-1 and TABLE 2-2)

N_i = number of days in the month

TABLE 2-1 Mean Possible Duration of Sunlight – Northern Hemisphere (Day-Length Correction Factor in Units of 30 Days of 12 Hours)

| Northern latitude | January | February | March | April | May | June | July | August | September | October | November | December |
|-------------------|---------|----------|-------|-------|------|------|------|--------|-----------|---------|----------|----------|
| 0 | 1.04 | 0.94 | 1.04 | 1.01 | 1.04 | 1.01 | 1.04 | 1.04 | 1.01 | 1.04 | 1.01 | 1.04 |
| 5 | 1.02 | 0.93 | 1.03 | 1.02 | 1.06 | 1.03 | 1.06 | 1.05 | 1.01 | 1.03 | 0.99 | 1.02 |
| 10 | 1.00 | 0.91 | 1.03 | 1.03 | 1.08 | 1.06 | 1.08 | 1.07 | 1.02 | 1.02 | 0.98 | 0.99 |
| 15 | 0.97 | 0.91 | 1.03 | 1.04 | 1.11 | 1.08 | 1.12 | 1.08 | 1.02 | 1.01 | 0.95 | 0.97 |
| 20 | 0.95 | 0.90 | 1.03 | 1.05 | 1.13 | 1.11 | 1.14 | 1.11 | 1.02 | 1.00 | 0.93 | 0.94 |
| 25 | 0.93 | 0.89 | 1.03 | 1.06 | 1.15 | 1.14 | 1.17 | 1.12 | 1.02 | 0.99 | 0.91 | 0.91 |
| 26 | 0.92 | 0.88 | 1.03 | 1.06 | 1.15 | 1.15 | 1.17 | 1.12 | 1.02 | 0.99 | 0.91 | 0.91 |
| 27 | 0.92 | 0.88 | 1.03 | 1.07 | 1.16 | 1.15 | 1.18 | 1.13 | 1.02 | 0.99 | 0.90 | 0.90 |
| 28 | 0.91 | 0.88 | 1.03 | 1.07 | 1.16 | 1.16 | 1.18 | 1.13 | 1.02 | 0.98 | 0.90 | 0.90 |
| 29 | 0.91 | 0.87 | 1.03 | 1.07 | 1.17 | 1.16 | 1.19 | 1.13 | 1.03 | 0.98 | 0.90 | 0.89 |
| 30 | 0.90 | 0.87 | 1.03 | 1.08 | 1.18 | 1.17 | 1.20 | 1.14 | 1.03 | 0.98 | 0.89 | 0.88 |
| 31 | 0.90 | 0.87 | 1.03 | 1.08 | 1.18 | 1.18 | 1.20 | 1.14 | 1.03 | 0.98 | 0.89 | 0.88 |
| 32 | 0.89 | 0.86 | 1.03 | 1.08 | 1.19 | 1.19 | 1.21 | 1.15 | 1.03 | 0.98 | 0.88 | 0.87 |
| 33 | 0.88 | 0.86 | 1.03 | 1.09 | 1.19 | 1.20 | 1.22 | 1.15 | 1.03 | 0.97 | 0.88 | 0.86 |
| 34 | 0.88 | 0.85 | 1.03 | 1.09 | 1.20 | 1.20 | 1.22 | 1.16 | 1.03 | 0.97 | 0.87 | 0.86 |
| 35 | 0.87 | 0.85 | 1.03 | 1.09 | 1.21 | 1.21 | 1.23 | 1.16 | 1.03 | 0.97 | 0.86 | 0.85 |
| 36 | 0.87 | 0.85 | 1.03 | 1.10 | 1.21 | 1.22 | 1.24 | 1.16 | 1.03 | 0.97 | 0.86 | 0.84 |
| 37 | 0.86 | 0.84 | 1.03 | 1.10 | 1.22 | 1.23 | 1.25 | 1.17 | 1.04 | 0.97 | 0.85 | 0.83 |
| 38 | 0.85 | 0.84 | 1.03 | 1.10 | 1.23 | 1.24 | 1.25 | 1.17 | 1.04 | 0.96 | 0.84 | 0.83 |
| 39 | 0.85 | 0.84 | 1.03 | 1.11 | 1.23 | 1.24 | 1.26 | 1.18 | 1.04 | 0.96 | 0.84 | 0.82 |
| 40 | 0.84 | 0.83 | 1.03 | 1.11 | 1.24 | 1.25 | 1.27 | 1.18 | 1.04 | 0.96 | 0.83 | 0.81 |
| 41 | 0.83 | 0.83 | 1.03 | 1.11 | 1.25 | 1.26 | 1.27 | 1.19 | 1.04 | 0.96 | 0.82 | 0.80 |
| 42 | 0.82 | 0.83 | 1.03 | 1.12 | 1.26 | 1.27 | 1.28 | 1.19 | 1.04 | 0.95 | 0.82 | 0.79 |
| 43 | 0.81 | 0.82 | 1.02 | 1.12 | 1.26 | 1.28 | 1.29 | 1.20 | 1.04 | 0.95 | 0.81 | 0.77 |
| 44 | 0.81 | 0.82 | 1.02 | 1.13 | 1.27 | 1.29 | 1.30 | 1.20 | 1.04 | 0.95 | 0.80 | 0.76 |
| 45 | 0.80 | 0.81 | 1.02 | 1.13 | 1.28 | 1.29 | 1.31 | 1.21 | 1.04 | 0.94 | 0.79 | 0.75 |
| 46 | 0.79 | 0.81 | 1.02 | 1.13 | 1.29 | 1.31 | 1.32 | 1.22 | 1.04 | 0.94 | 0.79 | 0.74 |
| 47 | 0.77 | 0.80 | 1.02 | 1.14 | 1.30 | 1.32 | 1.33 | 1.22 | 1.04 | 0.93 | 0.78 | 0.73 |
| 48 | 0.76 | 0.80 | 1.02 | 1.14 | 1.31 | 1.33 | 1.34 | 1.23 | 1.05 | 0.93 | 0.77 | 0.72 |
| 49 | 0.75 | 0.79 | 1.02 | 1.14 | 1.32 | 1.34 | 1.35 | 1.24 | 1.05 | 0.93 | 0.76 | 0.71 |
| 50 | 0.74 | 0.78 | 1.02 | 1.15 | 1.33 | 1.36 | 1.37 | 1.25 | 1.06 | 0.92 | 0.73 | 0.70 |

TABLE 2-2 Mean Possible Duration of Sunlight – Southern Hemisphere (Day-Length Correction Factor in Units of 30 Days of 12 Hours)

| Southern latitude | January | February | March | April | May | June | July | August | September | October | November | December |
|-------------------|---------|----------|-------|-------|------|------|------|--------|-----------|---------|----------|----------|
| 5 | 1.06 | 0.95 | 1.04 | 1.00 | 1.02 | 0.99 | 1.02 | 1.03 | 1.00 | 1.05 | 1.03 | 1.06 |
| 10 | 1.08 | 0.97 | 1.05 | 0.99 | 1.01 | 0.96 | 1.00 | 1.01 | 1.00 | 1.06 | 1.05 | 1.10 |
| 15 | 1.12 | 0.98 | 1.05 | 0.98 | 0.98 | 0.94 | 0.97 | 1.00 | 1.00 | 1.07 | 1.07 | 1.12 |
| 20 | 1.14 | 1.00 | 1.05 | 0.97 | 0.96 | 0.91 | 0.95 | 0.99 | 1.00 | 1.08 | 1.09 | 1.15 |
| 25 | 1.17 | 1.01 | 1.05 | 0.96 | 0.94 | 0.88 | 0.93 | 0.98 | 1.00 | 1.10 | 1.11 | 1.18 |
| 30 | 1.20 | 1.03 | 1.06 | 0.95 | 0.92 | 0.85 | 0.90 | 0.96 | 1.00 | 1.12 | 1.14 | 1.21 |
| 35 | 1.23 | 1.04 | 1.06 | 0.94 | 0.89 | 0.82 | 0.87 | 0.94 | 1.00 | 1.13 | 1.17 | 1.25 |
| 40 | 1.27 | 1.06 | 1.07 | 0.93 | 0.86 | 0.78 | 0.84 | 0.92 | 1.00 | 1.15 | 1.20 | 1.29 |
| 42 | 1.28 | 1.07 | 1.07 | 0.92 | 0.85 | 0.76 | 0.82 | 0.92 | 1.00 | 1.16 | 1.22 | 1.31 |
| 44 | 1.30 | 1.08 | 1.07 | 0.92 | 0.83 | 0.74 | 0.81 | 0.91 | 0.99 | 1.17 | 1.23 | 1.33 |
| 46 | 1.32 | 1.10 | 1.07 | 0.91 | 0.82 | 0.72 | 0.79 | 0.90 | 0.99 | 1.17 | 1.25 | 1.35 |
| 48 | 1.34 | 1.11 | 1.08 | 0.90 | 0.80 | 0.70 | 0.76 | 0.89 | 0.99 | 1.18 | 1.27 | 1.37 |
| 50 | 1.37 | 1.12 | 1.08 | 0.89 | 0.77 | 0.67 | 0.74 | 0.88 | 0.99 | 1.19 | 1.29 | 1.41 |

- Adjusted potential evapotranspiration [cm]:

$$PE = \sum PE_i \quad (2-7)$$

- Thornthwaite Moisture Index [dimensionless]:

$$TMI = 75 \left(\frac{P}{PE} - 1 \right) + 10 \quad (2-8)$$

where:

P = annual precipitation [cm]

t_i = mean monthly temperature [°C]

The equation is subjected to the following constraints: if the TMI predicted is greater than 100, TMI is set to 100. Conversely, if the TMI predicted value is less than -55, TMI is set equal to -55.

It should be noted that the TMI is calculated based on the average of one year of climatic data (precipitation and temperature). For the first year of the analysis, the climatic data to be used is the average of the first 12 months. For the subsequent months, the average of the last 12 months is used (floating average).

2.3.3.2 Suction, ψ (psi):

The TMI value predicted above is then used to estimate the suction value at equilibrium conditions. Two models are available: the first model is used to estimate the suction value for base course layers, while the second model is used to estimate suction in any other unbound layer of the pavement system.

If the layer is a base course, then the suction [kPa] is computed as follows:

$$h = \alpha + e^{[\beta + \gamma(TMI + 101)]} \tag{2-9}$$

where:

α, β, γ = constants obtained through a regression process. The values are function of the percent passing the US #200 sieve (P_{200}) if P_{200} is less than 16%. If P_{200} is greater than 16%, then the suction found for P_{200} equal to 16 should be used. The values for these constants are provided in TABLE 2-1 and are dimensionless.

TABLE 2-3 Constants for TMI-P200 Model for Base Coarse-grained Materials

| P_{200} | α | β | γ |
|-----------|----------|---------|----------|
| 0 | 3.649 | 3.338 | -0.05046 |
| 2 | 4.196 | 2.741 | -0.03824 |
| 4 | 5.285 | 3.473 | -0.04004 |
| 6 | 6.877 | 4.402 | -0.03726 |
| 8 | 8.621 | 5.379 | -0.03836 |
| 10 | 12.18 | 6.646 | -0.04688 |
| 12 | 15.59 | 7.599 | -0.04904 |
| 14 | 20.202 | 8.154 | -0.05164 |
| 16 | 23.564 | 8.283 | -0.05218 |

- Constraint: If $P_{200} > 16$, the $P_{200} = 16$ curve is to be used

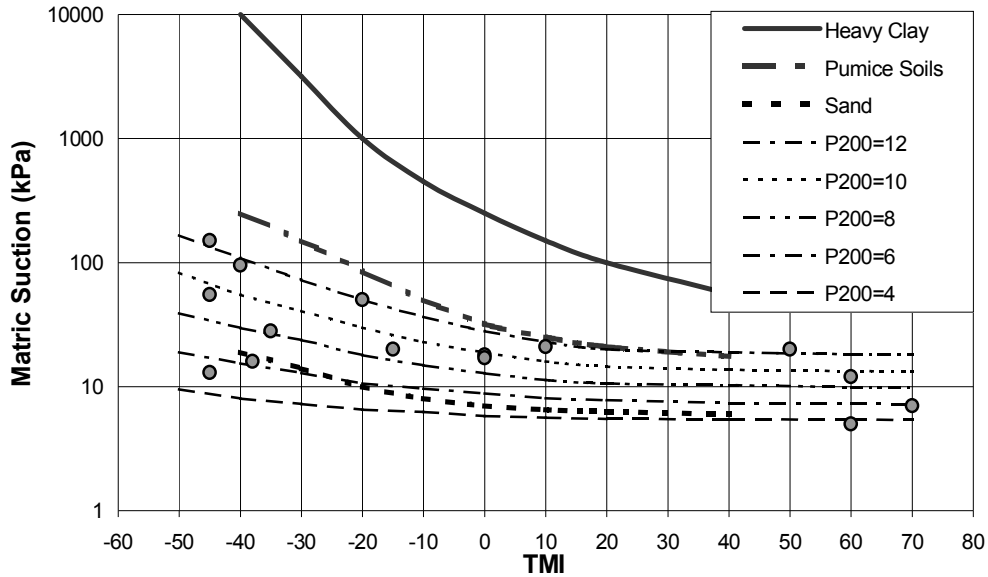


FIGURE 2-1 Curve used for estimated the suction of base material [kPa].

If the layer is not a base course, the suction [kPa] is computed as follows:

$$h = \alpha \left[e^{\left[\frac{\beta}{TMI + \gamma} \right]} + \delta \right] \quad (2-10)$$

where:

α , β , γ , and δ are constants obtained through the regression process as function of P_{200} and wPI ; where wPI is the product of P_{200} (decimal) and the Plasticity Index. Values are provided in TABLE 2-4 [treat as dimensionless]

TABLE 2-4 Regression Constants for TMI- P_{200} / wPI Model for Subbase/Subgrade Materials

| P_{200} | wPI | α | β | γ | δ |
|-----------|-------|----------|----------|----------|----------|
| 10 | | 0.3000 | 419.070 | 133.450 | 15.000 |
| 50 | 0.5 | 0.3000 | 521.500 | 137.300 | 16.000 |
| | 5 | 0.3000 | 663.500 | 142.500 | 17.500 |
| | 10 | 0.3000 | 801.000 | 147.600 | 25.000 |
| | 20 | 0.3000 | 975.000 | 152.500 | 32.000 |
| | 50 | 0.3000 | 1171.200 | 157.500 | 27.800 |

This equation is subjected to the following constraints:

- If $wPI > 50$, the $wPI = 50$ curve is to be used (FIGURE 2-2)
- If $wPI < 0.5$, default to a wPI value of 0.5
- If $wPI = 0$, check P_{200} .
- If P_{200} is $\geq 50\%$, default to the $P_{200} = 50$ curve
- If P_{200} is $< 10\%$, the suction should be calculated using equation [10].

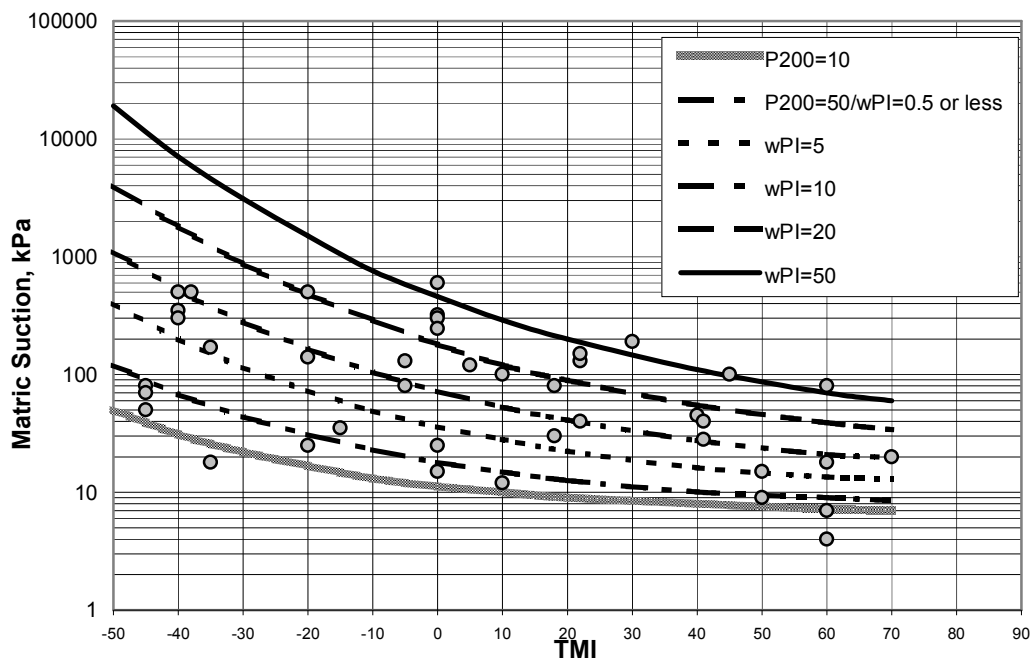


FIGURE 2-2 Curve used for estimated the suction [kPa] at $wPI = 50$.

2.3.3.3 Soil-atmosphere Interaction Predominance over Groundwater Table, GWT

Depth to GWT is a major factor which had been long believed to affect the soil moisture conditions. Russam and Coleman (1961) concluded that soil suctions are in static equilibrium with the water table when the depth to GWT is less than 10 to 15 feet or even 20 to 30 feet (10).

Russam (11) described three categories of design recommendations for predicting subgrade moisture conditions based on subgrade moisture studies.

- i. When the water table is within 20 feet of the surface, the soil suction dependant only on the position of ground water table and overburden pressure.
- ii. When the water table is deeper than 20 feet from the surface and seasonal rainfall exceeds 10 inches, ultimate suction of the subgrade can be estimated from the TMI and soil texture. The Plasticity Index can be used as guide to the soil texture and for a given climate the ratio of ultimate moisture content to plastic limit tends to be constant.
- iii. When the water table is deeper than 20 feet from the surface and the annual rainfall is less than 10 inches the soil suction is controlled by atmospheric humidity.

In the past, the suction was computed using the simple expression $y\gamma_w$. As shown in FIGURE 2-3, the distance from the groundwater table to the point of interest is y , and γ_w is the unit weight of water.

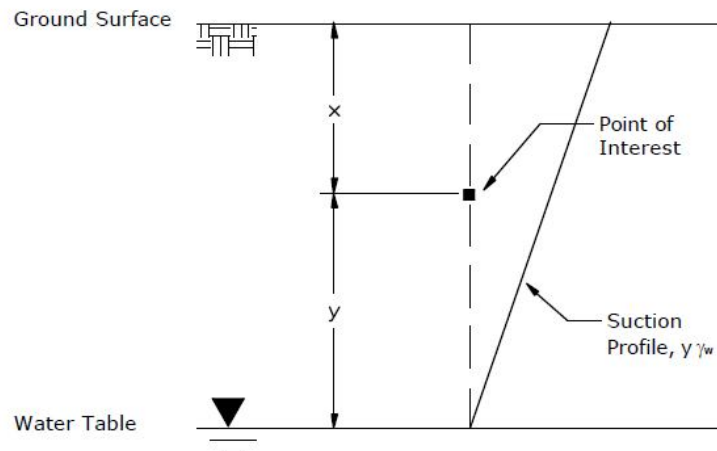


FIGURE 2-3 Suction profile using $y\gamma_w$.

It has been recognized that the estimation of suction based on the groundwater table depth is reasonable as long as the point of interest is relatively close to the GWT. However, the expression shown above yields very high suction values if the GWT is deep because it does not consider changes due to environmental effects. Therefore, relationships like that of Russam and Coleman (R/C), which relates soil suction to TMI are more appropriate in predicting the moisture content of subgrade materials than the negative pore water pressure or suction found by using $\gamma\gamma_w$.

Based on the test results from Perera (12), the suction beneath the pavement was found to be varying not only with the TMI but also with the soil type. The values of P200 and WPI were introduced into the relationship as parameters describing the soil type. The method proposed by the Perera dissertation, TMI-P200/wPI model, was described above in equation [2-10]

2.3.3.3.1 *If GWT is deeper than or at 4 ft from the top of the pavement*

If the GWT is deeper than or at 4 ft from the top of the pavement, the volumetric equilibrium water content will be calculated as follows:

- i. For the granular base, equilibrium suction and its corresponding volumetric water content will be calculated based on the TMI model for the upper nodal point.
- ii. For the second and subsequent layers (subbase, compacted subgrade, etc), the equilibrium suction and its corresponding volumetric water content will be calculated based on the TMI model for the middle point of the layer.
- iii. For the last layer (subgrade), the equilibrium suction and its corresponding volumetric water content will be calculated based on the TMI model for the nodal point located 1 foot below the subgrade.

- iv. Water table depth will dictate the point of zero suction or 100 % saturation.
- v. Go to step 2.3.3.4.

2.3.3.3.2 *If GWT is shallower than 4 ft from the top of the pavement structure, then*

When the groundwater table depth is located within the first 4 feet below the pavement surface, the suction at the top nodal point in the granular base ought to be calculated based on the TMI climatic model or the $P_{200 (w/c)}$ model as shown above. The lower suction boundary will correspond to zero suction at the groundwater table depth.

2.3.3.4 SWCC constants a_f , b_f , c_f , h_r and Degree of Saturation

The suction for the equilibrium condition expected at the design location is then used to predict the degree of saturation of the unbound layer material. The soil-water characteristic curve (SWCC), proposed by Fredlund and Xing (1994), is used in the EICM (13). The Fredlund and Xing model used to estimate the volumetric water content (θ_w) is shown below:

$$\theta_w = C(h) \times \left[\frac{\theta_{sat}}{\left[\ln \left[\exp(1) + \left(\frac{h}{a_f} \right)^{b_f} \right] \right]^{c_f}} \right] \quad [\%] \quad (2-11)$$

where:

$$C(h) = \left[1 - \frac{\ln \left(1 + \frac{h}{h_r} \right)}{\ln \left(1 + \frac{1 \times 10^6}{h_r} \right)} \right] \quad (2-12)$$

θ_{sat} = soil porosity or saturated volumetric water content

a_f , b_f , c_f , h_r are fitting parameters to the equation.

The following models have been proposed to estimate the Fredlund and Xing fitting parameters (14):

Estimate SWCC parameters for plastic materials ($wPI > 0$):

$$a_f = 32.835(\ln wPI) + 32.438 \quad (2-13)$$

$$b_f = 1.421wPI^{-0.3185} \quad (2-14)$$

$$c_f = -0.2154(\ln wPI) + 0.7145 \quad (2-15)$$

$$hr_f = 500 \quad (2-16)$$

These equations are subjected to the following constraints:

- If $a_f < 5$, then $a_f = 5$
- If $c_f < 0.01$, then $c_f = 0.03$

Once the SWCC parameters are determined, the volumetric water content (at the equilibrium conditions) is computed from equations [2-11] and [2-12].

For granular materials ($wPI < 2$), the volumetric water content is found by the following model, which overrides the SWCC model:

$$\theta_w = 4 + 1.5P_{200}^{0.6994} + 0.03TMI \quad (2-17)$$

where:

θ_w = volumetric water content (%)

P_{200} = percent passing #200 US Sieve (%)

TMI = Thornthwaite Moisture Index

This equation is subjected to the following set of constraints:

- If $P_{200} < 2\%$, use $P_{200} = 2\%$; then,
- If $\theta_w > 40$, then $\theta_w = 40 + 0.11(P_{200} - 53)$; then,
- If $\theta_w > \theta_{sat}$, make $\theta_w = \theta_{sat}$

Finally, the degree of saturation is found based on the following equation:

$$\%S = \frac{\theta_w}{\left(1 - \frac{\gamma_{dry}}{G_s * \gamma_{water}}\right)} \quad (2-18)$$

where:

S = the degree of saturation

γ_{water} = unit weight of water

γ_{dry} = dry unit weight

G_s = specific gravity of the solids

2.3.3.5 Degree of Saturation at Optimum Moisture Content Condition, $S_{opt}\%$

The degree of saturation at the optimum moisture condition, S_{opt} , is given by the following mass-volume relationship:

$$S_{opt} = \frac{w_{opt}}{\frac{\gamma_{water}}{\gamma_{d max}} + \frac{1}{G_s}} \quad (2-19)$$

where:

w_{opt} = optimum gravimetric moisture content

2.3.3.6 Environmental Factor, F_{env}

The environmental factor is computed by the equation presented by Cary and Zapata in 2010 (15):

$$F_{env} = 10 \left[\frac{m \times \left((\alpha + \beta \cdot e^{-wPI})^{-1} + \frac{(\delta + \gamma \cdot wPI^{0.5}) - (\alpha + \beta \cdot e^{-wPI})^{-1}}{\ln \left(\frac{-(\delta + \gamma \cdot wPI^{0.5})}{(\alpha + \beta \cdot e^{-wPI})^{-1}} \right) + (\rho + \omega \cdot e^{-wPI})^{0.5} \left(\frac{S - S_{opt}}{100} \right)} \right)}{1 + e} \right] \quad (2-20)$$

where:

$\alpha, \beta, \delta, \gamma, \rho$ and ω are fitting parameters.

$\alpha = -0.600, \beta = -1.87194, \delta = 0.800, \gamma = 0.080, \rho = 11.96518,$ and $\omega = -10.19111.$

It should be noted that equation [2-20] is not used by the EICM but rather is an enhanced equation incorporated in the ZAPMEDACA program.

2.3.3.7 Resilient Modulus, M_R

Finally, the expected resilient modulus at long-term equilibrium is found by multiplying the resilient modulus at optimum conditions (M_{Ropt}) by the environmental factor found from equation [2-20]:

$$M_R = M_{Ropt} \times F_{env} \quad (2-21)$$

2.3.4 Stress and Strain Analysis

The principle of Odemark's method (18) has been incorporated into ZAPMEDACA to transform the multilayer pavement system into an equivalent system where all layers have the same modulus. This allows Boussinesq's equations to be used. After the pavement section has been transformed, numerical integration of the Boussinesq solutions are conducted to rapidly compute the critical response parameters anywhere in the 3 dimensional half space (ie at the desired computational point). This is accomplished by the numerical integration of Boussinesq's equations (2,17) using a wide range of external boundary values dictating the pressure configuration and / or external load shape for the design vehicle (aircraft) in question.

2.3.4.1 ZAPMEDACA Pavement Response Solution Sequence

The method used in the program to calculate the stresses and strains in any pavement system is the method of equivalent thicknesses MET for short. This method is also known as Odemark's method (2). The basic idea of this method is to transform a system consisting of layers with different moduli into an equivalent system where all layers have the same modulus, and on which Boussinesq's equations will be utilized.

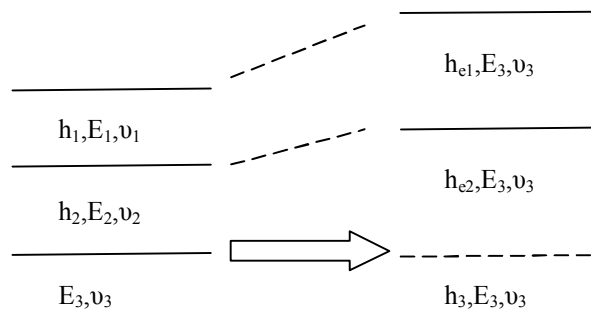


FIGURE 2-4 Transformations used in Odemark's method.

For a multi layer system, the equivalent thickness of the upper n-1 layers with respect to the modulus of layer n may be calculated as:

$$h_{ei} = f * \sum_{i=1}^{n-1} \left\{ h_i * [E_i / E_n]^{1/3} \right\} \quad (2-22)$$

Where:

h_{ei} = equivalent thickness for layer i, in

f = correction factor (assumed to be equal to one in ZAPMEDACA but changed in ZAPRAM to allow more accurate estimation of the pavement response variable)

h_i = actual thickness for layer i, in

E_i = modulus of layer i, psi

E_n = modulus of the lowest layer, psi

Boussinesq formulated a set of equations for calculating the stresses, strains and deflections of a homogenous, isotropic, and linear elastic semi-infinite mass due to a vertical point load applied at the ground surface (FIGURE 2-5).

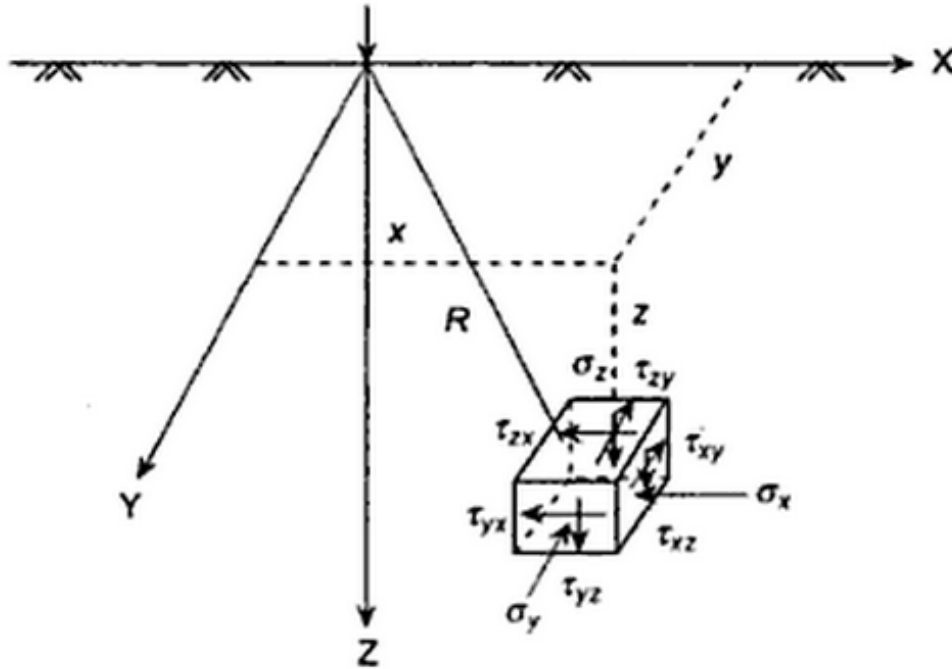


FIGURE 2-5 Stress in the soil due to point load at surface (rectangular coordinates).

Boussinesq obtained the expressions for stresses at a point (x, y, z) located at a distance, R from the origin of coordinates which is also the point of application of the vertical load, P . the stress components in Cartesian coordinates are given as:

- Normal stress in the z direction, σ_z :

$$\sigma_z = \frac{3P}{2\pi} \frac{z^3}{R^5} \quad (2-23)$$

- Normal stress in the x direction, σ_x :

$$\sigma_x = \frac{3P}{2\pi} \left[\frac{x^2 z}{R^5} - \frac{1-2\nu}{3} \left\{ -\frac{1}{R(R+z)} + \frac{(2R+z)x^2}{(R+z)^2 R^3} + \frac{z}{R^3} \right\} \right] \quad (2-24)$$

- Normal stress in the y direction, σ_y :

$$\sigma_y = \frac{3P}{2\pi} \left[\frac{y^2 z}{R^5} - \frac{1-2\nu}{3} \left\{ -\frac{1}{R(R+z)} + \frac{(2R+z)y^2}{(R+z)^2 R^3} + \frac{z}{R^3} \right\} \right] \quad (2-25)$$

- Shear stress in the xz plane, τ_{xz} :

$$\tau_{yz} = \frac{3P}{2\pi} \frac{yz^2}{R^5} \quad (2-26)$$

- Shear stress in the yz plane, τ_{yz} :

$$\tau_{xz} = \frac{3P}{2\pi} \frac{xz^2}{R^5} \quad (2-27)$$

- Shear stress in the xy plane, τ_{xy} :

$$\tau_{xy} = \frac{3P}{2\pi} \left[\frac{xyz}{R^5} - \frac{1-2\nu}{3} \left\{ \frac{(2R+z)xy}{(R+z)^2 R^3} \right\} \right] \quad (2-28)$$

- Strain in the x direction, ε_x :

$$\varepsilon_x = \frac{1}{E} (\sigma_x - \nu(\sigma_y + \sigma_z)) \quad (2-29)$$

- Strain in the y direction, ε_y :

$$\varepsilon_y = \frac{1}{E} (\sigma_y - \nu(\sigma_x + \sigma_z)) \quad (2-30)$$

- Strain in the z direction, ε_z :

$$\varepsilon_z = \frac{1}{E} (\sigma_z - \nu(\sigma_x + \sigma_y)) \quad (2-31)$$

where:

$$R = \sqrt{x^2 + y^2 + z^2}$$

ν = Poisson's ratio of the soil

A special adaptation/modification found in ZAPMEDACA is the ability to introduce the Frohlich Stress concentration to the computation factor (n_f) of the Boussinesq vertical stress. If a Frohlich number, n_f , is introduced, the following equation for vertical stress is given by:

$$\sigma_z = \frac{n_f P}{2\pi} \frac{\left(\frac{z}{R}\right)^{n_f}}{R^2} \quad (2-32)$$

where:

$$n_f = 2 \left[\frac{CBR}{6} \right]^{0.337}$$

This modification has been developed from recent research conducted by the USACE (24).

Finally, it should be recognized that the majority of vehicle (aircraft) gears are multi-tire gear configuration. Because of the assumption of linear elasticity, the direct utilization of stress superposition is utilized to combine the stress/strain values for each separate tire analysis. Obviously this additive process of stress/strain and displacement can only be correctly accomplished when Cartesian coordinate systems are utilized. This is the system used in both ZAPMEDACA and ZAPRAM.

CHAPTER 3 ENHANCEMENT OF ZAPMEDACA SOFTWARE

3.1 ZAPRAM Software

ZAPRAM, which stands for Zapata and Ramadan, is the second generation of ZAPMEDACA, a computer code created by graduate students at Arizona State University. This program was developed to primarily analyze the shear deformation performance of airfield flexible pavements. The user has a selection from a variety of mechanistic performance criteria inherent in the program. In addition, the program has an available aircraft library that includes information on the tire-gear properties for a wide range of aircraft types. Each aircraft shown within the library has the specific tire weights, pressure and geometric spacing of the specific multiple tire gear arrangement for the particular aircraft in question.

Another primary feature of ZAPRAM is that it contains the environmental effects models of ZAPMEDACA, previously described, that allow the analysis of the effect of the environmental region and the in-situ groundwater table characteristics at the design site to be incorporated within the pavement damage predictions. The program has an integrated library of cities which the user may select from, and contain all of the key environmental characteristics for the design location. The program will then output the latitude, longitude, and the monthly Thornthwaite Moisture Index (TMI) value for the selected city. For the Pavement Structural model, the program has the ability to have the user input a variable layer correction factor for the transformed thickness analysis. Guidance for the correction factor is contained in future sections of the thesis.

3.2 ZAPRAM Software Modules

The design inputs in ZAPRAM are the four main categories that were already mentioned in chapter 2: load configuration, pavement structure and material properties, and environmental affects. The ZAPRAM program has developed enhancements in each module to simplify the design inputs. Also, a new traffic module has been created to be one of the design inputs in program. This program was primarily developed to develop airfield pavement structural designs that are intended to guard against excessive shear deformation performance.

One of the major analysis and outputs of the program are the calculated vertical stress and strains at any given depth in the pavement system. In addition, the program determines the unit damage (per pass) and total damage on the pavement structure as a function of the predicted traffic level expected for the design aircraft. The final stage of the computational process is to determine the Annual Traffic (Passes), Annual Max Damage (%), Cumulative Traffic (Pass), Cumulative Max Damage (%), and lateral pavement Interval where the Maximum Damage is anticipated to occur. The following paragraph provides a description regarding the inputs, outputs and the most important enhancement for the modules that have been incorporated into ZAPRAM.

3.2.1 Improvement of Load Configuration

3.2.1.1 Library of Aircraft Icon

This library is located in the load configuration model. The user can utilize the Aircraft Library by clicking on the Select Aircraft Icon. This user-form has a huge library for numerous commercial aircraft. The user should utilize this icon when he or she chooses an Aircraft design type and needs to input data about specific aircraft. By clicking the

icon, the “Aircraft Company/Model” User-form will appear. TABLE 3-1 provides a listing of all the specific aircraft types that contain in the library.

TABLE 3-1 Listing of all the Specific Aircraft Types that Include d in the Library

| Dual (Tires) | | Dual Tandem | BOEING 747 family | Airbus 380 family | Galaxy |
|-------------------|-------------------|-------------|-------------------|-------------------|--------|
| BOEING 737 family | McDONNELL-DOUGLAS | | | | |
| B737-600 | MD-83 DC-9-51 | A300-C4 | B747-400 | A-380 | C-5A |
| B737-700 | MD-82 DC-9-41 | A300-B4 | B747-200 | A-380F | |
| B737-700C | MD-81 DC-9-32 | A310-300 | B747-200/300 | | |
| B737-800 | MD-87 DC-9-21 | A300-B2 | B747-100B/300 | | |
| B737-900ER | | DC-9-15 | A310-200 | B747-SP | |
| B747-100B/300SR | | | | | |

The most powerful aspect of this library is that all the critical gear properties of the selected aircraft are already incorporated into the program. As noted, the first step is to select an aircraft type from the current library of aircraft already embedded in the program. Once the aircraft is selected, the program automatically selects (for future input and analysis) the required number of tires, load per tire, tire pressure, number of main gear for each side of the aircraft, distance from x-axis to centerline of the main gear, and the gear tire spacing.

3.2.1.2 Aircraft Tire Location Icon

This Icon is located at the top middle of the load configuration model. The purpose of this icon is to show the user the specific plan view location for the specified aircraft main gear and tire location. By clicking this button, the program will automatically draw The Tires location graph. The figure is well organized and will give an idea for the user before the next model will be selected.

3.2.1.3 Time and Space Evaluation Study

This research task and findings of this study are explained in more detail within Chapter Four. The study focused mainly on the evaluation of resolution of vertical stresses, strain calculation and time in which the program should carry out the analysis in the minimum computational time but yet still achieve accurate predictions with currently used multi-layered elastic solutions. The purpose of the study was to identify the optimal number of runs in which the user would utilize the program. Furthermore, the investigation also identified the best condition and specification for elliptical tire imprint shape (number of longitudinal segments (dy) in tire imprint, number of transversal segments (dx) in tire imprint, number of radial segments (dr) in tire imprint, and size of angular segments ($d\theta$) in tire imprint). In addition, the study also demonstrated the same for circular tire imprint shape number of radial segments (dr) in tire imprint and the size of angular segments ($d\theta$) in tire imprint). As a result, definite recommendations regarding the suggested combination of differential areas (dA) used in the numerical integration scheme are provided in this chapter. This will assist the user to estimate the computational time for best results of stress and strain calculation.

3.2.2 Pavement Structure Enhancement

3.2.2.1 Equivalent Thickness Correction Factor Icon

This research task is explained in detail within Chapter Four. The method used in the program to calculate the stresses and strains in any pavement system is the method of equivalent thicknesses MET (18). This method is also known as Odemark's Transformed Section Analysis. The idea of this method is to transform a system consisting of layers with different moduli into an equivalent system where all layers have the same modulus, and on which Boussinesq's equations will be utilized. For a multi layer system, the

equivalent thickness of the upper $n-1$ layers with respect to the modulus of layer n may be calculated as was mentioned in equation [2-22].

The correction factor, f , was found to depend on layer thickness, the modular ratios, Poisson's ratios and the number of layers in the structure. A comprehensive study has been done with different loads, subgrade soils, and layer thickness, to evaluate the most accurate correction factor. The concept of the study was to compare the vertical stress and vertical strain results from the ZAPMEDACA (ZAPRAM) approach based upon multi-layer theory. After completing this study, it was concluded that the general results from ZAPMEDACA provided higher stresses and strains than those estimated by JULEA. By using a significant database, the percentage difference between the ZAPMEDACA one layer system and the JULEA three layer system was evaluated. The correction factor which was assumed to be 1 in the original ZAPMEDACA program, had to be changed to " f " instead of the original value of " $f=1.0$ ". The appropriate value for the correction factor has been recommended and is discussed in this section.

As a result of this study, a correction factor of 0.95 for the asphalt layer and a correction factor of 0.80 for all unbound layers were suggested. The correction factor icon is present within the Pavement Structure Model and located at the end of the input area. By clicking on this button, the program will automatically produce the correction factors for transformed system with the default value. The user has the ability to override these default values.

3.2.3 *Traffic Analysis Module:*

The interface to model traffic in ZAPMEDACA was combined between highway and airfield vehicle input requirements. The goal was to create a new module with a completely different programming code to make it easier for the user to interact with the

program. This module has two different menus; depending on which one the user selects for the analysis from the main menu. There are two lists of options that the user must deal with. If the user selects Type A analysis from the main menu, he or she will deal with the highway approach. On the other hand, if the user selects Types B or C of analysis from the main menu, he or she will work with the airfield pavement approach.

3.2.3.1 Input Variables for Traffic Analysis Module Selected Type A

The following are the required input parameters in the traffic analysis module if a flexible highway cross section is selected for the analysis:

- 1- ESAL_o at the Beginning of the Design Life
- 2- Annual Average Daily Traffic, AADT
- 3- Total Number of Lanes
- 4- Number of Lanes per Direction
- 5- Design Lane
- 6- Directional Distribution Factor, D_e
- 7- Lane Distribution Factor, L
- 8- Percentage of Trucks in the AADT, p_t
- 9- Truck Factor, T_f
- 10- Passes of Vehicle at End of Design Life, P_{jt}

3.2.3.2 Input Variables for Traffic Analysis Module Selected Type B and C

The main inputs for the traffic module are the number of passes during the base (initial) year, design life, and expected traffic growth rate. An aircraft traffic lateral wander standard deviation is then input and the critical design repetition are calculated across the pavement feature (taxiway or runway). The output result from the traffic analysis module

is the number of passes at end of the Design Life (P_{jt}). The program accordingly calculates the number of passes at the end of the design life. This value (P_{jt}) is calculated as follows:

$$P_{jt} = P_{j_o} * \frac{(1 + r_g)^{n-1}}{\ln\left(1 + \frac{r_g}{100}\right)} \quad (3-1)$$

where

P_{j_o} = Passes of Vehicle at Base Year, “0”

P_{jt} = Passes of Vehicle at End of Design Life

n = Design Life (yr)

r_g = Traffic Growth Rate (%)

3.2.4 *Environmental Effects Module Improvement*

In the ZAPMEDACA version, the user inputs monthly temperature and precipitation data from historic records in order to allow the program to calculate the monthly Thornthwaite Moisture Index (TMI) value. In the ZAPRAM version, the user has the ability either to select a certain design location (city) from the integrated library that currently includes 13 different cities in the United States. This library of environmental sites is continuously upgraded. TMI value is used in this module to account for the environmental effects on the resilient modulus for the unbound layers on a monthly basis. This program is considered very unique, compared to others available in the literature that deal with environmental changes on a seasonal basis. In addition, TMI values are utilized in the program to estimate other vital environmental parameters including suction, soil water characteristic curve parameters, and the degree of saturation. These parameters are then employed to calculate the environmental factor (F_{env}) for unbound materials (15, 19). This leads to the real time environmental effects to estimate the real time resilient

modulus response of any unbound material, above or below, the GWT (Ground Water Table).

3.2.4.1 *Select City Icon*

This Icon is located at the top middle of the environmental effects module. The objective of this icon is to have available some geographic and environmental stored information for the selected city listed in the city library. The library saves the time to calculate the environmental factors that were computed by the previous code (ZAZMEDACA). By clicking on this icon, the user will be led to a list of cities to choose from. The program contains a library of cities which the user has the ability to directly select a certain city from the integrated library. The library currently includes 13 different cities in the United States along with their longitudes, latitudes and the average TMI values for the cities (TABLE 3-2).

TABLE 3-2 The Currently Available Cities that are Included in the City Library

| Location | Longitude (decimal) | Latitude (decimal) | TMI |
|----------------|------------------------|-----------------------|--------|
| Athens-GA | -83.20 | 33.57 | 32.60 |
| Cleveland-OH | -81.51 | 41.24 | 41.65 |
| Dallas-TX | -97.02 | 32.54 | -1.89 |
| Los Angeles-CA | -118.25 | 33.56 | -31.62 |
| McAlester-OK | -95.54 | 34.54 | 2.51 |
| Miami-FL | -80.19 | 25.49 | 17.32 |
| Orlando-FL | -81.19 | 28.26 | 18.63 |
| Phoenix-AZ | -112.07 | 33.45 | -54.95 |
| Portland-ME | -70.18 | 43.38 | 59.31 |
| Raleigh-NC | -78.47 | 35.52 | 37.52 |
| Salem-OR | -123.00 | 44.55 | 50.84 |
| Seattle-WA | -122.19 | 47.28 | 40.57 |
| Shreveport-LA | -93.49 | 32.27 | 31.84 |

3.2.5 Stress and Strain Analysis Improvement

3.2.5.1 Analysis of Response Computational Points and Tire Locations by Aircraft

In the original ZAPMEDACA version, the user needed to input each desired computation point (Cartesian coordinate) in order to allow the program to calculate the stresses and strains value. In this version, a significant enhancement has been made. The user now has the ability either to input these values or to select a certain design load (aircraft) from the integrated library that currently includes 28 different airplanes. This library has already been noted to exist in the load configuration model. The user can reach it by clicking on the Select Aircraft Icon.

The X and Y coordinates of the recommended computational points are automatically selected for the user if a specific aircraft is selected from the library. The maximum number of the X and Y computational points of interest (for the most complex aircraft gear arrangement B-747 A-380) is 88 points. These points are the default computational value for every aircraft assembly type. The following Tables and Figures illustrate the x-y default computational values for each gear Arrangement.

TABLE 3-3 Input Type Gear Arrangement

| Type Gear Arrangement | User Inputs | Point of interest | Notes |
|--------------------------|--|----------------------|--------------|
| General Type of Aircraft | | | |
| Single | X_{j1}, Y_{j1} | $6x \times 2y = 12$ | |
| Dual (Tires) | X_{j1}, Y_{j1}, S_{d1} | $6x \times 2y = 12$ | |
| Single Tandem | X_{j1}, Y_{j1}, S_{t1} | $6x \times 3y = 18$ | |
| Dual Tandem | $X_{j1}, Y_{j1}, S_{d1}, S_{t1}$ | $6x \times 3y = 18$ | |
| Tri- Tandem | $X_{j1}, Y_{j1}, S_{d1}, S_{t1}$ | $6x \times 4y = 24$ | |
| Some Specific Aircraft | | | |
| C5A | $X_{j1}, Y_{j1}, X_{j2}, Y_{j2}, S_{d1}, S_{d2}, S_{d4}, S_{t1}, S_{t2}$ | $7x \times 7y = 49$ | 1Pass=2 Rep. |
| B52 | $X_{j1}, Y_{j1}, S_{d1}, S_{t1}$ | $7x \times 3y = 21$ | 1Pass=2 Rep. |
| A-380 | $X_{j1}, Y_{j1}, X_{j2}, Y_{j2}, S_{d1}, S_{t1}, S_{d2}, S_{t2}$ | $11x \times 8y = 88$ | |
| B-747 | $X_{j1}, Y_{j1}, X_{j2}, Y_{j2}, S_{d1}, S_{t1}, S_{d2}, S_{t2}$ | $11x \times 8y = 88$ | |

3.2.5.1.1 Single Tire

For aircraft having a single tire main gear the number of computational points is set at 12. These 12 points are divided into two lines, 6 for each. The coordinates for the 12 points are listed in TABLE 3-4.

TABLE 3-4 The Coordinate of Point of Interest for Single Tire Aircraft

| | | | | | | |
|---|--------------------|--------------------|--------------------|--------------------|--------------------|--------------------|
| X | 0 | $0.2x_{j1}$ | $0.4x_{j1}$ | $0.6x_{j1}$ | $0.8x_{j1}$ | x_{j1} |
| Y | Y_{j1} | Y_{j1} | Y_{j1} | Y_{j1} | Y_{j1} | Y_{j1} |
| X | 0 | $0.2x_{j1}$ | $0.4x_{j1}$ | $0.6x_{j1}$ | $0.8x_{j1}$ | x_{j1} |
| Y | $Y_{j1}-0.2X_{j2}$ | $Y_{j1}-0.2X_{j2}$ | $Y_{j1}-0.2X_{j2}$ | $Y_{j1}-0.2X_{j2}$ | $Y_{j1}-0.2X_{j2}$ | $Y_{j1}-0.2X_{j2}$ |

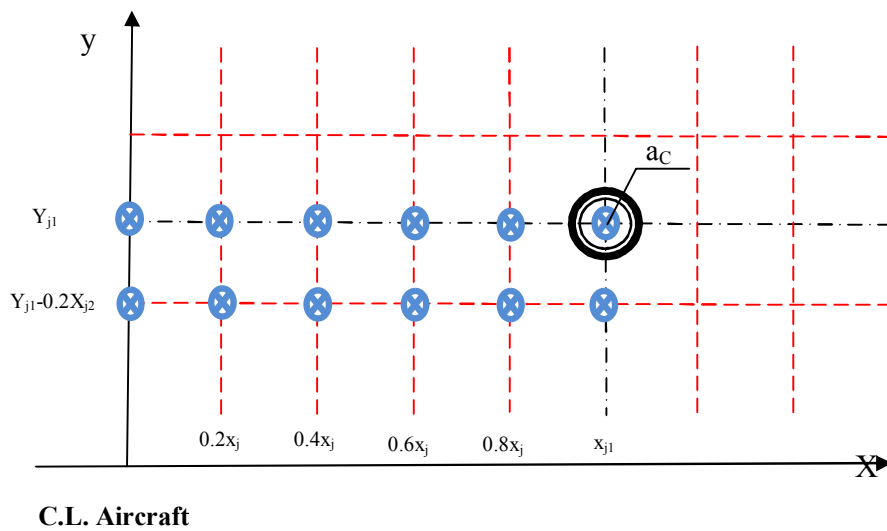


FIGURE 3-1 Type gear single tire.

3.2.5.1.2 Dual Tire

FIGURE 3-2, illustrates the computational points used in ZAPRAM. A total of 12 computational points are shown and their x-y coordinates are found in TABLE 3-5.

TABLE 3-5 The Coordinate of Point of Interest for Dual Tire Aircraft

| | | | | | | |
|---|-----------|-----------|-----------|-----------|------------|-----------|
| X | 0 | 0.2xj1 | 0.4xj1 | 0.6xj1 | xj1- Sd1/2 | xj1 |
| Y | Yj1 | Yj1 | Yj1 | Yj1 | Yj1 | Yj1 |
| X | 0 | 0.2xj1 | 0.4xj1 | 0.6xj1 | xj1- Sd1/2 | xj1 |
| Y | Yj1- 2 ac | Yj1- 2 ac | Yj1- 2 ac | Yj1- 2 ac | Yj1- 2 ac | Yj1- 2 ac |

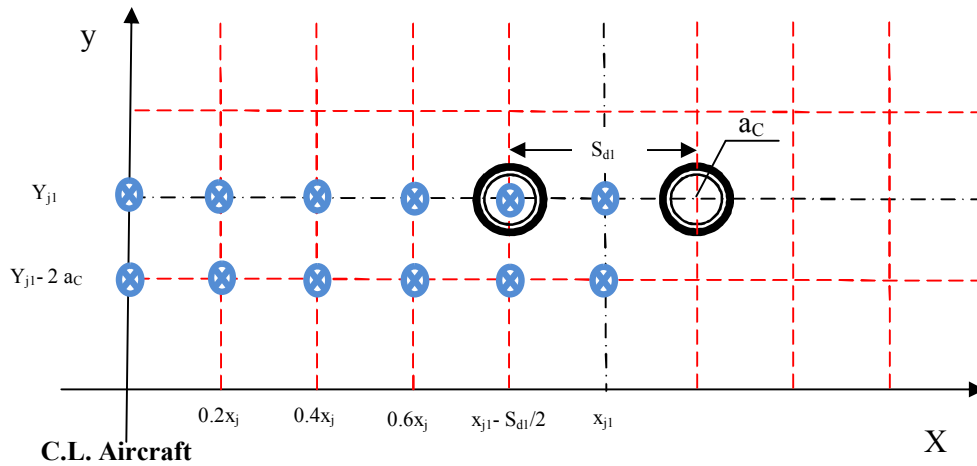


FIGURE 3-2 Type gear dual tire.

3.2.5.1.3 Single Tandem C-130

The main gear for the C-130 (Hercules) aircraft has 2 tires in tandem (one behind the other). The number of computational points will be 18. These 18 points are divided into three lines, with 6 for each line. The coordinates for the 18 points are listed in TABLE 3-6.

TABLE 3-6 The Coordinate of Point of Interest for Single Tandem Aircraft

| | | | | | | |
|---|------------|------------|------------|------------|------------|------------|
| X | 0 | 0.2xj1 | 0.4xj1 | 0.6xj1 | 0.8xj1 | xj1 |
| Y | Yj1 | Yj1 | Yj1 | Yj1 | Yj1 | Yj1 |
| X | 0 | 0.2xj1 | 0.4xj1 | 0.6xj1 | 0.8xj1 | xj1 |
| Y | Yj1- St1/2 | Yj1- St1/2 | Yj1- St1/2 | Yj1- St1/2 | Yj1- St1/2 | Yj1- St1/2 |
| X | 0 | 0.2xj1 | 0.4xj1 | 0.6xj1 | 0.8xj1 | xj1 |
| Y | Yj1- St1 | Yj1- St1 | Yj1- St1 | Yj1- St1 | Yj1- St1 | Yj1- St1 |

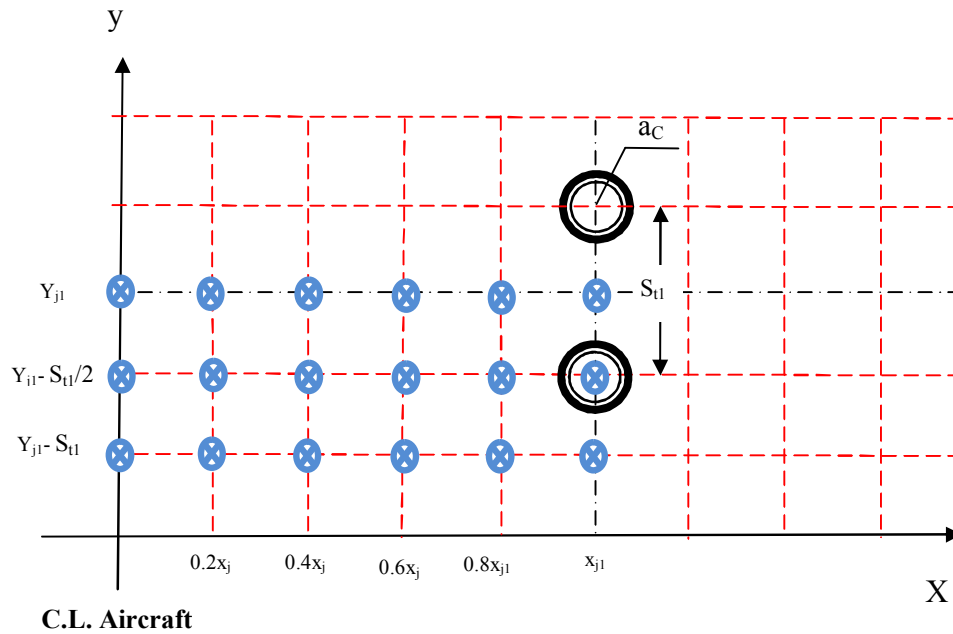


FIGURE 3-3 Type gear single tandem.

3.2.5.1.4 Dual Tandem

The main gear of this kind of aircraft has four tires. This main gear configuration is the typical gear found for many medium to heavy aircraft. FIGURE 3-4 illustrates the arrangement of the dual tandem gear and the computational points. There are 18 locations and the x-y coordinates of these points are shown in TABLE 3-7.

TABLE 3-7 The Coordinate of Point of Interest for Dual Tandem Aircraft

| | | | | | | |
|---|--------------------------------------|--------------------------------------|--------------------------------------|--------------------------------------|--------------------------------------|--------------------------------------|
| X | 0 | 0.2x _{j1} | 0.4x _{j1} | 0.6x _{j1} | x _{j1} - S _{d1} /2 | x _{j1} |
| Y | Y _{j1} | Y _{j1} | Y _{j1} | Y _{j1} | Y _{j1} | Y _{j1} |
| X | 0 | 0.2x _{j1} | 0.4x _{j1} | 0.6x _{j1} | x _{j1} - S _{d1} /2 | x _{j1} |
| Y | Y _{j1} - S _{t1} /4 | Y _{j1} - S _{t1} /4 | Y _{j1} - S _{t1} /4 | Y _{j1} - S _{t1} /4 | Y _{j1} - S _{t1} /4 | Y _{j1} - S _{t1} /4 |
| X | 0 | 0.2x _{j1} | 0.4x _{j1} | 0.6x _{j1} | x _{j1} - S _{d1} /2 | x _{j1} |
| Y | Y _{j1} - S _{t1} /2 | Y _{j1} - S _{t1} /2 | Y _{j1} - S _{t1} /2 | Y _{j1} - S _{t1} /2 | Y _{j1} - S _{t1} /2 | Y _{j1} - S _{t1} /2 |

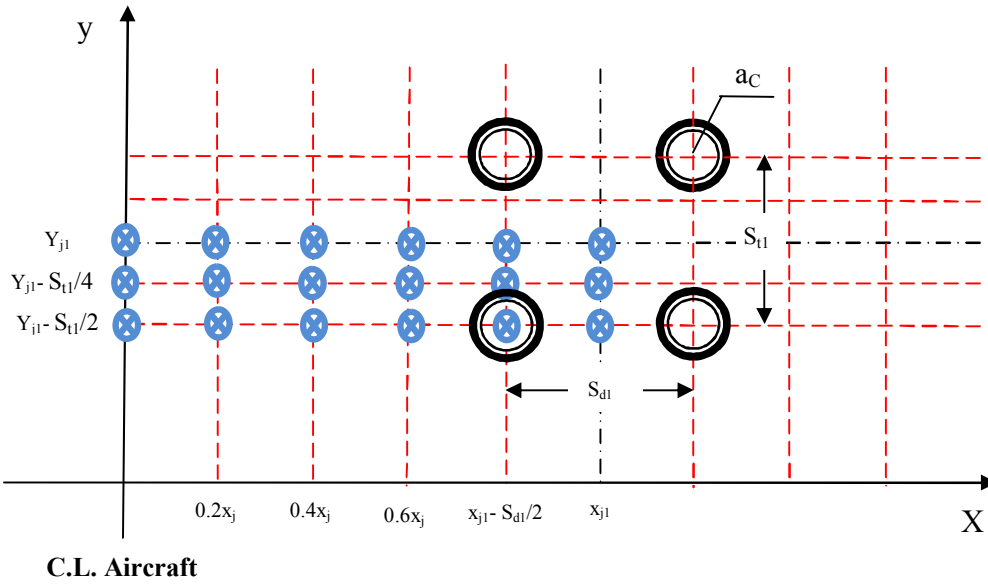


FIGURE 3-4 Type gear dual tandem.

3.2.5.1.5 Tri- Tandem B-777

The B-777 is an aircraft having a Tri-Tandem main gear. The number of computational points is 24. These 24 points are separated into four lines of 6 points per line. The coordinates for the 24 points listed are shown in TABLE 3-8.

TABLE 3-8 The Coordinate of Point of Interest for Tri-Tandem Aircraft

| | | | | | | |
|---|--------------|--------------|---------------|---------------|---------------|---------------|
| X | 0 | 0.2xj1 | 0.4xj1 | 0.6xj1 | 0.8xj1 | xj1 |
| Y | Yj1 | Yj1 | Yj1 | Yj1 | Yj1 | Yj1 |
| X | 0 | 0.2xj1 | 0.4xj1 | 0.6xj1 | 0.8xj1 | xj1 |
| Y | Yj1- St1/2 | Yj1- St1/2 | Yj1- St1/2 | Yj1- St1/2 | Yj1- St1/2 | Yj1- St1/2 |
| X | 0 | 0.2xj1 | 0.4xj1 | 0.6xj1 | 0.8xj1 | xj1 |
| Y | Yj1- St1 | Yj1- St1 | Yj1- St1 | Yj1- St1 | Yj1- St1 | Yj1- St1 |
| X | 0 | 0.2xj1 | 0.4xj1 | 0.6xj1 | 0.8xj1 | xj1 |
| Y | Yj1- 3*St1/2 | Yj1-3* St1/2 | Yj1- 3* St1/2 | Yj1- 3* St1/2 | Yj1- 3* St1/2 | Yj1- 3* St1/2 |

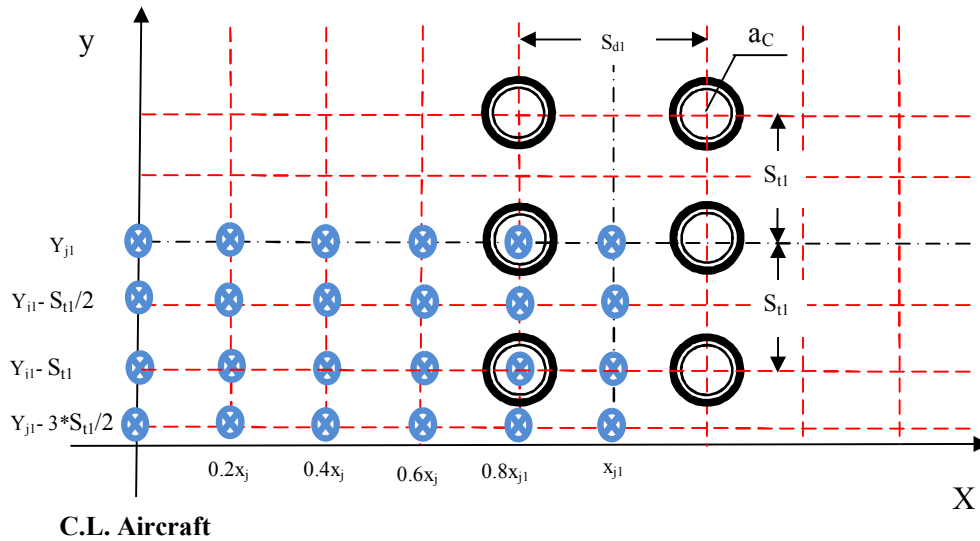


FIGURE 3-5 Type gear tri- tandem.

3.2.5.1.6 C5A Aircraft

The main gear of the C5A aircraft has two sets of 6 tires. It is shown in FIGURE 3-6. The required number of computational points are 49. TABLE 3-9 illustrates the specific location of each point. As a general rule, the damage to the pavement is generally due to that caused by one of the main gears (especially near the upper portions of the pavement structures). As a consequence, it is assumed that one pass of the C5A causes two unique stress/strain repetitions for the damage analysis (See TABLE 3-3).

TABLE 3-9 The Coordinate of Point of Interest for C5A Aircraft

| | | | | | | | |
|---|-------------------------------------|-------------------------------------|-------------------------------------|-------------------------------------|-------------------------------------|-------------------------------------|-------------------------------------|
| X | 0 | 0.2xj1 | 0.4xj1 | $xj_1 - \frac{Sd2}{2} - Sd_1$ | $xj_1 - \frac{Sd2}{2}$ | $xj_1 - \frac{Sd4}{2}$ | xj1 |
| Y | $Yj_1 + 2S_{t1} + S_{t2}$ | $Yj_1 + 2S_{t1} + S_{t2}$ | $Yj_1 + 2S_{t1} + S_{t2}$ | $Yj_1 + 2S_{t1} + S_{t2}$ | $Yj_1 + 2S_{t1} + S_{t2}$ | $Yj_1 + 2S_{t1} + S_{t2}$ | $Yj_1 + 2S_{t1} + S_{t2}$ |
| X | 0 | 0.2xj1 | 0.4xj1 | $xj_1 - \frac{Sd2}{2} - Sd_1$ | $xj_1 - \frac{Sd2}{2}$ | $xj_1 - \frac{Sd4}{2}$ | xj1 |
| Y | $Yj_1 + \frac{3S_{t1}}{2} + S_{t2}$ | $Yj_1 + \frac{3S_{t1}}{2} + S_{t2}$ | $Yj_1 + \frac{3S_{t1}}{2} + S_{t2}$ | $Yj_1 + \frac{3S_{t1}}{2} + S_{t2}$ | $Yj_1 + \frac{3S_{t1}}{2} + S_{t2}$ | $Yj_1 + \frac{3S_{t1}}{2} + S_{t2}$ | $Yj_1 + \frac{3S_{t1}}{2} + S_{t2}$ |
| X | 0 | 0.2xj1 | 0.4xj1 | $xj_1 - \frac{Sd2}{2} - Sd_1$ | $xj_1 - \frac{Sd2}{2}$ | $xj_1 - \frac{Sd4}{2}$ | xj1 |
| Y | $Yj_1 + S_{t1} + S_{t2}$ | $Yj_1 + S_{t1} + S_{t2}$ | $Yj_1 + S_{t1} + S_{t2}$ | $Yj_1 + S_{t1} + S_{t2}$ | $Yj_1 + S_{t1} + S_{t2}$ | $Yj_1 + S_{t1} + S_{t2}$ | $Yj_1 + S_{t1} + S_{t2}$ |
| X | 0 | 0.2xj1 | 0.4xj1 | $xj_1 - \frac{Sd2}{2} - Sd_1$ | $xj_1 - \frac{Sd2}{2}$ | $xj_1 - \frac{Sd4}{2}$ | xj1 |
| Y | $Yj_1 + S_{t1} + \frac{S_{t2}}{2}$ | $Yj_1 + S_{t1} + \frac{S_{t2}}{2}$ | $Yj_1 + S_{t1} + \frac{S_{t2}}{2}$ | $Yj_1 + S_{t1} + \frac{S_{t2}}{2}$ | $Yj_1 + S_{t1} + \frac{S_{t2}}{2}$ | $Yj_1 + S_{t1} + \frac{S_{t2}}{2}$ | $Yj_1 + S_{t1} + \frac{S_{t2}}{2}$ |
| X | 0 | 0.2xj1 | 0.4xj1 | $xj_1 - \frac{Sd2}{2} - Sd_1$ | $xj_1 - \frac{Sd2}{2}$ | $xj_1 - \frac{Sd4}{2}$ | xj1 |
| Y | $Yj_1 + S_{t1}$ | $Yj_1 + S_{t1}$ | $Yj_1 + S_{t1}$ | $Yj_1 + S_{t1}$ | $Yj_1 + S_{t1}$ | $Yj_1 + S_{t1}$ | $Yj_1 + S_{t1}$ |
| X | 0 | 0.2xj1 | 0.4xj1 | $xj_1 - \frac{Sd2}{2} - Sd_1$ | $xj_1 - \frac{Sd2}{2}$ | $xj_1 - \frac{Sd4}{2}$ | xj1 |
| Y | $Yj_1 + \frac{S_{t1}}{2}$ | $Yj_1 + \frac{S_{t1}}{2}$ | $Yj_1 + \frac{S_{t1}}{2}$ | $Yj_1 + \frac{S_{t1}}{2}$ | $Yj_1 + \frac{S_{t1}}{2}$ | $Yj_1 + \frac{S_{t1}}{2}$ | $Yj_1 + \frac{S_{t1}}{2}$ |
| X | 0 | 0.2xj1 | 0.4xj1 | $xj_1 - \frac{Sd2}{2} - Sd_1$ | $xj_1 - \frac{Sd2}{2}$ | $xj_1 - \frac{Sd4}{2}$ | xj1 |
| Y | Yj_1 | Yj_1 | Yj_1 | Yj_1 | Yj_1 | Yj_1 | Yj_1 |

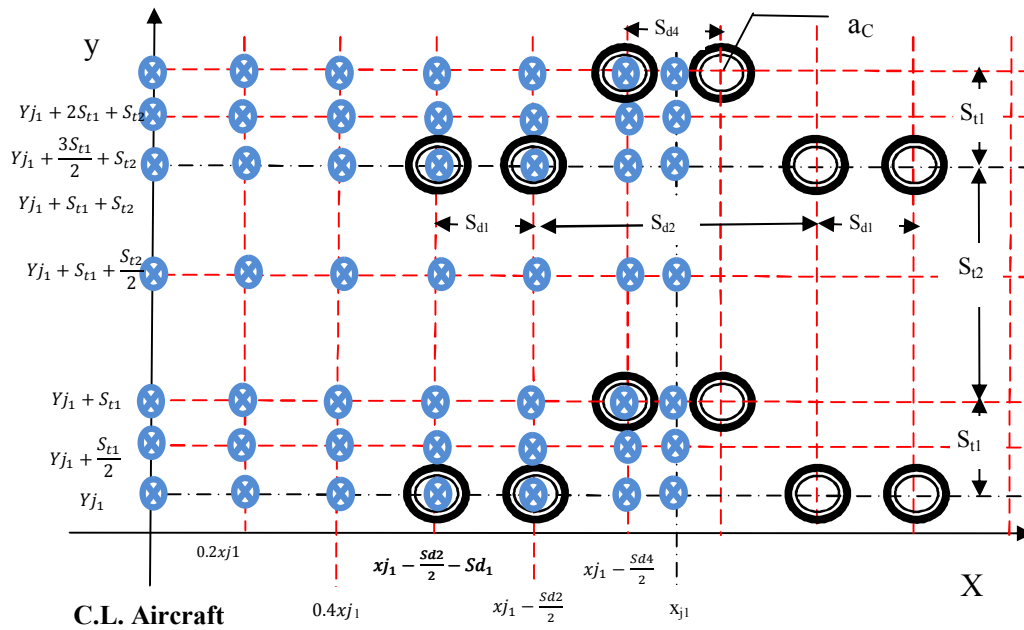


FIGURE 3-6 Type gear for C5A.

3.2.5.1.7 Twin-Twin B-52 Aircraft

The B-52 aircraft has four tires (twin-twin) for each main gear. As shown in the Figure 3-7, the distance between tires is S_{d1} , S_{t1} , and S_{d1} . TABLE 3-10 illustrates the location of the 18 computational points. It should be noted that the main gears are centered under the centerline of the aircraft fuselage. Because of this; it is assumed that one pass of a B-52 causes two stress/strain repetitions (See TABLE 3-3).

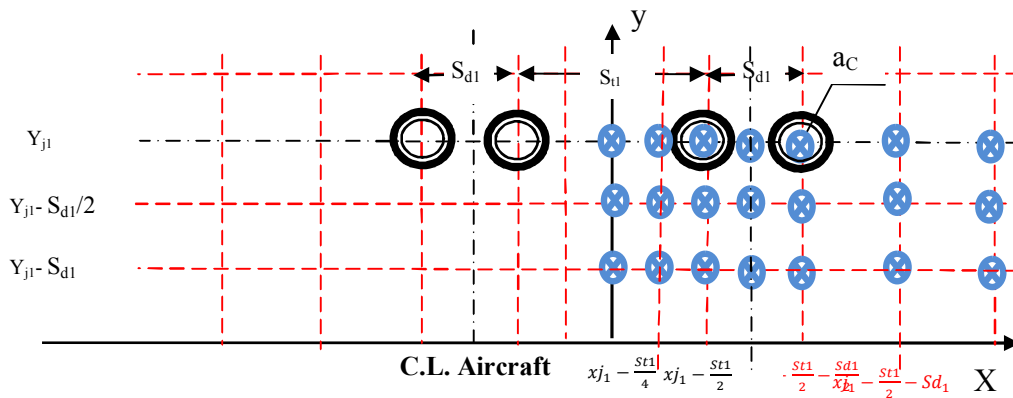


Figure 3-7 Type Gear for B-52

TABLE 3-10 The Coordinate of Point of Interest for Twin-Twin Aircraft

| | | | | | | | |
|---|---------------------------------------|---------------------------------------|--------------------------------------|---|--------------------------|--------------------------|------------------|
| X | $x_{j1} - \frac{St1}{2}$ $- 3Sd_1$ | $x_{j1} - \frac{St1}{2}$ $- 2Sd_1$ | $x_{j1} - \frac{St1}{2}$ $- Sd_1$ | $x_{j1} - \frac{St1}{2}$ $- \frac{Sd1}{2}$ | $x_{j1} - \frac{St1}{2}$ | $x_{j1} - \frac{St1}{4}$ | x_{j1} |
| Y | Y_{j1} | Y_{j1} | Y_{j1} | Y_{j1} | Y_{j1} | Y_{j1} | Y_{j1} |
| X | $x_{j1} - \frac{St1}{2}$ $- 3Sd_1$ | $x_{j1} - \frac{St1}{2}$ $- 2Sd_1$ | $x_{j1} - \frac{St1}{2}$ $- Sd_1$ | $x_{j1} - \frac{St1}{2}$ $- \frac{Sd1}{2}$ | $x_{j1} - \frac{St1}{2}$ | $x_{j1} - \frac{St1}{4}$ | x_{j1} |
| Y | $Y_{j1} - Sd1/2$ | $Y_{j1} - Sd1/2$ | $Y_{j1} - Sd1/2$ | $Y_{j1} - Sd1/2$ | $Y_{j1} - Sd1/2$ | $Y_{j1} - Sd1/2$ | $Y_{j1} - Sd1/2$ |
| X | $x_{j1} - \frac{St1}{2}$ $- 3Sd_1$ | $x_{j1} - \frac{St1}{2}$ $- 2Sd_1$ | $x_{j1} - \frac{St1}{2}$ $- Sd_1$ | $x_{j1} - \frac{St1}{2}$ $- \frac{Sd1}{2}$ | $x_{j1} - \frac{St1}{2}$ | $x_{j1} - \frac{St1}{4}$ | x_{j1} |
| Y | $Y_{j1} - Sd1$ | $Y_{j1} - Sd1$ | $Y_{j1} - Sd1$ | $Y_{j1} - Sd1$ | $Y_{j1} - Sd1$ | $Y_{j1} - Sd1$ | $Y_{j1} - Sd1$ |

3.2.5.1.8 A-380 Airbus

The A-380 aircraft has two main gears on each side of the aircraft centerline (a tri-tandem and dual tandem). FIGURE 3-8 illustrates the arrangement of the tires for the A-380 and the computational points. The number of these points is 88 and their locations are listed in the TABLE 3-11.

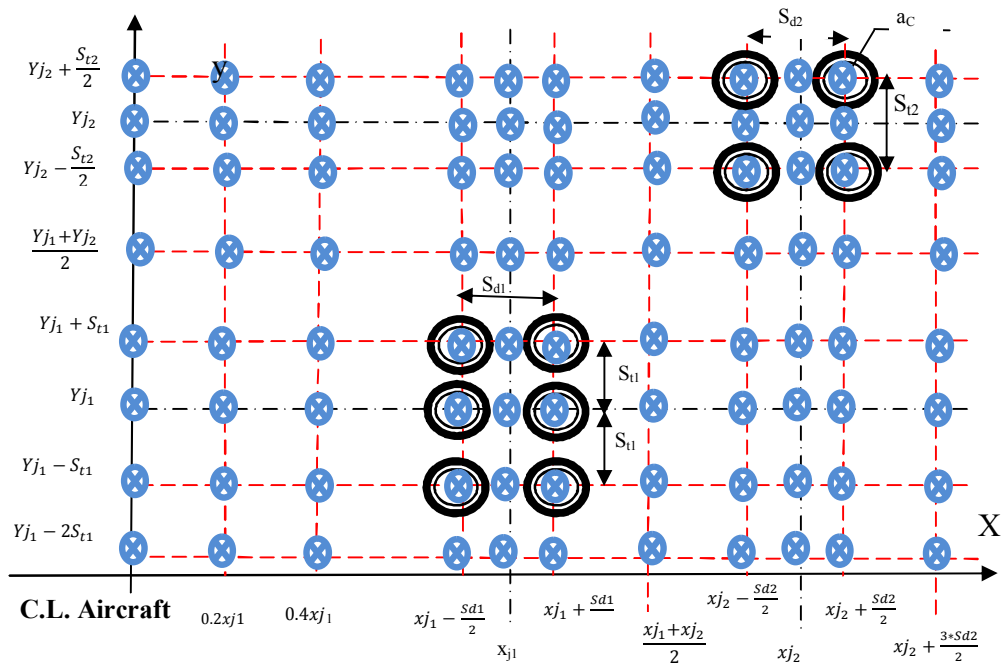


FIGURE 3-8 Type gear for A-380.

TABLE 3-11 The Coordinate of Point of Interest for A-380 Aircraft

| | | | | | | | | | | | |
|---|------------------------|------------------------|------------------------|------------------------|------------------------|------------------------|------------------------|------------------------|------------------------|------------------------|----------------------------|
| X | 0 | 0.2xj1 | 0.4xj1 | $xj_1 - \frac{Sd1}{2}$ | xj1 | $xj_1 + \frac{Sd1}{2}$ | $\frac{xj_1+xj_2}{2}$ | $xj_2 - \frac{Sd2}{2}$ | xj2 | $xj_2 + \frac{Sd2}{2}$ | $xj_2 + \frac{3 * Sd2}{2}$ |
| Y | $Yj_2 + \frac{St2}{2}$ | $Yj_2 + \frac{St2}{2}$ | $Yj_2 + \frac{St2}{2}$ | $Yj_2 + \frac{St2}{2}$ | $Yj_2 + \frac{St2}{2}$ | $Yj_2 + \frac{St2}{2}$ | $Yj_2 + \frac{St2}{2}$ | $Yj_2 + \frac{St2}{2}$ | $Yj_2 + \frac{St2}{2}$ | $Yj_2 + \frac{St2}{2}$ | $Yj_2 + \frac{St2}{2}$ |
| X | 0 | 0.2xj1 | 0.4xj1 | $xj_1 - \frac{Sd1}{2}$ | xj1 | $xj_1 + \frac{Sd1}{2}$ | $\frac{xj_1+xj_2}{2}$ | $xj_2 - \frac{Sd2}{2}$ | xj2 | $xj_2 + \frac{Sd2}{2}$ | $xj_2 + \frac{3 * Sd2}{2}$ |
| Y | Yj2 | Yj2 | Yj2 | Yj2 | Yj2 | Yj2 | Yj2 | Yj2 | Yj2 | Yj2 | Yj2 |
| X | 0 | 0.2xj1 | 0.4xj1 | $xj_1 - \frac{Sd1}{2}$ | xj1 | $xj_1 + \frac{Sd1}{2}$ | $\frac{xj_1+xj_2}{2}$ | $xj_2 - \frac{Sd2}{2}$ | xj2 | $xj_2 + \frac{Sd2}{2}$ | $xj_2 + \frac{3 * Sd2}{2}$ |
| Y | $Yj_2 - \frac{St2}{2}$ | $Yj_2 - \frac{St2}{2}$ | $Yj_2 - \frac{St2}{2}$ | $Yj_2 - \frac{St2}{2}$ | $Yj_2 - \frac{St2}{2}$ | $Yj_2 - \frac{St2}{2}$ | $Yj_2 - \frac{St2}{2}$ | $Yj_2 - \frac{St2}{2}$ | $Yj_2 - \frac{St2}{2}$ | $Yj_2 - \frac{St2}{2}$ | $Yj_2 - \frac{St2}{2}$ |
| X | 0 | 0.2xj1 | 0.4xj1 | $xj_1 - \frac{Sd1}{2}$ | xj1 | $xj_1 + \frac{Sd1}{2}$ | $\frac{xj_1+xj_2}{2}$ | $xj_2 - \frac{Sd2}{2}$ | xj2 | $xj_2 + \frac{Sd2}{2}$ | $xj_2 + \frac{3 * Sd2}{2}$ |
| Y | $\frac{Yj_1+Yj_2}{2}$ | $\frac{Yj_1+Yj_2}{2}$ | $\frac{Yj_1+Yj_2}{2}$ | $\frac{Yj_1+Yj_2}{2}$ | $\frac{Yj_1+Yj_2}{2}$ | $\frac{Yj_1+Yj_2}{2}$ | $\frac{Yj_1+Yj_2}{2}$ | $\frac{Yj_1+Yj_2}{2}$ | $\frac{Yj_1+Yj_2}{2}$ | $\frac{Yj_1+Yj_2}{2}$ | $\frac{Yj_1+Yj_2}{2}$ |
| X | 0 | 0.2xj1 | 0.4xj1 | $xj_1 - \frac{Sd1}{2}$ | xj1 | $xj_1 + \frac{Sd1}{2}$ | $\frac{xj_1+xj_2}{2}$ | $xj_2 - \frac{Sd2}{2}$ | xj2 | $xj_2 + \frac{Sd2}{2}$ | $xj_2 + \frac{3 * Sd2}{2}$ |
| Y | $Yj_1 + St1$ | $Yj_1 + St1$ | $Yj_1 + St1$ | $Yj_1 + St1$ | $Yj_1 + St1$ | $Yj_1 + St1$ | $Yj_1 + St1$ | $Yj_1 + St1$ | $Yj_1 + St1$ | $Yj_1 + St1$ | $Yj_1 + St1$ |
| X | 0 | 0.2xj1 | 0.4xj1 | $xj_1 - \frac{Sd1}{2}$ | xj1 | $xj_1 + \frac{Sd1}{2}$ | $\frac{xj_1+xj_2}{2}$ | $xj_2 - \frac{Sd2}{2}$ | xj2 | $xj_2 + \frac{Sd2}{2}$ | $xj_2 + \frac{3 * Sd2}{2}$ |
| Y | Yj1 | Yj1 | Yj1 | Yj1 | Yj1 | Yj1 | Yj1 | Yj1 | Yj1 | Yj1 | Yj1 |
| X | 0 | 0.2xj1 | 0.4xj1 | $xj_1 - \frac{Sd1}{2}$ | xj1 | $xj_1 + \frac{Sd1}{2}$ | $\frac{xj_1+xj_2}{2}$ | $xj_2 - \frac{Sd2}{2}$ | xj2 | $xj_2 + \frac{Sd2}{2}$ | $xj_2 + \frac{3 * Sd2}{2}$ |
| Y | $Yj_1 - St1$ | $Yj_1 - St1$ | $Yj_1 - St1$ | $Yj_1 - St1$ | $Yj_1 - St1$ | $Yj_1 - St1$ | $Yj_1 - St1$ | $Yj_1 - St1$ | $Yj_1 - St1$ | $Yj_1 - St1$ | $Yj_1 - St1$ |
| X | 0 | 0.2xj1 | 0.4xj1 | $xj_1 - \frac{Sd1}{2}$ | xj1 | $xj_1 + \frac{Sd1}{2}$ | $\frac{xj_1+xj_2}{2}$ | $xj_2 - \frac{Sd2}{2}$ | xj2 | $xj_2 + \frac{Sd2}{2}$ | $xj_2 + \frac{3 * Sd2}{2}$ |
| Y | $Yj_1 - 2St1$ | $Yj_1 - 2St1$ | $Yj_1 - 2St1$ | $Yj_1 - 2St1$ | $Yj_1 - 2St1$ | $Yj_1 - 2St1$ | $Yj_1 - 2St1$ | $Yj_1 - 2St1$ | $Yj_1 - 2St1$ | $Yj_1 - 2St1$ | $Yj_1 - 2St1$ |

3.2.5.1.9 B-747 Aircraft

The b-747 aircraft has two main gears (dual tandem) on each side of the aircraft centerline. FIGURE 3-9 illustrates the arrangement of the B-747 tires and the computational points. The number of these points is 88. The location of these points are listed in TABLE 3-12.

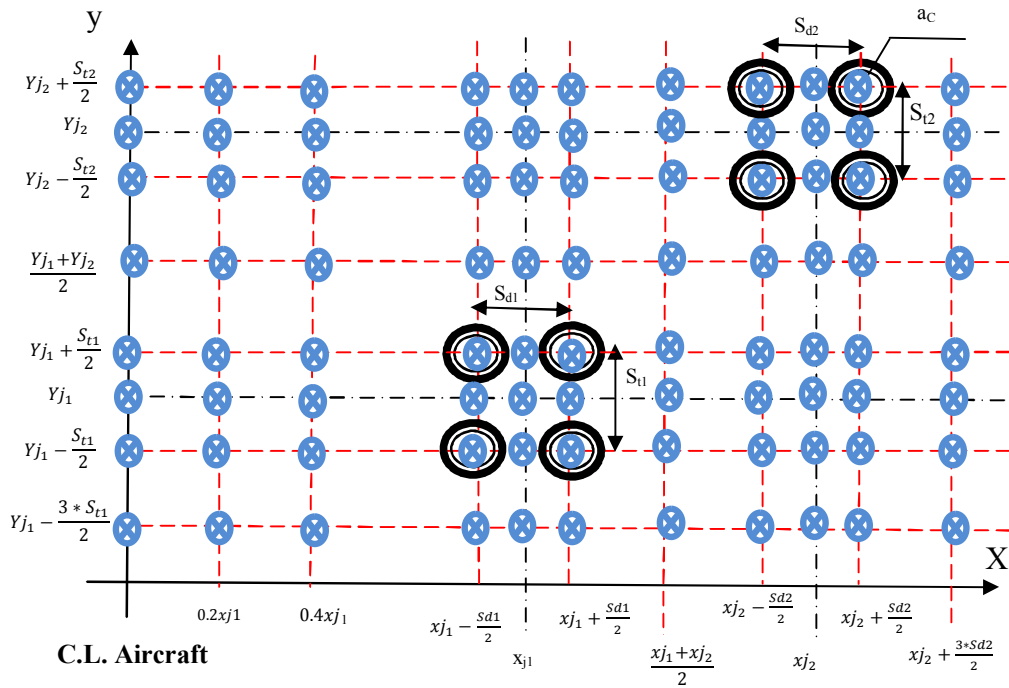


FIGURE 3-9 Type gear for B-747.

3.2.6 *Vertical Subgrade Strain Criteria*

3.2.6.1 *Introduction*

This module has been specifically developed for the ZAPRAM program. The inputs of this module are the summary of results obtained from the Stress and Strain Analysis Module just described. The user will click on the "Update Data" button to retrieve the input in a tabular format. The table has the x, y, and z coordinates of the points of interest for the maximum vertical strain at the top of the pavement layer in question for each lateral internal (x_i) evaluated for each aircraft. These strains are, in turn, utilized within a specific user defined limiting strain criteria, to compute the actual damage of the pavement system. While the limiting subgrade strain criteria typically utilizes the top of the subgrade layer as the critical computational depth; ZAPRAM may also be used to find the critical stresses or strains at the top of a saturated layer within a subgrade just described. Thus, critical locations of any layer, partially subjected to saturation within only a portion of the layer are generally evaluated at all critical possible points.

Once the critical strains are developed, the program allows the solution of one of four agency criteria, to calculate the allowable number of repetitions to failure as a function of the vertical strain at the top of the subgrade (These criteria will be explained in detail in next section). From this, the unit damage (damage per pass); total damage and design life can be quickly determined. This analysis is linked to the expected permanent deformation (rutting). For a given criteria, the unit damage of all computational points are developed. The four different criteria contained in ZAPRAM are the: Shell Oil Criteria (Airfields), MS-11 the Asphalt Institute (Airfields), USACE.WES (U.S. Army Corps of Engineers-Original MLET), and USACE.WES (U.S. Army Corps of Engineers-Revised β Approach). The user simply selects the criteria by clicking on the criteria name on the

top of the user form. The allowable number of repetitions to failure as a function of the vertical strain at the top of the subgrade and the unit damage of all computational points are computed.

The program then determines the actual design repetitions (or coverages) that will be used to design the Taxiway or Runway. This is accomplished by assuming that the lateral wander of the aircraft can be modeled by a normal probability distribution, having a standard deviation associated with the specific range of values commonly used in airfield pavement analysis (i.e., 3' to 20'). The wander value can simulate a range of aircraft operations simulating highly channelized taxiway operations, ($\sigma_w = 3.0'$) to runway landing simulation ($\sigma_w = 20.0'$). The user then has three options for each aircraft type: one main gear, two main gears in one path or two main gears in two paths. This is solely dependent upon the tracking of the main gears of the aircraft. The grooves “two main gears in one path” are used only for the C-5A and B-52 aircraft (see TABLE 3-3). The program then automatically retrieves the distance to the mean location of the load, (x_{j1}), distance to mean location of load (x_{j2}), if present, the gear wander standard deviation, (σ_{wj}), the desired design analysis width (centerline to pavement edge), and the name of the selected aircraft. These variables have already been input in previous modules. At this time the user has the ability to change the value of these inputs from the initial input. From this, the unit damage (per pass) and total damage on the pavement structure are then computed. The next stage of the computational process is to determine the Annual Traffic (Passes), Annual Max Damage (%), Cumulative Traffic (Pass), Cumulative Max Damage (%), and lateral pavement Interval where the Maximum Damage occurs.

The last stage of this module presents the graphical forms of the output. The user has a list of plots that can be chosen: strain profile, unit damage, and damage profile by one pass, damage profile at the end of the design life, damage versus time, and annual and cumulative traffic for each analysis.

3.2.6.2 Vertical Subgrade Strain Criteria Implemented in ZAPRAM

In pavement applications, a damage factor (DF) is defined as the ratio between the number of actual strain repetitions (n) and the number of allowable strains repetitions to failure (N_f).

$$DF = \frac{n}{N_f} \quad (3-2)$$

Where:

n = Number of effective (actual) strain repetitions;

N_f = Number of allowable strain repetitions to failure;

The cumulative damage factor is the sum of the damages factors for all aircrafts. The value of n is determined from the number of aircraft operations obtained from an assessment of the expected traffic repetitions that will be operating at the airport facility. It is very important to note that “n” represents the actual strain repetitions of a specific aircraft and not the actual passes of that aircraft. The value of N_f is determined from an assessment of the structural capacity of the pavement cross section and critical aircraft load (20) depending upon the agency “failure” criteria used.

In Limiting Strain design approaches; there are three different criteria to determine N_f , based upon the specific distress type being investigated:

- i. The allowable number of repetitions as a function of the vertical strain at the top of the subgrade. This analysis is linked to the expected shear deformation that leads to permanent deformation or rutting.
- ii. The allowable number of repetitions as a function of the horizontal strain at the bottom of the Asphalt concrete. This analysis is linked to the expected fatigue cracking life of the asphalt layer.
- iii. The allowable number of repetitions as a function of the horizontal strain at the bottom of a chemically stabilized base or chemically stabilized subbase. This analysis is linked to the development of fatigue cracking of the stabilized layer, which may reflect through the AC surface layer.

This section focuses on the criteria of the vertical strain at the top of the subgrade (ϵ_{vsg}) (the permanent deformation (rutting) distress). Use of these criteria will adjust the structural pavement cross section to minimize the shear deformation (rutting) in the subgrade to a specified maximum criterion level. Four currently used limiting subgrade strain criteria, each developed by a major pavement design agency have been incorporated in the ZAPRAM program. Each of these criteria has been used previously in practice to design / analyze major airfield pavements throughout the world.

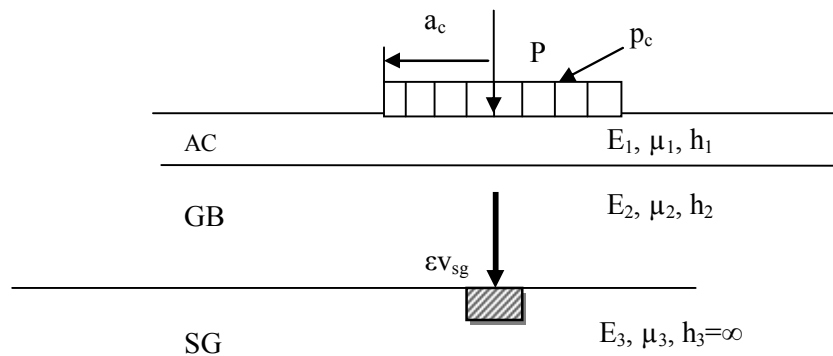


FIGURE 3-10 Vertical strain at the top of the subgrade (ϵ_{vsg}).

3.2.6.2.1 Shell Oil Criteria (Airfields)

The Shell Oil vertical strain criterion was established from a MLET analysis of pavements designed by empirical design techniques. The Shell Oil vertical strain criteria was initially developed by an analysis for various road structures designed in accordance with the CBR method and in the test sections at the AASHTO Road Test (21). The original Shell Oil Highway vertical strain criterion was later modified for airfield pavement applications (21).

The Shell Oil Airfield design vertical subgrade strain criteria is a linear Log-Log relationship between N_f and ϵ_{vsg} . Figure 3-11 illustrates, in a schematic fashion, this relationship. From this figure, the relationship is defined by:

$$N_f = K_1 \left(\frac{1}{\epsilon_{vsg}} \right)^{K_2} \quad (3-3)$$

Where:

K_1, K_2 = regression parameters (intercept ,slope);

N_f = allowable repetitions to failure;

ϵ_{vsg} = Vertical strain at the top of subgrade;

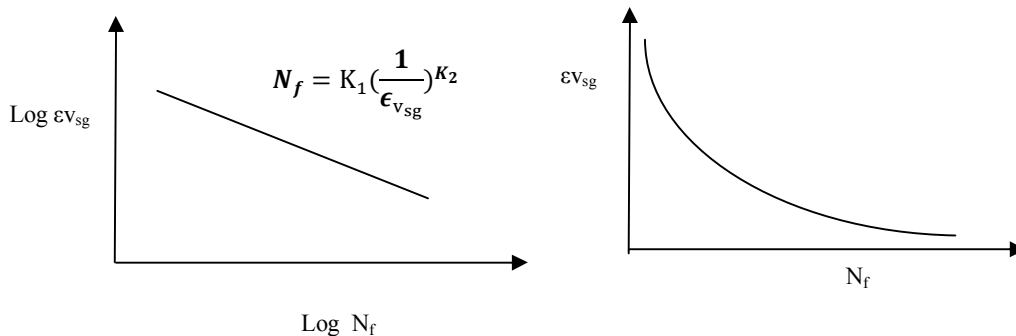


Figure 3-11 Relation between allowable repetitions and the vertical strain at the top of the subgrade (ϵ_{vsg}).

For the linear log-log relationship:

$$\text{Log } N_f = \text{Log } K_1 + K_2 \text{ Log } \epsilon_{vsg} \quad (3-4)$$

It should be recognized that K_2 will be a negative value, or that

$$N_f = K_1 \left(\frac{1}{\epsilon_{vsg}} \right)^{K_2} \quad (3-5)$$

With K_2 expressed as a positive integer.

TABLE 3-13 illustrates the Shell Oil limiting Vertical Strain Criteria Summary (20):

TABLE 3-13 Shell Oil Limiting Vertical Strain Criteria (Airfields)

| Limiting Vertical Strain Criteria Summary | | | |
|---|----------|---------------------------|---|
| | N_f | ϵ_{vsg} in/in | Regression Predicted $\epsilon_{vsg} = 0.0188565 * N_f^{-0.209}$ |
| Vertical Strain (Subgrade) | 1000 | 0.0045 | 0.00445 |
| | 10000 | 0.0027 | 0.00275 |
| | 100000 | 0.0017 | 0.00170 |
| | 1000000 | 0.00103 | 0.00105 |
| | 10000000 | 0.00065 | 0.00065 |
| | 1E+08 | 0.0004 | 0.00040 |

The finalized Shell Oil equation is the following:

$$N_f = 2.8626E+20 * (1 / \epsilon_{vsg})^{4.785} \quad (3-6)$$

where:

N_f = allowable repetitions to failure;

ϵ_{vsg} = Vertical strain at the top of subgrade ($\mu. / "$);

Or , the equation could be formulated with different units as follows:

$$N_f = 5.6056E-09 * (1/ \epsilon_{V_{sg}})^{4.785} \quad (3-7)$$

Where:

N_f = allowable repetitions to failure;

$\epsilon_{V_{sg}}$ = Vertical strain at the top of subgrade (" / ");

It is critically important for the user to note that the Shell Oil criterion *must use* an effective AC modulus (E1) of 150,000 psi when applying it to analysis/design of airfield pavement structures for permanent deformation. FIGURE 3-12 illustrates the limiting vertical subgrade strain criteria for Shell Oil criterion.

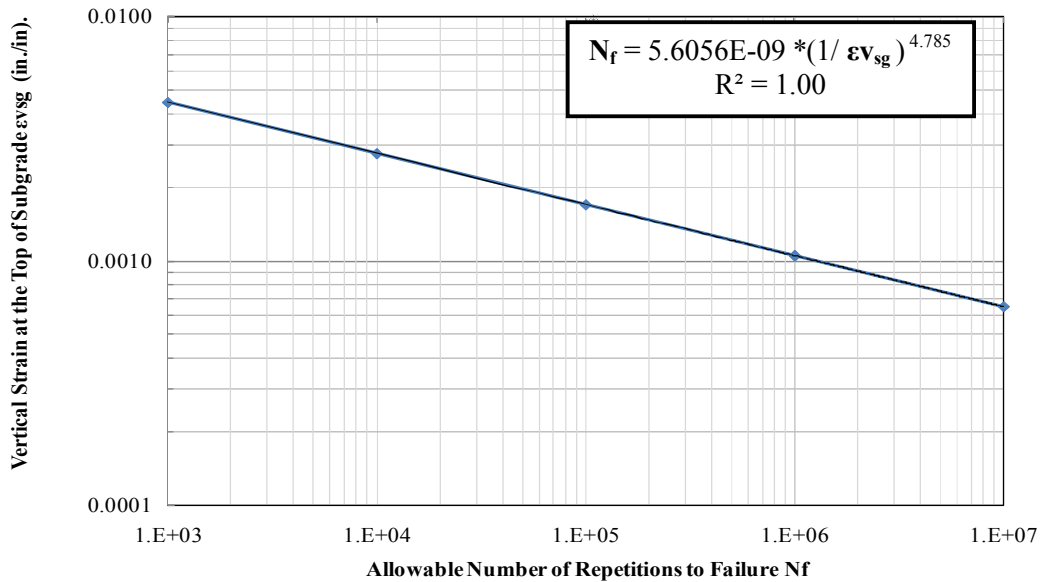


FIGURE 3-12 Allowable number of repetition as a function of the vertical strain at the top of the subgrade (shell oil - airfields).

3.2.6.2.2 MS-11 the Asphalt Institute Criteria (Airfields)

In the theoretical study, leading to the development of the limiting subgrade strain criteria used by the Asphalt Institute in their MS-11 Airfield Design Manual (20, 22), several important assumptions were utilized:

- i. Poisson’s ratio of 0.40 for asphalt concrete and 0.45 for unbound layer were used.
- ii. The subgrade modulus (E_s) was set equal to 1500 CBR.
- iii. A critical effective AC module of 100 ksi must be used.

The criterion for vertical strain that was developed by Witczak was derived through a MLET evaluation of the older, established CBR pavement design methodology of the USACE. This USACE approach utilized the “alpha procedure” for adjusting thickness based upon the design coverage and number of wheels used to establish the ESWL of the aircraft. In addition, the ESWL was based upon the use of equal interface deflection theory, using Boussinesq theory, developed by the USACE. A detailed derivation of this approach is explained by Witczak (22).

TABLE 3-14 summarizes the Limiting Vertical Strain Criteria developed from the USACE design procedure (with the α factor) and utilized in MS-11(17).

TABLE 3-14 The Limiting Vertical Strain Criteria Summary (MS-11) Airfield

| limiting Vertical Strain Criteria Summary | | | | | |
|---|----------|-----------------------------------|----------------|-----|------|
| | Nf | ϵ_{vsg} μ .inch/inch | E1psi | v1 | v2 |
| | 100 | 2548 | $1 \cdot 10^6$ | 0.4 | 0.45 |
| Vertical | 1000 | 1904 | | | |
| Strain | 10000 | 1646 | | | |
| (Subgrade) | 100000 | 1508 | | | |
| | 1000000 | 1423 | | | |
| | ∞ | 1060 | | | |

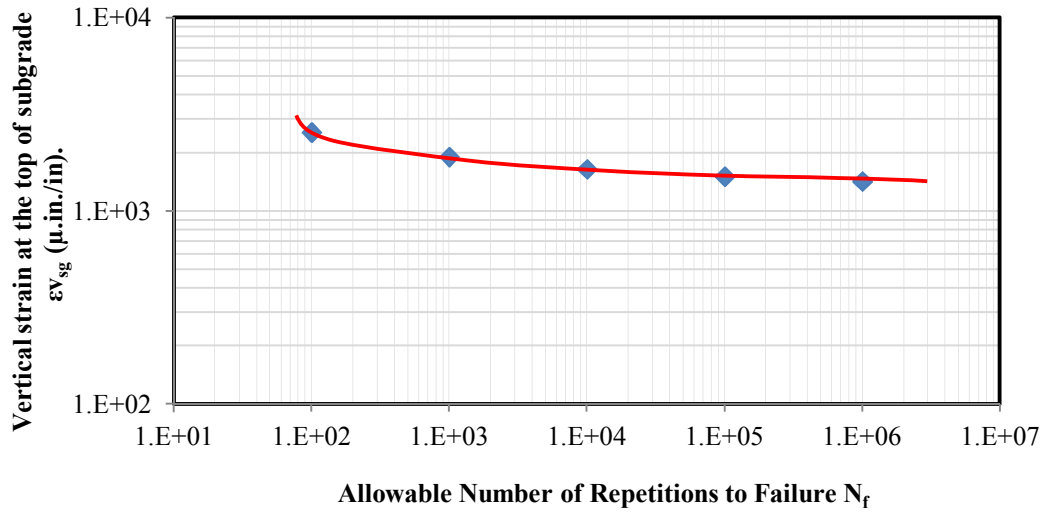


FIGURE 3-13 Allowable number of repetitions as a function of the vertical strain at the top of the subgrade (ms-11 airfield).

The relationship between the allowable number of repetitions and the vertical strain at the top of the subgrade for the MS-11 Airfield Pavement design procedure is a nonlinear Log-Log relationship. The limiting Strain criterion is given by the equation:

$$\log(\epsilon_{vsg}) = \frac{a + b * (\log(N_f))}{c + d * (\log(N_f))} \quad (3-8)$$

Where:

ϵ_{vsg} = Vertical strain at the top of subgrade ($\mu\text{in./in.}$);

N_f = allowable repetitions to failure;

a = 47.395

b = -195.221

c = 1.0

d = 65.627

TABLE 3-15 is a summary of the vertical subgrade strain criteria of the (MS-11 Airfield). As can be seen, for the previous model the regression number values for A, B, C, and D are listed in the table. These values work very well for the model with $R^2 = 100\%$.

TABLE 3-15 Limiting Vertical Strain Criteria (MS-11 Airfield)

| A | B | C | D | N_f | ϵ_{vsg} (""/") | ϵ_{vsg} Regression Predicted (""/") |
|--------|----------|---|--------|----------|----------------------------|---|
| | | | | 100 | 0.002548 | 0.002548 |
| | | | | 1000 | 0.001904 | 0.001905 |
| 47.395 | -195.221 | 1 | 65.627 | 10000 | 0.001646 | 0.001646 |
| | | | | 100000 | 0.001508 | 0.001508 |
| | | | | 1000000 | 0.001423 | 0.001422 |
| | | | | ∞ | 0.00106 | 0.001060 |

The ϵ_{vsg} criterion values shown in TABLE 3-15 are in 100% agreement with the criterion shown and computed from equation [8]. As a final point, FIGURE 3-14 is a final plot of the limiting strain - N_f equation for (MS-11 Airfield).

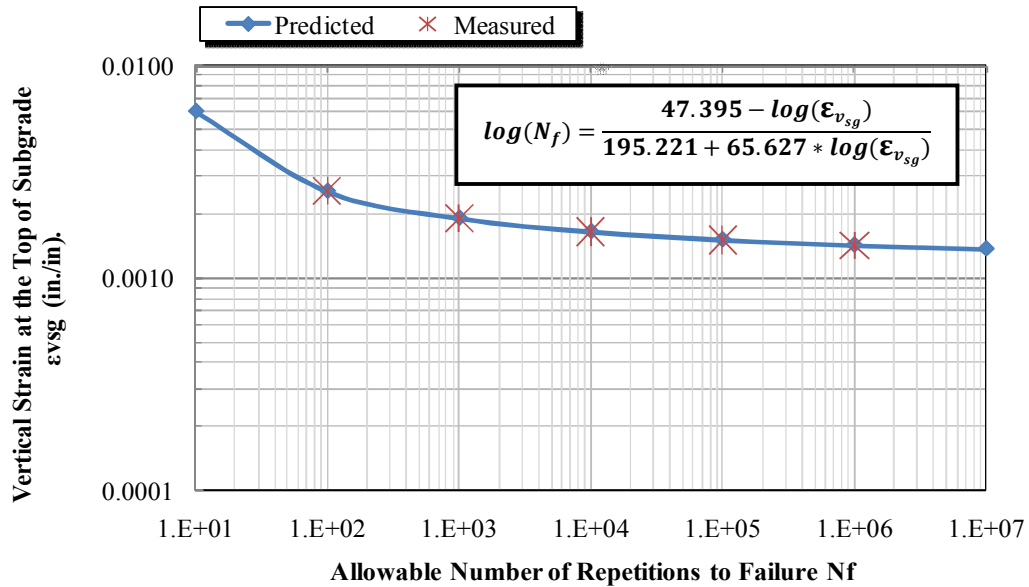


FIGURE 3-14 Allowable number of repetitions as a function of the vertical strain at the top of the subgrade (MS-11 Airfield).

3.2.6.2.3 USACE. WES (U.S. Army Corps of Engineers) ... (Original MLET)

The subgrade strain criteria used in the original MLET design by the U.S. Army Corps of Engineers was developed from the analysis of USACE field test data and present the allowable number of strain repetitions as a function of vertical subgrade strain magnitude. The criterion was subsequently used in all military airfields (Army TM 5-825-2-1; Air Force AFM 88-6, chap 2, section A), “Flexible Pavement Design for Airfields (Elastic Layered Method)”. The details of this model development are found in reference (23). The data analysis indicated that the relationship between allowable repetitions and strain magnitude was a function of the subgrade resilient moduli. The criterion is presented in FIGURE 3-15. According to the USACE-WES, the design equation is:

$$N_f = 10,000 * \left(\frac{A}{\epsilon_{vsg}}\right)^B \quad (3-9)$$

where:

N_f = allowable repetitions to failure;

A = $0.000247 + 0.000245 \log M_R$;

ϵ_{vsg} = Vertical strain at the top of subgrade (in/in);

B = $0.0658 * M_R^{0.559}$

M_R = resilient modulus of the subgrade (psi);

It is very important to note that the allowable N_f values is not only a function of the vertical subgrade strain level but also a function of the subgrade M_r value. FIGURE 3-15 illustrates the limiting vertical subgrade strain criteria for the USACE original MLET-Airfield criterion.

TABLE 3-16 Vertical Subgrade Strain Computations by Moduli

| Limiting Vertical Strain Criteria for Mr =4500 psi | | | | | |
|---|-------|----------|----------|---------------------------|----------------------------------|
| Nf | Mr | A | B | ϵ all. inch/inch | ϵ all. μ .inch/inch |
| 1000 | | | | 0.00157 | 1569 |
| 10000 | | | | 0.00114 | 1142 |
| 100000 | 4500 | 0.001142 | 7.250562 | 0.00083 | 831 |
| 1000000 | | | | 0.00061 | 605 |
| 10000000 | | | | 0.00044 | 440 |
| Limiting Vertical Strain Criteria for Mr =6000 psi | | | | | |
| Nf | Mr | A | B | ϵ all. inch/inch | ϵ all. μ .inch/inch |
| 1000 | | | | 0.00154 | 1537 |
| 10000 | | | | 0.00117 | 1173 |
| 100000 | 6000 | 0.001173 | 8.515545 | 0.00089 | 895 |
| 1000000 | | | | 0.00068 | 683 |
| 10000000 | | | | 0.00052 | 521 |
| Limiting Vertical Strain Criteria for Mr =9000 psi | | | | | |
| Nf | Mr | A | B | ϵ all. inch/inch | ϵ all. μ .inch/inch |
| 1000 | | | | 0.00151 | 1508 |
| 10000 | | | | 0.00122 | 1216 |
| 100000 | 9000 | 0.001216 | 10.68187 | 0.00098 | 980 |
| 1000000 | | | | 0.00079 | 790 |
| 10000000 | | | | 0.00064 | 637 |
| Limiting Vertical Strain Criteria for Mr =15000 psi | | | | | |
| Nf | Mr | A | B | ϵ all. inch/inch | ϵ all. μ .inch/inch |
| 1000 | | | | 0.00149 | 1494 |
| 10000 | | | | 0.00127 | 1270 |
| 100000 | 15000 | 0.00127 | 14.21219 | 0.00108 | 1080 |
| 1000000 | | | | 0.00092 | 919 |
| 10000000 | | | | 0.00078 | 781 |
| Limiting Vertical Strain Criteria for Mr =30000 psi | | | | | |
| Nf | Mr | A | B | ϵ all. inch/inch | ϵ all. μ .inch/inch |
| 1000 | | | | 0.00150 | 1500 |
| 10000 | | | | 0.00134 | 1344 |
| 100000 | 30000 | 0.001344 | 20.93807 | 0.00120 | 1204 |
| 1000000 | | | | 0.00108 | 1079 |
| 10000000 | | | | 0.00097 | 966 |

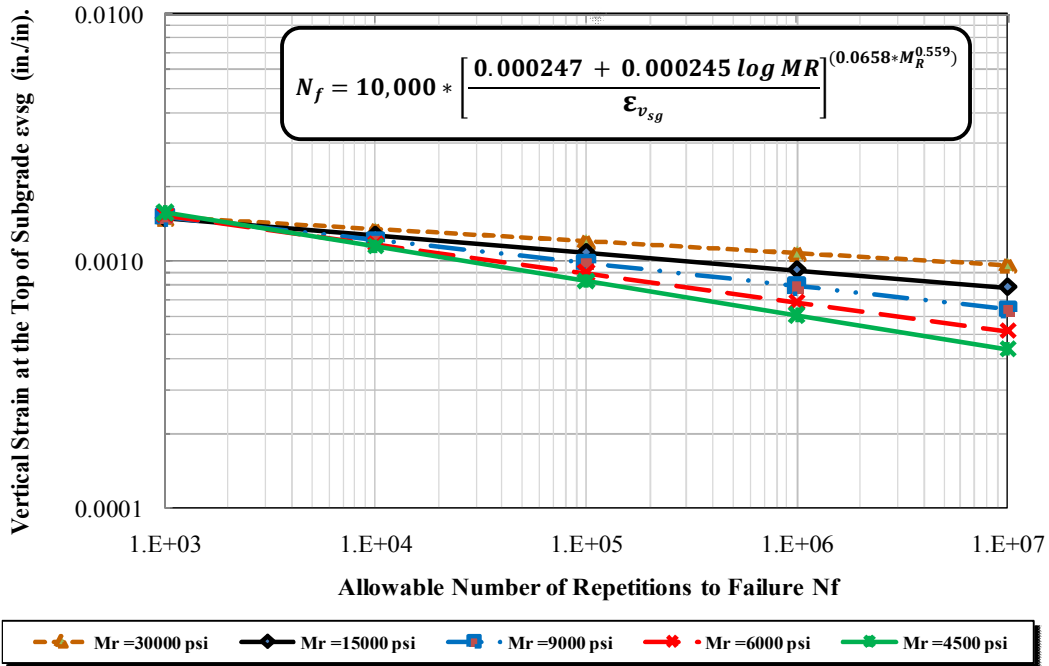


FIGURE 3-15 Design criteria based on the ϵ_{vsg} (USACE. original MLET-airfield).

3.2.6.2.4 Revised β Approach USACE Criteria

Since 2006, The USACE-WES has been developing a revised enhancement to the classical CBR airfield pavement procedure of the USACE (23). This latest enhancement, formally approved by the USACE Board of Consultants in 2010 is based upon the use of a variable Froehlich “n” concentration factor modifier to the Boussinesq vertical stress. In addition, the use of a “ β -Beta” factor to adjust the design thickness as a function of the stress to strength ratio of the unbound layers has been incorporated into the new approach. Barker and Gonzalez have also expressed this new CBR design criterion in terms of a completely revised limiting subgrade strain criteria. The details of this model development are presented by Barker and Gonzalez (24, 25).

The revised criterion by the new USACE-WES Beta approach can be expressed in the form of the following equation shown below:

$$\log(\epsilon_{vsg}) = \frac{a+b \cdot \log(N_f)}{c+d \cdot \log(N_f)} \quad (3-10)$$

where:

ϵ_{vsg} = Vertical strain at the top of subgrade (" / ");

N_f = Allowable repetitions to failure;

a = -2.1582

b = -1.3723

c = 1.0

d = 0.4115

According to Barker, the critical effective AC modulus that *must be* used in the rutting design analysis of flexible pavements is E = 300,000 psi. Table 3-17 is a summary of the vertical subgrade strain criteria of the newly revised USACE approach (elastic layered).

Table 3-17 USACE-WES Limiting Vertical Strain Criteria (β -Airfield)

| Limiting Vertical Strain Criteria(USACE- β Airfield) | | | |
|--|------------|--------------------------|-----------------------------------|
| | N_f | ϵ_{vsg} (" / ") | ϵ_{vsg} (μ . " / ") |
| Vertical Strain (Subgrade) | 100 | 0.002044 | 2044 |
| | 1,000 | 0.001555 | 1555 |
| | 10,000 | 0.001288 | 1288 |
| | 100,000 | 0.001122 | 1122 |
| | 1,000,000 | 0.001010 | 1010 |
| | 10,000,000 | 0.000930 | 930 |

FIGURE 3-16 illustrates USACE-WES derived plot of the correct limiting vertical subgrade strain criteria from references (24) and (25). As can be seen the revised ϵ_{vsg} criterion values shown in Table 3-17 are in 100% agreement with the criterion shown and computed from equation [3-10].

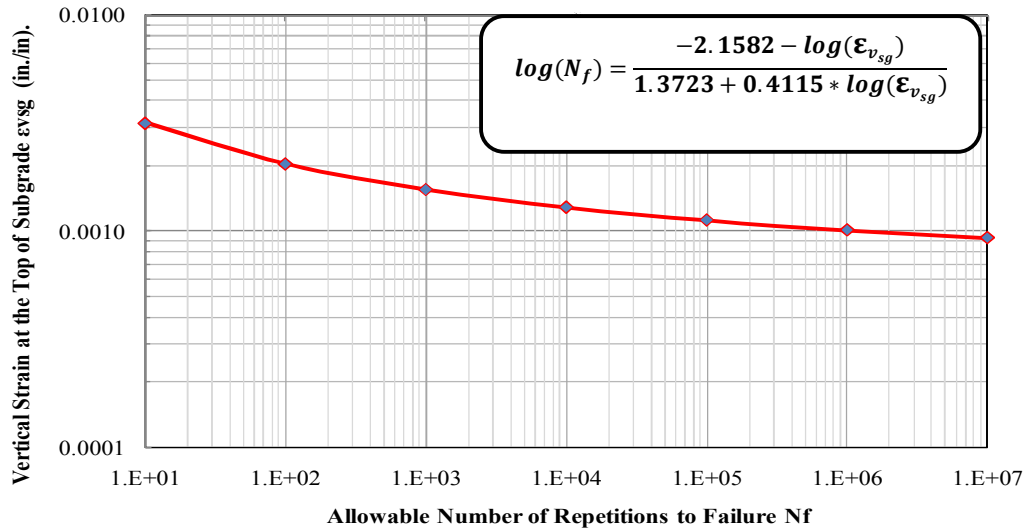


FIGURE 3-16 Allowable number of repetition as a function of the ϵ_{vsg} (USACE-WES (β -Airfield)).

FIGURE 3-17 illustrates the limiting vertical subgrade strain criteria for each of the 4 criteria that were used in this study. It is important to note that each criterion has its own unique effective E_1 moduli to be used.

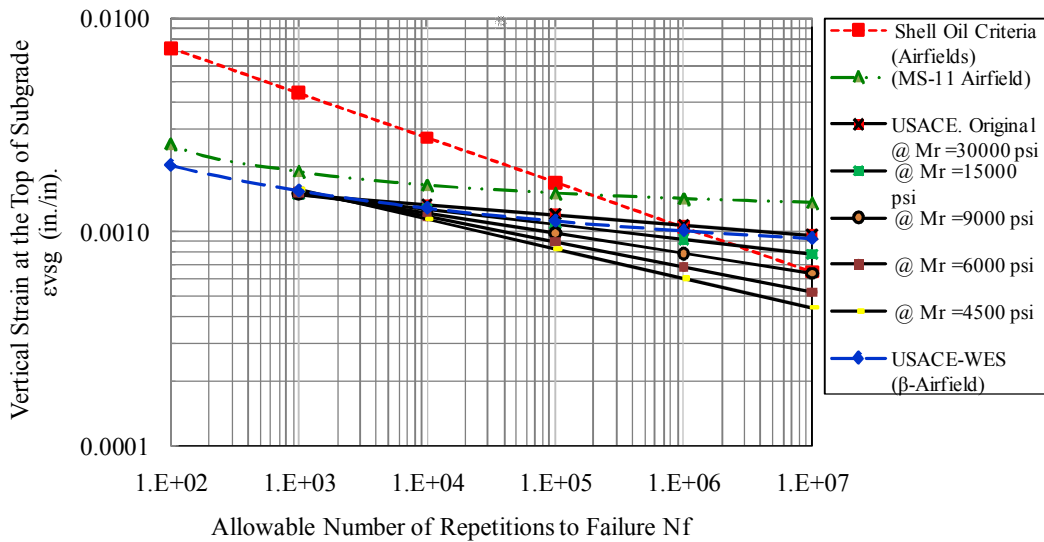


FIGURE 3-17 Allowable number of repetition as a function of the vertical strain at the top of the subgrade (from the previous four methods).

3.2.6.3 Determination of the Actual Design Deflection Repetitions (Coverage)

The program determines the actual design repetitions (or coverages) that will be used to design the Taxiway or Runway. This is accomplished by assuming that the lateral wander of the aircraft can be modeled by a normal probability distribution, having a standard deviation associated with the specific range of values commonly used in airfield pavement analysis (i.e. 3' to 20'). The steps that the ZAPRAM program follows to determine the actual design repetitions for any aircraft:

- i. Choose the aircraft that would be used to design the pavement.
- ii. The program has a list of aircrafts with their characterization that the user is able to choose one of them (for exp. B-737-900-ER).
- iii. Aircraft characteristics list for B-737-900-ER :
- iv. These values have already been input in previous modules
- v. Maximum gross weight $w_t = 188$ kips
- vi. CC tire spacing = 34.0 "
- vii. Tire pressure = 205 psi
- viii. Number of tires in the main gear = 2 tires
- ix. The load for B-737 carrying by the two main gears is: $P_t = 0.95 \times 188 = 178.6$ kips
- x. Find the maximum load on one tire (gear load) $P_g = 178.6 / 4 = 44.65$ kips

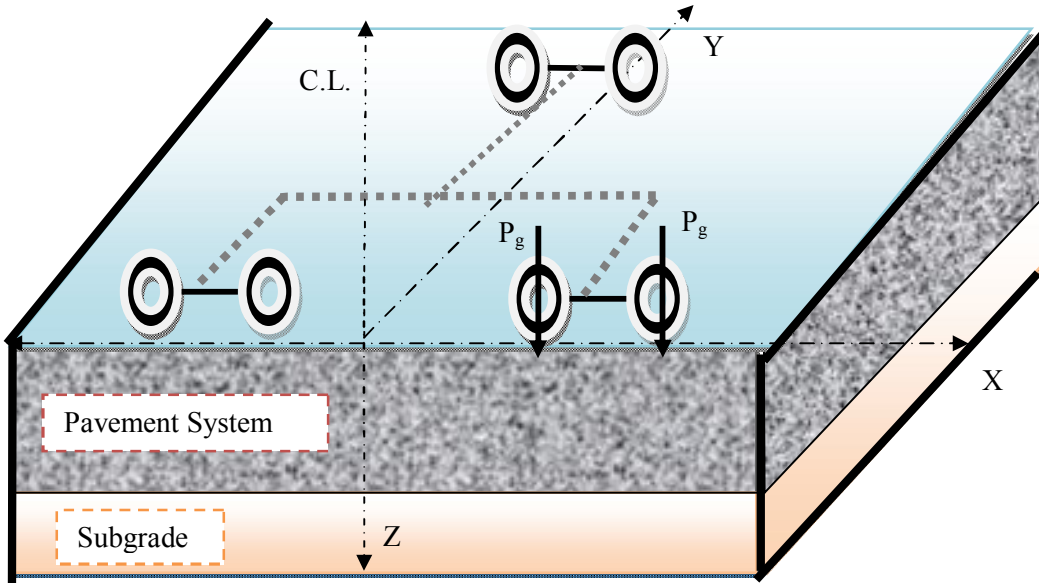


FIGURE 3-18 Load distribution for aircraft with dual tire gear.

- xi. Introduce the P_g , CC , and number of tires to the program to find the maximum strain at the top of subgrade (ϵ_{vsg}) that occurred by this load. Several items that should be kept in mind are that the location and the value of the maximum strain at the top of subgrade were found as described in section 3.2.5.1. To be noted, the location of this value depends upon many factors such as aircraft load, number of tires in the main gear, the tires arrangement and position of the main gear (below the aircraft's body or beneath the wings).
- xii. From the program, there are up to 88 points that the deflection can be calculated. In this case, these points would be located in the strip that has the maximum strain at the top of subgrade.

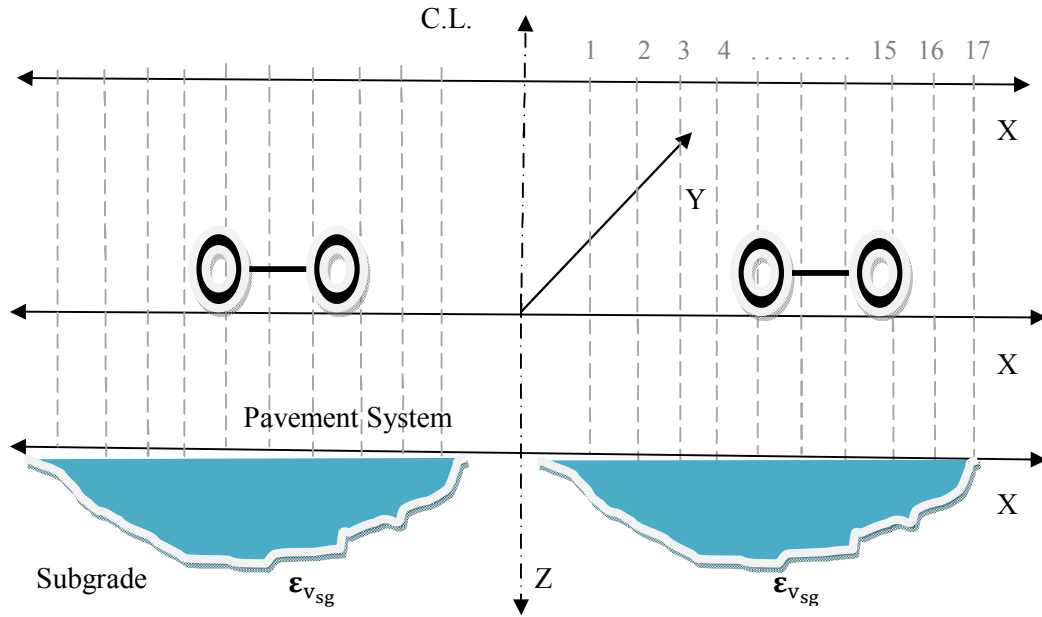


Figure 3-19 The maximum strain at the top of subgrade.

In the ZAPMRAM program, Boussinesq one-layer theory is used to calculate the strain for transformed pavement section. Also the contact area, A_c , for all tires of the multiple gear are assumed equal. For these assumptions, the maximum interface vertical strain at the given depth can be calculated.

xiii. After that, the program determines the largest strain along X_i .

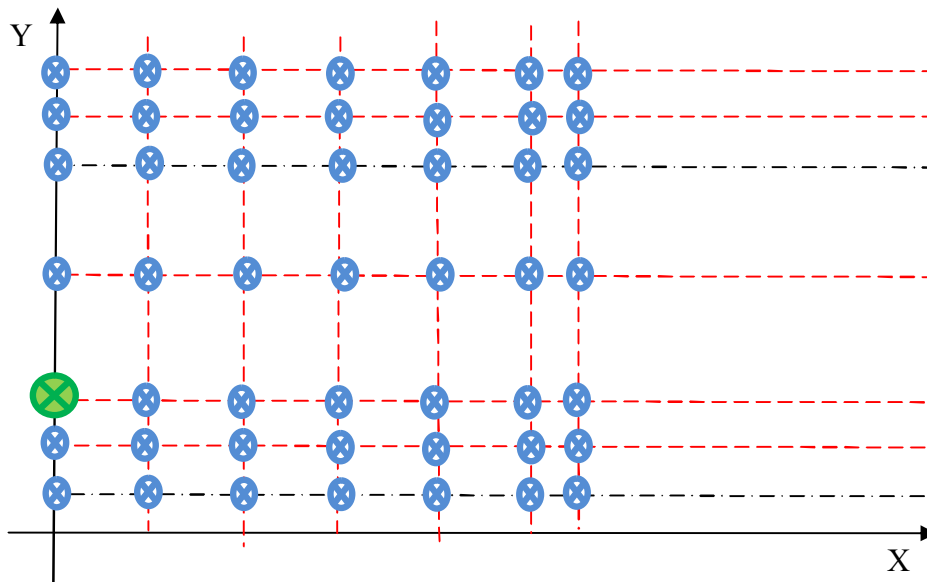


FIGURE 3-20 Determines the largest strain along X_i .

- xiv. The program will repeat selecting the largest strain for all X_i .
- xv. Develop the maximum strain for all the selected points along X_i .

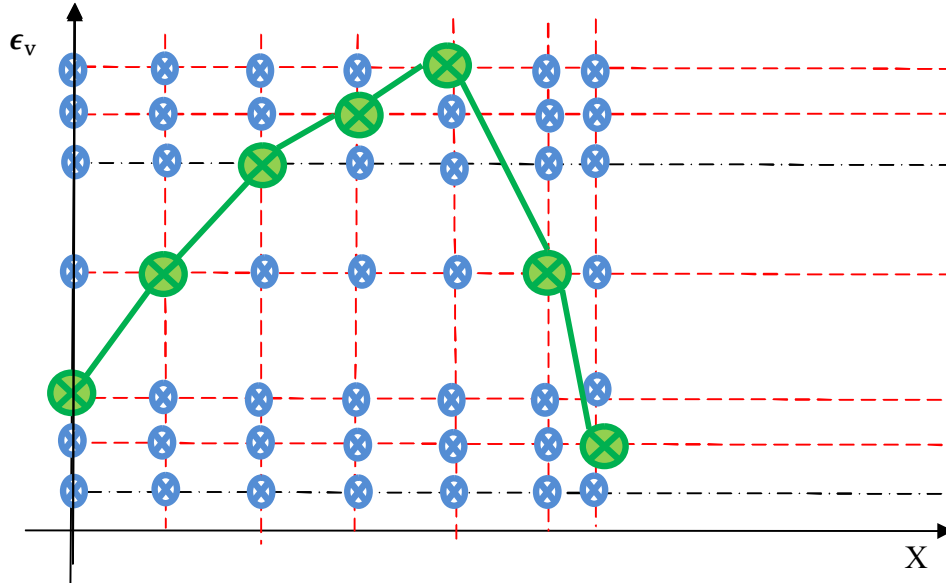


FIGURE 3-21 Maximum strain for all the points along X_i .

- xvi. It is desired to have the maximum strain beneath the multiple main gears. The vertical strains at the top of the subgrade are calculated for 88 points under the gear system. Rutting results of asphalt concrete have shown that the number of repetitions to failure N_f can be related to the strain at the top of the subgrade by several formulas developed from different agencies (see the section 3.2.6.2). For example the Shell Oil equation is:

$$N_f = 5.6056E-09 * (1 / \epsilon_{vsg})^{4.785} \quad (3-11)$$

Where:

N_f = allowable repetitions to failure;

ϵ_{vsg} = Vertical strain at the top of subgrade (" / ");

By using one of these equations, N_f can be calculated. FIGURE 3-22 illustrates the distribution N_f underneath the selected strip.

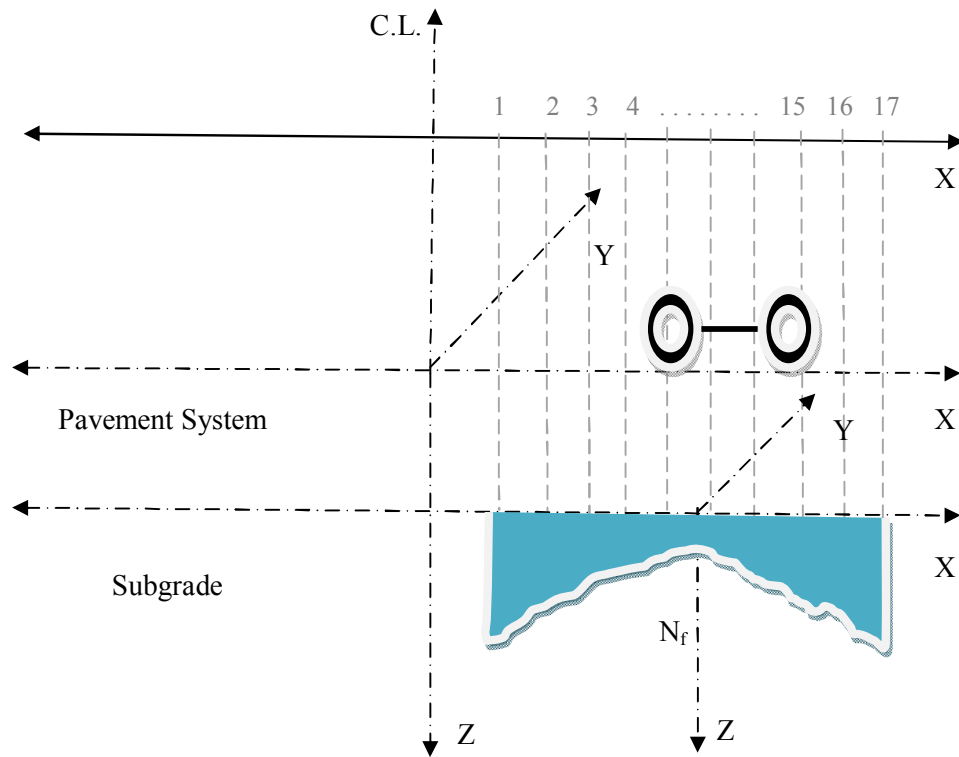


FIGURE 3-22 The distribution N_f underneath the selected strip.

xvii. Unit Damage Computation (d_j):

Unit damage defines the damage per pass caused to a specific pavement system by the vehicle; it is calculated by the equation.

$$\text{Unit damage } d_j = \frac{1}{N_{fj}} \quad (3-12)$$

Beneath every point of the computational points, the unit damage is determined.

Figure 3-23 illustrates the unit damage caused to a specific pavement by the specific aircraft.

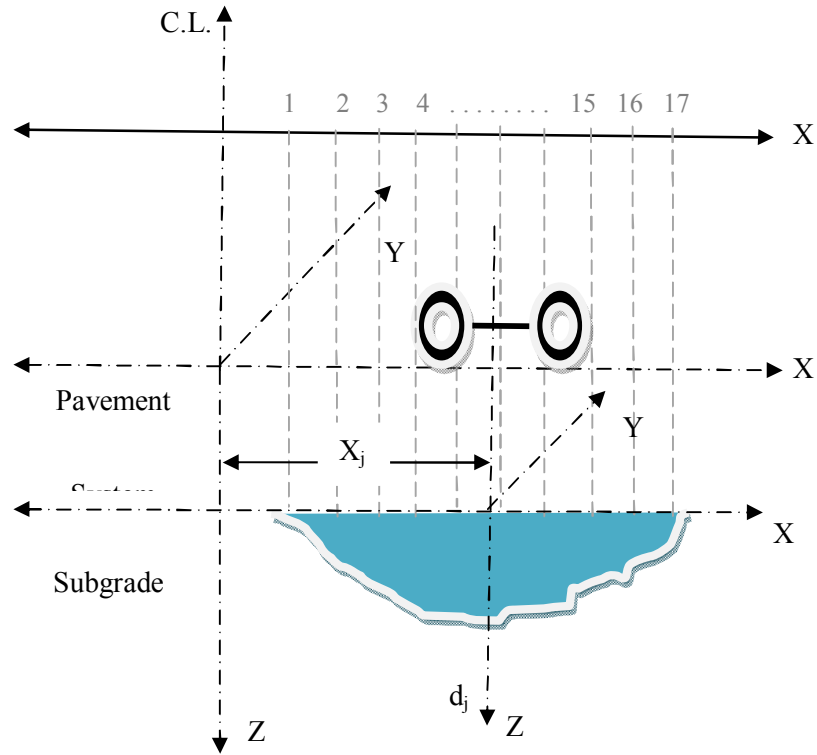


Figure 3-23 The unit damage caused to specific pavement by certain aircraft.

xviii. Aircraft Wander:

The general conditions used for developing the expression for traffic analysis of either highway or airfield pavements are the lateral wander of the vehicle. It is assumed to wander laterally such that the frequency of the deflection (stress, strain) repetitions of the j^{th} vehicle along the pavement interval will vary. This condition is shown in FIGURE 3-24:

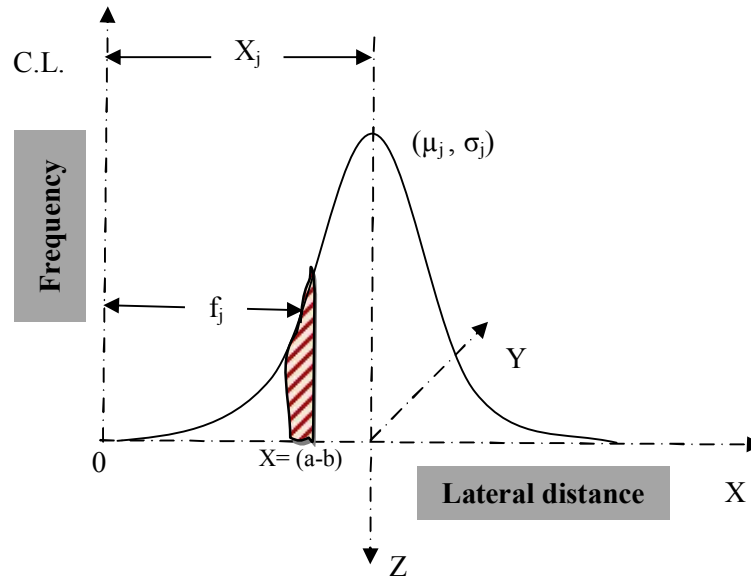


FIGURE 3-24 Distribution of wander laterally of the vehicle.

The value of X_j for Airfields represents the distance from the aircraft centerline to the geometric center of each main gear.

This distribution would be identified for specific aircraft and determined the $(x_j, \mu_j, \text{ and } \sigma_j)$. When the distribution of the wander laterally for a specific aircraft is known, f_j can be estimated at one foot intervals along the pavement interval $x(a-b)$.

xix. The Damage Distribution

Aircraft that are moving along an airfield pavement generally do not travel in the exact transverse locations since they pose some lateral wander associated with their movements.

When considering the effect that the wander has upon aircraft movements, the probable location of the maximum load repetitions and hence the probable maximum damage location should be taken in mind. For that reason the unit damage for particular aircraft will be constantly changing along the airfield pavement to match the phenomenon.

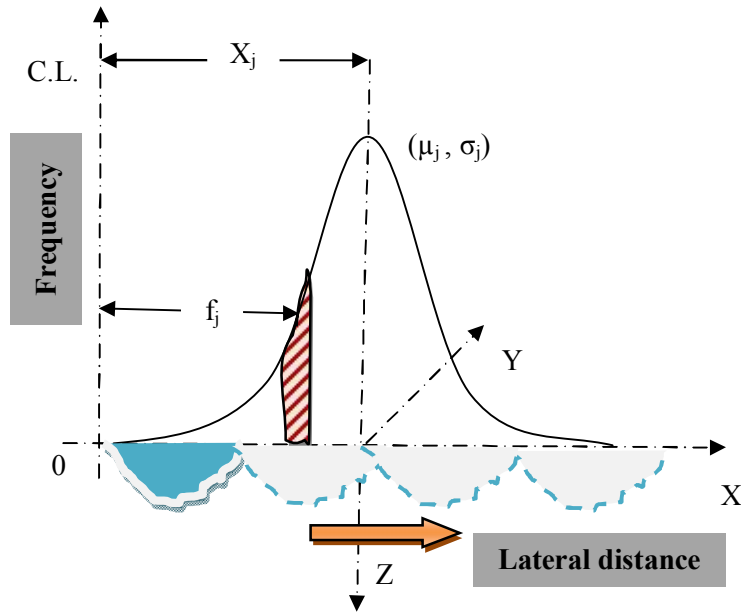


FIGURE 3-25 The unit damage for particular aircraft moving laterally long the airfield pavement.

xx. Total Damage Accumulated by the Aircraft

Considering one aircraft is moving on the pavement, the total damage accumulated by the aircraft, D_j , due to p_j passes within the time t , at any pavement interval can be calculated as:

$$D_j = P_j \times d_j \times f_j \quad (3-13)$$

This is schematically illustrated in FIGURE 3-26

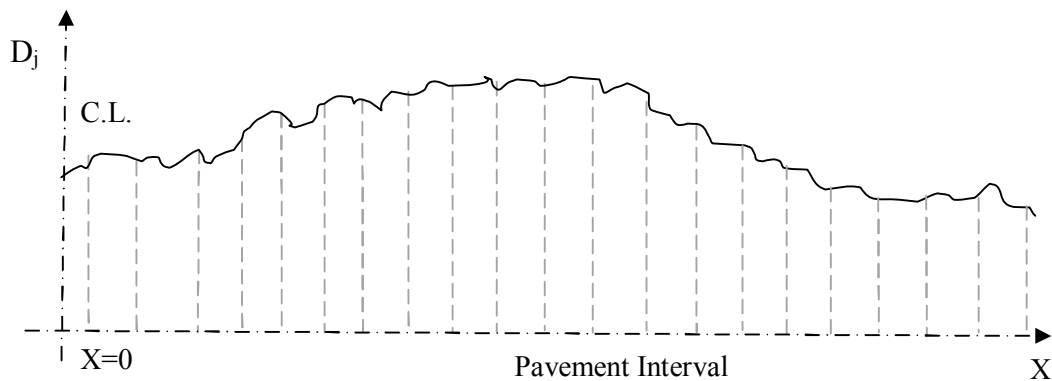


FIGURE 3-26 Total damage accumulated by the aircraft.

CHAPTER 4 EVALUATION OF OPTIMAL DIFFERENTIAL AREAS IN NUMERICAL INTEGRATION PROCESS

4.1 Introduction

This research task focused on the evaluation of the optimal differential areas used in the resolution of vertical stress and strain calculations. The size of the differential area used in the numerical integration process affects the precision of the pavement response prediction. This in turn, has a direct effect on the computational time involved in the analysis. Two different tire imprint shapes are used in ZAPRAM; circular and elliptical (rectangular) tire imprint shapes. The major objective of this study is to insure the minimum threshold number of computational points the user should use at a specific depth within the pavement system.

As noted, there is a direct tradeoff between the optimal number of runs that the user should perform to run the program and a reasonable minimal time to establish the computations. This investigation will identify the condition and specification for the elliptical (rectangular) tire imprint shape (number of longitudinal segments (dy) and transverse segments (dx) leading to the area (dA) of tire imprint and the number of radial segments (dr) and size of angular segments ($d\theta$) leading to the area (dA) of the tire imprint). In addition, it will also demonstrate the requirements for a circular tire imprint shape number through the optimum number of radial segments (dr) in tire imprint, and the size of angular segments ($d\theta$) in tire imprint.

4.2 Selected Aircraft:

ZAPRAM has a list of aircraft with their gear load characterizations, which the user can choose from. The Aircraft used for this investigation was the Airbus A-380 that is shown in FIGURE 4-1 and FIGURE 4-2.



FIGURE 4-1 The airbus A-380.

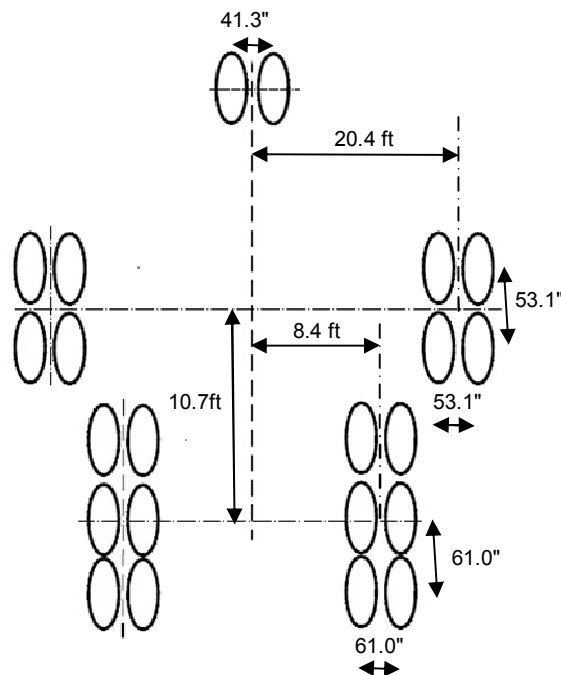


FIGURE 4-2 Tire configuration of the A-380 airbus.

4.2.1 Aircraft characteristics list for Airbus A-380:

- I. Maximum Gross Weight $w_t = 1258.9$ kips
- II. Number of tires in the main gear.
 - i. Two Dual Wheels (4 tires)
 - ii. Three Dual Wheels (6 tires)
- III. Load per Tire (lb)
 - i. Two Dual Wheels (59,400)
 - ii. Three Dual Wheels (59,400)
- IV. Distance between the loading points, S_d (in) .
 - i. Two Dual Wheels (53.1)
 - ii. Three Dual Wheels (61.0)
- V. Tire pressure (psi).
 - i. Two Dual Wheels (218)
 - ii. Three Dual Wheels (218)
- VI. Distance to Mean Location of Load, x_j (ft)
 - i. Two Dual Wheels ($X_j = 20.4$)
 - ii. Three Dual Wheels ($X_j = 8.4$)

The FIGURE 4-3 shows the tire location (in) for the chosen Aircraft:

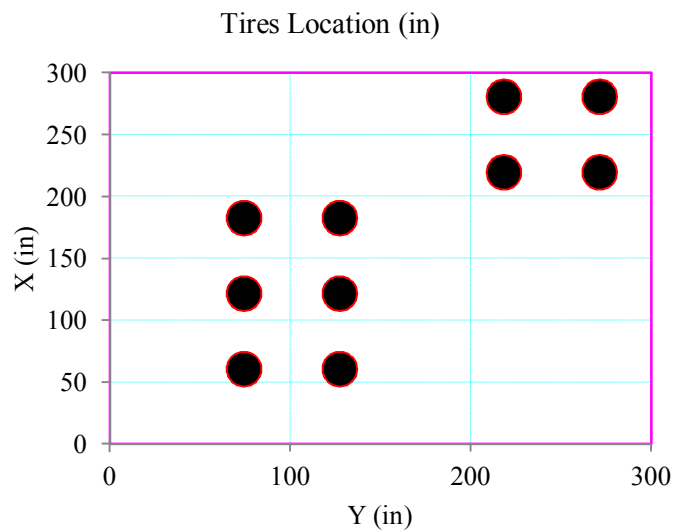


FIGURE 4-3 Tires location for airbus A380.

4.3 Pavement System Utilized:

A pavement system with three layers was used for the stress-study; this pavement is shown in FIGURE 4-4.

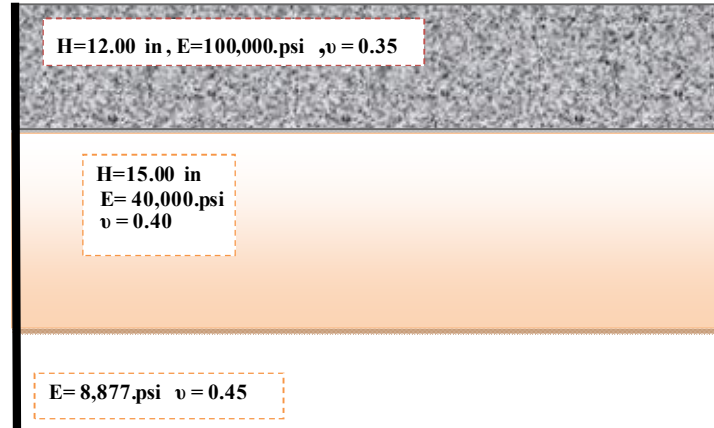


FIGURE 4-4 The pavement system that was used in comparison.

TABLE 4-1 illustrates the input parameters used in the pavement structure:

TABLE 4-1 Properties of Layer Materials in Pavement Structure

| Layer Number | 1 | 2 | 3 |
|---|---------|------------|----------|
| Material Type | Asphalt | Gran. Base | Subgrade |
| Thickness (in) | 12 | 30 | |
| Poisson Ratio, ν | 0.35 | 0.4 | 0.45 |
| E* or E at Optimum Conditions, (psi) | 100000 | 40000 | 8877 |
| CBR (%) | | | 7 |
| Soil Classification (AASHTO or SUCS) | | A-1-a | |
| Percentage Passing Sieve #200, P200 | | 9 | 80 |
| Plasticity Index, PI | | 0.8 | 28 |
| Specific Gravity of Solids, G_s | | 2.65 | 2.68 |
| Optimum Moisture Content, w_{opt} % | | 7 | 20 |
| Maximum Dry Density, γ_d max (pcf) | | 138 | 102 |
| Ground Water Table Depth, (ft). | | 90 | |

4.4 Plan Study:

Three different depths (deep- middle – shallow) were evaluated in this study. At each depth the program was conducted by using the two different tire imprint shapes

noted (circular and elliptical tire imprint shapes). The program was run 26 times for every tire imprint shape and at each specific depth by increasing the number of computational points, i.e., varying the size of the dA used in the numerical interpretation routine. The specific computational times required by the program to calculate the stresses and strains were then recorded, along with the values of the vertical strain and vertical stress. As the number of computational points increases, the stress and strain value will become more stable and converge to the specific (true) value. The true value (target) determined as the value of strain/stress which is calculated from the program at cycle 26 (The last cycle with largest number of computational points). Furthermore, the percentage difference between the calculated value and the target value was recorded for every cycle and summarized in tabular form.

The selected points for this study used the Cartesian coordinate $x=100.8$ in and $y=122.0$ in. This point was selected to be at the middle of the configuration of the aircraft assembly. The three depths, (Z Cartesian coordinate) selected for the study varied from:

Deep ($Z=150.00$ in) - Middle ($Z=79.57$ in) - Shallow ($Z=20.00$ in).

The total program runs were 156 times (3 depths, 2 tire imprint shapes, and 26 computational points).

4.5 The Study for Deep Depth ($Z=150.00$ in).

4.5.1 Analysis for Circular Tire Imprint Shape (Deep Depth)

TABLE 4-2 illustrates the input and the results for the circular tire imprint shape at a computational depth of $Z=150$ in. Also shown, are the times taken by the program to complete the run.

TABLE 4-2 Analysis for Circular Tire Imprint Shape (Z=150 in)

| X (in) Y (in) Z (in) | | | Time | | | | (ZAPMEDACA) | | | | Target Value | | Percentage Diff, % | |
|-----------------------|----|--------|---------------------------|-----------|--------|--------|----------------------|----------------------|----------------------|------------------------|----------------------|------------------------|--------------------|----------------|
| 100.8 122 150.00 | | | | | | | | | | | | | | |
| N | Dr | dφ (°) | # of computational points | 1/100 sec | sec | min | σ _z (psi) | σ _x (psi) | σ _y (psi) | ε _z (in/in) | σ _z (psi) | ε _z (in/in) | σ _z | ε _z |
| 1 | 1 | 72 | 5 | 2.7 | 0.027 | 0.0005 | 6.0212 | 0.45641 | 0.71960 | 0.0005663 | 6.0141 | 0.0005655 | 0.12 | 0.14 |
| 2 | 1 | 36 | 10 | 3.6 | 0.036 | 0.0006 | 6.0212 | 0.45641 | 0.71960 | 0.0005663 | 6.0141 | 0.0005655 | 0.12 | 0.14 |
| 3 | 2 | 30 | 24 | 4.4 | 0.044 | 0.0007 | 6.0159 | 0.45763 | 0.71971 | 0.0005657 | 6.0141 | 0.0005655 | 0.03 | 0.04 |
| 4 | 2 | 18 | 40 | 9 | 0.090 | 0.0015 | 6.0159 | 0.45763 | 0.71971 | 0.0005657 | 6.0141 | 0.0005655 | 0.03 | 0.04 |
| 5 | 3 | 15 | 72 | 12.6 | 0.126 | 0.0021 | 6.0149 | 0.45786 | 0.71973 | 0.0005656 | 6.0141 | 0.0005655 | 0.01 | 0.02 |
| 6 | 3 | 12 | 90 | 14.4 | 0.144 | 0.0024 | 6.0149 | 0.45786 | 0.71973 | 0.0005656 | 6.0141 | 0.0005655 | 0.01 | 0.02 |
| 7 | 4 | 12 | 120 | 18.4 | 0.184 | 0.0031 | 6.0145 | 0.45794 | 0.71974 | 0.0005655 | 6.0141 | 0.0005655 | 0.01 | 0.01 |
| 8 | 5 | 12 | 150 | 21.6 | 0.216 | 0.0036 | 6.0144 | 0.45798 | 0.71974 | 0.0005655 | 6.0141 | 0.0005655 | 0.00 | 0.01 |
| 9 | 6 | 10 | 216 | 26.8 | 0.268 | 0.0045 | 6.0143 | 0.45800 | 0.71974 | 0.0005655 | 6.0141 | 0.0005655 | 0.00 | 0.00 |
| 10 | 8 | 9 | 320 | 38.3 | 0.383 | 0.0064 | 6.0142 | 0.45802 | 0.71975 | 0.0005655 | 6.0141 | 0.0005655 | 0.00 | 0.00 |
| 11 | 10 | 8 | 450 | 52.8 | 0.528 | 0.0088 | 6.0142 | 0.45803 | 0.71975 | 0.0005655 | 6.0141 | 0.0005655 | 0.00 | 0.00 |
| 12 | 10 | 6 | 600 | 71.6 | 0.716 | 0.0119 | 6.0142 | 0.45803 | 0.71975 | 0.0005655 | 6.0141 | 0.0005655 | 0.00 | 0.00 |
| 13 | 12 | 6 | 720 | 85.2 | 0.852 | 0.0142 | 6.0141 | 0.45803 | 0.71975 | 0.0005655 | 6.0141 | 0.0005655 | 0.00 | 0.00 |
| 14 | 12 | 5 | 864 | 102.7 | 1.027 | 0.0171 | 6.0141 | 0.45803 | 0.71975 | 0.0005655 | 6.0141 | 0.0005655 | 0.00 | 0.00 |
| 15 | 15 | 5 | 1080 | 140.8 | 1.408 | 0.0235 | 6.0141 | 0.45804 | 0.71975 | 0.0005655 | 6.0141 | 0.0005655 | 0.00 | 0.00 |
| 16 | 14 | 4 | 1260 | 146.6 | 1.466 | 0.0244 | 6.0141 | 0.45803 | 0.71975 | 0.0005655 | 6.0141 | 0.0005655 | 0.00 | 0.00 |
| 17 | 17 | 4 | 1530 | 178.1 | 1.781 | 0.0297 | 6.0141 | 0.45804 | 0.71975 | 0.0005655 | 6.0141 | 0.0005655 | 0.00 | 0.00 |
| 18 | 20 | 4 | 1800 | 201.9 | 2.019 | 0.0337 | 6.0141 | 0.45804 | 0.71975 | 0.0005655 | 6.0141 | 0.0005655 | 0.00 | 0.00 |
| 19 | 18 | 3 | 2160 | 246.2 | 2.462 | 0.0410 | 6.0141 | 0.45804 | 0.71975 | 0.0005655 | 6.0141 | 0.0005655 | 0.00 | 0.00 |
| 20 | 25 | 3 | 3000 | 338.6 | 3.386 | 0.0564 | 6.0141 | 0.45804 | 0.71975 | 0.0005655 | 6.0141 | 0.0005655 | 0.00 | 0.00 |
| 21 | 24 | 2 | 4320 | 485.1 | 4.851 | 0.0809 | 6.0141 | 0.45804 | 0.71975 | 0.0005655 | 6.0141 | 0.0005655 | 0.00 | 0.00 |
| 22 | 30 | 2 | 5400 | 599 | 5.990 | 0.0998 | 6.0141 | 0.45804 | 0.71975 | 0.0005655 | 6.0141 | 0.0005655 | 0.00 | 0.00 |
| 23 | 35 | 2 | 6300 | 715.9 | 7.159 | 0.1193 | 6.0141 | 0.45804 | 0.71975 | 0.0005655 | 6.0141 | 0.0005655 | 0.00 | 0.00 |
| 24 | 20 | 1 | 7200 | 804.7 | 8.047 | 0.1341 | 6.0141 | 0.45804 | 0.71975 | 0.0005655 | 6.0141 | 0.0005655 | 0.00 | 0.00 |
| 25 | 23 | 1 | 8280 | 925.5 | 9.255 | 0.1543 | 6.0141 | 0.45804 | 0.71975 | 0.0005655 | 6.0141 | 0.0005655 | 0.00 | 0.00 |
| 26 | 25 | 1 | 9000 | 10039 | 10.039 | 0.1673 | 6.0141 | 0.45804 | 0.71975 | 0.0005655 | 6.0141 | 0.0005655 | 0.00 | 0.00 |

FIGURE 4-5 shows the relationship between time and the number of dA while FIGURE 4-6 shows the relationship between the vertical stress and the number of dA. The relationship between the vertical strain and the number of dA is shown in FIGURE 4-7.

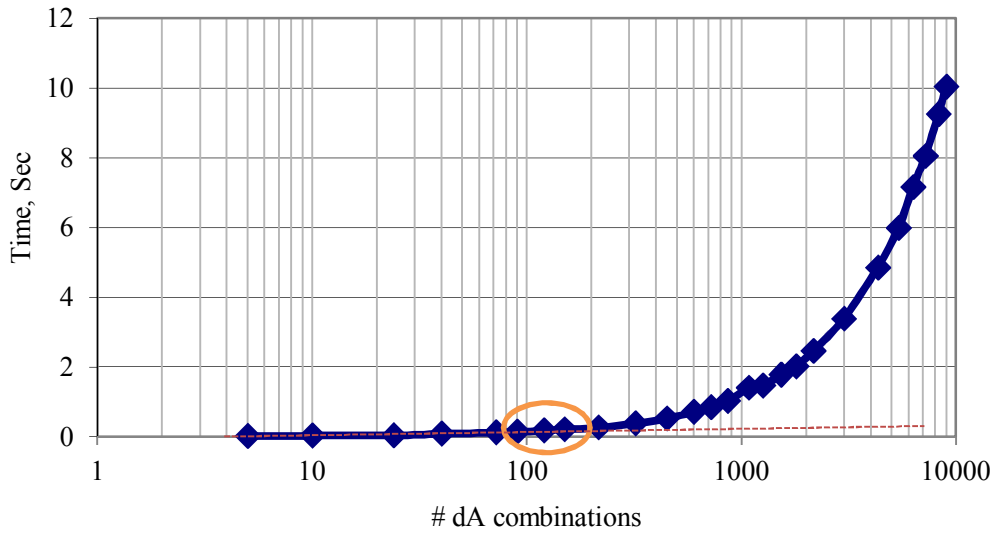


FIGURE 4-5 Time and number of dA analysis for circular tire imprint shape (Z=150 in).

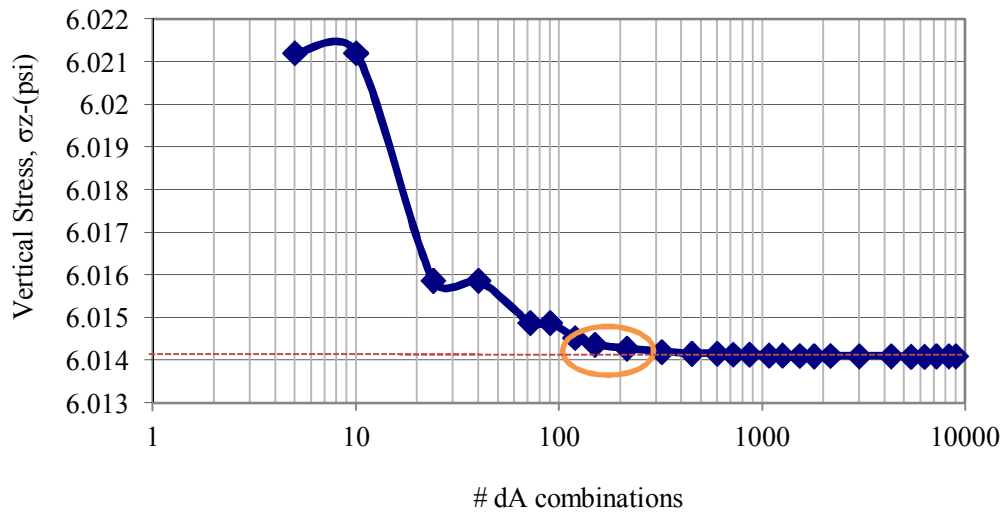


FIGURE 4-6 Vertical stress and number of dA analysis for circular tire imprint shape (Z=150 in).

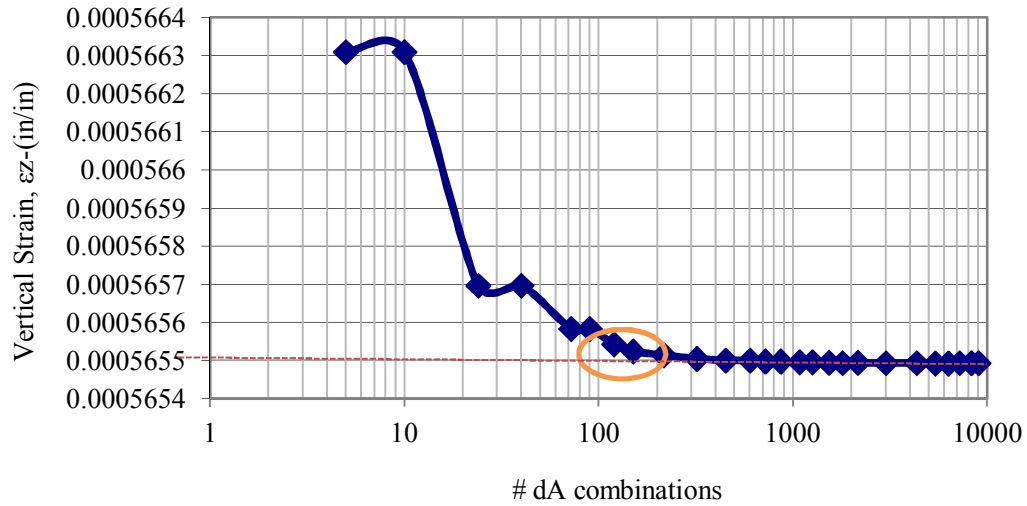


FIGURE 4-7 Vertical strain and number of dA analysis for circular tire imprint shape ($Z=150$ in).

From the previous tables and figures, the following points could be concluded:

- i. After a certain point (number of dA combinations), the number of sectors used leads to a stress/strain value that stabilizes at a certain value at which further increases in the number of dA areas in the segment does not matter.
- ii. For the circular tire shape at the deep depth, the range of # dA combinations (100-150) was found to be optimal in relation to time and best strain and stress values.
- iii. In general, a range of $dr = (3-5)$, and $d\phi = (10^\circ - 12^\circ)$ appears to be a good number to use for circular tire shape calculation with deep depth.

4.5.2 Analysis for Elliptical Tire Imprint Shape (Deep Depth)

TABLE 4-3 illustrates the input and the results for elliptical tire Imprint shape with $Z=150$ in. Moreover, the time taken by the program to do the run was recorded and listed.

TABLE 4-3 Analysis for Elliptical Tire Imprint Shape (Z=150 in)

| N | dx | dy | dr | X (in) | | Z (in) | 1/100 sec | Time sec | (ZAPMEDACA) | | | | | Target Value | | Percentage Diff, % | |
|----|----|----|----|--------|-------|--------|--------------|-------------|---------------------|---------------------|---------------------|-------------------------|---------------------|-------------------------|------------|-----------------------|------|
| | | | | 100.8 | 122.0 | 150.00 | | | σ_z (psi) | σ_x (psi) | σ_y (psi) | ϵ_z (in/in) | σ_z (psi) | ϵ_z (in/in) | σ_z | ϵ_z | |
| 1 | 1 | 4 | 1 | 90 | 4 | 8 | 2.2 | 0.022 | 0.0004 | 6.0193 | 0.45542 | 0.72025 | 0.0005661 | 6.0136 | 0.0005655 | 0.09 | 0.12 |
| 2 | 2 | 3 | 2 | 72 | 5 | 16 | 4.5 | 0.045 | 0.0008 | 6.0127 | 0.45468 | 0.72098 | 0.0005654 | 6.0136 | 0.0005655 | 0.02 | 0.01 |
| 3 | 2 | 5 | 2 | 60 | 6 | 22 | 6 | 0.060 | 0.0010 | 6.0150 | 0.45657 | 0.72026 | 0.0005656 | 6.0136 | 0.0005655 | 0.02 | 0.03 |
| 4 | 3 | 6 | 3 | 60 | 6 | 36 | 9 | 0.090 | 0.0015 | 6.0142 | 0.45678 | 0.72026 | 0.0005655 | 6.0136 | 0.0005655 | 0.01 | 0.01 |
| 5 | 4 | 7 | 4 | 60 | 6 | 52 | 11.1 | 0.111 | 0.0019 | 6.0139 | 0.45686 | 0.72026 | 0.0005655 | 6.0136 | 0.0005655 | 0.00 | 0.00 |
| 6 | 6 | 7 | 6 | 54 | 6.667 | 82 | 12.4 | 0.124 | 0.0021 | 6.3899 | 0.48283 | 0.76826 | 0.0006008 | 6.0136 | 0.0005655 | 6.26 | 6.25 |
| 7 | 6 | 10 | 6 | 54 | 6.667 | 100 | 13.6 | 0.136 | 0.0023 | 6.3898 | 0.48283 | 0.76826 | 0.0006008 | 6.0136 | 0.0005655 | 6.26 | 6.25 |
| 8 | 8 | 12 | 8 | 48 | 7.5 | 156 | 19.3 | 0.193 | 0.0032 | 6.2522 | 0.47148 | 0.75185 | 0.0005879 | 6.0136 | 0.0005655 | 3.97 | 3.97 |
| 9 | 10 | 16 | 10 | 48 | 7.5 | 235 | 30.4 | 0.304 | 0.0051 | 6.2487 | 0.47208 | 0.75103 | 0.0005876 | 6.0136 | 0.0005655 | 3.91 | 3.91 |
| 10 | 11 | 18 | 11 | 30 | 12 | 330 | 37.9 | 0.379 | 0.0063 | 6.0137 | 0.45694 | 0.72025 | 0.0005655 | 6.0136 | 0.0005655 | 0.00 | 0.00 |
| 11 | 14 | 20 | 14 | 30 | 12 | 448 | 49.9 | 0.499 | 0.0083 | 6.0136 | 0.45694 | 0.72025 | 0.0005655 | 6.0136 | 0.0005655 | 0.00 | 0.00 |
| 12 | 17 | 20 | 17 | 24 | 15 | 595 | 66.8 | 0.668 | 0.0111 | 6.0128 | 0.45631 | 0.72050 | 0.0005654 | 6.0136 | 0.0005655 | 0.01 | 0.01 |
| 13 | 18 | 24 | 18 | 24 | 15 | 702 | 82.4 | 0.824 | 0.0137 | 6.0128 | 0.45632 | 0.72050 | 0.0005654 | 6.0136 | 0.0005655 | 0.01 | 0.01 |
| 14 | 20 | 24 | 20 | 20 | 18 | 840 | 94.6 | 0.946 | 0.0158 | 6.0136 | 0.45694 | 0.72025 | 0.0005655 | 6.0136 | 0.0005655 | 0.00 | 0.00 |
| 15 | 22 | 26 | 22 | 20 | 18 | 968 | 106.9 | 1.069 | 0.0178 | 6.0136 | 0.45694 | 0.72025 | 0.0005655 | 6.0136 | 0.0005655 | 0.00 | 0.00 |
| 16 | 24 | 28 | 24 | 18 | 20 | 1152 | 124.4 | 1.244 | 0.0207 | 6.0136 | 0.45695 | 0.72025 | 0.0005655 | 6.0136 | 0.0005655 | 0.00 | 0.00 |
| 17 | 26 | 30 | 26 | 18 | 20 | 1300 | 146 | 1.460 | 0.0243 | 6.0136 | 0.45695 | 0.72025 | 0.0005655 | 6.0136 | 0.0005655 | 0.00 | 0.00 |
| 18 | 29 | 32 | 29 | 15 | 24 | 1624 | 174.1 | 1.741 | 0.0290 | 6.0136 | 0.45695 | 0.72025 | 0.0005655 | 6.0136 | 0.0005655 | 0.00 | 0.00 |
| 19 | 34 | 35 | 34 | 15 | 24 | 2006 | 216.9 | 2.169 | 0.0362 | 6.0136 | 0.45695 | 0.72025 | 0.0005655 | 6.0136 | 0.0005655 | 0.00 | 0.00 |
| 20 | 40 | 45 | 40 | 12 | 30 | 3000 | 319 | 3.190 | 0.0532 | 6.0136 | 0.45695 | 0.72025 | 0.0005655 | 6.0136 | 0.0005655 | 0.00 | 0.00 |
| 21 | 43 | 60 | 43 | 10 | 36 | 4128 | 467.4 | 4.674 | 0.0779 | 6.0136 | 0.45695 | 0.72025 | 0.0005655 | 6.0136 | 0.0005655 | 0.00 | 0.00 |
| 22 | 45 | 70 | 45 | 8 | 45 | 5175 | 552.9 | 5.529 | 0.0922 | 6.0134 | 0.45674 | 0.72033 | 0.0005654 | 6.0136 | 0.0005655 | 0.00 | 0.00 |
| 23 | 46 | 80 | 46 | 6 | 60 | 6440 | 691.4 | 6.914 | 0.1152 | 6.0136 | 0.45695 | 0.72025 | 0.0005655 | 6.0136 | 0.0005655 | 0.00 | 0.00 |
| 24 | 48 | 90 | 48 | 5 | 72 | 7776 | 822.4 | 8.224 | 0.1371 | 6.0136 | 0.45695 | 0.72025 | 0.0005655 | 6.0136 | 0.0005655 | 0.00 | 0.00 |
| 25 | 50 | 90 | 50 | 4 | 90 | 9000 | 973.7 | 9.737 | 0.1623 | 6.0136 | 0.45695 | 0.72025 | 0.0005655 | 6.0136 | 0.0005655 | 0.00 | 0.00 |
| 26 | 50 | 90 | 50 | 3 | 120 | 10500 | 1119.3 | 11.193 | 0.1866 | 6.0136 | 0.45695 | 0.72025 | 0.0005655 | 6.0136 | 0.0005655 | 0.00 | 0.00 |

FIGURE 4-8 shows the relationship between the vertical stress and number of dA load areas. FIGURE 4-9 shows the relationship between the vertical strain and number of dA values. The number of dA values analyzed was selected randomly. During this analysis, it was discovered that the program gives a wrong value for the strain and stress as shown in these figures. However, the reason was found to be a result of when the user chooses the $d\phi$, $360/d\phi$ combinations that revert in a non-integer value. As a result, the program was repeated one more time to correct the mistake.

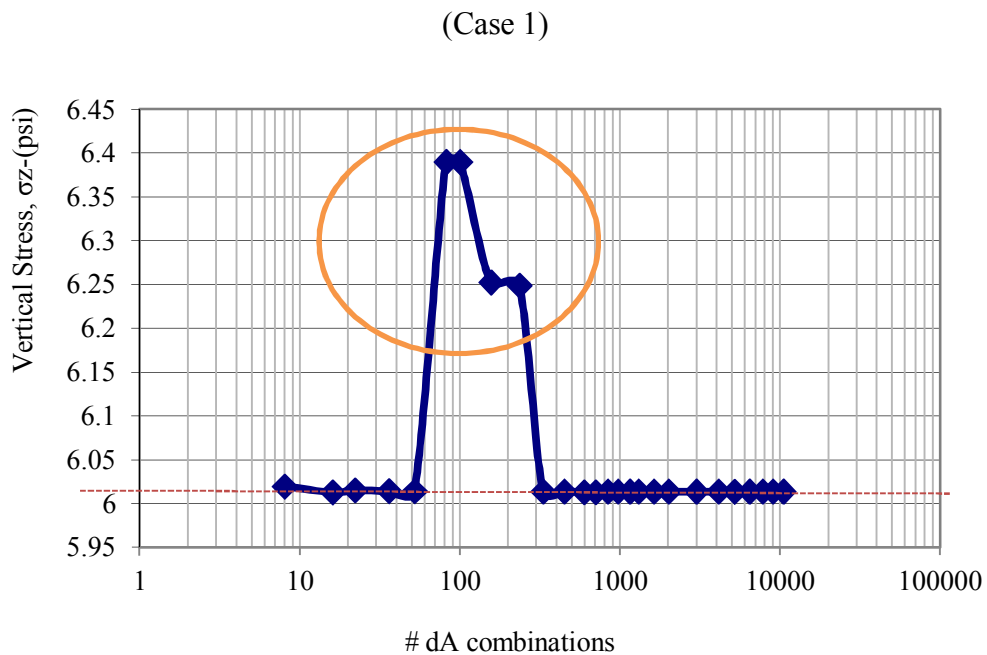


FIGURE 4-8 Vertical stress and number of dA analysis for elliptical tire imprint shape ($Z=150$ in).

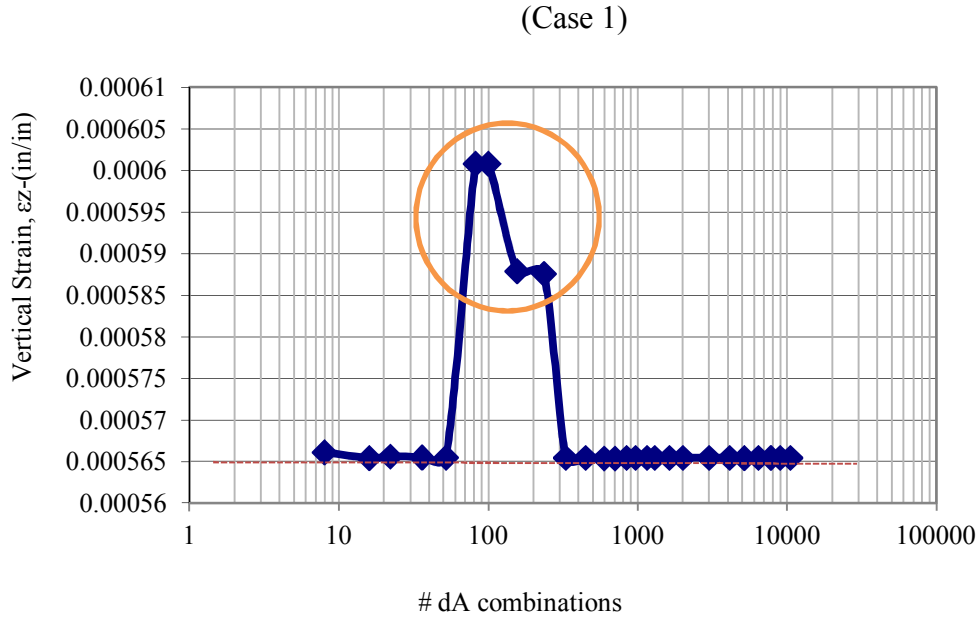


FIGURE 4-9 Vertical strain and number of da analysis for elliptical tire imprint shape (Z=150 in).

TABLE 4-4 illustrates the input and the results for an elliptical tire Imprint shape with Z=150 in and all $(360/d\phi)$ values as an integer. Also, the time taken by the program to do a run was recorded and listed.

After the $360/d\phi$ was corrected to be an integer value, for some reason, the program still give a mistaken value for the strain and stress values as shown in the figures below. To correct this, the $d\phi$, $360/d\phi$ was selected not to be an odd value. As a result, the program was run one more time to correct the mistake.

TABLE 4-4 Analysis for Elliptical Tire Imprint Shape (Z=150 in) - 360/dφ is Integer

| N | dx | dy | dr | X (in) | | Y (in) | | Z (in) | | Time | | | | Target Value | | Percentage Diff, % | |
|----|----|----|----|--------|-------|--------|-----------|--------|--------|----------------------|----------------------|----------------------|------------------------|----------------------|------------------------|--------------------|----------------|
| | | | | 100.8 | 122.0 | 150.00 | 1/100 sec | sec | min | σ _z (psi) | σ _x (psi) | σ _y (psi) | ε _z (in/in) | σ _z (psi) | ε _z (in/in) | σ _z | ε _z |
| 1 | 1 | 4 | 1 | 90 | 4 | 8 | 2.2 | 0.022 | 0.0004 | 6.0193 | 0.45542 | 0.72025 | 0.0005661 | 6.0136 | 0.0005655 | 0.09 | 0.12 |
| 2 | 2 | 3 | 2 | 72 | 5 | 16 | 4.5 | 0.045 | 0.0008 | 6.0127 | 0.45468 | 0.72098 | 0.0005654 | 6.0136 | 0.0005655 | 0.02 | 0.01 |
| 3 | 2 | 5 | 2 | 60 | 6 | 22 | 6 | 0.060 | 0.0010 | 6.0150 | 0.45657 | 0.72026 | 0.0005656 | 6.0136 | 0.0005655 | 0.02 | 0.03 |
| 4 | 3 | 6 | 3 | 60 | 6 | 36 | 9 | 0.090 | 0.0015 | 6.0142 | 0.45678 | 0.72026 | 0.0005655 | 6.0136 | 0.0005655 | 0.01 | 0.01 |
| 5 | 4 | 7 | 4 | 60 | 6 | 52 | 11.1 | 0.111 | 0.0019 | 6.0139 | 0.45686 | 0.72026 | 0.0005655 | 6.0136 | 0.0005655 | 0.00 | 0.00 |
| 6 | 6 | 7 | 6 | 45 | 8 | 90 | 13 | 0.130 | 0.0022 | 6.0137 | 0.45691 | 0.72026 | 0.0005655 | 6.0136 | 0.0005655 | 0.00 | 0.00 |
| 7 | 6 | 10 | 6 | 45 | 8 | 108 | 16.1 | 0.161 | 0.0027 | 6.0137 | 0.45691 | 0.72026 | 0.0005655 | 6.0136 | 0.0005655 | 0.00 | 0.00 |
| 8 | 8 | 12 | 8 | 40 | 9 | 168 | 23.6 | 0.236 | 0.0039 | 6.0123 | 0.45588 | 0.72067 | 0.0005654 | 6.0136 | 0.0005655 | 0.02 | 0.02 |
| 9 | 10 | 16 | 10 | 40 | 9 | 250 | 28.2 | 0.282 | 0.0047 | 6.0123 | 0.45589 | 0.72067 | 0.0005654 | 6.0136 | 0.0005655 | 0.02 | 0.02 |
| 10 | 11 | 18 | 11 | 30 | 12 | 330 | 37.9 | 0.379 | 0.0063 | 6.0137 | 0.45694 | 0.72025 | 0.0005655 | 6.0136 | 0.0005655 | 0.00 | 0.00 |
| 11 | 14 | 20 | 14 | 30 | 12 | 448 | 49.9 | 0.499 | 0.0083 | 6.0136 | 0.45694 | 0.72025 | 0.0005655 | 6.0136 | 0.0005655 | 0.00 | 0.00 |
| 12 | 17 | 20 | 17 | 24 | 15 | 595 | 66.8 | 0.668 | 0.0111 | 6.0128 | 0.45631 | 0.72050 | 0.0005654 | 6.0136 | 0.0005655 | 0.01 | 0.01 |
| 13 | 18 | 24 | 18 | 24 | 15 | 702 | 82.4 | 0.824 | 0.0137 | 6.0128 | 0.45632 | 0.72050 | 0.0005654 | 6.0136 | 0.0005655 | 0.01 | 0.01 |
| 14 | 20 | 24 | 20 | 20 | 18 | 840 | 94.6 | 0.946 | 0.0158 | 6.0136 | 0.45694 | 0.72025 | 0.0005655 | 6.0136 | 0.0005655 | 0.00 | 0.00 |
| 15 | 22 | 26 | 22 | 20 | 18 | 968 | 106.9 | 1.069 | 0.0178 | 6.0136 | 0.45694 | 0.72025 | 0.0005655 | 6.0136 | 0.0005655 | 0.00 | 0.00 |
| 16 | 24 | 28 | 24 | 18 | 20 | 1152 | 124.4 | 1.244 | 0.0207 | 6.0136 | 0.45695 | 0.72025 | 0.0005655 | 6.0136 | 0.0005655 | 0.00 | 0.00 |
| 17 | 26 | 30 | 26 | 18 | 20 | 1300 | 146 | 1.460 | 0.0243 | 6.0136 | 0.45695 | 0.72025 | 0.0005655 | 6.0136 | 0.0005655 | 0.00 | 0.00 |
| 18 | 29 | 32 | 29 | 15 | 24 | 1624 | 174.1 | 1.741 | 0.0290 | 6.0136 | 0.45695 | 0.72025 | 0.0005655 | 6.0136 | 0.0005655 | 0.00 | 0.00 |
| 19 | 34 | 35 | 34 | 15 | 24 | 2006 | 216.9 | 2.169 | 0.0362 | 6.0136 | 0.45695 | 0.72025 | 0.0005655 | 6.0136 | 0.0005655 | 0.00 | 0.00 |
| 20 | 40 | 45 | 40 | 12 | 30 | 3000 | 319 | 3.190 | 0.0532 | 6.0136 | 0.45695 | 0.72025 | 0.0005655 | 6.0136 | 0.0005655 | 0.00 | 0.00 |
| 21 | 43 | 60 | 43 | 10 | 36 | 4128 | 467.4 | 4.674 | 0.0779 | 6.0136 | 0.45695 | 0.72025 | 0.0005655 | 6.0136 | 0.0005655 | 0.00 | 0.00 |
| 22 | 45 | 70 | 45 | 8 | 45 | 5175 | 552.9 | 5.529 | 0.0922 | 6.0134 | 0.45674 | 0.72033 | 0.0005654 | 6.0136 | 0.0005655 | 0.00 | 0.00 |
| 23 | 46 | 80 | 46 | 6 | 60 | 6440 | 691.4 | 6.914 | 0.1152 | 6.0136 | 0.45695 | 0.72025 | 0.0005655 | 6.0136 | 0.0005655 | 0.00 | 0.00 |
| 24 | 48 | 90 | 48 | 5 | 72 | 7776 | 822.4 | 8.224 | 0.1371 | 6.0136 | 0.45695 | 0.72025 | 0.0005655 | 6.0136 | 0.0005655 | 0.00 | 0.00 |
| 25 | 50 | 90 | 50 | 4 | 90 | 9000 | 973.7 | 9.737 | 0.1623 | 6.0136 | 0.45695 | 0.72025 | 0.0005655 | 6.0136 | 0.0005655 | 0.00 | 0.00 |
| 26 | 50 | 90 | 50 | 3 | 120 | 10500 | 1119.3 | 11.193 | 0.1866 | 6.0136 | 0.45695 | 0.72025 | 0.0005655 | 6.0136 | 0.0005655 | 0.00 | 0.00 |

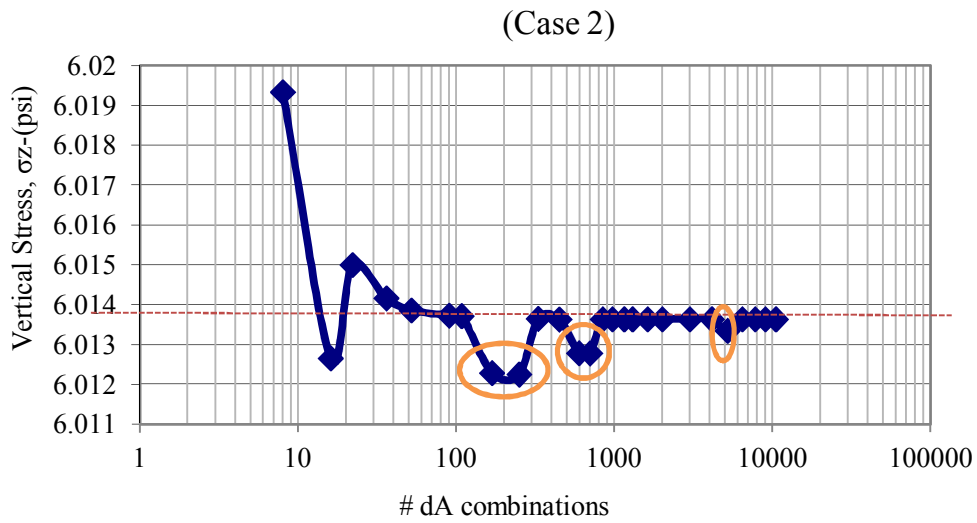


FIGURE 4-10 Vertical stress and number of dA analysis for elliptical tire imprint shape ($Z=150$ in).

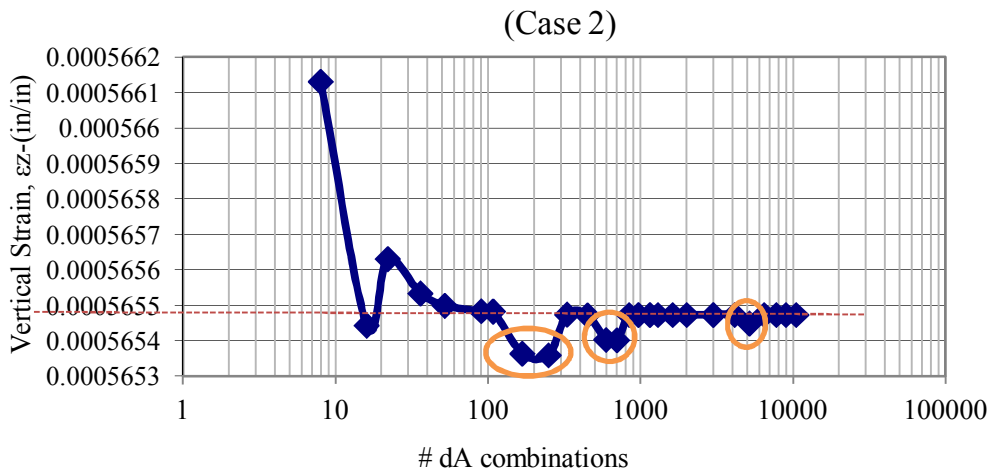


FIGURE 4-11 Vertical strain and number of dA analysis for elliptical tire imprint shape ($Z=150$ in).

TABLE 4-5 illustrates the input and the results for the elliptical tire Imprint shape with $Z=150$ in and all $360/d\phi$ being an even integer. Also, the time taken by the program to do the run was recorded and listed.

TABLE 4-5 Analysis for Elliptical Tire Imprint Shape (Z=150 in) - 360/dφ Is Integer and Even

| N | dx | dy | dr | X (in) | | Y (in) | | Z (in) | | Time | | (ZAPMEDACA) | | | | Target Value | | Percentage Diff, % | |
|----|----|----|----|--------|-------|--------|-----------|--------|--------|----------------------|----------------------|----------------------|------------------------|----------------------|------------------------|----------------|----------------|--------------------|--|
| | | | | 100.8 | 122.0 | 150.00 | 1/100 sec | sec | min | σ _z (psi) | σ _x (psi) | σ _y (psi) | ε _z (in/in) | σ _z (psi) | ε _z (in/in) | σ _z | ε _z | | |
| 1 | 1 | 4 | 1 | 90 | 4 | 8 | 2.2 | 0.022 | 0.0004 | 6.0193 | 0.45542 | 0.72025 | 0.0005661 | 6.0136 | 0.0005655 | 0.09 | 0.12 | | |
| 2 | 2 | 3 | 2 | 90 | 4 | 14 | 3.7 | 0.037 | 0.0006 | 6.0148 | 0.45657 | 0.72027 | 0.0005656 | 6.0136 | 0.0005655 | 0.02 | 0.02 | | |
| 3 | 2 | 5 | 2 | 60 | 6 | 22 | 6 | 0.060 | 0.0010 | 6.0150 | 0.45657 | 0.72026 | 0.0005656 | 6.0136 | 0.0005655 | 0.02 | 0.03 | | |
| 4 | 3 | 6 | 3 | 60 | 6 | 36 | 9 | 0.090 | 0.0015 | 6.0142 | 0.45678 | 0.72026 | 0.0005655 | 6.0136 | 0.0005655 | 0.01 | 0.01 | | |
| 5 | 4 | 7 | 4 | 60 | 6 | 52 | 11.1 | 0.111 | 0.0019 | 6.0139 | 0.45686 | 0.72026 | 0.0005655 | 6.0136 | 0.0005655 | 0.00 | 0.00 | | |
| 6 | 6 | 7 | 6 | 45 | 8 | 90 | 13 | 0.130 | 0.0022 | 6.0137 | 0.45691 | 0.72026 | 0.0005655 | 6.0136 | 0.0005655 | 0.00 | 0.00 | | |
| 7 | 6 | 10 | 6 | 45 | 8 | 108 | 16.1 | 0.161 | 0.0027 | 6.0137 | 0.45691 | 0.72026 | 0.0005655 | 6.0136 | 0.0005655 | 0.00 | 0.00 | | |
| 8 | 8 | 12 | 8 | 36 | 10 | 176 | 24.2 | 0.242 | 0.0040 | 6.0137 | 0.45693 | 0.72025 | 0.0005655 | 6.0136 | 0.0005655 | 0.00 | 0.00 | | |
| 9 | 10 | 16 | 10 | 36 | 10 | 260 | 31.3 | 0.313 | 0.0052 | 6.0137 | 0.45693 | 0.72025 | 0.0005655 | 6.0136 | 0.0005655 | 0.00 | 0.00 | | |
| 10 | 11 | 18 | 11 | 30 | 12 | 330 | 37.9 | 0.379 | 0.0063 | 6.0137 | 0.45694 | 0.72025 | 0.0005655 | 6.0136 | 0.0005655 | 0.00 | 0.00 | | |
| 11 | 14 | 20 | 14 | 30 | 12 | 448 | 49.9 | 0.499 | 0.0083 | 6.0136 | 0.45694 | 0.72025 | 0.0005655 | 6.0136 | 0.0005655 | 0.00 | 0.00 | | |
| 12 | 17 | 20 | 17 | 30 | 12 | 544 | 61.1 | 0.611 | 0.0102 | 6.0136 | 0.45694 | 0.72025 | 0.0005655 | 6.0136 | 0.0005655 | 0.00 | 0.00 | | |
| 13 | 18 | 24 | 18 | 20 | 18 | 756 | 88.8 | 0.888 | 0.0148 | 6.0136 | 0.45694 | 0.72025 | 0.0005655 | 6.0136 | 0.0005655 | 0.00 | 0.00 | | |
| 14 | 20 | 24 | 20 | 20 | 18 | 840 | 94.6 | 0.946 | 0.0158 | 6.0136 | 0.45694 | 0.72025 | 0.0005655 | 6.0136 | 0.0005655 | 0.00 | 0.00 | | |
| 15 | 22 | 26 | 22 | 20 | 18 | 968 | 106.9 | 1.069 | 0.0178 | 6.0136 | 0.45694 | 0.72025 | 0.0005655 | 6.0136 | 0.0005655 | 0.00 | 0.00 | | |
| 16 | 24 | 28 | 24 | 18 | 20 | 1152 | 124.4 | 1.244 | 0.0207 | 6.0136 | 0.45695 | 0.72025 | 0.0005655 | 6.0136 | 0.0005655 | 0.00 | 0.00 | | |
| 17 | 26 | 30 | 26 | 18 | 20 | 1300 | 146 | 1.460 | 0.0243 | 6.0136 | 0.45695 | 0.72025 | 0.0005655 | 6.0136 | 0.0005655 | 0.00 | 0.00 | | |
| 18 | 29 | 32 | 29 | 15 | 24 | 1624 | 174.1 | 1.741 | 0.0290 | 6.0136 | 0.45695 | 0.72025 | 0.0005655 | 6.0136 | 0.0005655 | 0.00 | 0.00 | | |
| 19 | 34 | 35 | 34 | 15 | 24 | 2006 | 216.9 | 2.169 | 0.0362 | 6.0136 | 0.45695 | 0.72025 | 0.0005655 | 6.0136 | 0.0005655 | 0.00 | 0.00 | | |
| 20 | 40 | 45 | 40 | 12 | 30 | 3000 | 319 | 3.190 | 0.0532 | 6.0136 | 0.45695 | 0.72025 | 0.0005655 | 6.0136 | 0.0005655 | 0.00 | 0.00 | | |
| 21 | 43 | 60 | 43 | 10 | 36 | 4128 | 467.4 | 4.674 | 0.0779 | 6.0136 | 0.45695 | 0.72025 | 0.0005655 | 6.0136 | 0.0005655 | 0.00 | 0.00 | | |
| 22 | 45 | 70 | 45 | 9 | 40 | 4950 | 507.6 | 5.076 | 0.0846 | 6.0136 | 0.45695 | 0.72025 | 0.0005655 | 6.0136 | 0.0005655 | 0.00 | 0.00 | | |
| 23 | 46 | 80 | 46 | 6 | 60 | 6440 | 691.4 | 6.914 | 0.1152 | 6.0136 | 0.45695 | 0.72025 | 0.0005655 | 6.0136 | 0.0005655 | 0.00 | 0.00 | | |
| 24 | 48 | 90 | 48 | 5 | 72 | 7776 | 822.4 | 8.224 | 0.1371 | 6.0136 | 0.45695 | 0.72025 | 0.0005655 | 6.0136 | 0.0005655 | 0.00 | 0.00 | | |
| 25 | 50 | 90 | 50 | 4 | 90 | 9000 | 973.7 | 9.737 | 0.1623 | 6.0136 | 0.45695 | 0.72025 | 0.0005655 | 6.0136 | 0.0005655 | 0.00 | 0.00 | | |
| 26 | 50 | 90 | 50 | 3 | 120 | 10500 | 1119.3 | 11.193 | 0.1866 | 6.0136 | 0.45695 | 0.72025 | 0.0005655 | 6.0136 | 0.0005655 | 0.00 | 0.00 | | |

FIGURE 4-12 illustrates the final relationship between the time and the number of dA. While, FIGURE 4-13 shows the relationship between vertical stress and the number of dA. FIGURE 4-14 shows the relationship between vertical strain and number of dA.

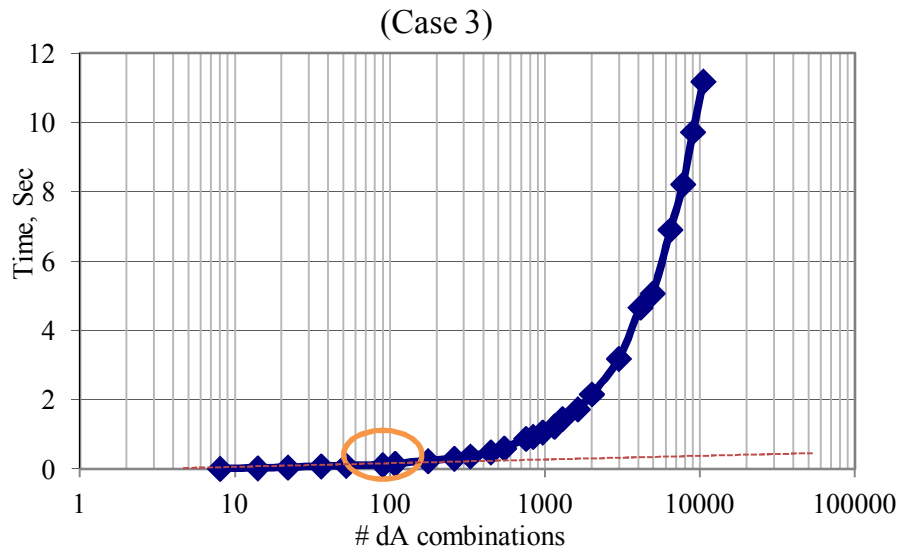


FIGURE 4-12 Time and number of dA analysis for elliptical tire imprint shape ($Z=150$ in).

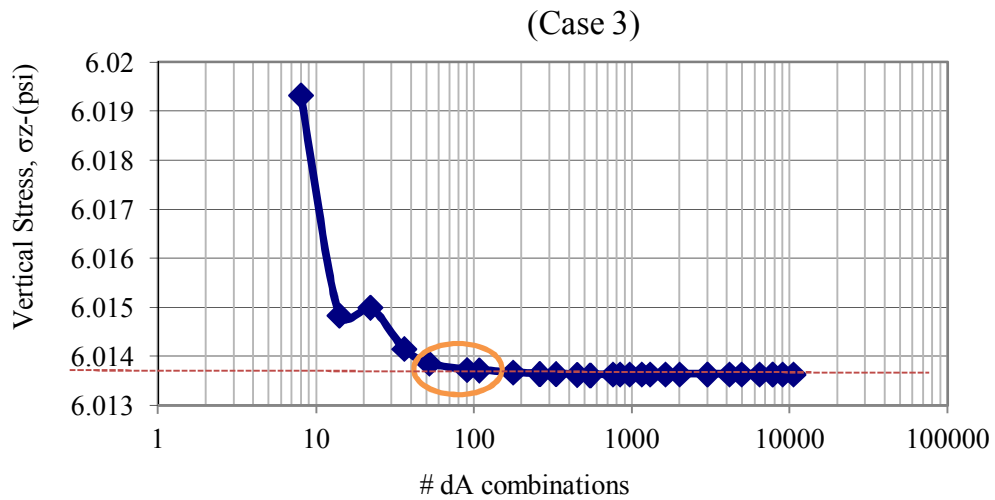


FIGURE 4-13 Vertical stress and number of dA analysis for elliptical tire imprint shape ($Z=150$ in).

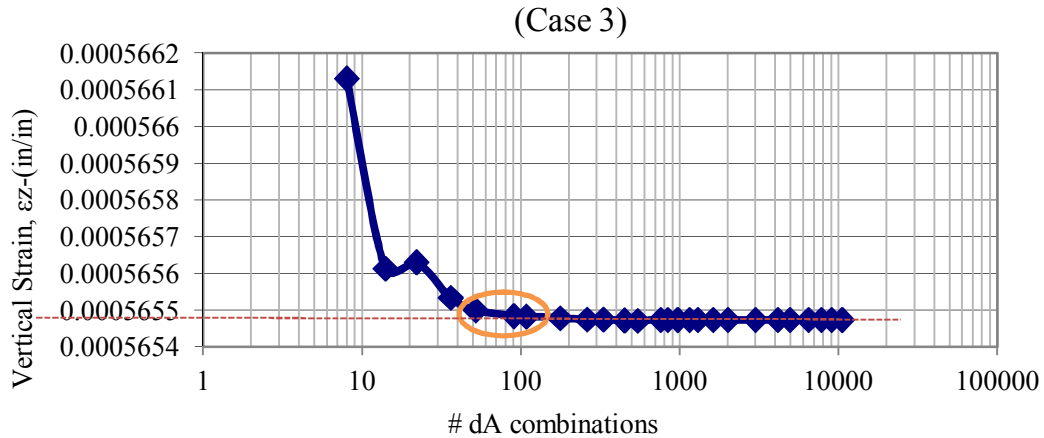


FIGURE 4-14 Vertical strain and number of da analysis for elliptical tire imprint shape ($Z=150$ in).

From the previous tables and figures, the following points could be concluded:

- i. After a certain point, the number of dA units used becomes stable at a certain value. At this point, the accuracy of the stress-strain prediction is not improved even as the number of dA areas is increased.
- ii. For an elliptical tire shape at deep depth, the range of # dA combinations (50-100) is the best that should be used for time concern and best strain and stress values.
- iii. The range of dx and $dr = (4-6)$, $dy = (7- 10)$, and $d\phi = (45^\circ -60^\circ)$ appear to be good numbers to use for an elliptical tire shape calculation.
- iv. $d\phi$ should not be an odd number.
- v. $360/d\phi$ should be an even integer.

4.6 The Study for Mid Depth ($Z=79.57$ in).

4.6.1 Analysis for Circular Tire Imprint Shape (Mid Depth)

TABLE 4-6 illustrates the input and the results for circular tire Imprint shape with $Z=79.57$ in.

TABLE 4-6 Analysis for Circular Tire Imprint Shape (Z=79.57 in)

| N | X (in) Y (in) Z (in) | | | Time | | | (ZAPMEDACA) | | | | Target Value | | Percentage Diff, % | |
|----|----------------------|--------|---------------------------|-----------|-------|--------|------------------|------------------|------------------|----------------------|------------------|----------------------|--------------------|--------------|
| | 00.8 | 122.0 | 79.57 | 1/100 sec | sec | min | σ_z (psi) | σ_x (psi) | σ_y (psi) | ϵ_z (in/in) | σ_z (psi) | ϵ_z (in/in) | σ_z | ϵ_z |
| | dr | dφ (°) | # of computational points | | | | | | | | | | | |
| 1 | 1 | 72 | 5 | 1.8 | 0.018 | 0.0003 | 11.7953 | 1.54539 | 2.87518 | 0.0010112 | 11.772 | 0.0010088 | 0.20 | 0.24 |
| 2 | 1 | 36 | 10 | 2.9 | 0.029 | 0.0005 | 11.7953 | 1.54539 | 2.87518 | 0.0010112 | 11.772 | 0.0010088 | 0.20 | 0.24 |
| 3 | 2 | 30 | 24 | 4.8 | 0.048 | 0.0008 | 11.7778 | 1.54602 | 2.87408 | 0.0010094 | 11.772 | 0.0010088 | 0.05 | 0.06 |
| 4 | 2 | 18 | 40 | 5.8 | 0.058 | 0.0010 | 11.7778 | 1.54602 | 2.87408 | 0.0010094 | 11.772 | 0.0010088 | 0.05 | 0.06 |
| 5 | 3 | 15 | 72 | 9.7 | 0.097 | 0.0016 | 11.7745 | 1.54615 | 2.87386 | 0.0010090 | 11.772 | 0.0010088 | 0.02 | 0.03 |
| 6 | 3 | 12 | 90 | 11.5 | 0.115 | 0.0019 | 11.7745 | 1.54615 | 2.87386 | 0.0010090 | 11.772 | 0.0010088 | 0.02 | 0.03 |
| 7 | 4 | 12 | 120 | 16.7 | 0.167 | 0.0028 | 11.7734 | 1.54620 | 2.87379 | 0.0010089 | 11.772 | 0.0010088 | 0.01 | 0.01 |
| 8 | 5 | 12 | 150 | 30.1 | 0.301 | 0.0050 | 11.7729 | 1.54622 | 2.87375 | 0.0010089 | 11.772 | 0.0010088 | 0.01 | 0.01 |
| 9 | 6 | 10 | 216 | 34.6 | 0.346 | 0.0058 | 11.7726 | 1.54623 | 2.87373 | 0.0010088 | 11.772 | 0.0010088 | 0.01 | 0.01 |
| 10 | 8 | 9 | 320 | 38.8 | 0.388 | 0.0065 | 11.7723 | 1.54625 | 2.87371 | 0.0010088 | 11.772 | 0.0010088 | 0.00 | 0.00 |
| 11 | 10 | 8 | 450 | 53.7 | 0.537 | 0.0090 | 11.7722 | 1.54625 | 2.87370 | 0.0010088 | 11.772 | 0.0010088 | 0.00 | 0.00 |
| 12 | 10 | 6 | 600 | 73.6 | 0.736 | 0.0123 | 11.7722 | 1.54625 | 2.87370 | 0.0010088 | 11.772 | 0.0010088 | 0.00 | 0.00 |
| 13 | 12 | 6 | 720 | 86.3 | 0.863 | 0.0144 | 11.7721 | 1.54626 | 2.87370 | 0.0010088 | 11.772 | 0.0010088 | 0.00 | 0.00 |
| 14 | 12 | 5 | 864 | 97.3 | 0.973 | 0.0162 | 11.7721 | 1.54626 | 2.87370 | 0.0010088 | 11.772 | 0.0010088 | 0.00 | 0.00 |
| 15 | 15 | 5 | 1080 | 119.9 | 1.199 | 0.0200 | 11.7720 | 1.54626 | 2.87369 | 0.0010088 | 11.772 | 0.0010088 | 0.00 | 0.00 |
| 16 | 14 | 4 | 1260 | 141 | 1.410 | 0.0235 | 11.7721 | 1.54626 | 2.87370 | 0.0010088 | 11.772 | 0.0010088 | 0.00 | 0.00 |
| 17 | 17 | 4 | 1530 | 173.5 | 1.735 | 0.0289 | 11.7720 | 1.54626 | 2.87369 | 0.0010088 | 11.772 | 0.0010088 | 0.00 | 0.00 |
| 18 | 20 | 4 | 1800 | 203.8 | 2.038 | 0.0340 | 11.7720 | 1.54626 | 2.87369 | 0.0010088 | 11.772 | 0.0010088 | 0.00 | 0.00 |
| 19 | 18 | 3 | 2160 | 247.1 | 2.471 | 0.0412 | 11.7720 | 1.54626 | 2.87369 | 0.0010088 | 11.772 | 0.0010088 | 0.00 | 0.00 |
| 20 | 25 | 3 | 3000 | 331 | 3.310 | 0.0552 | 11.7720 | 1.54626 | 2.87369 | 0.0010088 | 11.772 | 0.0010088 | 0.00 | 0.00 |
| 21 | 24 | 2 | 4320 | 475.1 | 4.751 | 0.0792 | 11.7720 | 1.54626 | 2.87369 | 0.0010088 | 11.772 | 0.0010088 | 0.00 | 0.00 |
| 22 | 30 | 2 | 5400 | 590 | 5.900 | 0.0983 | 11.7720 | 1.54626 | 2.87369 | 0.0010088 | 11.772 | 0.0010088 | 0.00 | 0.00 |
| 23 | 35 | 2 | 6300 | 689.7 | 6.897 | 0.1150 | 11.7720 | 1.54626 | 2.87369 | 0.0010088 | 11.772 | 0.0010088 | 0.00 | 0.00 |
| 24 | 20 | 1 | 7200 | 799.8 | 7.998 | 0.1333 | 11.7720 | 1.54626 | 2.87369 | 0.0010088 | 11.772 | 0.0010088 | 0.00 | 0.00 |
| 25 | 23 | 1 | 8280 | 929.5 | 9.295 | 0.1549 | 11.7720 | 1.54626 | 2.87369 | 0.0010088 | 11.772 | 0.0010088 | 0.00 | 0.00 |
| 26 | 25 | 1 | 9000 | 989.5 | 9.895 | 0.1649 | 11.7720 | 1.54626 | 2.87369 | 0.0010088 | 11.7720 | 0.0010088 | 0.00 | 0.00 |

FIGURE 4-15 illustrates the relationship between time and the number of dA. FIGURE 4-16 shows the relationship between vertical stress and number of dA; while, FIGURE 4-17 shows the relationship between the vertical strain and the number of dA.

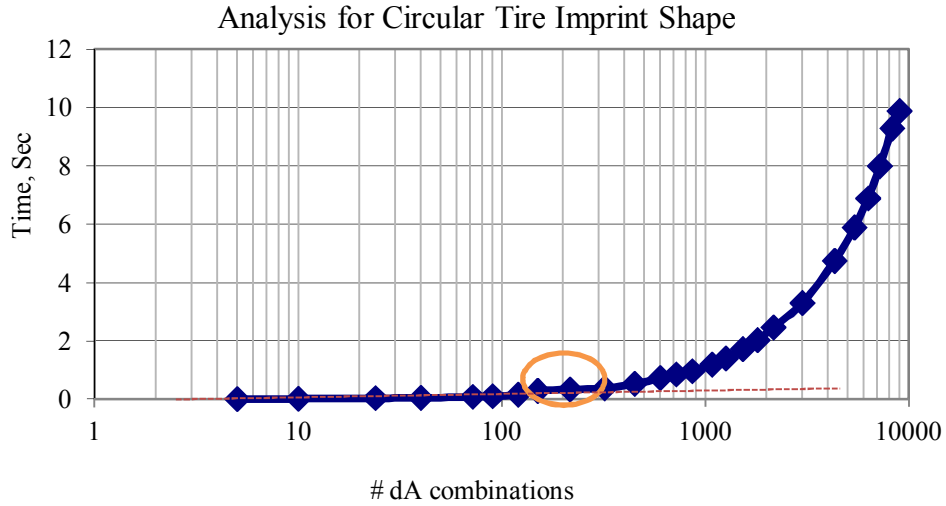


FIGURE 4-15 Time and number of dA analysis for circular tire imprint shape ($Z=79.57$ in).

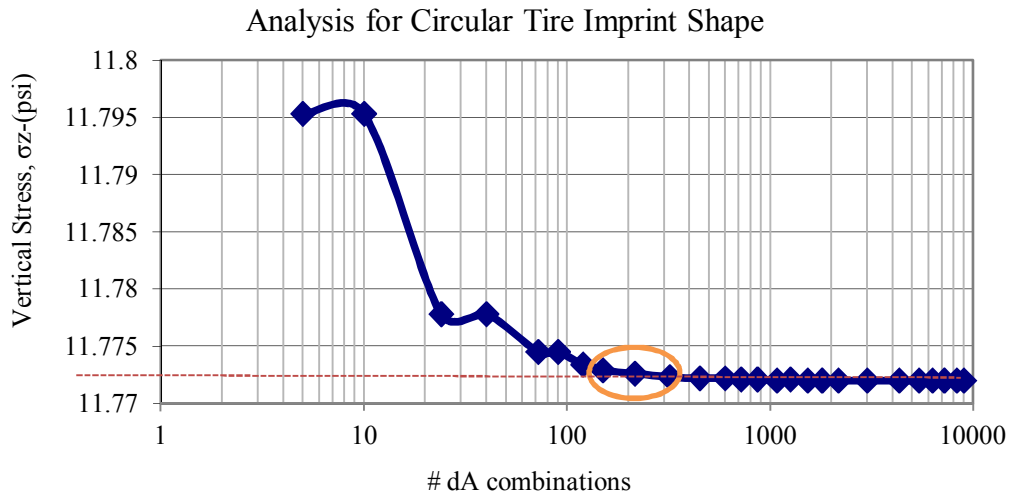


FIGURE 4-16 Vertical stress and number of dA analysis for circular tire imprint shape ($Z=79.57$ in).

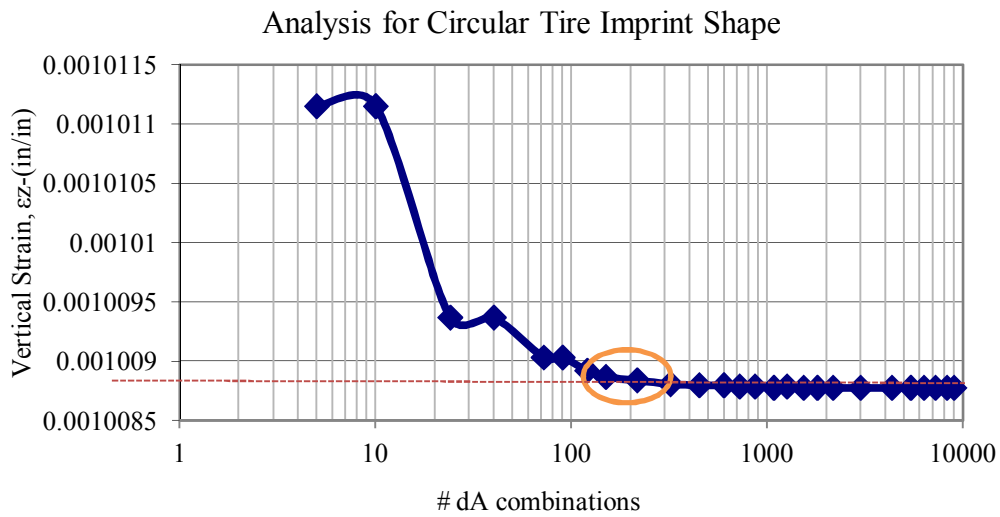


FIGURE 4-17 Vertical strain and number of dA analysis for circular tire imprint shape ($Z=79.57$ in).

From the previous tables and figures, the following points are made:

- i. After a certain point, the number of dA combinations used becomes stable. At this point, any increase in the number of areas in the segment does not improve the precision of the predicted value.
- ii. For circular tire shape at mid depth, the range of # dA combinations (150-250) appears to be the best that should be used for time concern and best strain and stress values.
- iii. A Range of $dr = (5-7)$, and $d\phi = (9^\circ -12^\circ)$ appears to be a good number to use for circular tire shape calculation with mid depth.

4.6.2 Analysis for Elliptical Tire Imprint Shape (Mid Depth)

TABLE 4-7 illustrates the input and the results for an elliptical tire imprint shape with a depth of $Z=79.57$ in. Also, the time taken by the program to do the run was recorded and listed.

TABLE 4-7 Analysis for Elliptical Tire Imprint Shape (Z=79.57 in)

| N | X (in) | | | Y (in) | Z (in) | Time | | | (ZAPMEDACA) | | | | Target Value | | Percentage Diff, % | |
|----|--------|----|----|--------|-------------------|-----------|--------|--------|----------------------|----------------------|----------------------|------------------------|----------------------|------------------------|--------------------|----------------|
| | dx | dy | dr | dφ (°) | # of comp. points | 1/100 sec | sec | min | σ _z (psi) | σ _x (psi) | σ _y (psi) | ε _z (in/in) | σ _z (psi) | ε _z (in/in) | σ _z | ε _z |
| 1 | 1 | 4 | 1 | 90 | 8 | 3.8 | 0.038 | 0.0006 | 11.7889 | 1.54377 | 2.87930 | 0.0010104 | 11.7707 | 0.0010086 | 0.15 | 0.18 |
| 2 | 2 | 3 | 2 | 90 | 14 | 3.6 | 0.036 | 0.0006 | 11.7745 | 1.54440 | 2.87783 | 0.0010089 | 11.7707 | 0.0010086 | 0.03 | 0.04 |
| 3 | 2 | 5 | 2 | 60 | 22 | 6 | 0.060 | 0.0010 | 11.7751 | 1.54443 | 2.87771 | 0.0010090 | 11.7707 | 0.0010086 | 0.04 | 0.04 |
| 4 | 3 | 6 | 3 | 60 | 36 | 8.8 | 0.088 | 0.0015 | 11.7724 | 1.54456 | 2.87744 | 0.0010087 | 11.7707 | 0.0010086 | 0.01 | 0.02 |
| 5 | 4 | 7 | 4 | 60 | 52 | 15.5 | 0.155 | 0.0026 | 11.7714 | 1.54461 | 2.87734 | 0.0010087 | 11.7707 | 0.0010086 | 0.01 | 0.02 |
| 6 | 6 | 7 | 6 | 45 | 90 | 12.6 | 0.126 | 0.0021 | 11.7710 | 1.54465 | 2.87723 | 0.0010086 | 11.7707 | 0.0010086 | 0.00 | 0.00 |
| 7 | 6 | 10 | 6 | 45 | 108 | 14 | 0.140 | 0.0023 | 11.7710 | 1.54465 | 2.87723 | 0.0010086 | 11.7707 | 0.0010086 | 0.00 | 0.00 |
| 8 | 8 | 12 | 8 | 36 | 176 | 19.8 | 0.198 | 0.0033 | 11.7708 | 1.54467 | 2.87719 | 0.0010086 | 11.7707 | 0.0010086 | 0.00 | 0.00 |
| 9 | 10 | 16 | 10 | 36 | 260 | 38.5 | 0.385 | 0.0064 | 11.7707 | 1.54467 | 2.87718 | 0.0010086 | 11.7707 | 0.0010086 | 0.00 | 0.00 |
| 10 | 11 | 18 | 11 | 30 | 330 | 44.1 | 0.441 | 0.0074 | 11.7708 | 1.54468 | 2.87717 | 0.0010086 | 11.7707 | 0.0010086 | 0.00 | 0.00 |
| 11 | 14 | 20 | 14 | 30 | 448 | 49.2 | 0.492 | 0.0082 | 11.7707 | 1.54468 | 2.87716 | 0.0010086 | 11.7707 | 0.0010086 | 0.00 | 0.00 |
| 12 | 17 | 20 | 17 | 30 | 544 | 58.1 | 0.581 | 0.0097 | 11.7707 | 1.54468 | 2.87716 | 0.0010086 | 11.7707 | 0.0010086 | 0.00 | 0.00 |
| 13 | 18 | 24 | 18 | 20 | 756 | 91.5 | 0.915 | 0.0153 | 11.7707 | 1.54469 | 2.87715 | 0.0010086 | 11.7707 | 0.0010086 | 0.00 | 0.00 |
| 14 | 20 | 24 | 20 | 20 | 840 | 97.6 | 0.976 | 0.0163 | 11.7707 | 1.54469 | 2.87714 | 0.0010086 | 11.7707 | 0.0010086 | 0.00 | 0.00 |
| 15 | 22 | 26 | 22 | 20 | 968 | 106 | 1.060 | 0.0177 | 11.7707 | 1.54469 | 2.87714 | 0.0010086 | 11.7707 | 0.0010086 | 0.00 | 0.00 |
| 16 | 24 | 28 | 24 | 18 | 1152 | 128 | 1.280 | 0.0213 | 11.7707 | 1.54469 | 2.87714 | 0.0010086 | 11.7707 | 0.0010086 | 0.00 | 0.00 |
| 17 | 26 | 30 | 26 | 18 | 1300 | 145.4 | 1.454 | 0.0242 | 11.7707 | 1.54469 | 2.87714 | 0.0010086 | 11.7707 | 0.0010086 | 0.00 | 0.00 |
| 18 | 29 | 32 | 29 | 15 | 1624 | 175.4 | 1.754 | 0.0292 | 11.7707 | 1.54469 | 2.87714 | 0.0010086 | 11.7707 | 0.0010086 | 0.00 | 0.00 |
| 19 | 34 | 35 | 34 | 15 | 2006 | 214.7 | 2.147 | 0.0358 | 11.7707 | 1.54469 | 2.87714 | 0.0010086 | 11.7707 | 0.0010086 | 0.00 | 0.00 |
| 20 | 40 | 45 | 40 | 12 | 3000 | 316.6 | 3.166 | 0.0528 | 11.7707 | 1.54469 | 2.87714 | 0.0010086 | 11.7707 | 0.0010086 | 0.00 | 0.00 |
| 21 | 43 | 60 | 43 | 10 | 4128 | 440.8 | 4.408 | 0.0735 | 11.7707 | 1.54469 | 2.87713 | 0.0010086 | 11.7707 | 0.0010086 | 0.00 | 0.00 |
| 22 | 45 | 70 | 45 | 9 | 4950 | 506.8 | 5.068 | 0.0845 | 11.7707 | 1.54469 | 2.87713 | 0.0010086 | 11.7707 | 0.0010086 | 0.00 | 0.00 |
| 23 | 46 | 80 | 46 | 6 | 6440 | 712.8 | 7.128 | 0.1188 | 11.7707 | 1.54469 | 2.87713 | 0.0010086 | 11.7707 | 0.0010086 | 0.00 | 0.00 |
| 24 | 48 | 90 | 48 | 5 | 7776 | 824.8 | 8.248 | 0.1375 | 11.7707 | 1.54469 | 2.87713 | 0.0010086 | 11.7707 | 0.0010086 | 0.00 | 0.00 |
| 25 | 50 | 90 | 50 | 4 | 9000 | 987.6 | 9.876 | 0.1646 | 11.7707 | 1.54469 | 2.87713 | 0.0010086 | 11.7707 | 0.0010086 | 0.00 | 0.00 |
| 26 | 50 | 90 | 50 | 3 | 10500 | 1107.6 | 11.076 | 0.1846 | 11.7707 | 1.54469 | 2.87713 | 0.0010086 | 11.7707 | 0.0010086 | 0.00 | 0.00 |

FIGURE 4-18 illustrates the relationship between time and number of dA. FIGURE 4-19 shows the relationship between vertical stress and number of dA and FIGURE 4-20 shows the relationship between vertical strain and the number of dA.

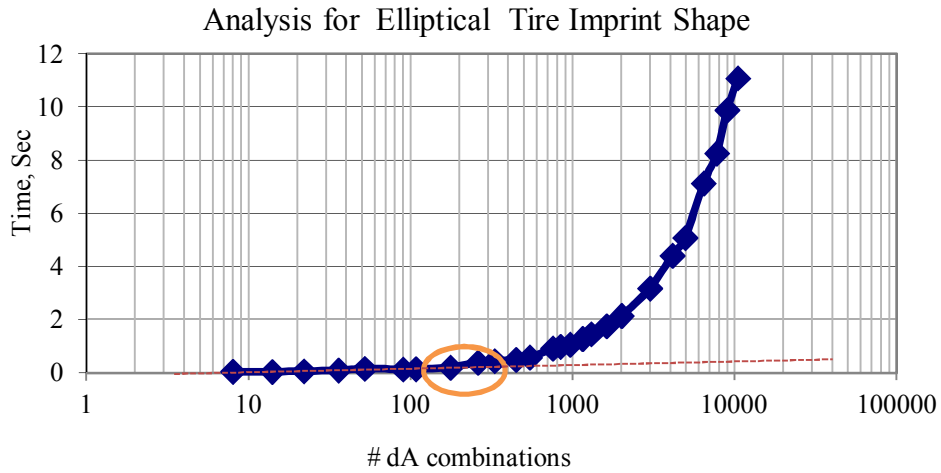


FIGURE 4-18 Time and number of dA analysis for elliptical tire imprint shape ($Z=79.57$ in).

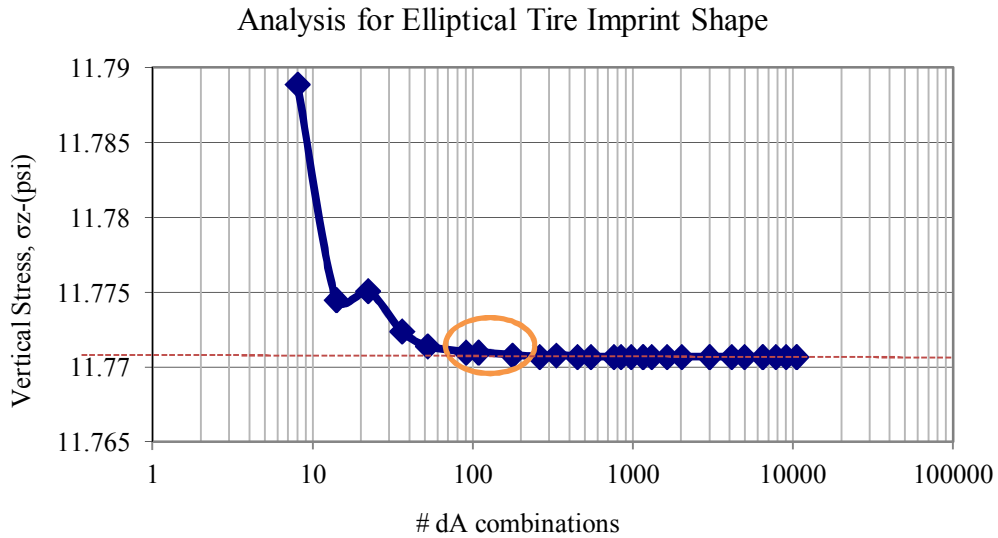


FIGURE 4-19 Vertical strain and number of dA analysis for elliptical tire imprint shape ($Z=79.57$ in).

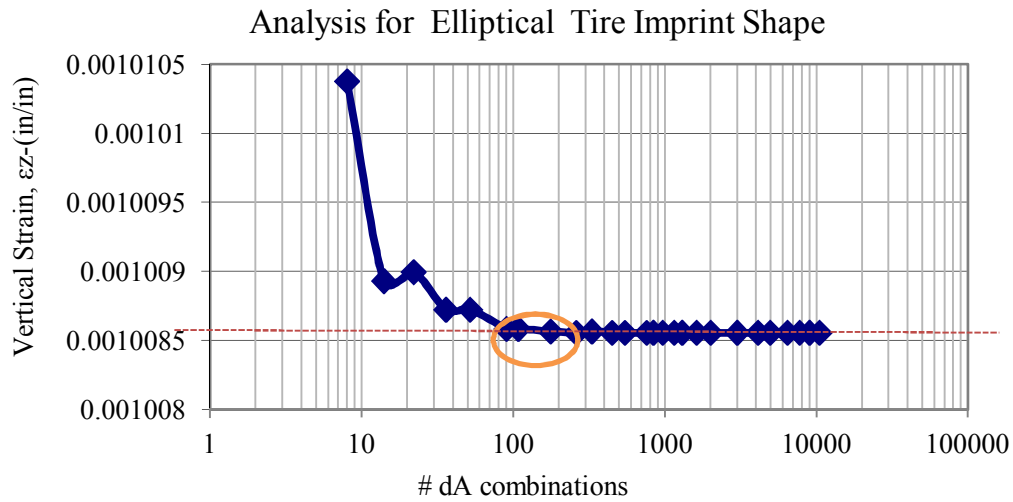


FIGURE 4-20 Vertical strain and number of dA analysis for elliptical tire imprint shape ($Z=79.57$ in).

From the previous tables and figures, the following points could be concluded:

- i. .After a certain point, the number of dA combinations used becomes stable. At this point, any increase in the number of areas in the segment does not improve the precision of the predicted value.
- ii. For elliptical tire shape at mid depth, the range of # dA combinations (100-200) is the best that should be used for time concern and the best strain and stress values.
- iii. The range of dx and $dr = (6-10)$, $dy = (10- 16)$, and $d\phi = (36^\circ -45^\circ)$ appears to be a good number to use for elliptical tire shape calculation with mid depth.

4.7 The Study for Shallow Depth ($Z=20.00$ in).

4.7.1 Analysis for Circular Tire Imprint Shape (Shallow Depth)

TABLE 4-8 illustrates the input and the results for circular tire imprint shape at a depth of $Z=20.00$ in. Also, the time taken by the program to do the run was recorded and listed.

TABLE 4-8 Analysis for Circular Tire Imprint Shape (Z=20 in)

| N | X (in) | | Y (in) | | Z (in) | | Time | | | (ZAPMEDACA) | | | Target Value | | Percentage Diff, % | |
|----|--------|--------|---------------------------|-----------|--------|--------|----------------------|----------------------|----------------------|------------------------|----------------------|------------------------|----------------|----------------|--------------------|--|
| | 100.8 | 122.0 | 20.00 | | | | | | | | | | | | | |
| | dr | dφ (°) | # of computational points | 1/100 sec | sec | min | σ _z (psi) | σ _x (psi) | σ _y (psi) | ε _z (in/in) | σ _z (psi) | ε _z (in/in) | σ _z | ε _z | | |
| 1 | 1 | 72 | 5 | 2.6 | 0.026 | 0.0004 | 12.4435 | 19.607 | 5.259 | 0.0001293 | 13.1512 | 0.0002095 | 5.38 | 38.28 | | |
| 2 | 1 | 36 | 10 | 3.6 | 0.036 | 0.0006 | 12.4435 | 19.607 | 5.259 | 0.0001293 | 13.1512 | 0.0002095 | 5.38 | 38.28 | | |
| 3 | 2 | 30 | 24 | 5.1 | 0.051 | 0.0009 | 12.9743 | 19.267 | 5.487 | 0.0001892 | 13.1512 | 0.0002095 | 1.35 | 9.66 | | |
| 4 | 2 | 18 | 40 | 8.3 | 0.083 | 0.0014 | 12.9743 | 19.267 | 5.487 | 0.0001892 | 13.1512 | 0.0002095 | 1.35 | 9.66 | | |
| 5 | 3 | 15 | 72 | 9.7 | 0.097 | 0.0016 | 13.0732 | 19.200 | 5.530 | 0.0002005 | 13.1512 | 0.0002095 | 0.59 | 4.26 | | |
| 6 | 3 | 12 | 90 | 15.9 | 0.159 | 0.0027 | 13.0732 | 19.200 | 5.530 | 0.0002005 | 13.1512 | 0.0002095 | 0.59 | 4.26 | | |
| 7 | 4 | 12 | 120 | 16.4 | 0.164 | 0.0027 | 13.1079 | 19.177 | 5.545 | 0.0002045 | 13.1512 | 0.0002095 | 0.33 | 2.37 | | |
| 8 | 5 | 12 | 150 | 19.5 | 0.195 | 0.0033 | 13.1239 | 19.166 | 5.552 | 0.0002063 | 13.1512 | 0.0002095 | 0.21 | 1.49 | | |
| 9 | 6 | 10 | 216 | 26.2 | 0.262 | 0.0044 | 13.1326 | 19.160 | 5.555 | 0.0002073 | 13.1512 | 0.0002095 | 0.14 | 1.02 | | |
| 10 | 8 | 9 | 320 | 39.2 | 0.392 | 0.0065 | 13.1413 | 19.154 | 5.559 | 0.0002083 | 13.1512 | 0.0002095 | 0.08 | 0.54 | | |
| 11 | 10 | 8 | 450 | 63.4 | 0.634 | 0.0106 | 13.1453 | 19.152 | 5.561 | 0.0002088 | 13.1512 | 0.0002095 | 0.04 | 0.32 | | |
| 12 | 10 | 6 | 600 | 77.5 | 0.775 | 0.0129 | 13.1453 | 19.152 | 5.561 | 0.0002088 | 13.1512 | 0.0002095 | 0.04 | 0.32 | | |
| 13 | 12 | 6 | 720 | 82.3 | 0.823 | 0.0137 | 13.1474 | 19.150 | 5.562 | 0.0002090 | 13.1512 | 0.0002095 | 0.03 | 0.21 | | |
| 14 | 12 | 5 | 864 | 99.6 | 0.996 | 0.0166 | 13.1474 | 19.150 | 5.562 | 0.0002090 | 13.1512 | 0.0002095 | 0.03 | 0.21 | | |
| 15 | 15 | 5 | 1080 | 123.1 | 1.231 | 0.0205 | 13.1492 | 19.149 | 5.562 | 0.0002092 | 13.1512 | 0.0002095 | 0.02 | 0.11 | | |
| 16 | 14 | 4 | 1260 | 142.5 | 1.425 | 0.0238 | 13.1488 | 19.149 | 5.562 | 0.0002092 | 13.1512 | 0.0002095 | 0.02 | 0.13 | | |
| 17 | 17 | 4 | 1530 | 174.4 | 1.744 | 0.0291 | 13.1499 | 19.148 | 5.563 | 0.0002093 | 13.1512 | 0.0002095 | 0.01 | 0.07 | | |
| 18 | 20 | 4 | 1800 | 201.1 | 2.011 | 0.0335 | 13.1506 | 19.148 | 5.563 | 0.0002094 | 13.1512 | 0.0002095 | 0.00 | 0.03 | | |
| 19 | 18 | 3 | 2160 | 241.5 | 2.415 | 0.0403 | 13.1502 | 19.148 | 5.563 | 0.0002093 | 13.1512 | 0.0002095 | 0.01 | 0.06 | | |
| 20 | 25 | 3 | 3000 | 334.5 | 3.345 | 0.0558 | 13.1512 | 19.148 | 5.563 | 0.0002095 | 13.1512 | 0.0002095 | 0.00 | 0.00 | | |
| 21 | 24 | 2 | 4320 | 481.5 | 4.815 | 0.0803 | 13.1512 | 19.148 | 5.563 | 0.0002095 | 13.1512 | 0.0002095 | 0.00 | 0.00 | | |
| 22 | 30 | 2 | 5400 | 608.4 | 6.084 | 0.1014 | 13.1516 | 19.147 | 5.564 | 0.0002095 | 13.1512 | 0.0002095 | 0.00 | 0.02 | | |
| 23 | 35 | 2 | 6300 | 702.8 | 7.028 | 0.1171 | 13.1518 | 19.147 | 5.564 | 0.0002095 | 13.1512 | 0.0002095 | 0.00 | 0.03 | | |
| 24 | 20 | 1 | 7200 | 799.8 | 7.998 | 0.1333 | 13.1506 | 19.148 | 5.563 | 0.0002094 | 13.1512 | 0.0002095 | 0.00 | 0.03 | | |
| 25 | 23 | 1 | 8280 | 914.8 | 9.148 | 0.1525 | 13.1510 | 19.148 | 5.563 | 0.0002094 | 13.1512 | 0.0002095 | 0.00 | 0.01 | | |
| 26 | 25 | 1 | 9000 | 990.5 | 9.905 | 0.1651 | 13.1512 | 19.148 | 5.563 | 0.0002095 | 13.1512 | 0.0002095 | 0.00 | 0.00 | | |

FIGURE 4-21 illustrates the relation between time and number of dA. FIGURE 4-22 shows the relationship between vertical stress and number of dA. FIGURE 4-23 shows the relationship between vertical strain and number of dA.

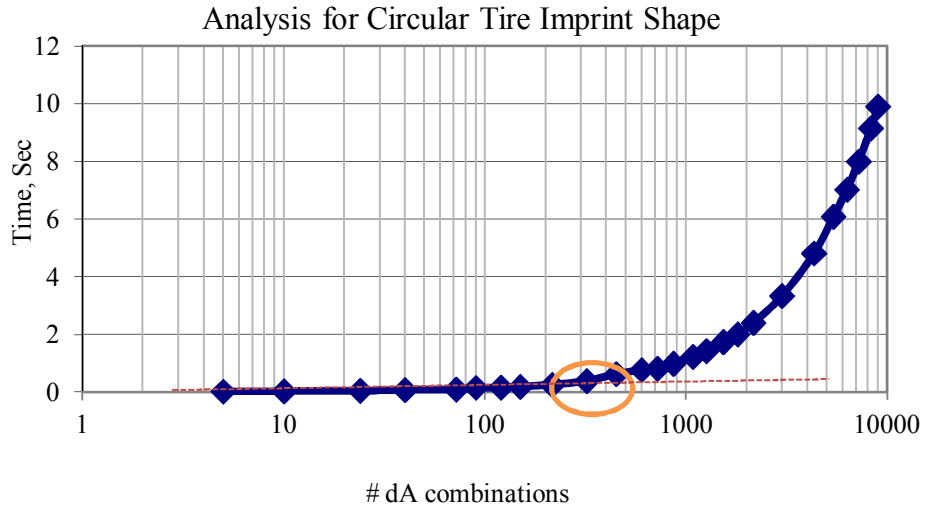


FIGURE 4-21 Time and number of dA analysis for circular tire imprint shape (Z=20 in).

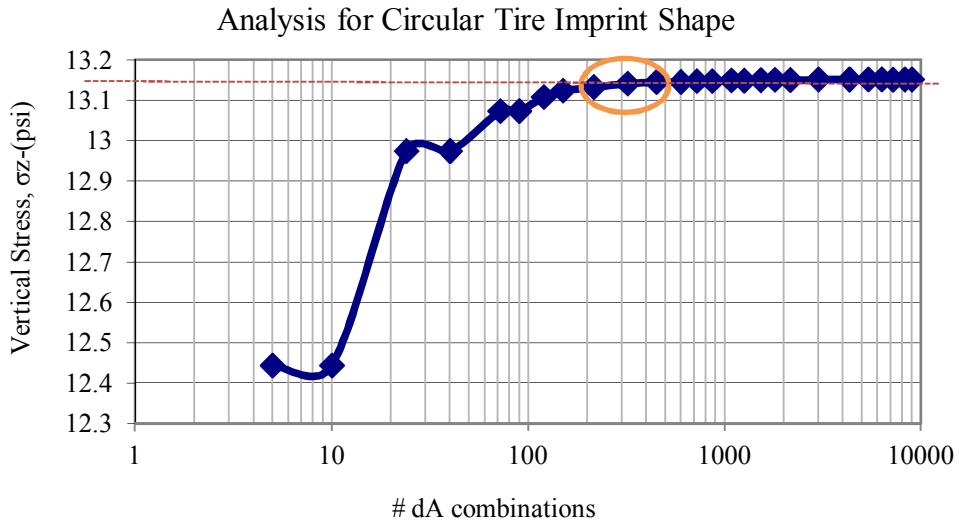


FIGURE 4-22 Vertical stress and number of dA analysis for circular tire imprint shape (Z=20.00 in).

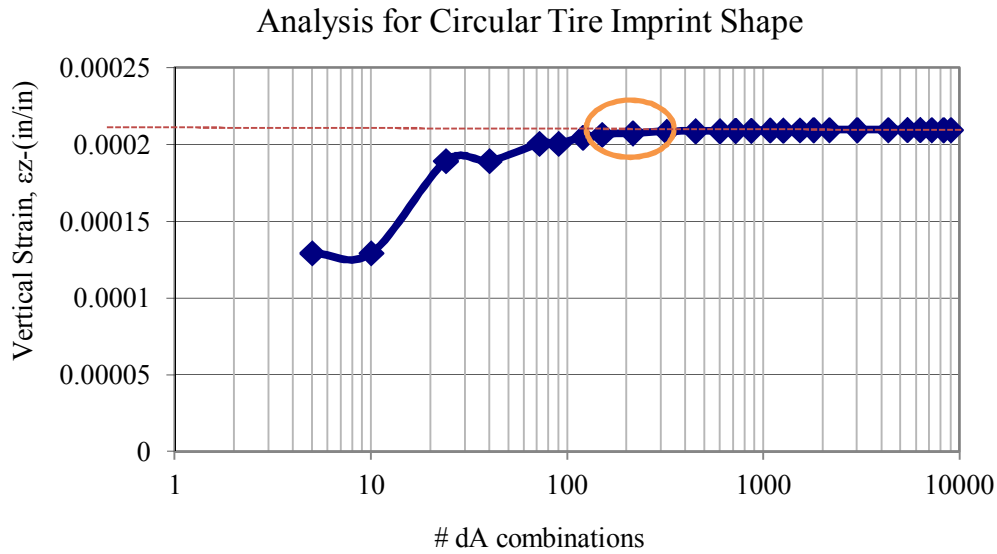


FIGURE 4-23 Vertical strain and number of dA analysis for circular tire imprint shape ($Z=20.00$ in).

From the previous tables and figures, the following points could be concluded:

- i. After a certain point, the number of dA combinations used becomes stable. At this point, any increase in the number of areas in the segment does not improve the precision of the predicted value.
- ii. For circular tire shape at shallow depth, range of # dA combinations (200-300) appears to be the optional that should use for time concern and best strain and stress value.
- iii. Range $d_r = (6-8)$, and $d_\phi = (9^\circ - 11^\circ)$ are reasonable numbers to use for circular tire shape calculation with shallow depth..

4.7.2 Analysis for Elliptical Tire Imprint Shape (Shallow Depth)

TABLE 4-9 illustrates the input and the results for an elliptical tire Imprint shape with $Z=20.00$ in. Also, the time which the program uses to do the run was recorded and listed.

TABLE 4-9 Analysis for Elliptical Tire Imprint Shape (Z=20 in)

| N | X (in) | | | | Y (in) | Z (in) | Time | | | | (ZAPMEDACA) | | | | Target Value | | Percentage Diff, % | |
|----|--------|----|----|--------|-------------------|-----------|-------|--------|----------------------|----------------------|----------------------|------------------------|----------------------|------------------------|----------------|----------------|--------------------|--|
| | dx | dy | dr | dφ (°) | # of comp. points | 1/100 sec | sec | min | σ _z (psi) | σ _x (psi) | σ _y (psi) | ε _z (in/in) | σ _z (psi) | ε _z (in/in) | σ _z | ε _z | | |
| 1 | 1 | 4 | 1 | 90 | 8 | 2.4 | 0.024 | 0.0004 | 11.3189 | 18.917 | 5.771 | 0.0000216 | 12.0857 | 0.0001037 | 6.34 | 79.17 | | |
| 2 | 2 | 3 | 2 | 90 | 14 | 3.3 | 0.033 | 0.0006 | 11.8312 | 18.729 | 5.915 | 0.0000764 | 12.0857 | 0.0001037 | 2.11 | 26.25 | | |
| 3 | 2 | 5 | 2 | 60 | 22 | 4.3 | 0.043 | 0.0007 | 11.8752 | 18.763 | 5.882 | 0.0000809 | 12.0857 | 0.0001037 | 1.74 | 21.94 | | |
| 4 | 3 | 6 | 3 | 60 | 36 | 5.1 | 0.051 | 0.0009 | 11.9783 | 18.723 | 5.908 | 0.0000922 | 12.0857 | 0.0001037 | 0.89 | 11.05 | | |
| 5 | 4 | 7 | 4 | 60 | 52 | 6.7 | 0.067 | 0.0011 | 12.0145 | 18.708 | 5.918 | 0.0000962 | 12.0857 | 0.0001037 | 0.59 | 7.20 | | |
| 6 | 6 | 7 | 6 | 45 | 90 | 11.4 | 0.114 | 0.0019 | 12.0534 | 18.711 | 5.913 | 0.0001003 | 12.0857 | 0.0001037 | 0.27 | 3.24 | | |
| 7 | 6 | 10 | 6 | 45 | 108 | 15.7 | 0.157 | 0.0026 | 12.0524 | 18.710 | 5.914 | 0.0001002 | 12.0857 | 0.0001037 | 0.28 | 3.33 | | |
| 8 | 8 | 12 | 8 | 36 | 176 | 23.2 | 0.232 | 0.0039 | 12.0665 | 18.712 | 5.911 | 0.0001017 | 12.0857 | 0.0001037 | 0.16 | 1.91 | | |
| 9 | 10 | 16 | 10 | 36 | 260 | 33.7 | 0.337 | 0.0056 | 12.0706 | 18.710 | 5.912 | 0.0001021 | 12.0857 | 0.0001037 | 0.12 | 1.47 | | |
| 10 | 11 | 18 | 11 | 30 | 330 | 41.4 | 0.414 | 0.0069 | 12.0744 | 18.713 | 5.910 | 0.0001025 | 12.0857 | 0.0001037 | 0.09 | 1.11 | | |
| 11 | 14 | 20 | 14 | 30 | 448 | 51.2 | 0.512 | 0.0085 | 12.0768 | 18.712 | 5.911 | 0.0001028 | 12.0857 | 0.0001037 | 0.07 | 0.85 | | |
| 12 | 17 | 20 | 17 | 30 | 544 | 64.4 | 0.644 | 0.0107 | 12.0781 | 18.711 | 5.911 | 0.0001029 | 12.0857 | 0.0001037 | 0.06 | 0.71 | | |
| 13 | 18 | 24 | 18 | 20 | 756 | 88.6 | 0.886 | 0.0148 | 12.0814 | 18.715 | 5.908 | 0.0001032 | 12.0857 | 0.0001037 | 0.04 | 0.42 | | |
| 14 | 20 | 24 | 20 | 20 | 840 | 105.2 | 1.052 | 0.0175 | 12.0819 | 18.715 | 5.908 | 0.0001033 | 12.0857 | 0.0001037 | 0.03 | 0.36 | | |
| 15 | 22 | 26 | 22 | 20 | 968 | 109.2 | 1.092 | 0.0182 | 12.0822 | 18.714 | 5.908 | 0.0001033 | 12.0857 | 0.0001037 | 0.03 | 0.33 | | |
| 16 | 24 | 28 | 24 | 18 | 1152 | 129.1 | 1.291 | 0.0215 | 12.0829 | 18.715 | 5.908 | 0.0001034 | 12.0857 | 0.0001037 | 0.02 | 0.26 | | |
| 17 | 26 | 30 | 26 | 18 | 1300 | 159.6 | 1.596 | 0.0266 | 12.0831 | 18.715 | 5.908 | 0.0001034 | 12.0857 | 0.0001037 | 0.02 | 0.24 | | |
| 18 | 29 | 32 | 29 | 15 | 1624 | 183.9 | 1.839 | 0.0307 | 12.0839 | 18.715 | 5.908 | 0.0001035 | 12.0857 | 0.0001037 | 0.01 | 0.17 | | |
| 19 | 34 | 35 | 34 | 15 | 2006 | 229.1 | 2.291 | 0.0382 | 12.0841 | 18.715 | 5.908 | 0.0001035 | 12.0857 | 0.0001037 | 0.01 | 0.15 | | |
| 20 | 40 | 45 | 40 | 12 | 3000 | 341.1 | 3.411 | 0.0569 | 12.0848 | 18.716 | 5.907 | 0.0001036 | 12.0857 | 0.0001037 | 0.01 | 0.08 | | |
| 21 | 43 | 60 | 43 | 10 | 4128 | 438.5 | 4.385 | 0.0731 | 12.0851 | 18.716 | 5.907 | 0.0001036 | 12.0857 | 0.0001037 | 0.00 | 0.06 | | |
| 22 | 45 | 70 | 45 | 9 | 4950 | 507.4 | 5.074 | 0.0846 | 12.0852 | 18.716 | 5.907 | 0.0001036 | 12.0857 | 0.0001037 | 0.00 | 0.05 | | |
| 23 | 46 | 80 | 46 | 6 | 6440 | 682.4 | 6.824 | 0.1137 | 12.0855 | 18.717 | 5.907 | 0.0001036 | 12.0857 | 0.0001037 | 0.00 | 0.02 | | |
| 24 | 48 | 90 | 48 | 5 | 7776 | 825.6 | 8.256 | 0.1376 | 12.0856 | 18.717 | 5.907 | 0.0001036 | 12.0857 | 0.0001037 | 0.00 | 0.01 | | |
| 25 | 50 | 90 | 50 | 4 | 9000 | 961.3 | 9.613 | 0.1602 | 12.0857 | 18.717 | 5.907 | 0.0001037 | 12.0857 | 0.0001037 | 0.00 | 0.00 | | |
| 26 | 50 | 90 | 50 | 3 | 10500 | 1126.4 | 11.26 | 0.1877 | 12.0857 | 18.717 | 5.907 | 0.0001037 | 12.0857 | 0.0001037 | 0.00 | 0.00 | | |

FIGURE 4-24 illustrates the relationship between time and the number of dA.

FIGURE 4-25 shows the relationship between vertical stress and the number of dA.

FIGURE 4-26 shows the relationship between vertical strain and the number of dA.

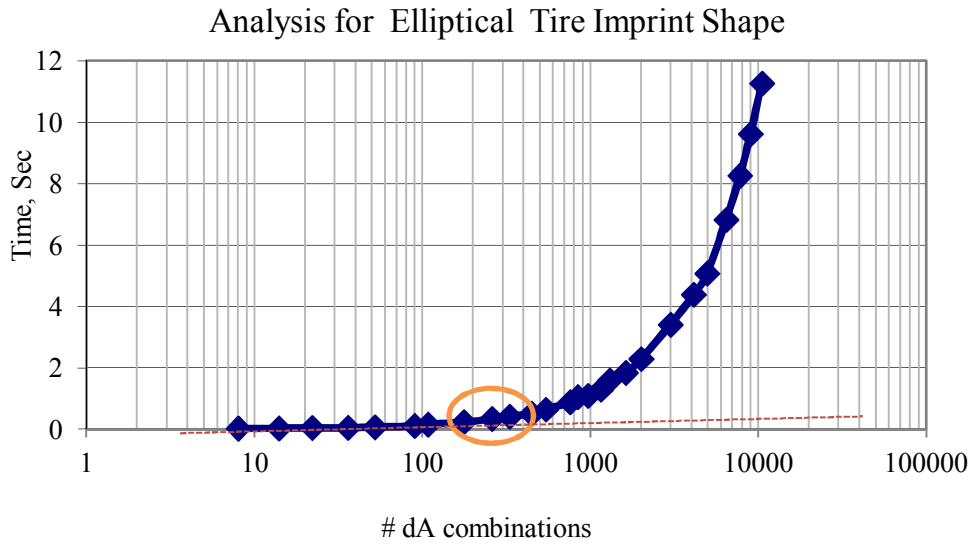


FIGURE 4-24 Time and number of dA analysis for elliptical tire imprint shape (Z=20 in).

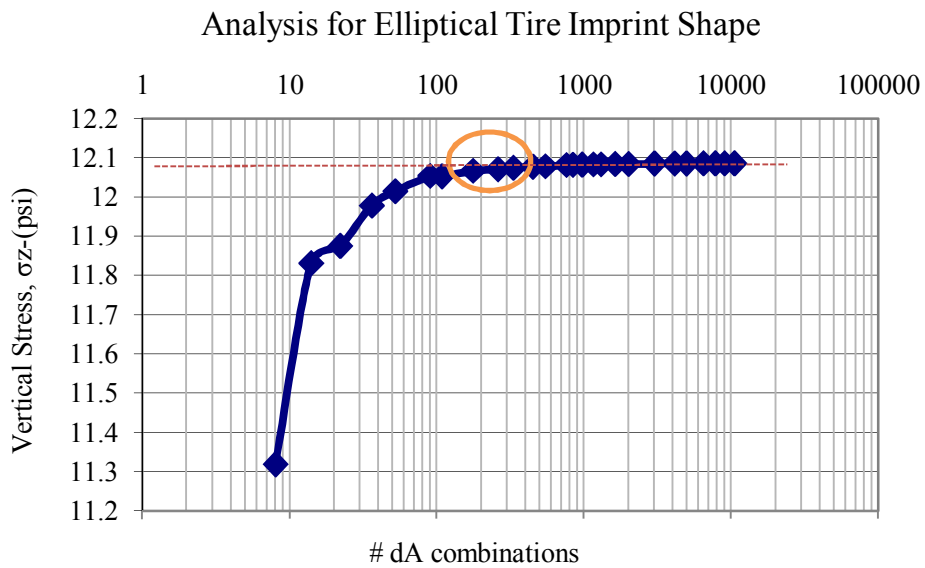


FIGURE 4-25 Vertical stress and number of dA analysis for elliptical tire imprint shape (Z=20.00 in).

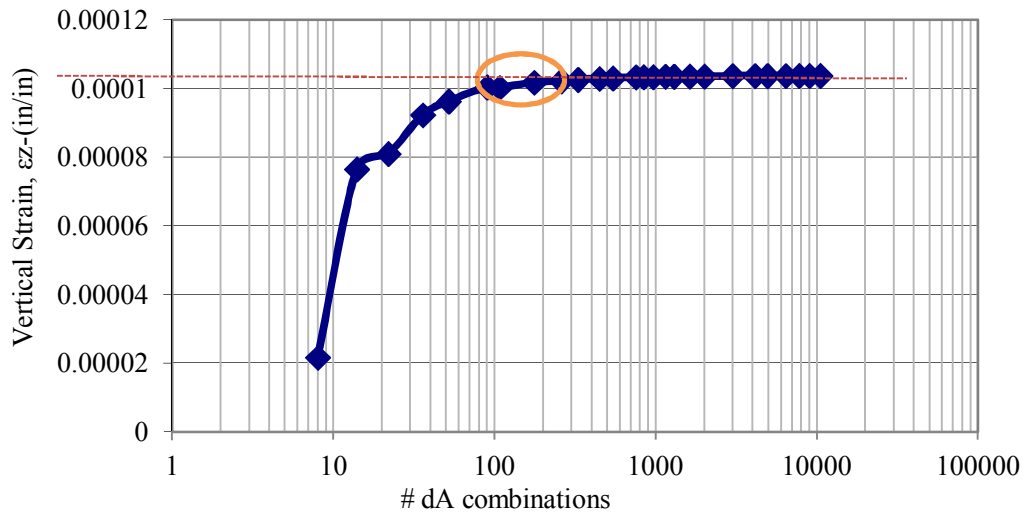


FIGURE 4-26 Vertical strain and number of dA analysis for elliptical tire imprint shape ($Z=20.00$ in).

From the previous tables and figures, the following points are concluded:

- i. After a certain point, the number of dA combinations used becomes stable. At this point, any increase in the number of areas in the segment does not improve the precision of the predicted value.
- ii. For elliptical tire shape at shallow depth, the range of # dA combinations (200-300) appears to be optimal that should be used for time concern and best strain and stress values.
- iii. The range of dx and $dr = (8-11)$, $dy = (12-18)$, and $d\phi = (30^\circ - 36^\circ)$ is a reasonable number to use for elliptical tire shape calculation with shallow depth.

4.8 Impact of the Computed Depth on Number of Computational Points

4.8.1 Analysis for Circular Tire Imprint Shape

TABLE 4-10 illustrates the results of stress and strain Percentage Diff, % between the target and calculated values for circular tire Imprint shape at the three depths

investigated: $z= 20.00, 79.57, 150.00$ in. FIGURE 4-27 illustrates the relationship between the stress percentage diff (calculated and target) and the number of computational points for 2 circular tire imprints. FIGURE 4-28 shows the relationship between vertical strain percentage diff (calculated and target) and the number of computational points of circular tire imprint shape for the three different depths.

TABLE 4-10 Analysis for Circular Tire Imprint Shape

| # of computational points | Percentage Diff, % | | | | | |
|---------------------------|--------------------|--------------|------------|--------------|-------------|--------------|
| | Z=20.00 in | | Z=79.57 in | | Z=150.00 in | |
| | σ_z | ϵ_z | σ_z | ϵ_z | σ_z | ϵ_z |
| 5 | 5.38 | 38.28 | 0.20 | 0.24 | 0.12 | 0.14 |
| 10 | 5.38 | 38.28 | 0.20 | 0.24 | 0.12 | 0.14 |
| 24 | 1.35 | 9.66 | 0.05 | 0.06 | 0.03 | 0.04 |
| 40 | 1.35 | 9.66 | 0.05 | 0.06 | 0.03 | 0.04 |
| 72 | 0.59 | 4.26 | 0.02 | 0.03 | 0.01 | 0.02 |
| 90 | 0.59 | 4.26 | 0.02 | 0.03 | 0.01 | 0.02 |
| 120 | 0.33 | 2.37 | 0.01 | 0.01 | 0.01 | 0.01 |
| 150 | 0.21 | 1.49 | 0.01 | 0.01 | 0.00 | 0.01 |
| 216 | 0.14 | 1.02 | 0.01 | 0.01 | 0.00 | 0.00 |
| 320 | 0.08 | 0.54 | 0.00 | 0.00 | 0.00 | 0.00 |
| 450 | 0.04 | 0.32 | 0.00 | 0.00 | 0.00 | 0.00 |
| 600 | 0.04 | 0.32 | 0.00 | 0.00 | 0.00 | 0.00 |
| 720 | 0.03 | 0.21 | 0.00 | 0.00 | 0.00 | 0.00 |
| 864 | 0.03 | 0.21 | 0.00 | 0.00 | 0.00 | 0.00 |
| 1080 | 0.02 | 0.11 | 0.00 | 0.00 | 0.00 | 0.00 |
| 1260 | 0.02 | 0.13 | 0.00 | 0.00 | 0.00 | 0.00 |
| 1530 | 0.01 | 0.07 | 0.00 | 0.00 | 0.00 | 0.00 |
| 1800 | 0.00 | 0.03 | 0.00 | 0.00 | 0.00 | 0.00 |
| 2160 | 0.01 | 0.06 | 0.00 | 0.00 | 0.00 | 0.00 |
| 3000 | 0.00 | 0.00 | 0.00 | 0.00 | 0.00 | 0.00 |
| 4320 | 0.00 | 0.00 | 0.00 | 0.00 | 0.00 | 0.00 |
| 5400 | 0.00 | 0.02 | 0.00 | 0.00 | 0.00 | 0.00 |
| 6300 | 0.00 | 0.03 | 0.00 | 0.00 | 0.00 | 0.00 |
| 7200 | 0.00 | 0.03 | 0.00 | 0.00 | 0.00 | 0.00 |
| 8280 | 0.00 | 0.01 | 0.00 | 0.00 | 0.00 | 0.00 |
| 9000 | 0.00 | 0.00 | 0.00 | 0.00 | 0.00 | 0.00 |

From TABLE 4-10 and the figures, the following points are concluded:

- i. For both stress and strain calculation, the accuracy of the program will increase as the number of computational points increases for all depths.
- ii. For both stress and strain calculations, the percentage difference between the target and calculated stress/strain values decreases as the selected depth for the stress and strain calculation increases. This is highly logical and allows one to conclude that the greatest number of dA used should occur closer to the pavement surface where the external loads are applied. As deeper depths are used, the prediction of stress/strain can be approximated by a single point surface load for each tire. As a result, the appropriated number of computational points will decrease as the selected depth is increases.

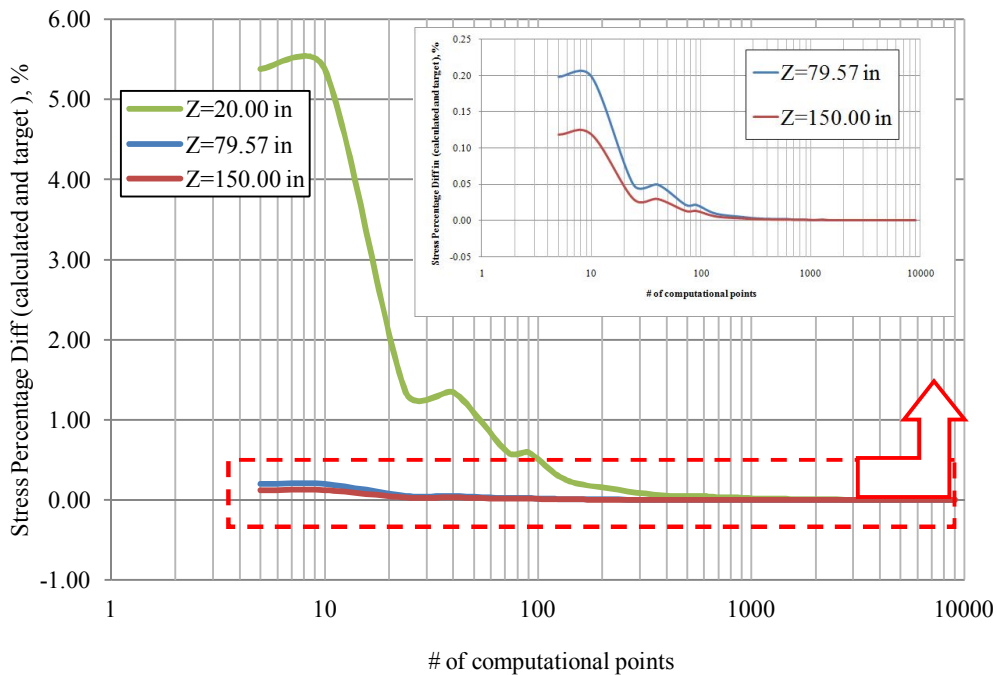


FIGURE 4-27 Relationship between stress percentage diff (%) and number of computational points of circular tire imprint shape.

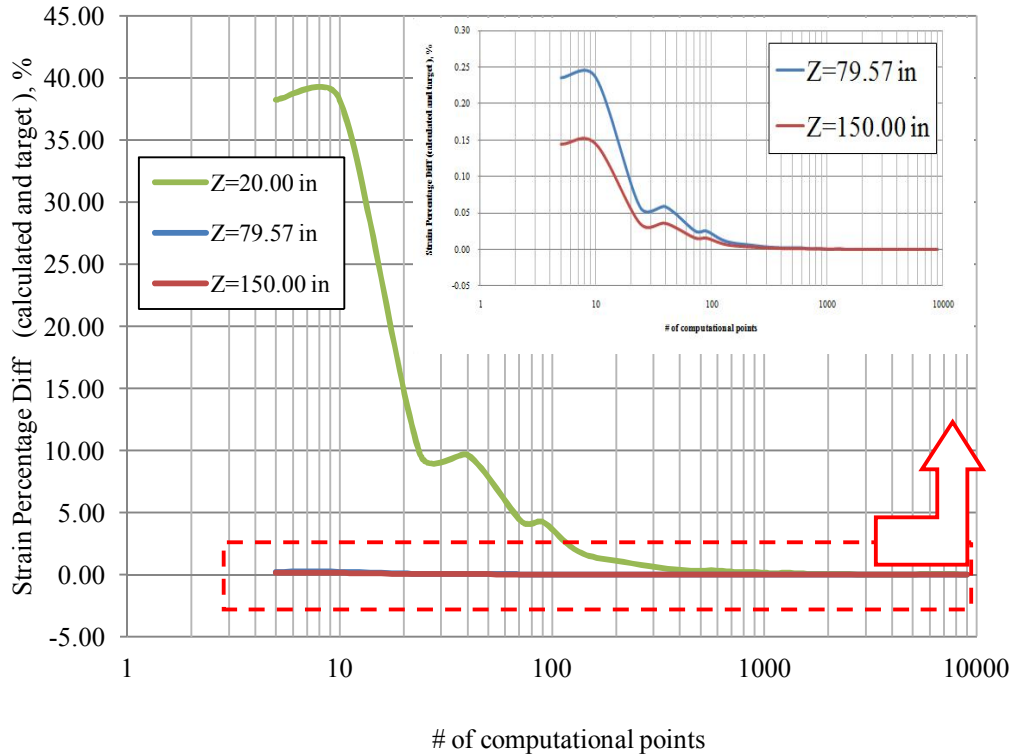


FIGURE 4-28 Relationship between strain percentage diff (%) and number of computational points of circular tire imprint shape.

4.8.1 Analysis for Elliptical Tire Imprint Shape

TABLE 4-11 illustrates the results of stress and strain percentage diff, % between target and calculated value for the elliptical tire imprint shape at three depths $z = 20.00$, 79.57 , and 150.00 in. FIGURE 4-29 illustrates the relationship between the stress percentages differences (calculated and target) and the number of computational points of elliptical tire imprint shape for three different depths. Finally, FIGURE 4-30 shows the relationship between the vertical strain percentage diff (calculated and target) and the number of computational points of elliptical tire imprint shape for three different depths.

TABLE 4-11 Analysis for Elliptical Tire Imprint Shape

| # of computational points | Percentage Diff, % | | | | | |
|---------------------------|--------------------|--------------|------------|--------------|-------------|--------------|
| | Z=20.00 in | | Z=79.57 in | | Z=150.00 in | |
| | σ_z | ϵ_z | σ_z | ϵ_z | σ_z | ϵ_z |
| 8 | 6.34 | 79.17 | 0.15 | 0.18 | 0.09 | 0.12 |
| 14 | 2.11 | 26.25 | 0.03 | 0.04 | 0.02 | 0.02 |
| 22 | 1.74 | 21.94 | 0.04 | 0.04 | 0.02 | 0.03 |
| 36 | 0.89 | 11.05 | 0.01 | 0.02 | 0.01 | 0.01 |
| 52 | 0.59 | 7.20 | 0.01 | 0.02 | 0.00 | 0.00 |
| 90 | 0.27 | 3.24 | 0.00 | 0.00 | 0.00 | 0.00 |
| 108 | 0.28 | 3.33 | 0.00 | 0.00 | 0.00 | 0.00 |
| 176 | 0.16 | 1.91 | 0.00 | 0.00 | 0.00 | 0.00 |
| 260 | 0.12 | 1.47 | 0.00 | 0.00 | 0.00 | 0.00 |
| 330 | 0.09 | 1.11 | 0.00 | 0.00 | 0.00 | 0.00 |
| 448 | 0.07 | 0.85 | 0.00 | 0.00 | 0.00 | 0.00 |
| 544 | 0.06 | 0.71 | 0.00 | 0.00 | 0.00 | 0.00 |
| 756 | 0.04 | 0.42 | 0.00 | 0.00 | 0.00 | 0.00 |
| 840 | 0.03 | 0.36 | 0.00 | 0.00 | 0.00 | 0.00 |
| 968 | 0.03 | 0.33 | 0.00 | 0.00 | 0.00 | 0.00 |
| 1152 | 0.02 | 0.26 | 0.00 | 0.00 | 0.00 | 0.00 |
| 1300 | 0.02 | 0.24 | 0.00 | 0.00 | 0.00 | 0.00 |
| 1624 | 0.01 | 0.17 | 0.00 | 0.00 | 0.00 | 0.00 |
| 2006 | 0.01 | 0.15 | 0.00 | 0.00 | 0.00 | 0.00 |
| 3000 | 0.01 | 0.08 | 0.00 | 0.00 | 0.00 | 0.00 |
| 4128 | 0.00 | 0.06 | 0.00 | 0.00 | 0.00 | 0.00 |
| 4950 | 0.00 | 0.05 | 0.00 | 0.00 | 0.00 | 0.00 |
| 6440 | 0.00 | 0.02 | 0.00 | 0.00 | 0.00 | 0.00 |
| 7776 | 0.00 | 0.01 | 0.00 | 0.00 | 0.00 | 0.00 |
| 9000 | 0.00 | 0.00 | 0.00 | 0.00 | 0.00 | 0.00 |
| 10500 | 0.00 | 0.00 | 0.00 | 0.00 | 0.00 | 0.00 |

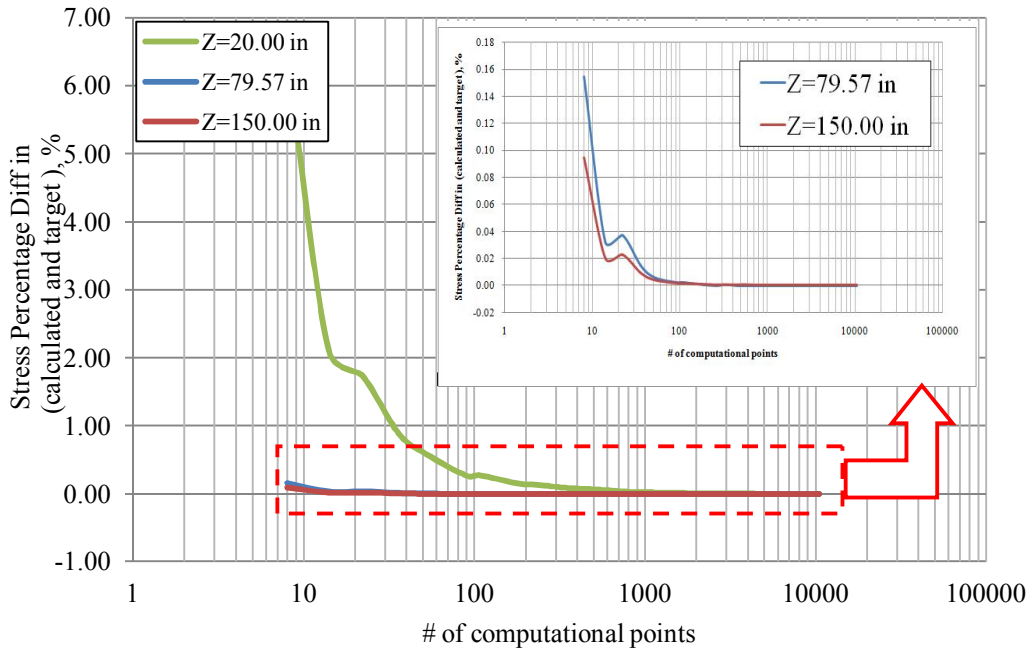


FIGURE 4-29 Relationship between stress percentage diff (%) and N_0 of computational points of elliptical tire imprint shape.

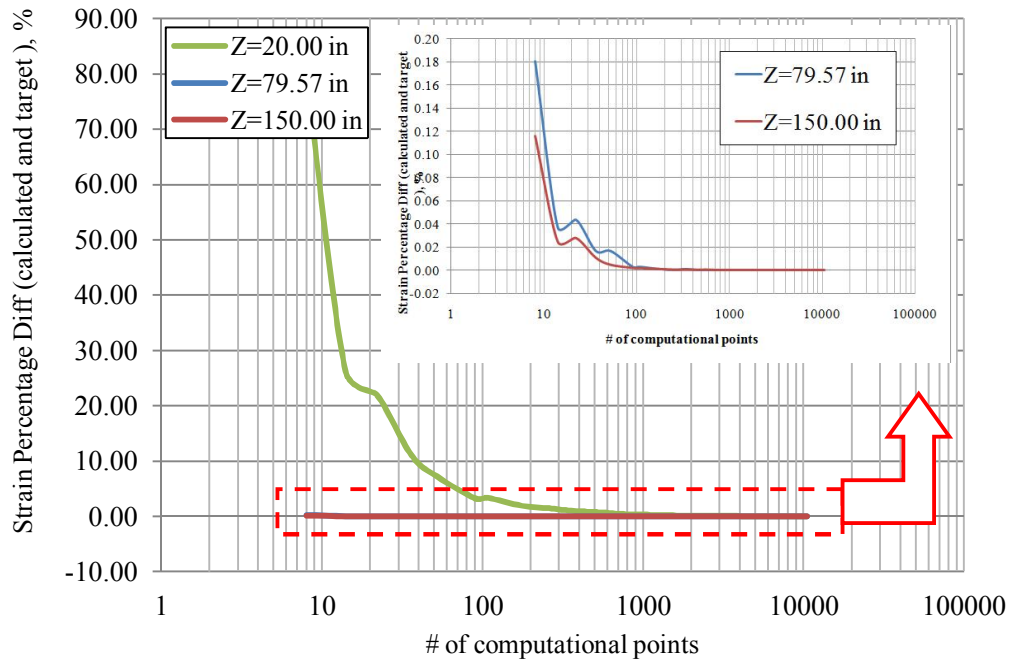


FIGURE 4-30 Relationship between strain percentage diff (%) and N_0 of computational points of elliptical tire imprint shape.

From TABLE 4-11 and the figures, the following points are concluded:

- i. For both stress and strain calculation, the accuracy of the program will increase as the number of computational points increases for all depths.
- ii. For both stress and strain calculations, the percentage difference between the target and calculated stress/strain values decreases as the selected depth for the stress and strain calculation increases. Thus, one can conclude that the greatest number of dA used should occur closer to pavement surface where the external loads are applied. As deeper depths are used, the prediction of stress/strain can be approximated by a single point surface load for each tire. As a result, the appropriated number of computational points will decrease as the selected depth is increases.

4.9 Conclusions of the Study:

Based upon the findings from this study, the following points are concluded:

- i. The larger the number of computational dA values selected, the time taken to run the program will increase direct in proportion to the time per point.
- ii. After a certain point of dA values; the pavement response value becomes stable. At this point, further increases in the number of areas (dA) in the segment will not improve the precision.
- iii. For circular tire shapes at deep depth, the range of # dA combinations (100-150) is a general optimal number of dA that should be used for time concern and precision of the strain and stress values.
- iv. The range of $dr = (3-5)$, and $d\phi = (10^\circ - 12^\circ)$ is a reasonable number to use for circular tire shape calculation with deep depth.

- v. For an elliptical tire shape at a deep depth, the range of # dA combinations (50-100) is the best that should be used for time concern and best strain and stress values.
- vi. The range of dx and dr = (4-6), dy = (7- 10), and $d\phi = (45^\circ -60^\circ)$ could be a good number to use for elliptical tire shape calculation.
- vii. For an elliptical tire shape, $d\phi$ must not be an even integer.
- viii. For an elliptical tire shape, $360/d\phi$ should not be an odd number. Also, $360/d\phi$ should be an integer number.
- ix. For a circular tire shape at mid depth, the range of # dA combinations (150-250) is the best that should be used for time concern and best strain and stress values.
- x. The range of dr = (5-7), and $d\phi = (9^\circ -12^\circ)$ is a good number to use for circular tire shape calculation with mid depth.
- xi. For elliptical tire shape at mid depth, the range of # dA combinations (100-200) is an optimal value that should be used for time concern and best strain and stress values.
- xii. The range of dx and dr = (6-10), dy = (10- 16), and $d\phi = (36^\circ -45^\circ)$ could be a good number to use for elliptical tire shape calculation with mid depth.
- xiii. For circular tire shape at shallow depth, the range of # dA combinations (200-300) is the best that should be used for time concern and best strain and stress value.
- xiv. The range of dr = (6-8), and $d\phi = (9^\circ -11^\circ)$ could be a good number to use for circular tire shape calculation with shallow depth.

- xv. For elliptical tire shape at shallow depth, the range of # dA combinations (200-300) is the best that should be used for time concern and best strain and stress values.
- xvi. The range of dx and dr = (8-11), dy = (12-18), and $d\phi = (30^\circ - 36^\circ)$ could be a good number to use for elliptical tire shape calculation with shallow depth.
- xvii. For both stress and strain calculation, the accuracy of the program will increase as the number of computational points increases for all depths.
- xviii. For both stress and strain calculation, the percentage difference between target and calculated values decreases by increasing the selected depth for both stress and strain calculation. As a result, the appropriate number of computational points will decrease as the selected depth increases.

CHAPTER 5 STRESS AND STRAIN ANALYSIS IN ZAPRAM

5.1 Introduction

The method used in ZAPRAM to calculate the stresses and strains in any pavement system is based upon the method of equivalent thicknesses (MET). This method is also known as Odemark's method. The general idea of this method is to transform a pavement system consisting of layers of different moduli into an equivalent system where all layers have the same modulus, and on which Boussinesq's equations can be utilized. Boussinesq solutions are available for stress, strain, and deflection at a point (x, y, z) located at a distance, R from the origin of coordinates which is also the point of application of the vertical load, P . The stress components in Cartesian coordinates are given in section 2.3.4.1.

While the Odemark procedure has been used in practice for many decades, program ZAPRAM was subsequently verified to existing multilayered elastic responses to insure its general compliance to provide reasonably accurate stress solutions.

5.2 Corroborate the Validity of the Program

After identifying the system of equations used in the program (section 2.3.4.1); the validity of the program was verified in a variety of ways. The next sub-section explains the comparative studies undertaken.

5.2.1 ZAPRAM and Manual Computation Comparison

In this section, the set of equations used in the program were first verified manually to the Boussinesq solutions. A three layered pavement system was used for the comparison. Figure 5-1 illustrates the pavement system that was used.

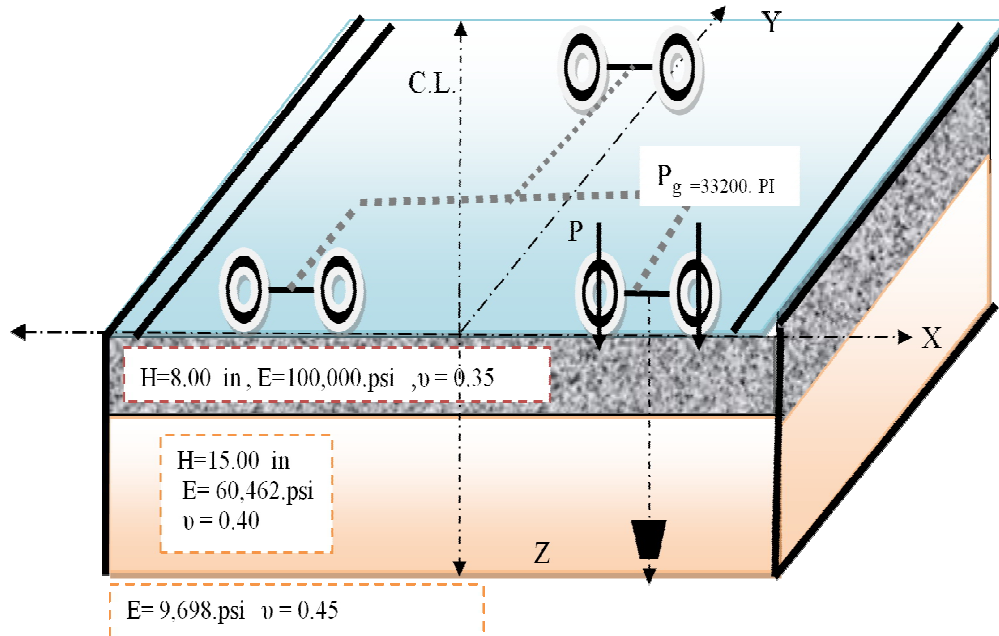


FIGURE 5-1 Pavement system used in the stress comparison.

For the comparison, a B-737-600 aircraft was used in the study. This plane contains 2 wheels in the main gear (Dual Tires). In this comparison, the stresses and strain on the surface of the subgrade layer and at the middle of the distance between the dual wheels were calculated. In addition, the values which were calculated from the program were then compared by the values that were obtained from an Excel sheet with the results from a numerical computational solution of the equation.

- The equivalent thickness for a given layer is :

$$h_e = f_i * h_i * \sqrt[3]{\frac{(E_i(1-\mu_n^2))}{(E_n(1-\mu_i^2))}} \quad (5-1)$$

- The equivalent thickness for both layers (using a f=1.0) is:

| h1 | E1 | E2 | μ1 | μ2 | He |
|----------------------------|--------|------|------|------|---------------|
| 8 | 100000 | 9698 | 0.35 | 0.45 | 16.866 |
| 15 | 60462 | 9698 | 0.4 | 0.45 | 27.134 |
| The equivalent thickness = | | | | | <u>44.000</u> |

- R Value:

$$R = \sqrt{x^2 + y^2 + z^2} \quad (5-2)$$

| X | Y | Z | R |
|----|---|----|--------|
| 17 | 0 | 44 | 47.170 |

- Normal stress in the z direction, σ_z :

$$\sigma_z = \frac{3P z^3}{2\pi R^5} \quad (5-3)$$

| P | Z | R | $\Sigma \sigma z$ |
|-----------|----|--------|-------------------|
| 33200 | 44 | 47.170 | 5.782 |
| Two Tires | | | 11.565 |

- Normal stress in the x direction, σ_x :

$$\sigma_x = \frac{3P}{2\pi} \left[\frac{x^2 z}{R^5} - \frac{1-2\nu}{3} \left\{ -\frac{1}{R(R+z)} + \frac{(2R+z)x^2}{(R+z)^2 R^3} + \frac{z}{R^3} \right\} \right] \quad (5-4)$$

| P | x | z | R | μ | $\Sigma \sigma x$ |
|-----------|----|----|--------|-------|-------------------|
| 33200 | 17 | 44 | 47.170 | 0.450 | 0.740 |
| Two Tires | | | | | 1.481 |

- Normal stress in the y direction, σ_y :

$$\sigma_y = \frac{3P}{2\pi} \left[\frac{y^2 z}{R^5} - \frac{1-2\nu}{3} \left\{ -\frac{1}{R(R+z)} + \frac{(2R+z)y^2}{(R+z)^2 R^3} + \frac{z}{R^3} \right\} \right] \quad (5-5)$$

| P | Y | Z | R | μ | $\Sigma \sigma y$ |
|-----------|---|----|--------|-------|-------------------|
| 33200 | 0 | 44 | 47.170 | 0.450 | -0.061 |
| Two Tires | | | | | -0.122 |

- Strain in the z direction, ϵ_z :

$$\varepsilon_z = \frac{1}{E}(\sigma_z - \nu(\sigma_x + \sigma_y)) \quad (5-6)$$

| | | | | | |
|------------|------|------------|------------|-------|-----------------|
| σ_z | E2 | σ_x | σ_y | μ | ε_z |
| 11.565 | 9698 | 1.481 | -0.122 | 0.450 | 0.00113 |

- The result from the program and the manual calculation comparison are:

| | | ZAPRAM | | | | | | Manual Calculation | | | | |
|----|----|---------|------|------------|------------|------------|-----------------|--------------------|------------|------------|------------|-----------------|
| h1 | h2 | CBR (%) | Z | σ_z | σ_x | σ_y | ε_z | Z | σ_z | σ_x | σ_y | ε_z |
| 8 | 15 | 7 | 44.0 | 11.3839 | 1.4372 | -0.1216 | 0.0011 | 44.00 | 11.565 | 1.481 | -0.122 | 0.00113 |

According to this brief calculation, the ZAMRAM predicted stresses are correctly computed relation to the Boussinesq equations. Since the triaxial strains are simply a function of a constant E and the state of triaxial stress; it can also be concluded that the ZAPRAM predicted normal strains are also equivalent to those normally computed from the One Layer Boussinesq case.

5.2.2 ZAPRAM and JULEA Comparison

For this comparison, two different types of aircraft were used; Boeing B737-600 which has 2 wheels in the main gear (Dual Tires) and AIRBUS INDUSTRIE A300-C4 having 4 wheels in the main gear (Dual Tandem). The geometric center point for both aircraft was selected for the (x, y) coordinate. The depth z was chosen at the top of the subgrade for all runs. As explained in the previous section, ZAPRAM is programmed to calculate the stresses and strains from the MET method. As a result, if any layer section is transformed to one layer and introduced to the JULEA program and the results compared, there should be no difference between the programs. (However, while this conceptually may be true, it must be recognized that a correction factor, for each layer, may be necessary to “calibrate” the transformed state of stress to the predicted from a precise multi-layered theoretical solution.)

5.2.2.1 Compare JULEA (1 Layer) with ZAPRAM:

For each aircraft, every program was run 8 times for 8 different systems (two values for the 1st layer thickness, two values for the 2nd layer thickness, and 2 CBR values for the subgrade). Figure 5-2 shows the pavement system with all alternative choices for this comparison study.

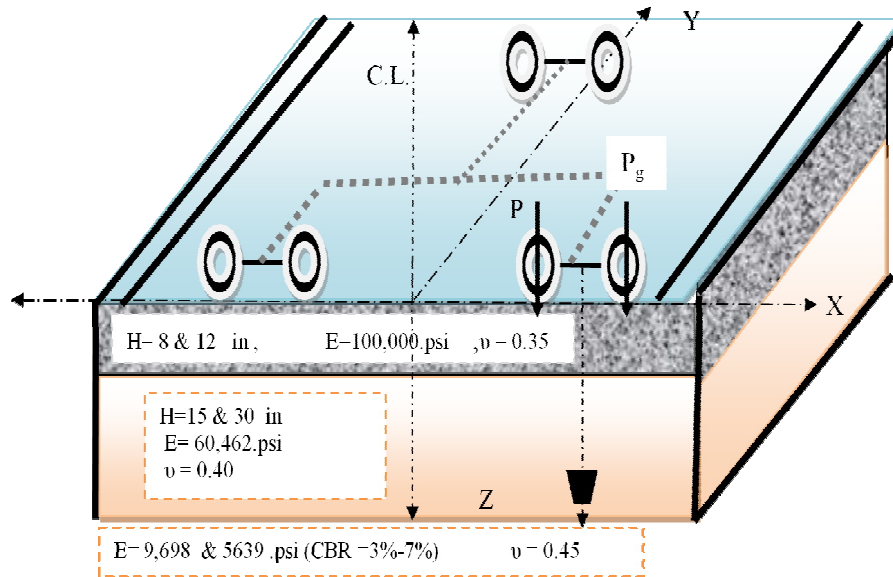


FIGURE 5-2 The pavement system with all the option.

FIGURE 5-1 and FIGURE 5-2, illustrate the results of computational runs from both programs, with both aircraft respectively. The last four columns show the percentage different for the ZAPRAM results compare to the JULEA one layer system. As can be seen, this percentage was 0% for all different runs with all different possible combination.

TABLE 5-1 JULEA (1 Layer) and ZAPRAM Comparison for Boeing B737-600

| Boeing B737-600 | | | ZAPRAM | | | | | JULEA(1 Layer) | | | | | Percentage Diff, % | | | |
|-----------------|-------|---------|--------|------------|------------|------------|--------------|----------------|------------|------------|------------|--------------|--------------------|------------|------------|--------------|
| h_1 | h_2 | CBR (%) | Z | σ_z | σ_x | σ_y | ϵ_z | Z | σ_z | σ_x | σ_y | ϵ_z | σ_z | σ_x | σ_y | ϵ_z |
| 8 | 15 | 3 | 52.70 | 8.7846 | 0.7420 | -0.1101 | 0.0015 | 52.70 | 8.7900 | 0.7418 | -0.1099 | 0.0015 | 0 | 0 | 0 | 0 |
| 8 | 15 | 7 | 44.00 | 11.3839 | 1.4372 | -0.1216 | 0.0011 | 44.00 | 11.3800 | 1.4360 | -0.1214 | 0.0011 | 0 | 0 | 0 | 0 |
| 8 | 30 | 3 | 85.23 | 3.9303 | 0.0904 | -0.0594 | 0.0007 | 85.23 | 3.9300 | 0.0897 | -0.0587 | 0.0007 | 0 | 1 | 1 | 0 |
| 8 | 30 | 7 | 71.13 | 5.4008 | 0.2153 | -0.0779 | 0.0006 | 71.13 | 5.4010 | 0.2141 | -0.0773 | 0.0006 | 0 | 1 | 1 | 0 |
| 12 | 15 | 3 | 62.82 | 6.6555 | 0.3685 | -0.0917 | 0.0012 | 62.82 | 6.6570 | 0.3668 | -0.0912 | 0.0012 | 0 | 0 | 1 | 0 |
| 12 | 15 | 7 | 52.43 | 8.8567 | 0.7575 | -0.1106 | 0.0009 | 52.43 | 8.8570 | 0.7563 | -0.1104 | 0.0009 | 0 | 0 | 0 | 0 |
| 12 | 30 | 3 | 95.33 | 3.2065 | 0.0485 | -0.0493 | 0.0006 | 95.33 | 3.2060 | 0.0482 | -0.0487 | 0.0006 | 0 | 1 | 1 | 0 |
| 12 | 30 | 7 | 79.57 | 4.4426 | 0.1276 | -0.0661 | 0.0005 | 79.57 | 4.4420 | 0.1268 | -0.0655 | 0.0005 | 0 | 1 | 1 | 0 |

TABLE 5-2 JULEA (1 Layer) and ZAPRAM Comparison for Airbus INDUSTRIE A300-C4

| AIRBUS INDUSTRIE A300-C4 | | | ZAPRAM | | | | | JULEA(1 Layer) | | | | | Percentage Diff, % | | | |
|--------------------------|-------|---------|--------|------------|------------|------------|--------------|----------------|------------|------------|------------|--------------|--------------------|------------|------------|--------------|
| h_1 | h_2 | CBR (%) | Z | σ_z | σ_x | σ_y | ϵ_z | Z | σ_z | σ_x | σ_y | ϵ_z | σ_z | σ_x | σ_y | ϵ_z |
| 8 | 15 | 3 | 52.70 | 11.4162 | 1.2891 | 3.2947 | 0.0017 | 52.70 | 11.4200 | 1.2910 | 3.2980 | 0.0017 | 0 | 0 | 0 | 0 |
| 8 | 15 | 7 | 44.00 | 12.0027 | 2.0120 | 4.9909 | 0.0009 | 44.00 | 12.0100 | 2.0120 | 4.9900 | 0.0009 | 0 | 0 | 0 | 0 |
| 8 | 30 | 3 | 85.23 | 7.4284 | 0.2518 | 0.7663 | 0.0012 | 85.23 | 7.4320 | 0.2513 | 0.7655 | 0.0012 | 0 | 0 | 0 | 0 |
| 8 | 30 | 7 | 71.13 | 9.1210 | 0.5059 | 1.4044 | 0.0009 | 71.13 | 9.1210 | 0.5062 | 1.4060 | 0.0009 | 0 | 0 | 0 | 0 |
| 12 | 15 | 3 | 62.82 | 10.2071 | 0.7690 | 2.0483 | 0.0016 | 62.82 | 10.2100 | 0.7698 | 2.0500 | 0.0016 | 0 | 0 | 0 | 0 |
| 12 | 15 | 7 | 52.43 | 11.4448 | 1.3081 | 3.3396 | 0.0010 | 52.43 | 11.4500 | 1.3090 | 3.3400 | 0.0010 | 0 | 0 | 0 | 0 |
| 12 | 30 | 3 | 95.33 | 6.4058 | 0.1529 | 0.5092 | 0.0011 | 95.33 | 6.4100 | 0.1524 | 0.5079 | 0.0011 | 0 | 0 | 0 | 0 |
| 12 | 30 | 7 | 79.57 | 8.0739 | 0.3328 | 0.9723 | 0.0008 | 79.57 | 8.0760 | 0.3323 | 0.9719 | 0.0008 | 0 | 0 | 0 | 0 |

The next four figures (Figs 5-3 to 5-6) show the computed stresses and strain from both programs. It is readily observable that the lines are identical from each analysis. This merely reaffirms the results shown by Tables 5-1 and 5-2. Similar to the first comparison conducted with the normal solution of the Boussinesq and ZAPRAM states of stress; it is perfectly clear that the Boussinesq stress/strain solution, programmed in ZAPRAM are completely identical to the Boussinesq solution used in either a manual solution of through sophisticated multi-layered Elastic Theory computer solutions (such as JULEA), solved for a Boussinesq One Layer solution with multiple tire loads.

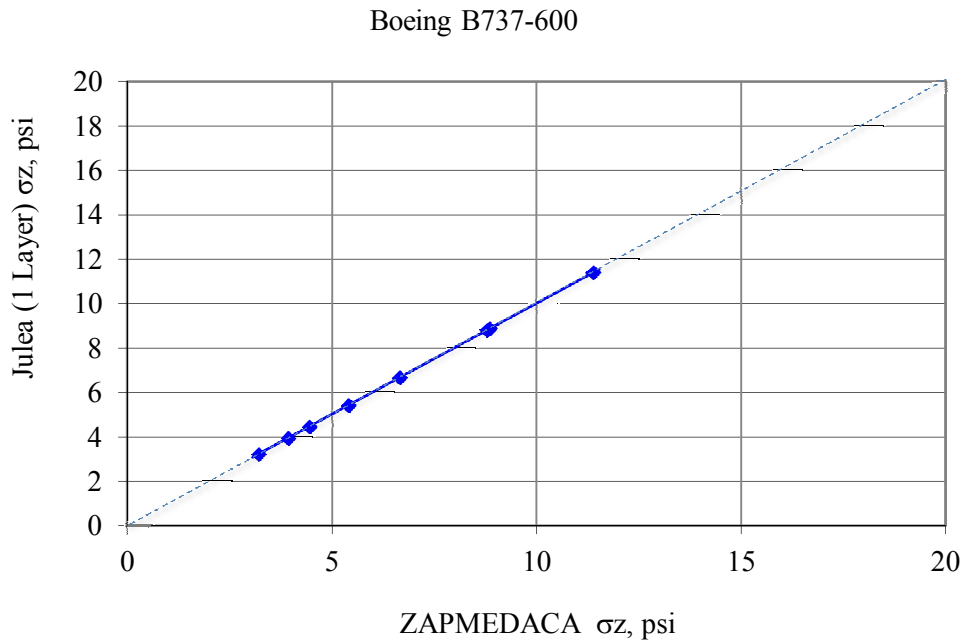


FIGURE 5-3 Calculated stresses from JULEA (1 Layer) and ZAPRAM by using Boeing B737-600.

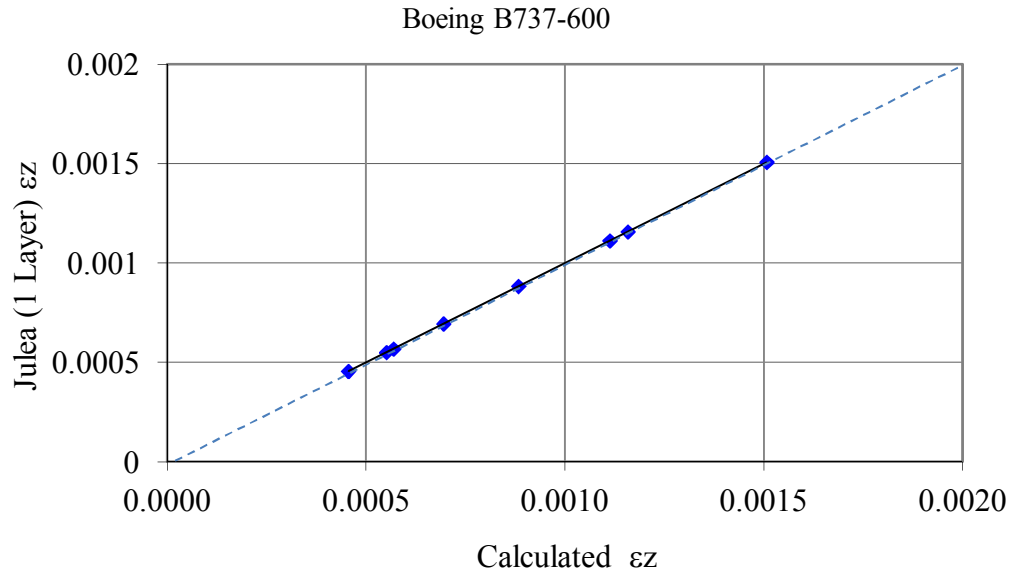


FIGURE 5-4 Calculated strain from JULEA (1 Layer) and ZAPRAM by using Boeing B737-600.

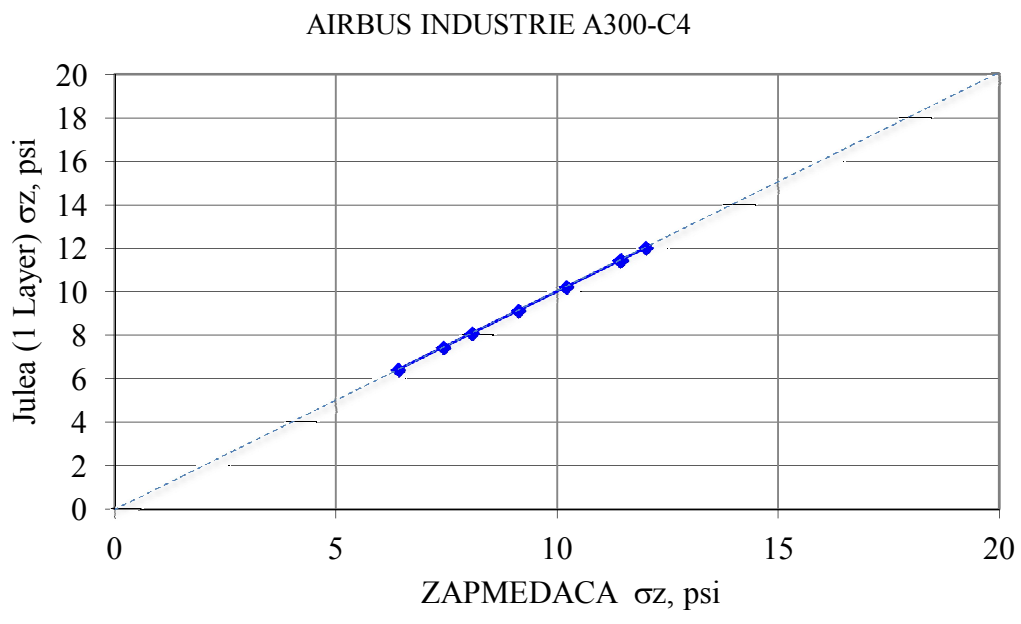


FIGURE 5-5 Calculated stresses from JULEA (1 Layer) and ZAPRAM by using airbus INDUSTRIE A300-C4.

AIRBUS INDUSTRIE A300-C4

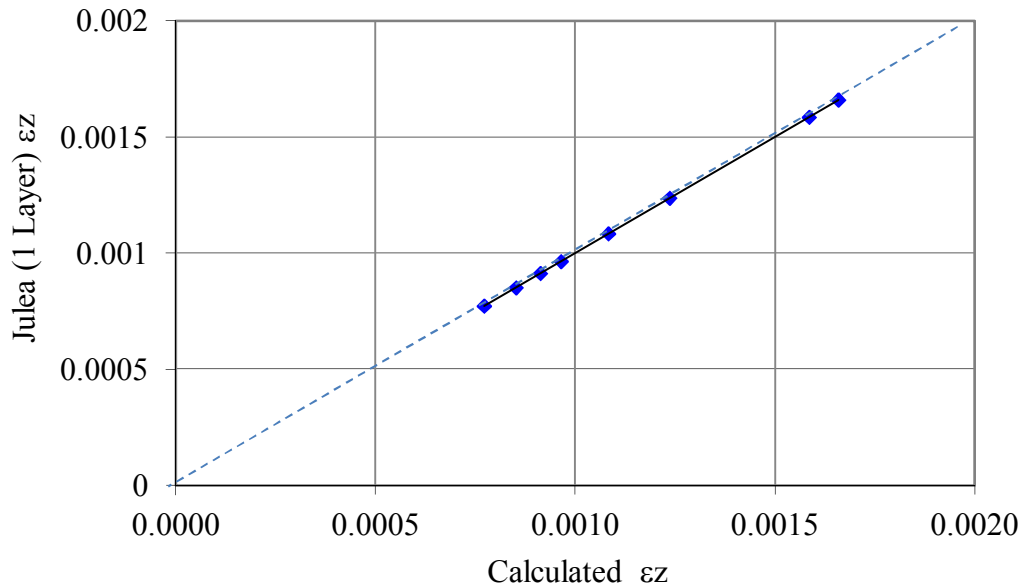


FIGURE 5-6 Calculated strain from JULEA (1 Layer) and ZAPRAM by using airbus INDUSTRIE A300-C.

5.2.2.2 Compare JULEA (3 Layers) to ZAPRAM:

In this comparative study, the comparison was extended to the prediction of multilayered structures. Thus, for the first time; the influence of the influence of the correction factor, f , (Odemark Transformed Section Correction Factor) comes into play with the comparative prediction of stress/strain by ZAPRAM and a 3 layered JULEA MLET Solution. The program solutions were conducted 48 times per aircraft. This was completed on 12 different systems (three values for the 1st layer thickness, two values for the 2nd layer thickness, and 2 CBR values for the subgrade). The following figure shows the pavement system utilized with all alternatives. It is important to recognize that these initial sets of runs were conducted using a $f_1 = f_2 = 1.0$.

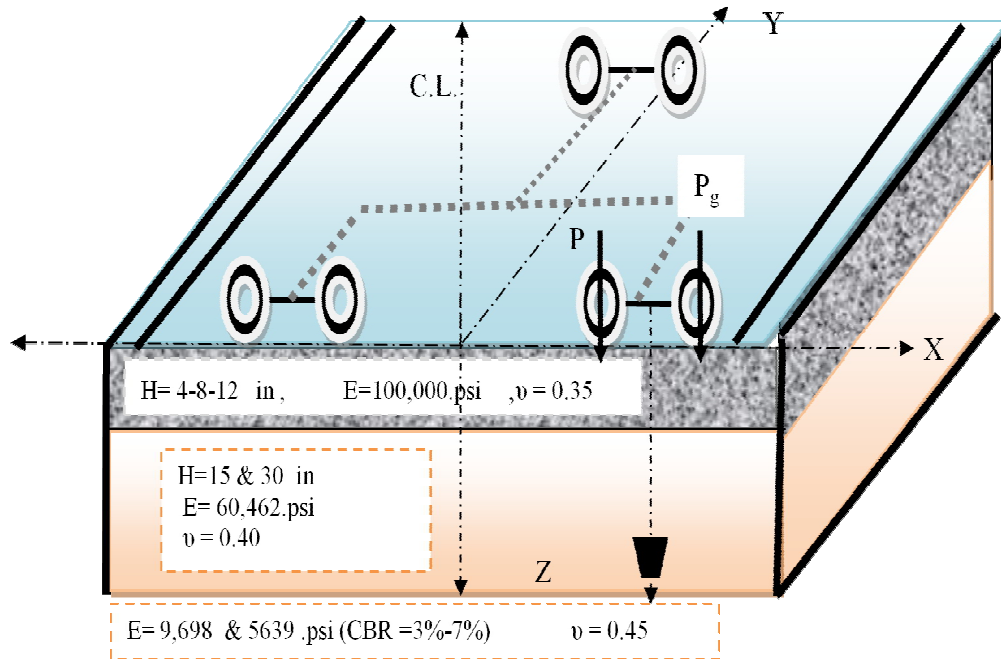


FIGURE 5-7 The pavement system with all options.

TABLE 5-3 and TABLE 5-4 summarize the results of the 48 runs for each aircraft analyzed. The last four columns show the percent difference for the ZAPRAM results compared to use of the JULEA three layer-system. It can be observed that the differences between program types now become quite significant.

The percentage is especially high for the strain value when the heavier A300 Airbus load was used. It should be recalled that the transformation of the layered system into a Boussinesq solution utilized a correction factor $f = 1.0$. These results clearly show that the use of an Odemark Transformed Section analysis, using a f_i (correction) = 1.0; will result in significant differences in the states of stress/strain that are predicted from the most accurate MLET models available (eg. JULEA MLET). As the original ZAPMEDACA used a $f_i = 1.0$; the predicted pavement response variables should be considered as suggest. The next section of this Chapter starts the investigation relative to what would be the most accurate values of f_i to be used in the Odemark Transformed Section produced within ZAPRAM.

TABLE 5-3 JULEA (3 Layers) and ZAPRAM Comparison for Boeing B737-600

| B737-600 | | | ZAPRAM | | | | | JULEA(3 Layers) | | | | | Percentage Diff, % | | | |
|----------|----|--------|--------|------------|------------|------------|--------------|-----------------|------------|------------|------------|--------------|--------------------|------------|------------|--------------|
| h1 | h2 | CBR(%) | Z | σ_z | σ_x | σ_y | ϵ_z | Z | σ_z | σ_x | σ_y | ϵ_z | σ_z | σ_x | σ_y | ϵ_z |
| 4 | 15 | 3 | 42.61 | 11.8783 | 1.6060 | -0.1220 | 0.0020 | 19 | 12.2700 | 5.6920 | 2.5280 | 0.0015 | 3 | 72 | 105 | 31 |
| 4 | 15 | 7 | 35.57 | 14.7628 | 2.9040 | -0.1090 | 0.0014 | 19 | 14.9500 | 7.2510 | 2.4440 | 0.0011 | 1 | 60 | 104 | 28 |
| 4 | 30 | 3 | 75.12 | 4.9144 | 0.1678 | -0.0720 | 0.0009 | 34 | 6.0690 | 1.5690 | 0.8241 | 0.0009 | 19 | 89 | 109 | 2 |
| 4 | 30 | 7 | 62.70 | 6.6766 | 0.3715 | -0.0919 | 0.0007 | 34 | 8.0050 | 1.9280 | 0.7728 | 0.0007 | 17 | 81 | 112 | 4 |
| 8 | 15 | 3 | 52.70 | 8.7846 | 0.7420 | -0.1101 | 0.0015 | 23 | 9.7670 | 3.6360 | 1.6910 | 0.0013 | 10 | 80 | 107 | 15 |
| 8 | 15 | 7 | 44.00 | 11.3839 | 1.4372 | -0.1216 | 0.0011 | 23 | 12.3500 | 4.6290 | 1.6410 | 0.0010 | 8 | 69 | 107 | 13 |
| 8 | 30 | 3 | 85.23 | 3.9303 | 0.0904 | -0.0594 | 0.0007 | 38 | 5.0600 | 1.1350 | 0.6246 | 0.0008 | 22 | 92 | 110 | 8 |
| 8 | 30 | 7 | 71.13 | 5.4008 | 0.2153 | -0.0779 | 0.0006 | 38 | 6.7580 | 1.3770 | 0.5836 | 0.0006 | 20 | 84 | 113 | 9 |
| 12 | 15 | 3 | 62.82 | 6.6555 | 0.3685 | -0.0917 | 0.0012 | 27 | 7.8360 | 2.4330 | 1.2000 | 0.0011 | 15 | 85 | 108 | 5 |
| 12 | 15 | 7 | 52.43 | 8.8567 | 0.7575 | -0.1106 | 0.0009 | 27 | 10.1400 | 3.0680 | 1.1590 | 0.0008 | 13 | 75 | 110 | 4 |
| 12 | 30 | 3 | 95.33 | 3.2065 | 0.0485 | -0.0493 | 0.0006 | 42 | 4.2580 | 0.8503 | 0.4959 | 0.0006 | 25 | 94 | 110 | 12 |
| 12 | 30 | 7 | 79.57 | 4.4426 | 0.1276 | -0.0661 | 0.0005 | 42 | 5.7300 | 1.0160 | 0.4633 | 0.0005 | 22 | 87 | 114 | 13 |

TABLE 5-4 JULEA (3 Layers) and ZAPRAM Comparison for Airbus INDUSTRIE A300-C4

| A300-C4 | | | ZAPRAM | | | | | JULEA(3 Layers) | | | | | Percentage Diff, % | | | |
|---------|----|---------|--------|------------|------------|------------|--------------|-----------------|------------|------------|------------|--------------|--------------------|------------|------------|--------------|
| h1 | h2 | CBR (%) | Z | σ_z | σ_x | σ_y | ϵ_z | Z | σ_z | σ_x | σ_y | ϵ_z | σ_z | σ_x | σ_y | ϵ_z |
| 4 | 15 | 3 | 42.61 | 12.0194 | 2.1573 | 5.3278 | 0.0015 | 19 | 12.0500 | 6.1710 | 8.7930 | 0.0009 | 0 | 65 | 39 | 63 |
| 4 | 15 | 7 | 35.57 | 11.5875 | 3.0390 | 7.3453 | 0.0007 | 19 | 11.7900 | 6.4220 | 10.0400 | 0.0005 | 2 | 53 | 27 | 58 |
| 4 | 30 | 3 | 75.12 | 8.6146 | 0.4147 | 1.1779 | 0.0014 | 34 | 8.3830 | 2.7940 | 3.9580 | 0.0009 | 3 | 85 | 70 | 48 |
| 4 | 30 | 7 | 62.70 | 10.2229 | 0.7738 | 2.0598 | 0.0009 | 34 | 9.7670 | 3.0920 | 4.8420 | 0.0006 | 5 | 75 | 57 | 44 |
| 8 | 15 | 3 | 52.70 | 11.4162 | 1.2891 | 3.2947 | 0.0017 | 23 | 11.0800 | 4.8410 | 6.8780 | 0.0010 | 3 | 73 | 52 | 61 |
| 8 | 15 | 7 | 44.00 | 12.0027 | 2.0120 | 4.9909 | 0.0009 | 23 | 11.6700 | 5.2190 | 8.1470 | 0.0006 | 3 | 61 | 39 | 57 |
| 8 | 30 | 3 | 85.23 | 7.4284 | 0.2518 | 0.7663 | 0.0012 | 38 | 7.4620 | 2.2030 | 3.1290 | 0.0009 | 0 | 89 | 76 | 38 |
| 8 | 30 | 7 | 71.13 | 9.1210 | 0.5059 | 1.4044 | 0.0009 | 38 | 8.9680 | 2.4540 | 3.8590 | 0.0006 | 2 | 79 | 64 | 35 |
| 12 | 15 | 3 | 62.82 | 10.2071 | 0.7690 | 2.0483 | 0.0016 | 27 | 9.9820 | 3.8080 | 5.3760 | 0.0010 | 2 | 80 | 62 | 53 |
| 12 | 15 | 7 | 52.43 | 11.4448 | 1.3081 | 3.3396 | 0.0010 | 27 | 11.0900 | 4.1930 | 6.5050 | 0.0006 | 3 | 69 | 49 | 49 |
| 12 | 30 | 3 | 95.33 | 6.4058 | 0.1529 | 0.5092 | 0.0011 | 42 | 6.6980 | 1.7740 | 2.5040 | 0.0008 | 4 | 91 | 80 | 28 |
| 12 | 30 | 7 | 79.57 | 8.0739 | 0.3328 | 0.9723 | 0.0008 | 42 | 8.2450 | 1.9790 | 3.0940 | 0.0006 | 2 | 83 | 69 | 26 |

Figures 5-8 to 5-11 show the computed stresses and strains from both programs. It is noted that the line of equivalency is not applicable with the study involving the two correction value equal to 1.0. This difference is very significant when the strain was calculated. Even the slopes for both lines are variable. With a correction factor of $f = 1.0$; it is concluded that the results in general from ZAPRAM (or ZAPMEDACA) may be significantly different than those estimated by JULEA.

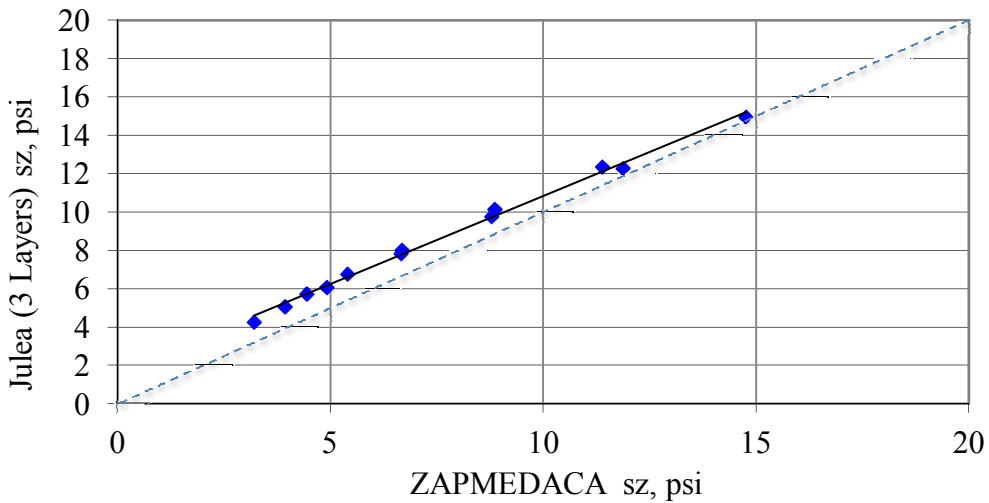


FIGURE 5-8 Calculated stresses from JULEA (3 Layers) and ZAPRAM by using Boeing B737-600.

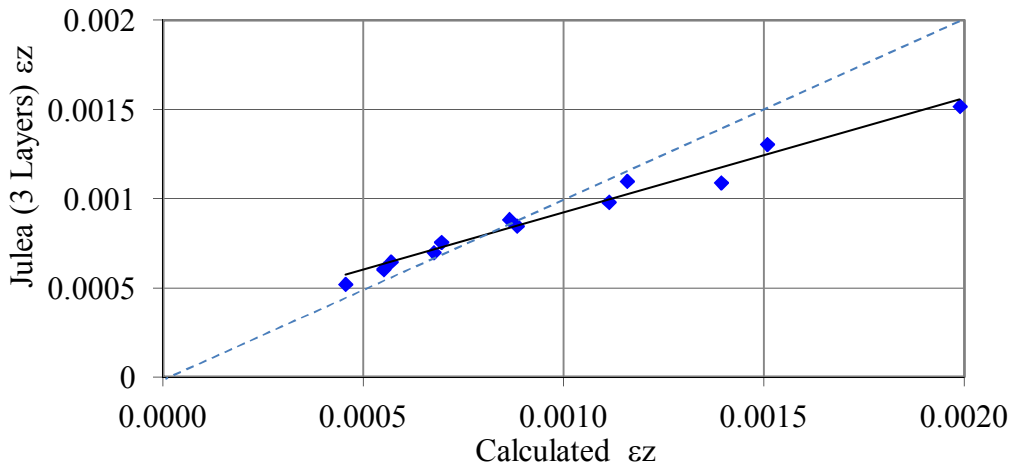


FIGURE 5-9 Calculated strain from JULEA (3 Layers) and ZAPRAM by using Boeing B737-600.

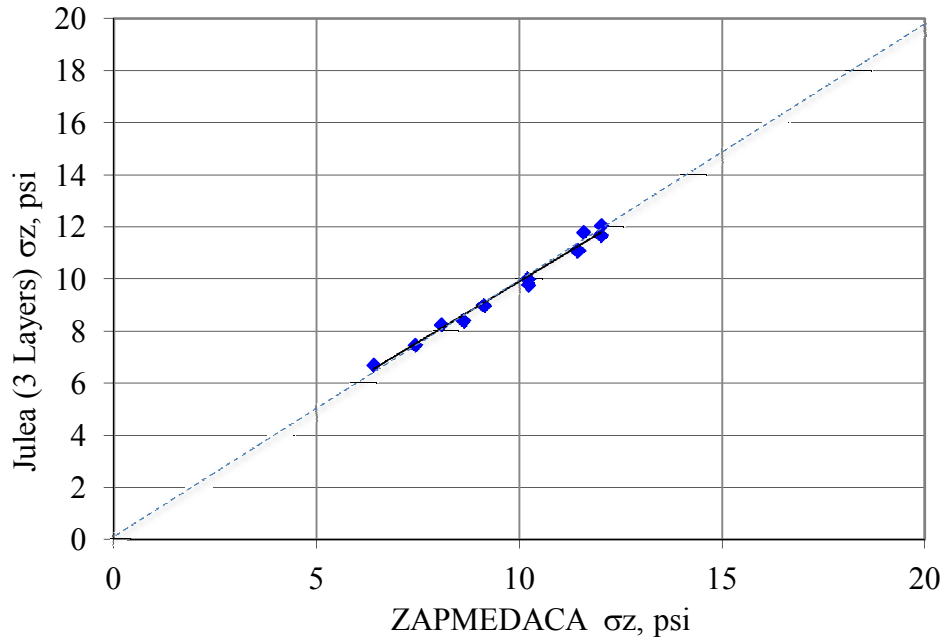


FIGURE 5-10 Calculated stresses from JULEA (3 Layers) and ZAPRAM by using airbus INDUSTRIE A300-C4

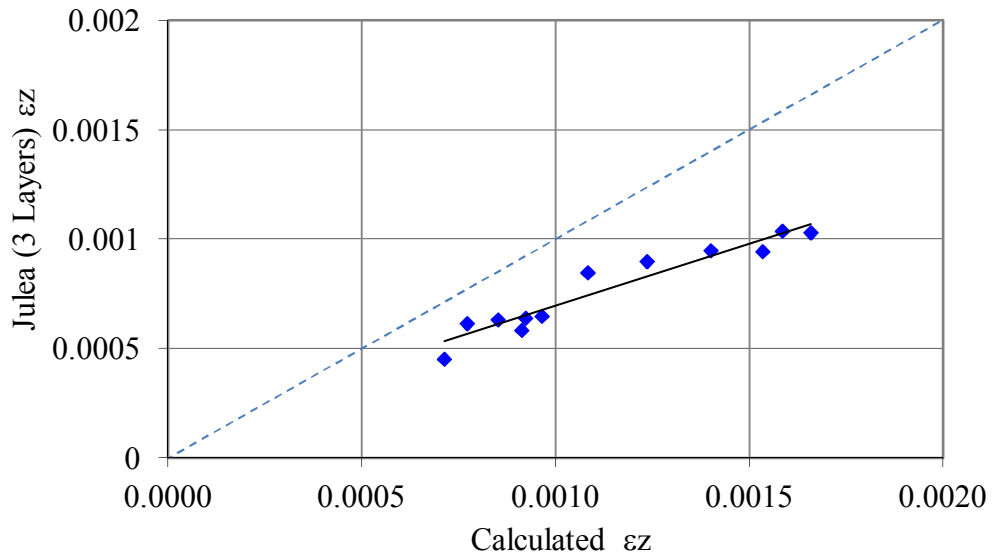


Figure 5-11 Calculated strain from JULEA (3 Layers) and ZAPRAM by using airbus INDUSTRIE A300-C.

5.3 The Correction Factor “f”:

Based upon the results of the previous studies, it was prudent to start an investigation to ascertain what the most accurate set of layered correction factors (f_i), for the Odemark Transformed Section analysis would be to provide stress and strain predictions comparable to the “true values” obtained from MLET computer codes. From a literature review, the correction factor, f , appears to depend on layer thickness, modular ratio, Poisson’s ratios and the number of layers in the structure. Frequently referenced values were found to range from $f_i = 1.0$ to 0.8 in the literature. In this section, a study is presented to determine the most accurate value for the correction factor that might be recommended to decrease the prediction differences found in the previous study.

Nine sets for f_1, f_2 were used in the initial study and are as follows:

| | |
|---|--------------------|
| 1 | $f_1=0.8, f_2=0.8$ |
| 2 | $f_1=0.8, f_2=0.9$ |
| 3 | $f_1=0.9, f_2=0.8$ |
| 4 | $f_1=0.9, f_2=0.9$ |
| 5 | $f_1=1.0, f_2=0.8$ |
| 6 | $f_1=1.0, f_2=0.9$ |
| 7 | $f_1=1.0, f_2=1.0$ |
| 8 | $f_1=1.0, f_2=1.1$ |
| 9 | $f_1=1.1, f_2=1.1$ |

For each integrated set, the percentage difference between the ZAPRAM one layer system and JULEA three layers system were calculated. An evaluation was then made to ascertain the best combinations of the f correction values to use. This study utilized 2 Aircraft types and eight pavement systems. TABLE 5-5 to TABLE 5-20 illustrate all of program results.

TABLE 5-5 JULEA (3 Layers) and ZAPRAM comparison for the 1st pavement system with different correction factors.

| Boeing B737-600 | | | | | | | | | | | ZAPRAM | | | | JULEA(3 Layer) | | | | | Percentage Diff, % | | | |
|-----------------------|--------|------|---------|---------|-------|-----|-----|-------|-------|-------|------------|------------|------------|--------------|----------------|------------|------------|------------|--------------|--------------------|------------|------------|--------------|
| h1 | E1 | E2 | μ_1 | μ_2 | He | f1 | f2 | he1 | he2 | he | σ_z | σ_x | σ_y | ϵ_z | Z | σ_z | σ_x | σ_y | ϵ_z | σ_z | σ_x | σ_y | ϵ_z |
| 8 | 100000 | 5639 | 0.35 | 0.45 | 20.21 | 0.8 | 0.8 | 16.17 | 26.01 | 42.17 | 2.0404 | 1.6643 | 0.1220 | 0.0020 | 23 | 9.767 | 3.636 | 1.6910 | 0.0013 | 23 | 54 | 107 | 54 |
| 15 | 60462 | 5639 | 0.4 | 0.45 | 32.51 | 0.8 | 0.9 | 16.17 | 29.26 | 45.42 | 0.9007 | 1.2846 | 0.1205 | 0.0018 | 23 | 9.767 | 3.636 | 1.6910 | 0.0013 | 12 | 65 | 107 | 41 |
| equivalent thickness= | | | | | 52.72 | 0.9 | 0.8 | 18.19 | 26.01 | 44.19 | 1.3167 | 1.4153 | 0.1215 | 0.0019 | 23 | 9.767 | 3.636 | 1.6910 | 0.0013 | 16 | 61 | 107 | 46 |
| | | | | | | 0.9 | 0.9 | 18.19 | 29.26 | 47.44 | 0.2563 | 1.0987 | 0.1183 | 0.0017 | 23 | 9.767 | 3.636 | 1.6910 | 0.0013 | 5 | 70 | 107 | 33 |
| | | | | | | 1 | 0.8 | 20.21 | 26.01 | 46.21 | 0.6429 | 1.2079 | 0.1198 | 0.0018 | 23 | 9.767 | 3.636 | 1.6910 | 0.0013 | 9 | 67 | 107 | 38 |
| | | | | | | 1 | 0.9 | 20.21 | 29.26 | 49.47 | 9.6579 | 0.9429 | 0.1155 | 0.0016 | 23 | 9.767 | 3.636 | 1.6910 | 0.0013 | 1 | 74 | 107 | 26 |
| | | | | | | 1 | 1 | 20.21 | 32.51 | 52.72 | 8.7849 | 0.7421 | 0.1101 | 0.0015 | 23 | 9.767 | 3.636 | 1.6910 | 0.0013 | 10 | 80 | 107 | 15 |
| | | | | | | 1 | 1.1 | 20.21 | 35.76 | 55.97 | 8.0115 | 0.5884 | 0.1042 | 0.0014 | 23 | 9.767 | 3.636 | 1.6910 | 0.0013 | 18 | 84 | 106 | 6 |
| | | | | | | 1.1 | 1.1 | 22.23 | 35.76 | 57.99 | 7.5757 | 0.5112 | 0.1005 | 0.0013 | 23 | 9.767 | 3.636 | 1.6910 | 0.0013 | 22 | 86 | 106 | 0 |

122

TABLE 5-6 JULEA (3 Layers) and ZAPRAM comparison for the 2nd pavement system with different correction factors.

| Boeing B737-600 | | | | | | | | | | | ZAPRAM | | | | JULEA(3 Layer) | | | | | Percentage Diff, % | | | |
|-----------------------|--------|------|---------|---------|-------|-----|-----|-------|-------|-------|------------|------------|------------|--------------|----------------|------------|------------|------------|--------------|--------------------|------------|------------|--------------|
| h1 | E1 | E2 | μ_1 | μ_2 | He | f1 | f2 | he1 | he2 | he | σ_z | σ_x | σ_y | ϵ_z | Z | σ_z | σ_x | σ_y | ϵ_z | σ_z | σ_x | σ_y | ϵ_z |
| 8 | 100000 | 9698 | 0.35 | 0.45 | 16.86 | 0.8 | 0.8 | 13.49 | 21.71 | 35.20 | 14.9292 | 2.9989 | -0.1072 | 0.0014 | 23 | 12.35 | 4.6290 | 1.6410 | 0.0010 | 21 | 35 | 107 | 43 |
| 15 | 60462 | 9698 | 0.4 | 0.45 | 27.13 | 0.8 | 0.9 | 13.49 | 24.42 | 37.91 | 13.7347 | 2.3715 | -0.1172 | 0.0013 | 23 | 12.35 | 4.6290 | 1.6410 | 0.0010 | 11 | 49 | 107 | 33 |
| equivalent thickness= | | | | | 44.00 | 0.9 | 0.8 | 15.18 | 21.71 | 36.89 | 14.1767 | 2.5895 | -0.1142 | 0.0013 | 23 | 12.35 | 4.6290 | 1.6410 | 0.0010 | 15 | 44 | 107 | 37 |
| | | | | | | 0.9 | 0.9 | 15.18 | 24.42 | 39.60 | 13.0365 | 2.0569 | -0.1203 | 0.0013 | 23 | 12.35 | 4.6290 | 1.6410 | 0.0010 | 6 | 56 | 107 | 28 |
| | | | | | | 1 | 0.8 | 16.87 | 21.71 | 38.57 | 13.4573 | 2.2423 | -0.1186 | 0.0013 | 23 | 12.35 | 4.6290 | 1.6410 | 0.0010 | 9 | 52 | 107 | 31 |
| | | | | | | 1 | 0.9 | 16.87 | 24.42 | 41.29 | 12.3741 | 1.7890 | -0.1218 | 0.0012 | 23 | 12.35 | 4.6290 | 1.6410 | 0.0010 | 0 | 61 | 107 | 22 |
| | | | | | | 1 | 1 | 16.87 | 27.13 | 44.00 | 11.3839 | 1.4372 | -0.1216 | 0.0011 | 23 | 12.35 | 4.6290 | 1.6410 | 0.0010 | 8 | 69 | 107 | 13 |
| | | | | | | 1 | 1.1 | 16.87 | 29.85 | 46.71 | 10.4841 | 1.1622 | -0.1192 | 0.0010 | 23 | 12.35 | 4.6290 | 1.6410 | 0.0010 | 15 | 75 | 107 | 5 |
| | | | | | | 1.1 | 1.1 | 18.55 | 29.85 | 48.40 | 9.9679 | 1.0217 | -0.1170 | 0.0010 | 23 | 12.35 | 4.6290 | 1.6410 | 0.0010 | 19 | 78 | 107 | 0 |

TABLE 5-7 JULEA (3 Layers) and ZAPRAM comparison for the 3rd pavement system with different correction factors.

| Boeing B737-600 | | | | | | | | | | | ZAPRAM | | | | JULEA(3 Layer) | | | | Percentage Diff, % | | | | |
|-----------------|-----------------------|------|---------|---------|--------|-----|-----|-------|-------|-------|------------|------------|------------|--------------|----------------|------------|------------|------------|-----------------------|------------|------------|------------|--------------|
| h1 | E1 | E2 | μ_1 | μ_2 | He | f1 | f2 | he1 | he2 | he | σ_z | σ_x | σ_y | ϵ_z | Z | σ_z | σ_x | σ_y | ϵ_z | σ_z | σ_x | σ_y | ϵ_z |
| 8 | 100000 | 5639 | 0.35 | 0.45 | 20.208 | 0.8 | 0.8 | 16.17 | 52.01 | 68.18 | 5.8056 | 0.2598 | -0.0825 | 0.0010 | 38 | 5.06 | 1.1350 | 0.6246 | 0.0008 | 15 | 77 | 113 | 34 |
| 30 | 60462 | 5639 | 0.4 | 0.45 | 65.018 | 0.8 | 0.9 | 16.17 | 58.52 | 74.68 | 4.9651 | 0.1725 | -0.0726 | 0.0009 | 38 | 5.06 | 1.1350 | 0.6246 | 0.0008 | 2 | 85 | 112 | 15 |
| | equivalent thickness= | | | | 85.223 | 0.9 | 0.8 | 18.19 | 52.01 | 70.20 | 5.5242 | 0.2284 | -0.0793 | 0.0010 | 38 | 5.06 | 1.1350 | 0.6246 | 0.0008 | 9 | 80 | 113 | 28 |
| | | | | | | 0.9 | 0.9 | 18.19 | 58.52 | 76.70 | 4.7389 | 0.1522 | -0.0698 | 0.0008 | 38 | 5.06 | 1.1350 | 0.6246 | 0.0008 | 6 | 87 | 111 | 10 |
| | | | | | | 1 | 0.8 | 20.21 | 52.01 | 72.22 | 5.2616 | 0.2011 | -0.0762 | 0.0009 | 38 | 5.06 | 1.1350 | 0.6246 | 0.0008 | 4 | 82 | 112 | 22 |
| | | | | | | 1 | 0.9 | 20.21 | 58.52 | 78.72 | 4.5270 | 0.1344 | -0.0672 | 0.0008 | 38 | 5.06 | 1.1350 | 0.6246 | 0.0008 | 11 | 88 | 111 | 5 |
| | | | | | | 1 | 1 | 20.21 | 65.02 | 85.23 | 3.9304 | 0.0904 | -0.0594 | 0.0007 | 38 | 5.06 | 1.1350 | 0.6246 | 0.0008 | 22 | 92 | 110 | 8 |
| | | | | | | 1 | 1.1 | 20.21 | 71.52 | 91.73 | 3.4406 | 0.0607 | -0.0527 | 0.0006 | 38 | 5.06 | 1.1350 | 0.6246 | 0.0008 | 32 | 95 | 108 | 19 |
| | | | | | | 1.1 | 1.1 | 22.23 | 71.52 | 93.75 | 3.3064 | 0.0536 | -0.0509 | 0.0006 | 38 | 5.06 | 1.1350 | 0.6246 | 0.0008 | 35 | 95 | 108 | 23 |

TABLE 5-8 JULEA (3 Layers) and ZAPRAM comparison for the 4th pavement system with different correction factors.

| Boeing B737-600 | | | | | | | | | | | ZAPRAM | | | | JULEA(3 Layer) | | | | Percentage Diff, % | | | | |
|-----------------|-----------------------|------|---------|---------|--------|-----|-----|-------|-------|-------|------------|------------|------------|--------------|----------------|------------|------------|------------|-----------------------|------------|------------|------------|--------------|
| h1 | E1 | E2 | μ_1 | μ_2 | He | f1 | f2 | he1 | he2 | he | σ_z | σ_x | σ_y | ϵ_z | Z | σ_z | σ_x | σ_y | ϵ_z | σ_z | σ_x | σ_y | ϵ_z |
| 8 | 100000 | 9698 | 0.35 | 0.45 | 16.866 | 0.8 | 0.8 | 13.49 | 43.41 | 56.91 | 7.8048 | 0.5510 | -0.1025 | 0.0008 | 38 | 6.7580 | 1.3770 | 0.5836 | 0.0006 | 15 | 60 | 118 | 29 |
| 30 | 60462 | 9698 | 0.4 | 0.45 | 54.267 | 0.8 | 0.9 | 13.49 | 48.84 | 62.33 | 6.7413 | 0.3807 | -0.0925 | 0.0007 | 38 | 6.7580 | 1.3770 | 0.5836 | 0.0006 | 0 | 72 | 116 | 13 |
| | equivalent thickness= | | | | 71.134 | 0.9 | 0.8 | 15.18 | 43.41 | 58.59 | 7.4513 | 0.4903 | -0.0994 | 0.0008 | 38 | 6.7580 | 1.3770 | 0.5836 | 0.0006 | 10 | 64 | 117 | 24 |
| | | | | | | 0.9 | 0.9 | 15.18 | 48.84 | 64.02 | 6.4512 | 0.3404 | -0.0896 | 0.0007 | 38 | 6.7580 | 1.3770 | 0.5836 | 0.0006 | 5 | 75 | 115 | 8 |
| | | | | | | 1 | 0.8 | 16.87 | 43.41 | 60.28 | 7.1191 | 0.4370 | -0.0963 | 0.0007 | 38 | 6.7580 | 1.3770 | 0.5836 | 0.0006 | 5 | 68 | 116 | 19 |
| | | | | | | 1 | 0.9 | 16.87 | 48.84 | 65.71 | 6.1780 | 0.3048 | -0.0867 | 0.0006 | 38 | 6.7580 | 1.3770 | 0.5836 | 0.0006 | 9 | 78 | 115 | 3 |
| | | | | | | 1 | 1 | 16.87 | 54.27 | 71.13 | 5.4008 | 0.2153 | -0.0779 | 0.0006 | 38 | 6.7580 | 1.3770 | 0.5836 | 0.0006 | 20 | 84 | 113 | 9 |
| | | | | | | 1 | 1.1 | 16.87 | 59.69 | 76.56 | 4.7543 | 0.1535 | -0.0700 | 0.0005 | 38 | 6.7580 | 1.3770 | 0.5836 | 0.0006 | 30 | 89 | 112 | 20 |
| | | | | | | 1.1 | 1.1 | 18.55 | 59.69 | 78.25 | 4.5758 | 0.1384 | -0.0678 | 0.0005 | 38 | 6.7580 | 1.3770 | 0.5836 | 0.0006 | 32 | 90 | 112 | 23 |

TABLE 5-9 JULEA (3 Layers) and ZAPRAM comparison for the 5th pavement system with different correction factors.

| Boeing B737-600 | | | | | | | | | | | ZAPRAM | | | | JULEA(3 Layer) | | | | Percentage Diff, % | | | | |
|-----------------|-----------------------|------|---------|---------|--------|-----|-----|-------|-------|-------|------------|------------|------------|--------------|----------------|------------|------------|------------|--------------------|------------|------------|------------|--------------|
| h1 | E1 | E2 | μ_1 | μ_2 | He | f1 | f2 | he1 | he2 | he | σ_z | σ_x | σ_y | ϵ_z | Z | σ_z | σ_x | σ_y | ϵ_z | σ_z | σ_x | σ_y | ϵ_z |
| 12 | 100000 | 5639 | 0.35 | 0.45 | 30.312 | 0.8 | 0.8 | 24.25 | 26.01 | 50.26 | 9.4358 | 0.8889 | -0.1142 | 0.0016 | 27 | 7.8360 | 2.4330 | 1.2000 | 0.0011 | 20 | 63 | 110 | 47 |
| 15 | 60462 | 5639 | 0.4 | 0.45 | 32.509 | 0.8 | 0.9 | 24.25 | 29.26 | 53.51 | 8.5880 | 0.7009 | -0.1087 | 0.0015 | 27 | 7.8360 | 2.4330 | 1.2000 | 0.0011 | 10 | 71 | 109 | 34 |
| | equivalent thickness= | | | | 62.820 | 0.9 | 0.8 | 27.28 | 26.01 | 53.29 | 8.6422 | 0.7121 | -0.1091 | 0.0015 | 27 | 7.8360 | 2.4330 | 1.2000 | 0.0011 | 10 | 71 | 109 | 35 |
| | | | | | | 0.9 | 0.9 | 27.28 | 29.26 | 56.54 | 7.8850 | 0.5653 | -0.1032 | 0.0014 | 27 | 7.8360 | 2.4330 | 1.2000 | 0.0011 | 1 | 77 | 109 | 24 |
| | | | | | | 1 | 0.8 | 30.31 | 26.01 | 56.32 | 7.9334 | 0.5741 | -0.1036 | 0.0014 | 27 | 7.8360 | 2.4330 | 1.2000 | 0.0011 | 1 | 76 | 109 | 24 |
| | | | | | | 1 | 0.9 | 30.31 | 29.26 | 59.57 | 7.2566 | 0.4586 | -0.0976 | 0.0013 | 27 | 7.8360 | 2.4330 | 1.2000 | 0.0011 | 7 | 81 | 108 | 14 |
| | | | | | | 1 | 1 | 30.31 | 32.51 | 62.82 | 6.6558 | 0.3685 | -0.0917 | 0.0012 | 27 | 7.8360 | 2.4330 | 1.2000 | 0.0011 | 15 | 85 | 108 | 5 |
| | | | | | | 1 | 1.1 | 30.31 | 35.76 | 66.07 | 6.1211 | 0.2977 | -0.0860 | 0.0011 | 27 | 7.8360 | 2.4330 | 1.2000 | 0.0011 | 22 | 88 | 107 | 3 |
| | | | | | | 1.1 | 1.1 | 33.34 | 35.76 | 69.10 | 5.6748 | 0.2449 | -0.0811 | 0.0010 | 27 | 7.8360 | 2.4330 | 1.2000 | 0.0011 | 28 | 90 | 107 | 10 |

TABLE 5-10 JULEA (3 Layers) and ZAPRAM comparison for the 6th pavement system with different correction factors.

| Boeing B737-600 | | | | | | | | | | | ZAPRAM | | | | JULEA(3 Layer) | | | | Percentage Diff, % | | | | |
|-----------------|-----------------------|------|---------|---------|--------|-----|-----|-------|-------|-------|------------|------------|------------|--------------|----------------|------------|------------|------------|--------------------|------------|------------|------------|--------------|
| h1 | E1 | E2 | μ_1 | μ_2 | He | f1 | f2 | he1 | he2 | he | σ_z | σ_x | σ_y | ϵ_z | Z | σ_z | σ_x | σ_y | ϵ_z | σ_z | σ_x | σ_y | ϵ_z |
| 12 | 100000 | 9698 | 0.35 | 0.45 | 25.300 | 0.8 | 0.8 | 20.24 | 21.71 | 41.95 | 12.1247 | 1.6952 | -0.1220 | 0.0012 | 27 | 10.1400 | 3.0680 | 1.1590 | 0.0008 | 20 | 45 | 111 | 39 |
| 15 | 60462 | 9698 | 0.4 | 0.45 | 27.134 | 0.8 | 0.9 | 20.24 | 24.42 | 44.66 | 11.1569 | 1.3641 | -0.1212 | 0.0011 | 27 | 10.1400 | 3.0680 | 1.1590 | 0.0008 | 10 | 56 | 110 | 29 |
| | equivalent thickness= | | | | 52.433 | 0.9 | 0.8 | 22.77 | 21.71 | 44.48 | 11.2195 | 1.3840 | -0.1213 | 0.0011 | 27 | 10.1400 | 3.0680 | 1.1590 | 0.0008 | 11 | 55 | 110 | 29 |
| | | | | | | 0.9 | 0.9 | 22.77 | 24.42 | 47.19 | 10.3350 | 1.1204 | -0.1186 | 0.0010 | 27 | 10.1400 | 3.0680 | 1.1590 | 0.0008 | 2 | 63 | 110 | 20 |
| | | | | | | 1 | 0.8 | 25.30 | 21.71 | 47.01 | 10.3920 | 1.1363 | -0.1189 | 0.0010 | 27 | 10.1400 | 3.0680 | 1.1590 | 0.0008 | 2 | 63 | 110 | 21 |
| | | | | | | 1 | 0.9 | 25.30 | 24.42 | 49.72 | 9.5858 | 0.9251 | -0.1151 | 0.0010 | 27 | 10.1400 | 3.0680 | 1.1590 | 0.0008 | 5 | 70 | 110 | 12 |
| | | | | | | 1 | 1 | 25.30 | 27.13 | 52.43 | 8.8568 | 0.7575 | -0.1106 | 0.0009 | 27 | 10.1400 | 3.0680 | 1.1590 | 0.0008 | 13 | 75 | 110 | 4 |
| | | | | | | 1 | 1.1 | 25.30 | 29.85 | 55.15 | 8.1980 | 0.6235 | -0.1057 | 0.0008 | 27 | 10.1400 | 3.0680 | 1.1590 | 0.0008 | 19 | 80 | 109 | 3 |
| | | | | | | 1.1 | 1.1 | 27.83 | 29.85 | 57.68 | 7.6408 | 0.5223 | -0.1011 | 0.0008 | 27 | 10.1400 | 3.0680 | 1.1590 | 0.0008 | 25 | 83 | 109 | 10 |

TABLE 5-11 JULEA (3 Layers) and ZAPRAM comparison for the 7th pavement system with different correction factors.

| Boeing B737-600 | | | | | | ZAPRAM | | | | JULEA(3 Layer) | | | | Percentage Diff, % | | | | | | | | | | |
|-----------------|-----------------------|------|---------|---------|--------|--------|-----|-------|-------|----------------|------------|------------|------------|--------------------|--------|------------|------------|------------|--------------|------------|------------|------------|--------------|----|
| h1 | E1 | E2 | μ_1 | μ_2 | He | f1 | f2 | he1 | he2 | he | σ_z | σ_x | σ_y | ϵ_z | Z | σ_z | σ_x | σ_y | ϵ_z | σ_z | σ_x | σ_y | ϵ_z | |
| 12 | 100000 | 5639 | 0.35 | 0.45 | 30.312 | 0.8 | 0.8 | 24.25 | 52.01 | 76.26 | 4.7868 | 0.1564 | -0.0704 | 0.0008 | 42 | 4.2580 | 0.8503 | 0.4959 | 0.0006 | 12 | 82 | 114 | 30 | |
| 30 | 60462 | 5639 | 0.4 | 0.45 | 65.018 | 0.8 | 0.9 | 24.25 | 58.52 | 82.77 | 4.1421 | 0.1050 | -0.0622 | 0.0007 | 42 | 4.2580 | 0.8503 | 0.4959 | 0.0006 | 3 | 88 | 113 | 13 | |
| | equivalent thickness= | | | | | 95.329 | 0.9 | 0.8 | 27.28 | 52.01 | 79.29 | 4.4696 | 0.1298 | -0.0664 | 0.0008 | 42 | 4.2580 | 0.8503 | 0.4959 | 0.0006 | 5 | 85 | 113 | 22 |
| | | | | | | | 0.9 | 0.9 | 27.28 | 58.52 | 85.80 | 3.8835 | 0.0873 | -0.0588 | 0.0007 | 42 | 4.2580 | 0.8503 | 0.4959 | 0.0006 | 9 | 90 | 112 | 6 |
| | | | | | | | 1 | 0.8 | 30.31 | 52.01 | 82.33 | 4.1817 | 0.1078 | -0.0627 | 0.0007 | 42 | 4.2580 | 0.8503 | 0.4959 | 0.0006 | 2 | 87 | 113 | 14 |
| | | | | | | | 1 | 0.9 | 30.31 | 58.52 | 88.83 | 3.6475 | 0.0725 | -0.0556 | 0.0006 | 42 | 4.2580 | 0.8503 | 0.4959 | 0.0006 | 14 | 91 | 111 | 0 |
| | | | | | | | 1 | 1 | 30.31 | 65.02 | 95.33 | 3.2066 | 0.0485 | -0.0495 | 0.0006 | 42 | 4.2580 | 0.8503 | 0.4959 | 0.0006 | 25 | 94 | 110 | 12 |
| | | | | | | | 1 | 1.1 | 30.31 | 71.52 | 101.83 | 2.8390 | 0.0319 | -0.0442 | 0.0005 | 42 | 4.2580 | 0.8503 | 0.4959 | 0.0006 | 33 | 96 | 109 | 22 |
| | | | | | | | 1.1 | 1.1 | 33.34 | 71.52 | 104.86 | 2.6883 | 0.0260 | -0.0420 | 0.0005 | 42 | 4.2580 | 0.8503 | 0.4959 | 0.0006 | 37 | 97 | 108 | 26 |

Table 5-12 JULEA (3 Layers) and ZAPRAM comparison for the 8th pavement system with different correction factors.

| Boeing B737-600 | | | | | | ZAPRAM | | | | JULEA(3 Layer) | | | | Percentage Diff, % | | | | | | | | | | |
|-----------------|-----------------------|------|---------|---------|--------|--------|-----|-------|-------|----------------|------------|------------|------------|--------------------|--------|------------|------------|------------|--------------|------------|------------|------------|--------------|----|
| h1 | E1 | E2 | μ_1 | μ_2 | He | f1 | f2 | he1 | he2 | he | σ_z | σ_x | σ_y | ϵ_z | Z | σ_z | σ_x | σ_y | ϵ_z | σ_z | σ_x | σ_y | ϵ_z | |
| 12 | 100000 | 9698 | 0.35 | 0.45 | 25.300 | 0.8 | 0.8 | 20.24 | 43.41 | 63.65 | 5.5128 | 0.3488 | -0.0902 | 0.0007 | 42 | 5.7300 | 1.0160 | 0.4633 | 0.0005 | 14 | 66 | 119 | 26 | |
| 30 | 60462 | 9698 | 0.4 | 0.45 | 54.267 | 0.8 | 0.9 | 20.24 | 48.84 | 69.08 | 5.6779 | 0.2453 | -0.0811 | 0.0006 | 42 | 5.7300 | 1.0160 | 0.4633 | 0.0005 | 1 | 76 | 118 | 11 | |
| | equivalent thickness= | | | | | 79.567 | 0.9 | 0.8 | 22.77 | 43.41 | 66.18 | 6.1037 | 0.2955 | -0.0859 | 0.0006 | 42 | 5.7300 | 1.0160 | 0.4633 | 0.0005 | 7 | 71 | 119 | 19 |
| | | | | | | | 0.9 | 0.9 | 22.77 | 48.84 | 71.61 | 5.3392 | 0.2090 | -0.0772 | 0.0005 | 42 | 5.7300 | 1.0160 | 0.4633 | 0.0005 | 7 | 79 | 117 | 4 |
| | | | | | | | 1 | 0.8 | 25.30 | 43.41 | 68.71 | 5.7295 | 0.2511 | -0.0817 | 0.0006 | 42 | 5.7300 | 1.0160 | 0.4633 | 0.0005 | 0 | 75 | 118 | 12 |
| | | | | | | | 1 | 0.9 | 25.30 | 48.84 | 74.14 | 5.0283 | 0.1784 | -0.0734 | 0.0005 | 42 | 5.7300 | 1.0160 | 0.4633 | 0.0005 | 12 | 82 | 116 | 2 |
| | | | | | | | 1 | 1 | 25.30 | 54.27 | 79.57 | 4.4426 | 0.1276 | -0.0661 | 0.0005 | 42 | 5.7300 | 1.0160 | 0.4633 | 0.0005 | 22 | 87 | 114 | 13 |
| | | | | | | | 1 | 1.1 | 25.30 | 59.69 | 84.99 | 3.9497 | 0.0917 | -0.0596 | 0.0004 | 42 | 5.7300 | 1.0160 | 0.4633 | 0.0005 | 31 | 91 | 113 | 22 |
| | | | | | | | 1.1 | 1.1 | 27.83 | 59.69 | 87.52 | 3.7464 | 0.0786 | -0.0569 | 0.0004 | 42 | 5.7300 | 1.0160 | 0.4633 | 0.0005 | 35 | 92 | 112 | 26 |

TABLE 5-13 JULEA (3 Layers) and ZAPRAM comparison for the 1st pavement system with different correction factors.

| AIRBUS INDUSTRIE A300-C4 | | | | | | ZAPRAM | | | | JULEA(3 Layer) | | | | Percentage Diff, % | | | | | | | | | |
|--------------------------|--------|------|---------|---------|-------|--------|-----|-------|-------|----------------|------------|------------|------------|--------------------|----|------------|------------|------------|-----------------|------------|------------|------------|-----------------|
| h1 | E1 | E2 | μ_1 | μ_2 | He | f1 | f2 | he1 | he2 | he | σ_z | σ_x | σ_y | ε_z | Z | σ_z | σ_x | σ_y | ε_z | σ_z | σ_x | σ_y | ε_z |
| 8 | 100000 | 5639 | 0.35 | 0.45 | 20.21 | 0.8 | 0.8 | 16.17 | 26.01 | 42.17 | 12.0188 | 2.2054 | 5.4390 | 0.0015 | 23 | 11.0800 | 4.8410 | 6.8780 | 0.0010 | 8 | 54 | 21 | 48 |
| 15 | 60462 | 5639 | 0.4 | 0.45 | 32.51 | 0.8 | 0.9 | 16.17 | 29.26 | 45.42 | 11.9587 | 1.8721 | 4.6652 | 0.0016 | 23 | 11.0800 | 4.8410 | 6.8780 | 0.0010 | 8 | 61 | 32 | 55 |
| equivalent thickness= | | | | | 52.72 | 0.9 | 0.8 | 18.19 | 26.01 | 44.19 | 11.9982 | 1.9924 | 4.9454 | 0.0016 | 23 | 11.0800 | 4.8410 | 6.8780 | 0.0010 | 8 | 59 | 28 | 53 |
| | | | | | | 0.9 | 0.9 | 18.19 | 29.26 | 47.44 | 11.8556 | 1.6891 | 4.2374 | 0.0016 | 23 | 11.0800 | 4.8410 | 6.8780 | 0.0010 | 7 | 65 | 38 | 58 |
| | | | | | | 1 | 0.8 | 20.21 | 26.01 | 46.21 | 11.9236 | 1.7984 | 4.4931 | 0.0016 | 23 | 11.0800 | 4.8410 | 6.8780 | 0.0010 | 8 | 63 | 35 | 57 |
| | | | | | | 1 | 0.9 | 20.21 | 29.26 | 49.47 | 11.7125 | 1.5232 | 3.8478 | 0.0016 | 23 | 11.0800 | 4.8410 | 6.8780 | 0.0010 | 6 | 69 | 44 | 60 |
| | | | | | | 1 | 1 | 20.21 | 32.51 | 52.72 | 11.4163 | 1.2892 | 3.2948 | 0.0017 | 23 | 11.0800 | 4.8410 | 6.8780 | 0.0010 | 3 | 73 | 52 | 61 |
| | | | | | | 1 | 1.1 | 20.21 | 35.76 | 55.97 | 11.0613 | 1.0912 | 2.8234 | 0.0016 | 23 | 11.0800 | 4.8410 | 6.8780 | 0.0010 | 0 | 77 | 59 | 60 |
| | | | | | | 1.1 | 1.1 | 22.23 | 35.76 | 57.99 | 10.8203 | 0.9839 | 2.5665 | 0.0016 | 23 | 11.0800 | 4.8410 | 6.8780 | 0.0010 | 2 | 80 | 63 | 59 |

TABLE 5-14 JULEA (3 Layers) and ZAPRAM comparison for the 2nd pavement system with different correction factors.

| AIRBUS INDUSTRIE A300-C4 | | | | | | ZAPRAM | | | | JULEA(3 Layer) | | | | Percentage Diff % | | | | | | | | | |
|--------------------------|--------|------|---------|---------|--------|--------|-----|-------|-------|----------------|------------|------------|------------|-------------------|----|------------|------------|------------|-----------------|------------|------------|------------|-----------------|
| h1 | E1 | E2 | μ_1 | μ_2 | He | f1 | f2 | he1 | he2 | he | σ_z | σ_x | σ_y | ε_z | Z | σ_z | σ_x | σ_y | ε_z | σ_z | σ_x | σ_y | ε_z |
| 8 | 100000 | 9698 | 0.35 | 0.45 | 16.866 | 0.8 | 0.8 | 13.49 | 21.71 | 35.20 | 11.5364 | 3.0913 | 7.4634 | 0.0007 | 23 | 11.6700 | 5.2190 | 8.1470 | 0.0006 | 1 | 41 | 8 | 20 |
| 15 | 60462 | 9698 | 0.4 | 0.45 | 27.134 | 0.8 | 0.9 | 13.49 | 24.42 | 37.91 | 11.8414 | 2.7189 | 6.6184 | 0.0008 | 23 | 11.6700 | 5.2190 | 8.1470 | 0.0006 | 1 | 48 | 19 | 35 |
| equivalent thickness= | | | | | 44.000 | 0.9 | 0.8 | 15.18 | 21.71 | 36.89 | 11.7455 | 2.8559 | 6.9302 | 0.0008 | 23 | 11.6700 | 5.2190 | 8.1470 | 0.0006 | 1 | 45 | 15 | 30 |
| | | | | | | 0.9 | 0.9 | 15.18 | 24.42 | 39.60 | 11.9516 | 2.5050 | 6.1290 | 0.0008 | 23 | 11.6700 | 5.2190 | 8.1470 | 0.0006 | 2 | 52 | 25 | 43 |
| | | | | | | 1 | 0.8 | 16.87 | 21.71 | 38.57 | 11.8913 | 2.6336 | 6.4235 | 0.0008 | 23 | 11.6700 | 5.2190 | 8.1470 | 0.0006 | 2 | 50 | 21 | 38 |
| | | | | | | 1 | 0.9 | 16.87 | 24.42 | 41.29 | 12.0083 | 2.3049 | 5.6689 | 0.0009 | 23 | 11.6700 | 5.2190 | 8.1470 | 0.0006 | 3 | 56 | 30 | 49 |
| | | | | | | 1 | 1 | 16.87 | 27.13 | 44.00 | 12.0027 | 2.0120 | 4.9909 | 0.0009 | 23 | 11.6700 | 5.2190 | 8.1470 | 0.0006 | 3 | 61 | 39 | 57 |
| | | | | | | 1 | 1.1 | 16.87 | 29.85 | 46.71 | 11.8980 | 1.7533 | 4.3877 | 0.0009 | 23 | 11.6700 | 5.2190 | 8.1470 | 0.0006 | 2 | 66 | 46 | 62 |
| | | | | | | 1.1 | 1.1 | 18.55 | 29.85 | 48.40 | 11.7925 | 1.6086 | 4.0486 | 0.0010 | 23 | 11.6700 | 5.2190 | 8.1470 | 0.0006 | 1 | 69 | 50 | 64 |

TABLE 5-15 JULEA (3 Layers) and ZAPRAM comparison for the 3rd pavement system with different correction factors.

| AIRBUS INDUSTRIE A300-C4 | | | | | | | | | | | ZAPRAM | | | | JULEA(3 Layer) | | | | Percentage Diff, % | | | | |
|--------------------------|-----------------------|------|---------|---------|--------|-----|-----|-------|-------|-------|------------|------------|------------|--------------|----------------|------------|------------|------------|--------------------|------------|------------|------------|--------------|
| h1 | E1 | E2 | μ_1 | μ_2 | He | f1 | f2 | he1 | he2 | he | σ_z | σ_x | σ_y | ϵ_z | Z | σ_z | σ_x | σ_y | ϵ_z | σ_z | σ_x | σ_y | ϵ_z |
| 8 | 100000 | 5639 | 0.35 | 0.45 | 20.208 | 0.8 | 0.8 | 16.17 | 52.01 | 68.18 | 9.5050 | 0.5866 | 1.6033 | 0.0015 | 38 | 7.4620 | 2.2030 | 3.1290 | 0.0009 | 27 | 73 | 49 | 68 |
| 30 | 60462 | 5639 | 0.4 | 0.45 | 65.018 | 0.8 | 0.9 | 16.17 | 58.52 | 74.68 | 8.6697 | 0.4239 | 1.2008 | 0.0014 | 38 | 7.4620 | 2.2030 | 3.1290 | 0.0009 | 16 | 81 | 62 | 57 |
| | equivalent thickness= | | | | 85.225 | 0.9 | 0.8 | 18.19 | 52.01 | 70.20 | 9.2416 | 0.5300 | 1.4641 | 0.0015 | 38 | 7.4620 | 2.2030 | 3.1290 | 0.0009 | 24 | 76 | 53 | 65 |
| | | | | | | 0.9 | 0.9 | 18.19 | 58.52 | 76.70 | 8.4193 | 0.3834 | 1.0997 | 0.0014 | 38 | 7.4620 | 2.2030 | 3.1290 | 0.0009 | 13 | 83 | 65 | 53 |
| | | | | | | 1 | 0.8 | 20.21 | 52.01 | 72.22 | 8.9812 | 0.4791 | 1.3381 | 0.0014 | 38 | 7.4620 | 2.2030 | 3.1290 | 0.0009 | 20 | 78 | 57 | 61 |
| | | | | | | 1 | 0.9 | 20.21 | 58.52 | 78.72 | 8.1744 | 0.3469 | 1.0080 | 0.0013 | 38 | 7.4620 | 2.2030 | 3.1290 | 0.0009 | 10 | 84 | 68 | 49 |
| | | | | | | 1 | 1 | 20.21 | 65.02 | 85.23 | 7.4286 | 0.2518 | 0.7663 | 0.0012 | 38 | 7.4620 | 2.2030 | 3.1290 | 0.0009 | 0 | 89 | 76 | 38 |
| | | | | | | 1 | 1.1 | 20.21 | 71.52 | 91.73 | 6.7515 | 0.1828 | 0.5877 | 0.0011 | 38 | 7.4620 | 2.2030 | 3.1290 | 0.0009 | 10 | 92 | 81 | 27 |
| | | | | | | 1.1 | 1.1 | 22.23 | 71.52 | 93.75 | 6.5551 | 0.1654 | 0.5421 | 0.0011 | 38 | 7.4620 | 2.2030 | 3.1290 | 0.0009 | 12 | 92 | 83 | 23 |

TABLE 5-16 JULEA (3 Layers) and ZAPRAM comparison for the 4th pavement system with different correction factors.

| AIRBUS INDUSTRIE A300-C4 | | | | | | | | | | | ZAPRAM | | | | JULEA(3 Layer) | | | | Percentage Diff, % | | | | |
|--------------------------|-----------------------|------|---------|---------|--------|-----|-----|-------|-------|-------|------------|------------|------------|--------------|----------------|------------|------------|------------|--------------------|------------|------------|------------|--------------|
| h1 | E1 | E2 | μ_1 | μ_2 | He | f1 | f2 | he1 | he2 | he | σ_z | σ_x | σ_y | ϵ_z | Z | σ_z | σ_x | σ_y | ϵ_z | σ_z | σ_x | σ_y | ϵ_z |
| 8 | 100000 | 9698 | 0.35 | 0.45 | 16.866 | 0.8 | 0.8 | 13.49 | 43.41 | 56.91 | 10.9508 | 1.0399 | 2.7007 | 0.0010 | 38 | 8.9680 | 2.4540 | 3.8590 | 0.0006 | 22 | 58 | 30 | 51 |
| 30 | 60462 | 9698 | 0.4 | 0.45 | 54.267 | 0.8 | 0.9 | 13.49 | 48.84 | 62.33 | 10.2705 | 0.7883 | 2.0951 | 0.0009 | 38 | 8.9680 | 2.4540 | 3.8590 | 0.0006 | 15 | 68 | 46 | 46 |
| | equivalent thickness= | | | | 71.134 | 0.9 | 0.8 | 15.18 | 43.41 | 58.59 | 10.7459 | 0.9539 | 2.4945 | 0.0009 | 38 | 8.9680 | 2.4540 | 3.8590 | 0.0006 | 20 | 61 | 35 | 50 |
| | | | | | | 0.9 | 0.9 | 15.18 | 48.84 | 64.02 | 10.0507 | 0.7237 | 1.9381 | 0.0009 | 38 | 8.9680 | 2.4540 | 3.8590 | 0.0006 | 12 | 71 | 50 | 44 |
| | | | | | | 1 | 0.8 | 16.87 | 43.41 | 60.28 | 10.5343 | 0.8752 | 2.3050 | 0.0009 | 38 | 8.9680 | 2.4540 | 3.8590 | 0.0006 | 17 | 64 | 40 | 49 |
| | | | | | | 1 | 0.9 | 16.87 | 48.84 | 65.71 | 9.8295 | 0.6645 | 1.7939 | 0.0009 | 38 | 8.9680 | 2.4540 | 3.8590 | 0.0006 | 10 | 73 | 54 | 42 |
| | | | | | | 1 | 1 | 16.87 | 54.27 | 71.13 | 9.1210 | 0.5059 | 1.4044 | 0.0009 | 38 | 8.9680 | 2.4540 | 3.8590 | 0.0006 | 2 | 79 | 64 | 35 |
| | | | | | | 1 | 1.1 | 16.87 | 59.69 | 76.56 | 8.4367 | 0.3861 | 1.1065 | 0.0008 | 38 | 8.9680 | 2.4540 | 3.8590 | 0.0006 | 6 | 84 | 71 | 27 |
| | | | | | | 1.1 | 1.1 | 18.55 | 59.69 | 78.25 | 8.2316 | 0.3552 | 1.0288 | 0.0008 | 38 | 8.9680 | 2.4540 | 3.8590 | 0.0006 | 8 | 86 | 73 | 24 |

TABLE 5-17 JULEA (3 Layers) and ZAPRAM comparison for the 5th pavement system with different correction factors.

| AIRBUS INDUSTRIE A300-C4 | | | | | | ZAPRAM | | | | JULEA(3 Layer) | | | | Percentage Diff, % | | | | | | | | | |
|--------------------------|-----------------------|------|---------|---------|--------|--------|-----|-------|-------|----------------|------------|------------|------------|--------------------|----|------------|------------|------------|-----------------|------------|------------|------------|-----------------|
| h1 | E1 | E2 | μ_1 | μ_2 | He | f1 | f2 | he1 | he2 | he | σ_z | σ_x | σ_y | ε_z | Z | σ_z | σ_x | σ_y | ε_z | σ_z | σ_x | σ_y | ε_z |
| 12 | 100000 | 5639 | 0.35 | 0.45 | 30.312 | 0.8 | 0.8 | 24.25 | 26.01 | 50.26 | 11.6472 | 1.4627 | 3.7052 | 0.0017 | 27 | 9.9820 | 3.8080 | 5.3760 | 0.0010 | 17 | 62 | 31 | 59 |
| 15 | 60462 | 5639 | 0.4 | 0.45 | 32.509 | 0.8 | 0.9 | 24.25 | 29.26 | 53.51 | 11.3345 | 1.2379 | 3.1731 | 0.0017 | 27 | 9.9820 | 3.8080 | 5.3760 | 0.0010 | 14 | 67 | 41 | 60 |
| | equivalent thickness= | | | | 62.820 | 0.9 | 0.8 | 27.28 | 26.01 | 53.29 | 11.3576 | 1.2520 | 3.2065 | 0.0017 | 27 | 9.9820 | 3.8080 | 5.3760 | 0.0010 | 14 | 67 | 40 | 60 |
| | | | | | | 0.9 | 0.9 | 27.28 | 29.26 | 56.54 | 10.9945 | 1.0597 | 2.7482 | 0.0016 | 27 | 9.9820 | 3.8080 | 5.3760 | 0.0010 | 10 | 72 | 49 | 59 |
| | | | | | | 1 | 0.8 | 30.31 | 26.01 | 56.32 | 11.0204 | 1.0717 | 2.7769 | 0.0016 | 27 | 9.9820 | 3.8080 | 5.3760 | 0.0010 | 10 | 72 | 48 | 59 |
| | | | | | | 1 | 0.9 | 30.31 | 29.26 | 59.57 | 10.6241 | 0.9075 | 2.3829 | 0.0016 | 27 | 9.9820 | 3.8080 | 5.3760 | 0.0010 | 6 | 76 | 56 | 56 |
| | | | | | | 1 | 1 | 30.31 | 32.51 | 62.82 | 10.2073 | 0.7691 | 2.0484 | 0.0016 | 27 | 9.9820 | 3.8080 | 5.3760 | 0.0010 | 2 | 80 | 62 | 53 |
| | | | | | | 1 | 1.1 | 30.31 | 35.76 | 66.07 | 9.7816 | 0.6524 | 1.7643 | 0.0015 | 27 | 9.9820 | 3.8080 | 5.3760 | 0.0010 | 2 | 83 | 67 | 49 |
| | | | | | | 1.1 | 1.1 | 33.34 | 35.76 | 69.10 | 9.3845 | 0.5601 | 1.5380 | 0.0015 | 27 | 9.9820 | 3.8080 | 5.3760 | 0.0010 | 6 | 85 | 71 | 44 |

TABLE 5-18 JULEA (3 Layers) and ZAPRAM comparison for the 6th pavement system with different correction factors.

| AIRBUS INDUSTRIE A300-C4 | | | | | | ZAPRAM | | | | JULEA(3 Layer) | | | | Percentage Diff, % | | | | | | | | | |
|--------------------------|-----------------------|------|---------|---------|--------|--------|-----|-------|-------|----------------|------------|------------|------------|--------------------|----|------------|------------|------------|-----------------|------------|------------|------------|-----------------|
| h1 | E1 | E2 | μ_1 | μ_2 | He | f1 | f2 | he1 | he2 | he | σ_z | σ_x | σ_y | ε_z | Z | σ_z | σ_x | σ_y | ε_z | σ_z | σ_x | σ_y | ε_z |
| 12 | 100000 | 9698 | 0.35 | 0.45 | 25.300 | 0.8 | 0.8 | 20.24 | 21.71 | 41.95 | 12.0173 | 2.2304 | 5.4970 | 0.0009 | 27 | 11.0900 | 4.1930 | 6.5050 | 0.0006 | 8 | 47 | 15 | 36 |
| 15 | 60462 | 9698 | 0.4 | 0.45 | 27.134 | 0.8 | 0.9 | 20.24 | 24.42 | 44.66 | 11.9855 | 1.9460 | 4.8375 | 0.0009 | 27 | 11.0900 | 4.1930 | 6.5050 | 0.0006 | 8 | 54 | 26 | 42 |
| | equivalent thickness= | | | | 52.433 | 0.9 | 0.8 | 22.77 | 21.71 | 44.48 | 11.9908 | 1.9641 | 4.8797 | 0.0009 | 27 | 11.0900 | 4.1930 | 6.5050 | 0.0006 | 8 | 53 | 25 | 42 |
| | | | | | | 0.9 | 0.9 | 22.77 | 24.42 | 47.19 | 11.8710 | 1.7112 | 4.2892 | 0.0009 | 27 | 11.0900 | 4.1930 | 6.5050 | 0.0006 | 7 | 59 | 34 | 46 |
| | | | | | | 1 | 0.8 | 25.30 | 21.71 | 47.01 | 11.8817 | 1.7273 | 4.3269 | 0.0009 | 27 | 11.0900 | 4.1930 | 6.5050 | 0.0006 | 7 | 59 | 33 | 46 |
| | | | | | | 1 | 0.9 | 25.30 | 24.42 | 49.72 | 11.6920 | 1.5035 | 3.8013 | 0.0010 | 27 | 11.0900 | 4.1930 | 6.5050 | 0.0006 | 5 | 64 | 42 | 48 |
| | | | | | | 1 | 1 | 25.30 | 27.13 | 52.43 | 11.4448 | 1.3081 | 3.3396 | 0.0010 | 27 | 11.0900 | 4.1930 | 6.5050 | 0.0006 | 3 | 69 | 49 | 49 |
| | | | | | | 1 | 1.1 | 25.30 | 29.85 | 55.15 | 11.1553 | 1.1381 | 2.9353 | 0.0010 | 27 | 11.0900 | 4.1930 | 6.5050 | 0.0006 | 1 | 73 | 55 | 49 |
| | | | | | | 1.1 | 1.1 | 27.83 | 29.85 | 57.68 | 10.8583 | 0.9997 | 2.6045 | 0.0010 | 27 | 11.0900 | 4.1930 | 6.5050 | 0.0006 | 2 | 76 | 60 | 47 |

TABLE 5-19 JULEA (3 Layers) and ZAPRAM comparison for the 7th pavement system with different correction factors.

| AIRBUS INDUSTRIE A300-C4 | | | | | | | | | | | ZAPRAM | | | | JULEA(3 Layer) | | | | Percentage Diff, % | | | | |
|--------------------------|-----------------------|------|------|------|--------|-----|-----|-------|-------|--------|----------------|----------------|----------------|----------------|----------------|----------------|----------------|----------------|--------------------|----------------|----------------|----------------|----------------|
| h1 | E1 | E2 | μ1 | μ2 | He | f1 | f2 | he1 | he2 | he | σ _z | σ _x | σ _y | ε _z | Z | σ _z | σ _x | σ _y | ε _z | σ _z | σ _x | σ _y | ε _z |
| 12 | 100000 | 5639 | 0.35 | 0.45 | 30.312 | 0.8 | 0.8 | 24.25 | 52.01 | 76.26 | 8.4733 | 0.3919 | 1.1208 | 0.0014 | 42 | 6.6980 | 1.7740 | 2.5040 | 0.0008 | 27 | 78 | 55 | 63 |
| 30 | 60462 | 5639 | 0.4 | 0.45 | 65.018 | 0.8 | 0.9 | 24.25 | 58.52 | 82.77 | 7.7029 | 0.2842 | 0.8492 | 0.0013 | 42 | 6.6980 | 1.7740 | 2.5040 | 0.0008 | 15 | 84 | 66 | 51 |
| | equivalent thickness= | | | | 95.329 | 0.9 | 0.8 | 27.28 | 52.01 | 79.29 | 8.1063 | 0.3373 | 0.9837 | 0.0013 | 42 | 6.6980 | 1.7740 | 2.5040 | 0.0008 | 21 | 81 | 61 | 57 |
| | | | | | | 0.9 | 0.9 | 27.28 | 58.52 | 85.80 | 7.3664 | 0.2448 | 0.7484 | 0.0012 | 42 | 6.6980 | 1.7740 | 2.5040 | 0.0008 | 10 | 86 | 70 | 45 |
| | | | | | | 1 | 0.8 | 30.31 | 52.01 | 82.33 | 7.7530 | 0.2904 | 0.8650 | 0.0013 | 42 | 6.6980 | 1.7740 | 2.5040 | 0.0008 | 16 | 84 | 65 | 52 |
| | | | | | | 1 | 0.9 | 30.31 | 58.52 | 88.83 | 7.0449 | 0.2109 | 0.6609 | 0.0012 | 42 | 6.6980 | 1.7740 | 2.5040 | 0.0008 | 5 | 88 | 74 | 39 |
| | | | | | | 1 | 1 | 30.31 | 65.02 | 95.33 | 6.4060 | 0.1530 | 0.5092 | 0.0011 | 42 | 6.6980 | 1.7740 | 2.5040 | 0.0008 | 4 | 91 | 80 | 28 |
| | | | | | | 1 | 1.1 | 30.31 | 71.52 | 101.83 | 5.8338 | 0.1104 | 0.3954 | 0.0010 | 42 | 6.6980 | 1.7740 | 2.5040 | 0.0008 | 13 | 94 | 84 | 17 |
| | | | | | | 1.1 | 1.1 | 33.34 | 71.52 | 104.86 | 5.5885 | 0.0945 | 0.3523 | 0.0010 | 42 | 6.6980 | 1.7740 | 2.5040 | 0.0008 | 17 | 95 | 86 | 13 |

TABLE 5-20 JULEA (3 Layers) and ZAPRAM comparison for the 8th pavement system with different correction factors.

| AIRBUS INDUSTRIE A300-C4 | | | | | | | | | | | ZAPRAM | | | | JULEA(3 Layer) | | | | Percentage Diff, % | | | | |
|--------------------------|-----------------------|------|------|------|--------|-----|-----|-------|-------|-------|----------------|----------------|----------------|----------------|----------------|----------------|----------------|----------------|--------------------|----------------|----------------|----------------|----------------|
| h1 | E1 | E2 | μ1 | μ2 | He | f1 | f2 | he1 | he2 | he | σ _z | σ _x | σ _y | ε _z | Z | σ _z | σ _x | σ _y | ε _z | σ _z | σ _x | σ _y | ε _z |
| 12 | 100000 | 9698 | 0.35 | 0.45 | 25.300 | 0.8 | 0.8 | 20.24 | 43.41 | 63.65 | 10.0986 | 0.7372 | 1.9711 | 0.0009 | 42 | 8.2450 | 1.9790 | 3.0940 | 0.0006 | 22 | 63 | 36 | 49 |
| 30 | 60462 | 9698 | 0.4 | 0.45 | 54.267 | 0.8 | 0.9 | 20.24 | 48.84 | 69.08 | 9.3874 | 0.5607 | 1.5396 | 0.0009 | 42 | 8.2450 | 1.9790 | 3.0940 | 0.0006 | 14 | 72 | 50 | 42 |
| | equivalent thickness= | | | | 79.567 | 0.9 | 0.8 | 22.77 | 43.41 | 66.18 | 9.7669 | 0.6487 | 1.7553 | 0.0009 | 42 | 8.2450 | 1.9790 | 3.0940 | 0.0006 | 18 | 67 | 43 | 46 |
| | | | | | | 0.9 | 0.9 | 22.77 | 48.84 | 71.61 | 9.0597 | 0.4940 | 1.3749 | 0.0008 | 42 | 8.2450 | 1.9790 | 3.0940 | 0.0006 | 10 | 75 | 56 | 38 |
| | | | | | | 1 | 0.8 | 25.30 | 43.41 | 68.71 | 9.4353 | 0.5711 | 1.5652 | 0.0009 | 42 | 8.2450 | 1.9790 | 3.0940 | 0.0006 | 14 | 71 | 49 | 42 |
| | | | | | | 1 | 0.9 | 25.30 | 48.84 | 74.14 | 8.7377 | 0.4354 | 1.2296 | 0.0008 | 42 | 8.2450 | 1.9790 | 3.0940 | 0.0006 | 6 | 78 | 60 | 34 |
| | | | | | | 1 | 1 | 25.30 | 54.27 | 79.57 | 8.0739 | 0.3328 | 0.9723 | 0.0008 | 42 | 8.2450 | 1.9790 | 3.0940 | 0.0006 | 2 | 83 | 69 | 26 |
| | | | | | | 1 | 1.1 | 25.30 | 59.69 | 84.99 | 7.4540 | 0.2547 | 0.7737 | 0.0007 | 42 | 8.2450 | 1.9790 | 3.0940 | 0.0006 | 10 | 87 | 75 | 17 |
| | | | | | | 1.1 | 1.1 | 27.83 | 59.69 | 87.52 | 7.1813 | 0.2249 | 0.6970 | 0.0007 | 42 | 8.2450 | 1.9790 | 3.0940 | 0.0006 | 13 | 89 | 77 | 14 |

The study to estimate the optimum set of correction factors used four different approaches. These approaches were: (1) Smallest Percent Difference Between Vertical Stresses and Strains, (2) The Best Slope Line for Every Combination of Correction Factors, (3) The Least Square Error for Every Combination of Correction Factors, (4) the Backcalculation to Estimate f_2 .

5.3.1 Smallest Percentage Difference, Between Vertical Stresses and Strains

In this procedure, the best combination has been chosen that resulted in the smallest percentage difference from the estimated stress and strain from both programs using the B737-600 airplane.

Table 5-21 The Best Section for f_1 , f_2 Value up to the Smallest σ_z , Percentage Diff, % for B737-600

| section number | h_1 | h_2 | CBR (%) | f_1 | f_2 | σ_z , Percentage Diff, % |
|----------------|-------|-------|---------|-------|-------|---------------------------------|
| 1 | 8 | 15 | 3 | 1.0 | 0.9 | 1 |
| 2 | 8 | 15 | 7 | 1.0 | 0.9 | 0 |
| 3 | 8 | 30 | 3 | 0.8 | 0.9 | 2 |
| 4 | 8 | 30 | 7 | 0.8 | 0.9 | 0 |
| 5 | 12 | 15 | 3 | 1.0 | 0.8 | 1 |
| 6 | 12 | 15 | 7 | 1.0 | 0.8 | 2 |
| 7 | 12 | 30 | 3 | 1.0 | 0.8 | 2 |
| 8 | 12 | 30 | 7 | 1.0 | 0.8 | 0 |

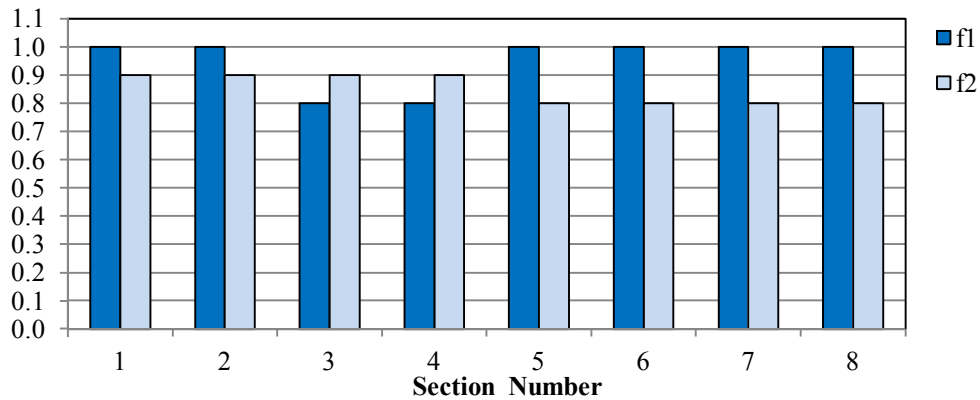


FIGURE 5-12 The best section for f_1 , f_2 value up to the smallest σ_z , percentage diff, % for B737-600.

It can be estimated that the best value for f_1 is approximately 1.00. Also, the best value for f_2 ranges between 0.8-0.9.

If the vertical strain criterion is used, the best combinations of both programs for the B737-600 airplane are shown in Table 5-12.

TABLE 5-22 The Best Section for f_1 , f_2 Value up to the Smallest ϵ_z , Percentage Diff, % for B737-600

| section number | h1 | h2 | CBR (%) | f_1 | f_2 | ϵ_z , Percentage Diff, % |
|----------------|----|----|---------|-------|-------|-----------------------------------|
| 1 | 8 | 15 | 3 | 1.1 | 1.1 | 0 |
| 2 | 8 | 15 | 7 | 1.1 | 1.1 | 0 |
| 3 | 8 | 30 | 3 | 1.0 | 0.9 | 5 |
| 4 | 8 | 30 | 7 | 1.0 | 0.9 | 3 |
| 5 | 12 | 15 | 3 | 1.0 | 1.0 | 5 |
| 6 | 12 | 15 | 7 | 1.0 | 1.0 | 4 |
| 7 | 12 | 30 | 3 | 1.0 | 0.9 | 0 |
| 8 | 12 | 30 | 7 | 1.0 | 0.9 | 2 |

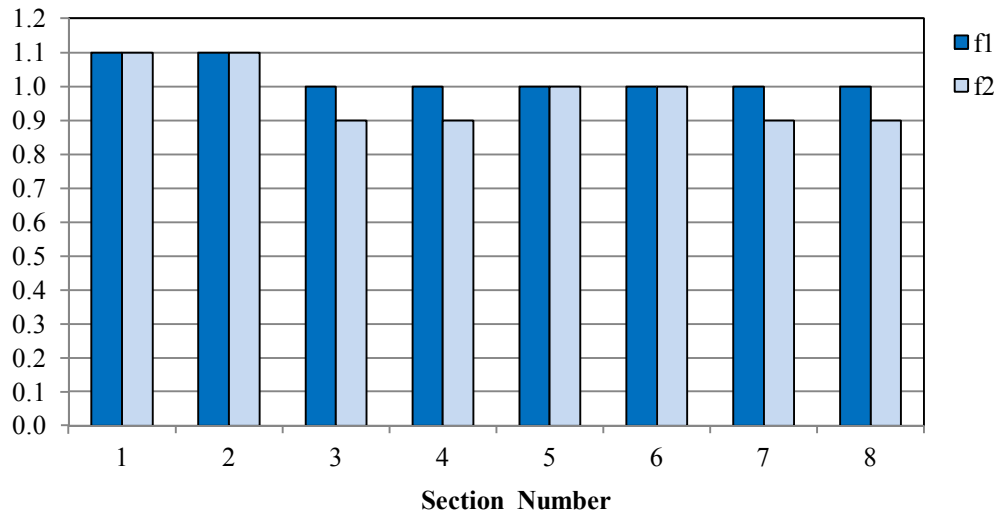


FIGURE 5-13 The best section for f_1, f_2 value up to the smallest ϵ_z , percentage diff, % for B737-600.

As a general conclusion, it appears that the best value for f_1 is 1.10, while the best value for f_2 ranges between 0.9-1.0.

The same analysis was then developed using the A300-C4 airplane. These results (for the stress difference) are shown in Table 5-23,

TABLE 5-23 The Best Section for f_1 , f_2 Value up to the Smallest σ_z , Percentage Diff, % for A300-C4

| Section number | h1 | h2 | CBR (%) | f_1 | f_2 | σ_z , Percentage Diff, % |
|----------------|----|----|---------|-------|-------|---------------------------------|
| 1 | 8 | 15 | 3 | 1.0 | 1.1 | 0 |
| 2 | 8 | 15 | 7 | 0.9 | 0.8 | 1 |
| 3 | 8 | 30 | 3 | 1.0 | 1.0 | 0 |
| 4 | 8 | 30 | 7 | 1.0 | 1.0 | 2 |
| 5 | 12 | 15 | 3 | 1.0 | 1.1 | 2 |
| 6 | 12 | 15 | 7 | 1.0 | 1.1 | 1 |
| 7 | 12 | 30 | 3 | 1.0 | 1.0 | 4 |
| 8 | 12 | 30 | 7 | 1.0 | 1.0 | 2 |

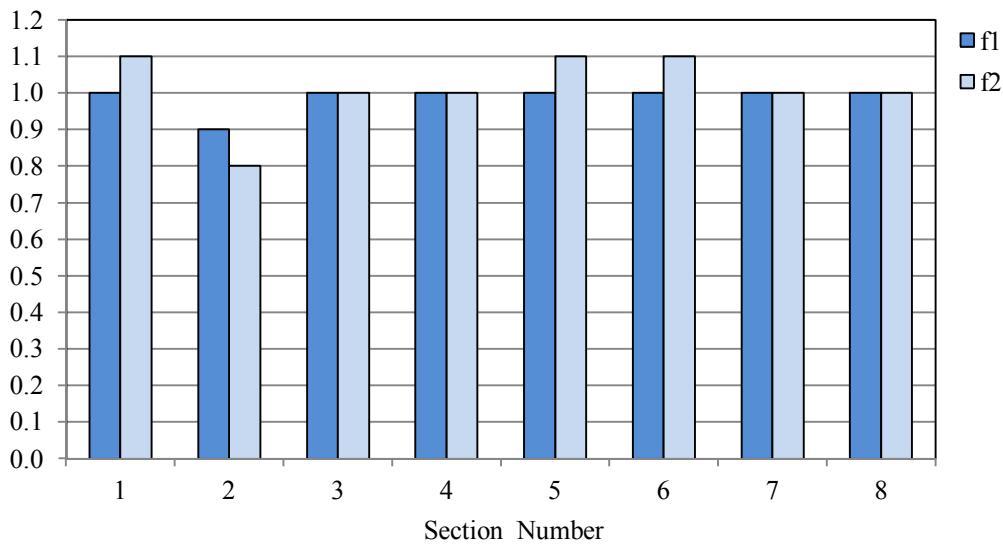


FIGURE 5-14 The best section for f_1 , f_2 value up to the smallest σ_z , percentage diff, % for A300-C4.

For this study, it appears that the best combination of both f_1 and f_2 are close to a value of $f_1 = f_2 = 1.0$.

The best combination has been chosen up to the smallest percentage difference from the estimated strain from both programs by A300-C4 airplane.

TABLE 5-24 The Best Section for f_1, f_2 Value up to the Smallest ϵ_z , Percentage Diff, % with A300-C4

| Section number | h1 | h2 | CBR (%) | f_1 | f_2 | ϵ_z , Percentage Diff, % |
|----------------|----|----|---------|-------|-------|-----------------------------------|
| 1 | 8 | 15 | 3 | 0.8 | 0.8 | 48 |
| 2 | 8 | 15 | 7 | 0.8 | 0.8 | 20 |
| 3 | 8 | 30 | 3 | 1.1 | 1.1 | 23 |
| 4 | 8 | 30 | 7 | 1.1 | 1.1 | 24 |
| 5 | 12 | 15 | 3 | 1.1 | 1.1 | 44 |
| 6 | 12 | 15 | 7 | 0.8 | 0.8 | 36 |
| 7 | 12 | 30 | 3 | 1.1 | 1.1 | 13 |
| 8 | 12 | 30 | 7 | 1.1 | 1.1 | 14 |

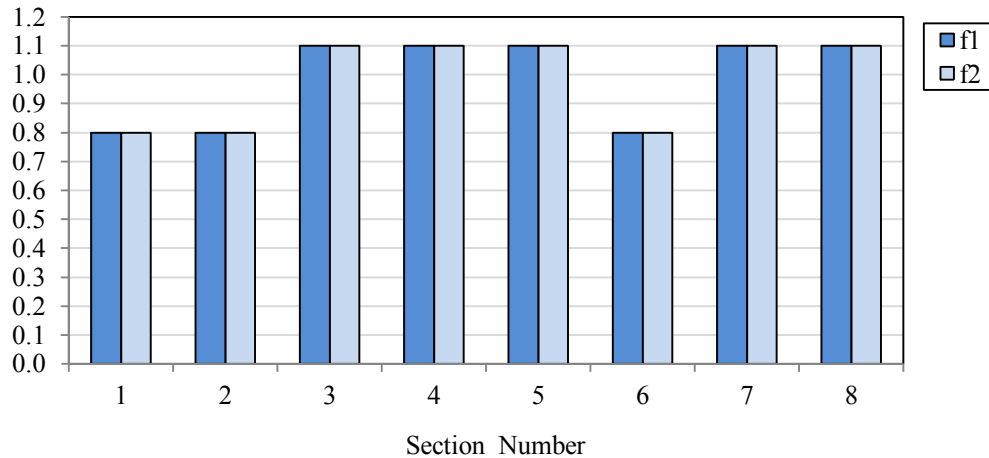


FIGURE 5-15 The best section for f_1, f_2 value up to the smallest ϵ_z , percentage diff, % with A300-C4.

It should be noted that the strain varies by a huge value between the programs when the heavier A-300 airplane is used. It is concluded that for both f_1 and f_2 , there appears to be no single best estimated value.

5.3.2 The Best Slope Line for Every Combination of Correction Factors

The next four figures utilize an approach based upon using the relationships found between f_i combination and the line of equality to select the “best” combination of f_i values. These lines were obtained for the eight different pavement systems.

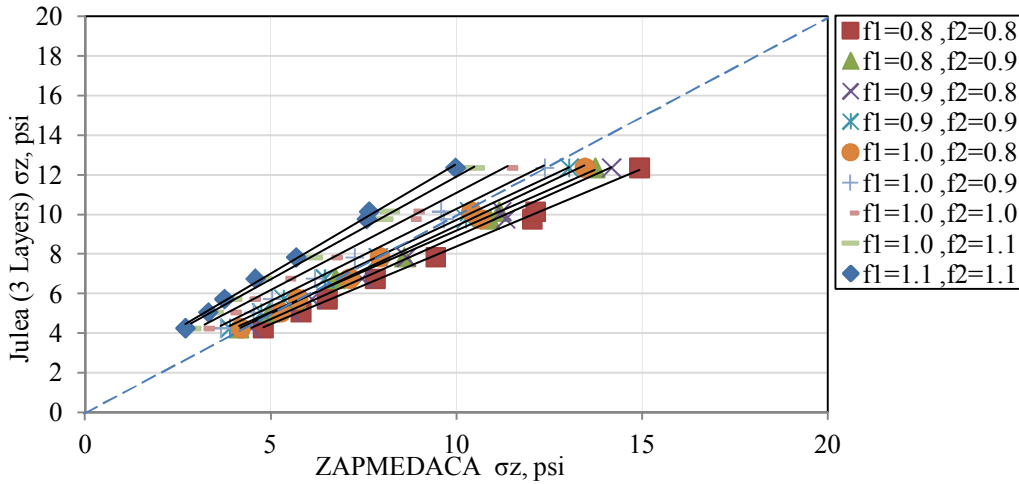


FIGURE 5-16 Correction factor for different combination of different pavement system with Boeing B737-600.

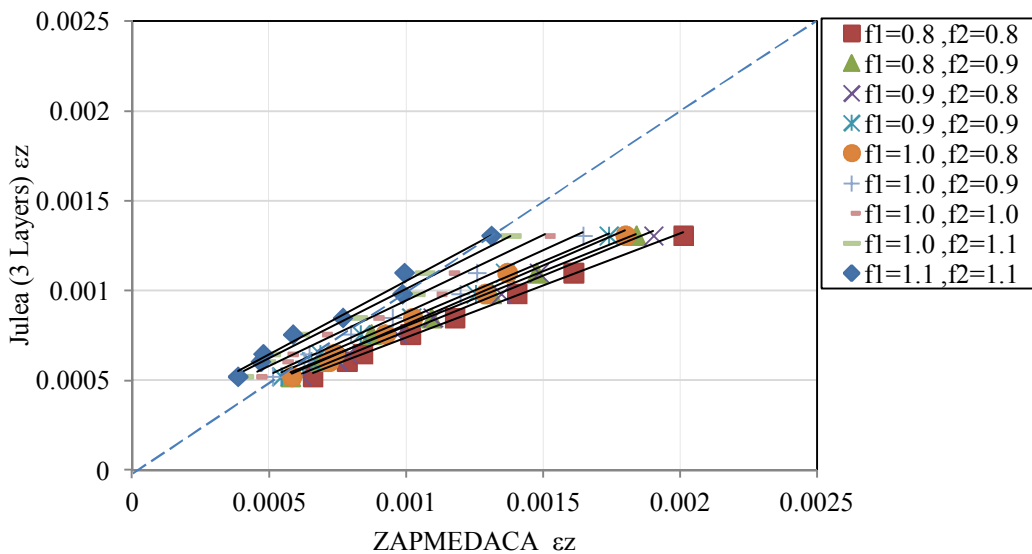


FIGURE 5-17 Correction factor for different combination of different pavement system with boeing B737-600.

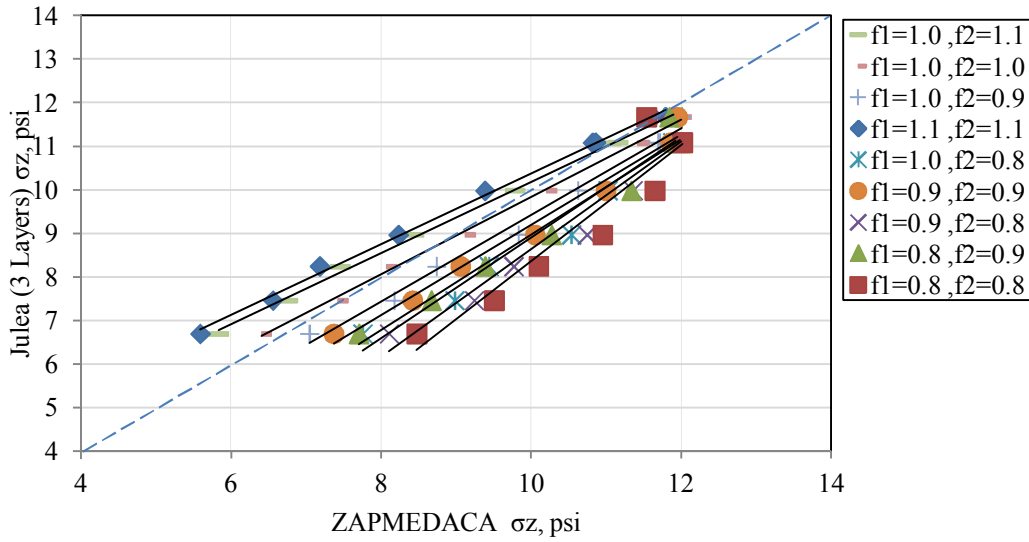


FIGURE 5-18 Correction factor for different combination of different pavement system with A300-C4.

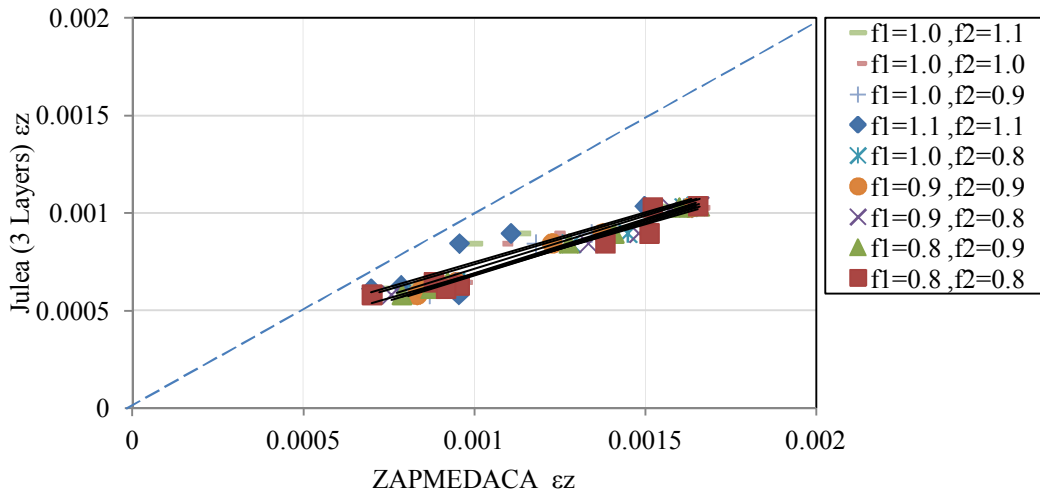


FIGURE 5-19 Correction factor for different combination of different pavement system with A300-C4.

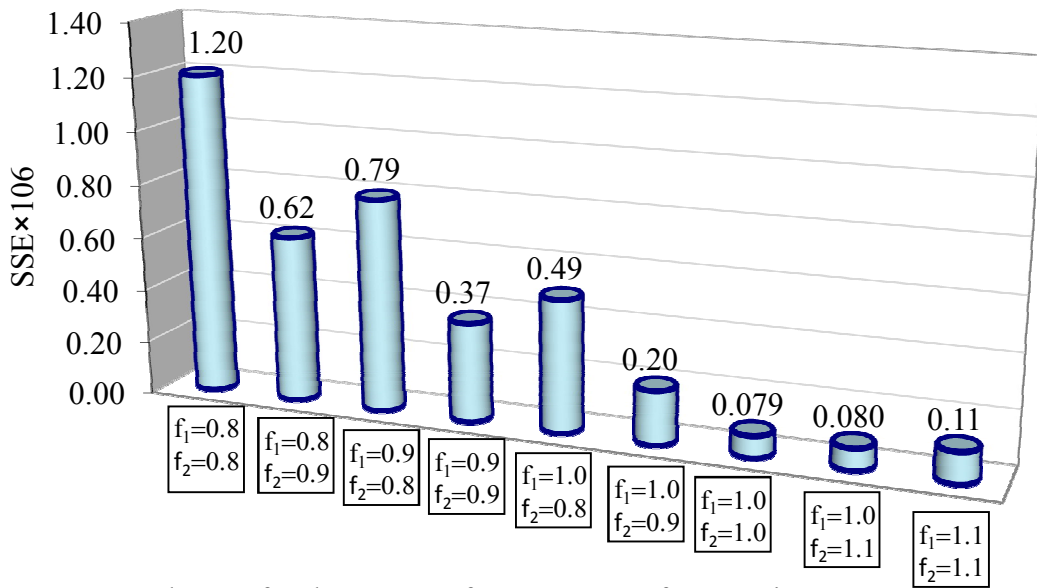
The first three figures show that the "best" line is the one near the $f_1=1.0, f_2=1.0$ condition. The points of these lines happen to be close to the line of equality. For the last figure all the lines are very far from 0-0 line due to the big difference for the calculated strain value. Thus, this conclusion like the previous conclusion is that there appears to be no accurate combination of f_1-f_2 that would adequately predict the vertical strains between the ZAPRAM and JULEA programs.

5.3.3 The Least Square Error for Every Combination of Correction factors

The next approach was based upon computing the Sum of Squared Errors for each set of f1-f2 combinations evaluated and then selecting the “Least Square Error” . Tables 5-25 and 5-26, along with Figures 5-20 to 5-23 present the results of the SSE as a function of the Correction Factor Set. This information is shown by stress and strain for each of the two aircraft types investigated.

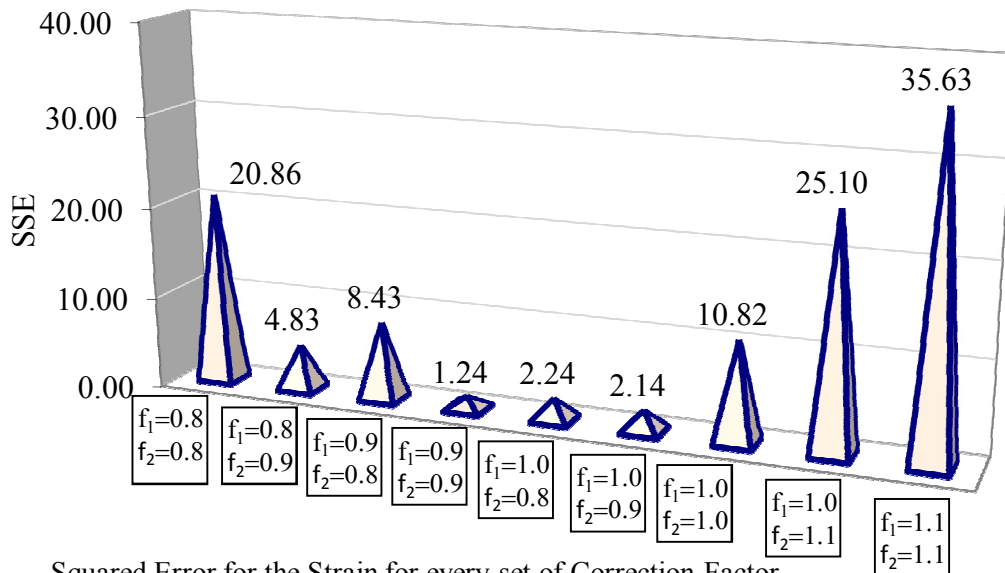
TABLE 5-25 Squared Error for the Strain for Every Set of Correction Factors for Different Pavement Systems with Boeing B737-600

| Correction Factor | | σ_z | | ϵ_z |
|-------------------|-----|------------|-------------------|--------------|
| f1 | f2 | SSE | SSE $\times 10^6$ | SSE |
| 0.8 | 0.8 | 1.201E-06 | 1.20 | 20.86 |
| 0.8 | 0.9 | 6.224E-07 | 0.62 | 4.83 |
| 0.9 | 0.8 | 7.931E-07 | 0.79 | 8.43 |
| 0.9 | 0.9 | 3.694E-07 | 0.37 | 1.24 |
| 1 | 0.8 | 4.930E-07 | 0.49 | 2.24 |
| 1 | 0.9 | 1.996E-07 | 0.20 | 2.14 |
| 1 | 1 | 7.937E-08 | 0.079 | 10.82 |
| 1 | 1.1 | 7.998E-08 | 0.080 | 25.10 |
| 1.1 | 1.1 | 1.135E-07 | 0.11 | 35.63 |



Squared Error for the Stresses for Every Set of Correction Factor for Different Pavement system with Boeing B737-600

FIGURE 5-20 Squared error versus correction factor set for stress (B-737).



Squared Error for the Strain for every set of Correction Factor for Different Pavement system with Boeing B737-600

FIGURE 5-21 Squared error versus correction factor set for strain (B-737).

TABLE 5-26 Squared Error for the Stress and Strain for every Set of Correction Factors for Different Pavement Systems with A600

| Correction Factor | | σ_z | | ϵ_z |
|-------------------|-----|------------|---------------------|--------------|
| f1 | f2 | SSE | SSE×10 ⁶ | SSE |
| 0.8 | 0.8 | 1.547E-06 | 1.55 | 19.22 |
| 0.8 | 0.9 | 1.423E-06 | 1.42 | 8.90 |
| 0.9 | 0.8 | 1.540E-06 | 1.54 | 14.18 |
| 0.9 | 0.9 | 1.387E-06 | 1.39 | 5.51 |
| 1 | 0.8 | 1.504E-06 | 1.50 | 9.76 |
| 1 | 0.9 | 1.327E-06 | 1.33 | 2.90 |
| 1 | 1 | 1.149E-06 | 1.149 | 0.54 |
| 1 | 1.1 | 9.841E-07 | 0.984 | 2.26 |
| 1.1 | 1.1 | 8.941E-07 | 0.89 | 4.22 |

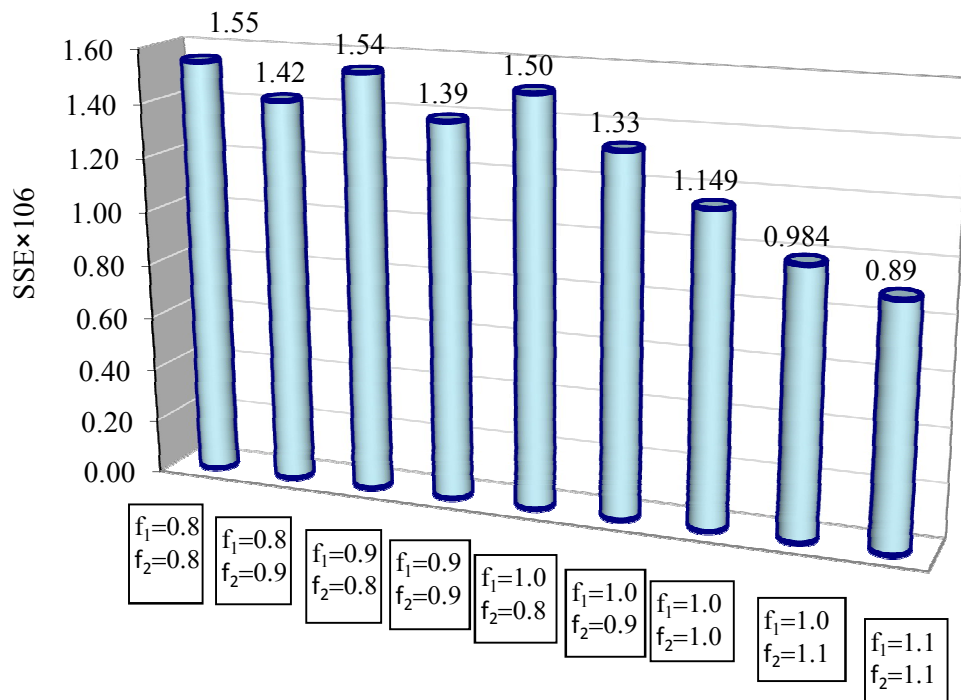


FIGURE 5-22 Squared error versus correction factor set for stress (A-300).

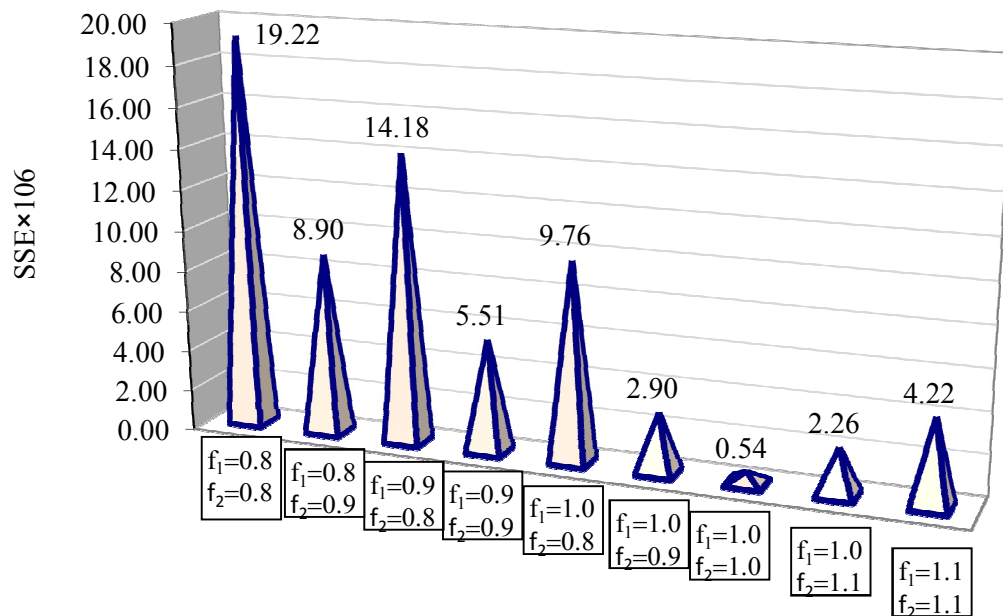


FIGURE 5-23 Squared error versus correction factor set for strains (A-300).

From this study, several points can be concluded:

- i. The f_1 and f_2 factors are functions of several variables (layer thickness, modular ratios, Poisson's ratios and the number of layers in the structure).
- ii. The least square errors calculated for the strain comparison are much higher than the ones calculated for the stress prediction.
- iii. The differences in vertical stress between the two approaches (ZAPRAM and JULEA) are not quite large.
- iv. In general, the values of $f_1=1.0$ and $f_2=0.8-1.0$ yielded the smallest squared error overall. That can be seen graphically in Figure 5-20 to Figure 5-23 and Table 5-25 and 5-26.

5.3.4 The Back Calculation to Estimate f_2

From the previous study it is apparent that the f_2 value is not really constant. Rather it is variable and dependent upon many factors. In this study the value of f_1 was set equal to $f_1 = 1.0$ and the resultant values for f_2 were determined as a function of the thickness (h_1) used. The h_1 thicknesses used are ($h_1 = 4.0- 8.0- 12$ in). All the other characterizations for the three layer system were held constant. Both the programs run and results are shown in Table 5-27:

TABLE 5-27 Strain and Stress Value from Both Programs with Changes of h_1

| Boeing B737-600 | | | JULEA(3 Layer) | | | ZAPRAM | | |
|-----------------|-------|---------|----------------|------------|--------------|--------|------------|--------------|
| h_1 | h_2 | CBR (%) | Z | σ_z | ϵ_z | Z | σ_z | ϵ_z |
| 4.00 | 15.00 | 3.00 | 19.00 | 12.27 | 0.0015 | 42.61 | 11.88 | 0.0020 |
| 8.00 | 15.00 | 3.00 | 23.00 | 9.77 | 0.0013 | 52.70 | 8.78 | 0.0015 |
| 12.00 | 15.00 | 3.00 | 27.00 | 7.84 | 0.0011 | 62.82 | 6.66 | 0.0012 |

After this, the stress from the ZAPRAM program was plotted against the effective (equivalent) thicknesses, extending horizontal lines from the ZAPRAM stress intersect with the curve, until it intersects the trend line; the "true" equivalent thickness can be determined.

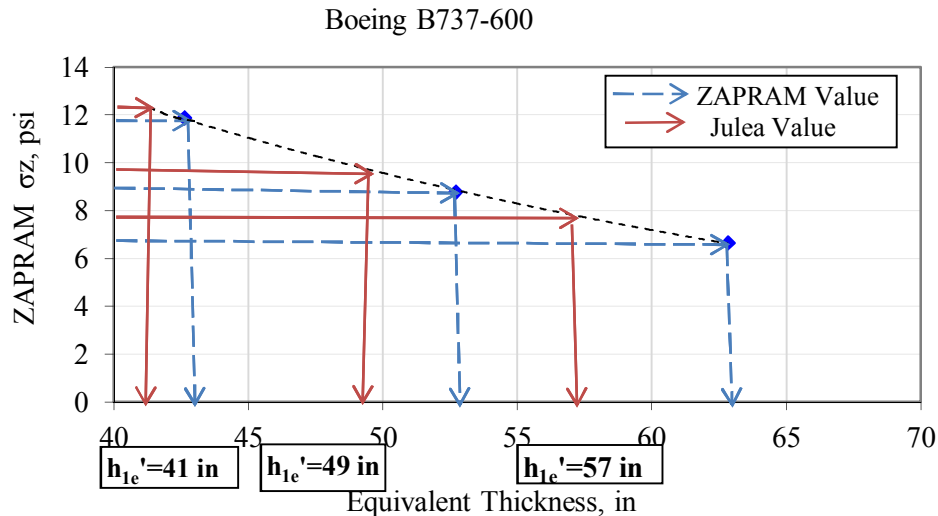


FIGURE 5-24 Estimate the equivalent depth that the stresses must be calculated.

By applying the variable into equation [5-7], the "best" correction factor for each layer can then be estimated.

$$h_{eT} = h_{1e} + h_{2e} \quad (5-7)$$

$$h_{eT} = f_1 h_1^3 \sqrt{\frac{(E_1(1-\mu_3^2))}{(E_3(1-\mu_1^2))}} + f_2 h_2^3 \sqrt{\frac{(E_2(1-\mu_3^2))}{(E_3(1-\mu_2^2))}} \quad (5-8)$$

Also, applying the same steps with the change of thickness for the first layer, it is possible to determine what the range of the correction factor (f_2) is. Table 5-28 is an example solution that contains all of computations and final conclusions that are obtained by this study.

TABLE 5-28 Steps of Best Correction Factor Calculation

| h1 | E1 | E2 | μ_1 | μ_2 | He | f1 | f2 | he1 | he | he2 | he1' | he' | he2' | f2 |
|----|--------|------|---------|---------|-----------------------|-------|----|-------|-------|-------|-------|-------|-------|------|
| 4 | 100000 | 5639 | 0.35 | 0.45 | 10.10 | 1 | 1 | 10.10 | 42.61 | 32.51 | 10.10 | 41.00 | 30.90 | 0.95 |
| 15 | 60462 | 5639 | 0.4 | 0.45 | 32.51 | | | | | | | | | |
| | | | | | equivalent thickness= | 42.61 | | | | | | | | |
| h1 | E1 | E2 | μ_1 | μ_2 | he | f1 | f2 | he1 | he | he2 | he1' | he' | he2' | f2 |
| 8 | 100000 | 5639 | 0.35 | 0.45 | 20.21 | 1 | 1 | 20.21 | 52.72 | 32.51 | 20.21 | 49.00 | 28.79 | 0.89 |
| 15 | 60462 | 5639 | 0.4 | 0.45 | 32.51 | | | | | | | | | |
| | | | | | equivalent thickness= | 52.72 | | | | | | | | |
| h1 | E1 | E2 | μ_1 | μ_2 | he | f1 | f2 | he1 | he | he2 | he1' | he' | he2' | f2 |
| 12 | 100000 | 5639 | 0.35 | 0.45 | 30.31 | 1 | 1 | 30.31 | 62.82 | 32.51 | 30.31 | 57.00 | 26.69 | 0.82 |
| 15 | 60462 | 5639 | 0.4 | 0.45 | 32.51 | | | | | | | | | |
| | | | | | equivalent thickness= | 62.82 | | | | | | | | |

Twelve different pavement systems with the Boeing B737-600 were analyzed with the same steps shown in Table 5-28. This investigation was completed for 12 systems to estimate f_2 for both the vertical stress and vertical strain at the top of subgrade. As a result 24 values for f_2 were estimated. The results are presented in the Table 5-29

TABLE 5-29 f_2 Estimations for Vertical Stress and Vertical Strain Value

| Pavement system | | | Back calculation σ_z | | Back calculation ϵ_z | |
|-----------------|----|---------|-----------------------------|------|-------------------------------|------|
| h1 | h2 | CBR (%) | f1 | f2 | f1 | f2 |
| 4 | 15 | 3 | 1 | 0.95 | 1 | 1.29 |
| 8 | | | 1 | 0.89 | 1 | 1.15 |
| 12 | | | 1 | 0.82 | 1 | 1.04 |
| 4 | 15 | 7 | 1 | 1.00 | 1 | 1.32 |
| 8 | | | 1 | 0.92 | 1 | 1.15 |
| 12 | | | 1 | 0.85 | 1 | 1.04 |
| 4 | 30 | 3 | 1 | 0.85 | 1 | 0.97 |
| 8 | | | 1 | 0.83 | 1 | 0.93 |
| 12 | | | 1 | 0.80 | 1 | 0.89 |
| 4 | 30 | 7 | 1 | 0.87 | 1 | 0.98 |
| 8 | | | 1 | 0.84 | 1 | 0.94 |
| 12 | | | 1 | 0.81 | 1 | 0.91 |

From the previous table, it can be observed that:

- The calculated f_2 values, associated with the stress predictions, range from 0.8 – 1.0 with an average value of $f_2 = 0.87$
- For the case where the strain predictions were evaluated, the f_2 values range from 0.9 to 1.3 with an average value of $f_2 = 1.05$
- For a given pavement system (structure) the ratio of the f_2 values computed by strain/stress yield ranges from 1.12 to 1.37 with the mean ratio being $R = 1.20$. (In general the f_2 value is approximately 20% greater than the f_2 value associated with stress)
- The tabular summary also shows that as the thickness of the AC layer increases; the f_2 values (stress and strain) decrease for all Base thicknesses (h_2) and CBR.
- Likewise, as the Base thicknesses increases, the f_2 (stress or strain) decreases for levels of AC thickness (h_1) and CBR.

- Finally, as the subgrade support increases, the f_2 (stress or strain) increases for all AC and Base layer Thicknesses (h_1 and h_2).

5.3.5 Vehicle-Airplane Study

While the prior analysis specifically concentrated on the range of correction factors to the Odemark f_i factor for two relatively heavy aircraft types; it was decided to expand the study to ascertain the influence of the f_i factors for a much wider range of load conditions. As a result an additional study investigating the impact of an 18KSAL (truck) (Load: 9kips; Pressure = 100 psi) as well as a very heavy “aircraft single wheel” (load: 100, 000 lbs and Pressure: 300 psi) was conducted. For each truck and aircraft specifications, each program (ZAPRAM and JULEA) were run 48 times for 48 different systems (three values for the 1st layer thickness, two values for the 2nd layer thickness, and 4 CBR values for the subgrade). The values used for h_1 were 4,8,12 inches; the values used for h_2 were 15, 30 inches and the CBR subgrade values were 3, 7, 12, and 20.

TABLE 5-30 and TABLE 5-31 illustrate the results of the 96 runs from both programs for the Truck and Aircraft respectively. The last four columns have the percentage different for the ZAPRAM results compared to the JULEA three layer-systems. ***It is emphasized that these studies used a f_1 correction of 1.0 for both layers in the ZAPRAM Odemark analysis.*** It can be observed that the percentage was never close to zero for all different runs with all different possible combination.

The percentage of error shown is high for all strain and stress values and is definitely related to the correction factor being assumed to be one. It should also be noted that the percent difference between the horizontal stresses are very large (as has been previously noted in this study).

TABLE 5-30 JULEA (3 Layers) and ZAPRAM Comparison for Truck

| Truck | | | ZAPRAM | | | | | JULEA(3 Layer) | | | | | Percentage Diff, % | | | |
|-------|-------|--------|--------|------------|------------|------------|--------------|----------------|------------|------------|------------|--------------|--------------------|------------|------------|--------------|
| h_1 | h_2 | CBR(%) | Z | σ_z | σ_x | σ_y | ϵ_z | Z | σ_z | σ_x | σ_y | ϵ_z | σ_z | σ_x | σ_y | ϵ_z |
| 4 | 15 | 3 | 42.61 | 2.3205 | -0.0299 | -0.0299 | 0.0004 | 19 | 3.4340 | 0.3553 | 0.3553 | 0.0006 | 32 | 108 | 108 | 25 |
| 4 | 15 | 7 | 35.57 | 3.3033 | -0.0372 | -0.0372 | 0.0003 | 19 | 4.7400 | 0.3422 | 0.3422 | 0.0005 | 30 | 111 | 111 | 25 |
| 4 | 15 | 12 | 31.70 | 4.1280 | -0.0408 | -0.0408 | 0.0003 | 19 | 5.7320 | 0.3271 | 0.3271 | 0.0004 | 28 | 112 | 112 | 23 |
| 4 | 15 | 20 | 28.43 | 5.0907 | -0.0421 | -0.0421 | 0.0003 | 19 | 6.7680 | 0.3158 | 0.3158 | 0.0003 | 25 | 113 | 113 | 21 |
| 4 | 30 | 3 | 75.12 | 0.7566 | -0.0117 | -0.0117 | 0.0001 | 34 | 1.1420 | 0.1066 | 0.1066 | 0.0002 | 34 | 111 | 111 | 27 |
| 4 | 30 | 7 | 62.70 | 1.0831 | -0.0162 | -0.0162 | 0.0001 | 34 | 1.5820 | 0.0962 | 0.0962 | 0.0002 | 32 | 117 | 117 | 27 |
| 4 | 30 | 12 | 55.89 | 1.3600 | -0.0197 | -0.0197 | 0.0001 | 34 | 1.9170 | 0.0859 | 0.0859 | 0.0001 | 29 | 123 | 123 | 25 |
| 4 | 30 | 20 | 50.12 | 1.6865 | -0.0235 | -0.0235 | 0.0001 | 34 | 2.2680 | 0.0758 | 0.0758 | 0.0001 | 26 | 131 | 131 | 22 |
| 8 | 15 | 3 | 52.72 | 1.5264 | -0.0217 | -0.0217 | 0.0003 | 23 | 2.2910 | 0.2243 | 0.2243 | 0.0004 | 33 | 110 | 110 | 26 |
| 8 | 15 | 7 | 44.00 | 2.1791 | -0.0286 | -0.0286 | 0.0002 | 23 | 3.1710 | 0.2130 | 0.2130 | 0.0003 | 31 | 113 | 113 | 26 |
| 8 | 15 | 12 | 39.22 | 2.7298 | -0.0334 | -0.0334 | 0.0002 | 23 | 3.8420 | 0.2026 | 0.2026 | 0.0003 | 29 | 116 | 116 | 25 |
| 8 | 15 | 20 | 35.17 | 3.3759 | -0.0376 | -0.0376 | 0.0002 | 23 | 4.5490 | 0.1965 | 0.1965 | 0.0002 | 26 | 119 | 119 | 22 |
| 8 | 30 | 3 | 85.23 | 0.5886 | -0.0093 | -0.0093 | 0.0001 | 38 | 0.8967 | 0.0811 | 0.0811 | 0.0001 | 34 | 111 | 111 | 28 |
| 8 | 30 | 7 | 71.13 | 0.8432 | -0.0129 | -0.0129 | 0.0001 | 38 | 1.2450 | 0.0734 | 0.0734 | 0.0001 | 32 | 118 | 118 | 28 |
| 8 | 30 | 12 | 63.41 | 1.0593 | -0.0158 | -0.0158 | 0.0001 | 38 | 1.5110 | 0.0661 | 0.0661 | 0.0001 | 30 | 124 | 124 | 26 |
| 8 | 30 | 20 | 56.86 | 1.3144 | -0.0191 | -0.0191 | 0.0001 | 38 | 1.7910 | 0.0595 | 0.0595 | 0.0001 | 27 | 132 | 132 | 23 |
| 12 | 15 | 3 | 62.82 | 1.0789 | -0.0161 | -0.0161 | 0.0002 | 27 | 1.6290 | 0.1533 | 0.1533 | 0.0003 | 34 | 111 | 111 | 27 |
| 12 | 15 | 7 | 52.43 | 1.5428 | -0.0219 | -0.0219 | 0.0002 | 27 | 2.2560 | 0.1427 | 0.1427 | 0.0002 | 32 | 115 | 115 | 27 |
| 12 | 15 | 12 | 46.74 | 1.9353 | -0.0262 | -0.0262 | 0.0001 | 27 | 2.7370 | 0.1340 | 0.1340 | 0.0002 | 29 | 120 | 120 | 25 |
| 12 | 15 | 20 | 41.91 | 2.3972 | -0.0306 | -0.0306 | 0.0001 | 27 | 3.2460 | 0.1295 | 0.1295 | 0.0002 | 26 | 124 | 124 | 23 |
| 12 | 30 | 3 | 95.33 | 0.4709 | -0.0075 | -0.0075 | 0.0001 | 42 | 0.7197 | 0.0647 | 0.0647 | 0.0001 | 35 | 112 | 112 | 28 |
| 12 | 30 | 7 | 79.57 | 0.6749 | -0.0105 | -0.0105 | 0.0001 | 42 | 1.0000 | 0.0588 | 0.0588 | 0.0001 | 33 | 118 | 118 | 28 |
| 12 | 30 | 12 | 70.92 | 0.8481 | -0.0130 | -0.0130 | 0.0001 | 42 | 1.2150 | 0.0534 | 0.0534 | 0.0001 | 30 | 124 | 124 | 26 |
| 12 | 30 | 20 | 63.60 | 1.0529 | -0.0158 | -0.0158 | 0.0001 | 42 | 1.4410 | 0.0489 | 0.0489 | 0.0001 | 27 | 132 | 132 | 24 |

TABLE 5-31 JULEA (3 Layers) and ZAPRAM Comparison for Heavy Load

| Truck | | | ZAPRAM | | | | | JULEA(3 Layer) | | | | | Percentage Diff, % | | | |
|-------|----|---------|--------|--------|---------|---------|--------|----------------|--------|--------|--------|--------|--------------------|-----|-----|----|
| h1 | h2 | CBR (%) | Z | σz | σx | σy | εz | Z | σz | σx | σy | εz | σz | σx | σy | εz |
| 4 | 15 | 3 | 42.61 | 24.505 | -0.0721 | -0.0721 | 0.0044 | 19 | 33.300 | 4.8300 | 4.8300 | 0.0051 | 26 | 101 | 101 | 15 |
| 4 | 15 | 7 | 35.57 | 34.158 | 0.0969 | 0.0969 | 0.0035 | 19 | 45.090 | 5.1760 | 5.1760 | 0.0042 | 24 | 98 | 98 | 16 |
| 4 | 15 | 12 | 31.70 | 41.951 | 0.3218 | 0.3218 | 0.0030 | 19 | 53.850 | 5.3950 | 5.3950 | 0.0036 | 22 | 94 | 94 | 15 |
| 4 | 15 | 20 | 28.43 | 50.709 | 0.6744 | 0.6744 | 0.0026 | 19 | 62.850 | 5.6720 | 5.6720 | 0.0030 | 19 | 88 | 88 | 13 |
| 4 | 30 | 3 | 75.12 | 8.267 | -0.1007 | -0.1007 | 0.0015 | 34 | 12.080 | 1.3100 | 1.3100 | 0.0019 | 32 | 108 | 108 | 23 |
| 4 | 30 | 7 | 62.70 | 11.750 | -0.1204 | -0.1204 | 0.0012 | 34 | 16.620 | 1.2670 | 1.2670 | 0.0016 | 29 | 110 | 110 | 23 |
| 4 | 30 | 12 | 55.89 | 14.665 | -0.1263 | -0.1263 | 0.0011 | 34 | 20.050 | 1.2090 | 1.2090 | 0.0014 | 27 | 110 | 110 | 22 |
| 4 | 30 | 20 | 50.12 | 18.057 | -0.1207 | -0.1207 | 0.0010 | 34 | 23.630 | 1.1580 | 1.1580 | 0.0012 | 24 | 110 | 110 | 20 |
| 8 | 15 | 3 | 52.72 | 16.400 | -0.1251 | -0.1251 | 0.0029 | 23 | 23.160 | 2.9380 | 2.9380 | 0.0036 | 29 | 104 | 104 | 20 |
| 8 | 15 | 7 | 44.00 | 23.083 | -0.0872 | -0.0872 | 0.0024 | 23 | 31.620 | 3.0640 | 3.0640 | 0.0030 | 27 | 103 | 103 | 20 |
| 8 | 15 | 12 | 39.22 | 28.575 | -0.0153 | -0.0153 | 0.0021 | 23 | 37.990 | 3.1450 | 3.1450 | 0.0026 | 25 | 100 | 100 | 19 |
| 8 | 15 | 20 | 35.17 | 34.856 | 0.1137 | 0.1137 | 0.0018 | 23 | 44.620 | 3.2830 | 3.2830 | 0.0022 | 22 | 97 | 97 | 17 |
| 8 | 30 | 3 | 85.23 | 6.456 | -0.0851 | -0.0851 | 0.0012 | 38 | 9.588 | 0.9792 | 0.9792 | 0.0015 | 33 | 109 | 109 | 25 |
| 8 | 30 | 7 | 71.13 | 9.196 | -0.1073 | -0.1073 | 0.0010 | 38 | 13.240 | 0.9385 | 0.9385 | 0.0013 | 31 | 111 | 111 | 25 |
| 8 | 30 | 12 | 63.41 | 11.498 | -0.1194 | -0.1194 | 0.0008 | 38 | 16.020 | 0.8928 | 0.8928 | 0.0011 | 28 | 113 | 113 | 24 |
| 8 | 30 | 20 | 56.86 | 14.188 | -0.1260 | -0.1260 | 0.0008 | 38 | 18.920 | 0.8578 | 0.8578 | 0.0010 | 25 | 115 | 115 | 21 |
| 12 | 15 | 3 | 62.82 | 11.707 | -0.1203 | -0.1203 | 0.0021 | 27 | 16.880 | 1.9550 | 1.9550 | 0.0027 | 31 | 106 | 106 | 22 |
| 12 | 15 | 7 | 52.43 | 16.570 | -0.1248 | -0.1248 | 0.0017 | 27 | 23.150 | 1.9780 | 1.9780 | 0.0022 | 28 | 106 | 106 | 22 |
| 12 | 15 | 12 | 46.74 | 20.609 | -0.1075 | -0.1075 | 0.0015 | 27 | 27.910 | 1.9930 | 1.9930 | 0.0019 | 26 | 105 | 105 | 21 |
| 12 | 15 | 20 | 41.91 | 25.274 | -0.0630 | -0.0630 | 0.0013 | 27 | 32.900 | 2.0580 | 2.0580 | 0.0016 | 23 | 103 | 103 | 18 |
| 12 | 30 | 3 | 95.33 | 5.179 | -0.0718 | -0.0718 | 0.0009 | 42 | 7.757 | 0.7684 | 0.7684 | 0.0013 | 33 | 109 | 109 | 26 |
| 12 | 30 | 7 | 79.57 | 7.388 | -0.0936 | -0.0936 | 0.0008 | 42 | 10.730 | 0.7322 | 0.7322 | 0.0010 | 31 | 113 | 113 | 26 |
| 12 | 30 | 12 | 70.92 | 9.249 | -0.1076 | -0.1076 | 0.0007 | 42 | 12.990 | 0.6959 | 0.6959 | 0.0009 | 29 | 115 | 115 | 24 |
| 12 | 30 | 20 | 63.60 | 11.430 | -0.1192 | -0.1192 | 0.0006 | 42 | 15.370 | 0.6716 | 0.6716 | 0.0008 | 26 | 118 | 118 | 22 |

Figures 5-15 to 5-28 illustrate the computed stresses and strain from both programs. It is noted that the line of equality is not a factor with the calculated line for the programs. It can be also observed that even the slopes for both lines vary. Finally, it is concluded that the results from the JULEA are higher than those estimated by ZAPRAM.

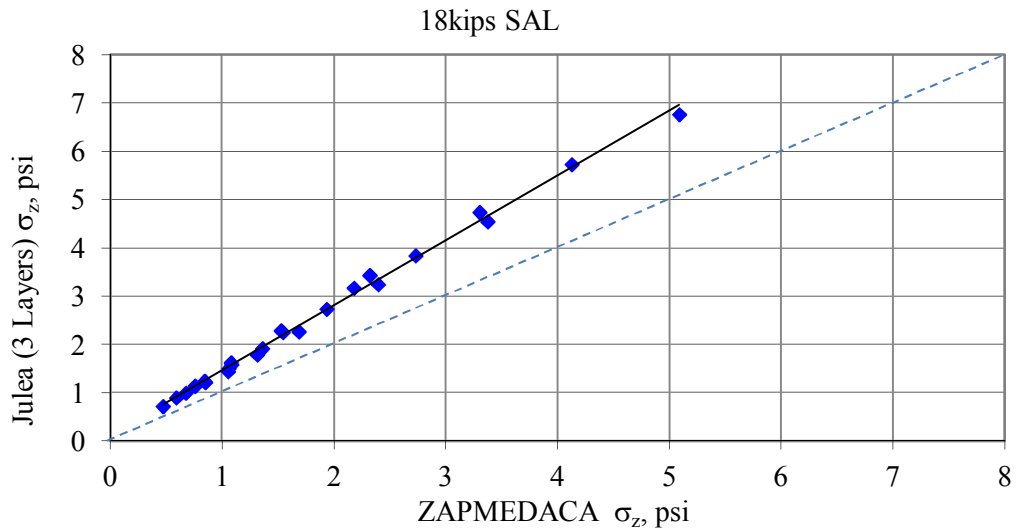


FIGURE 5-25 Calculated stresses from JULEA (3 Layers) and ZAPRAM for light load.

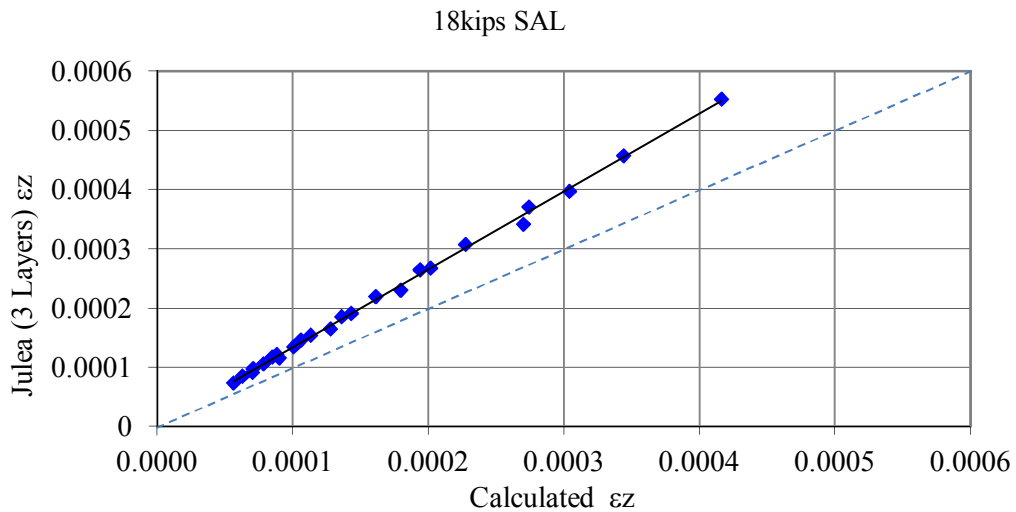


FIGURE 5-26 Calculated strain from JULEA (3 Layers) and ZAPRAM for light load.

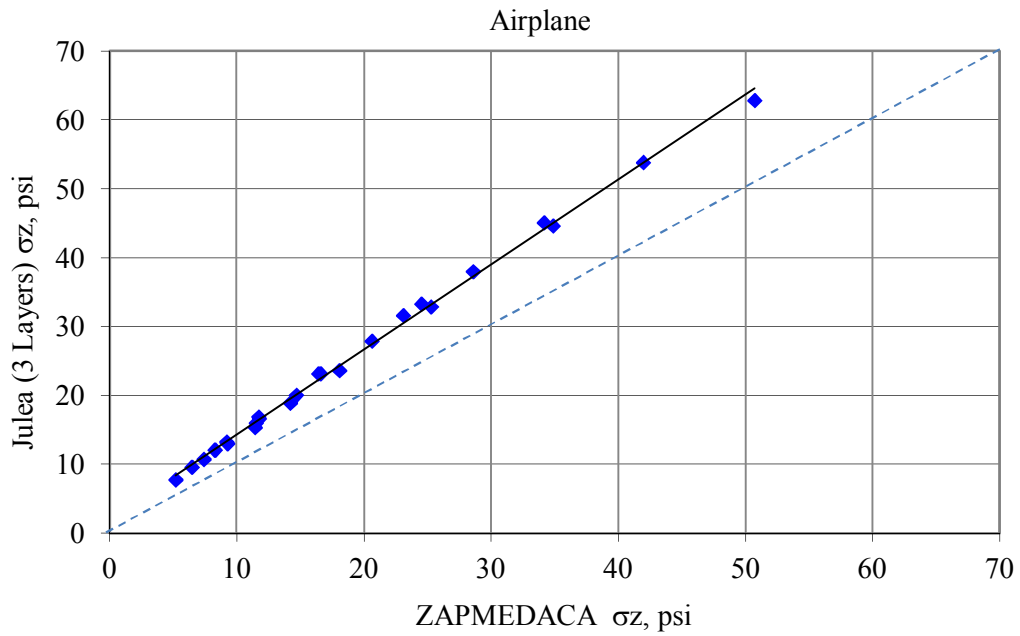


FIGURE 5-27 Calculated Stresses from JULEA (3 Layers) and ZAPRAM for heavy load.

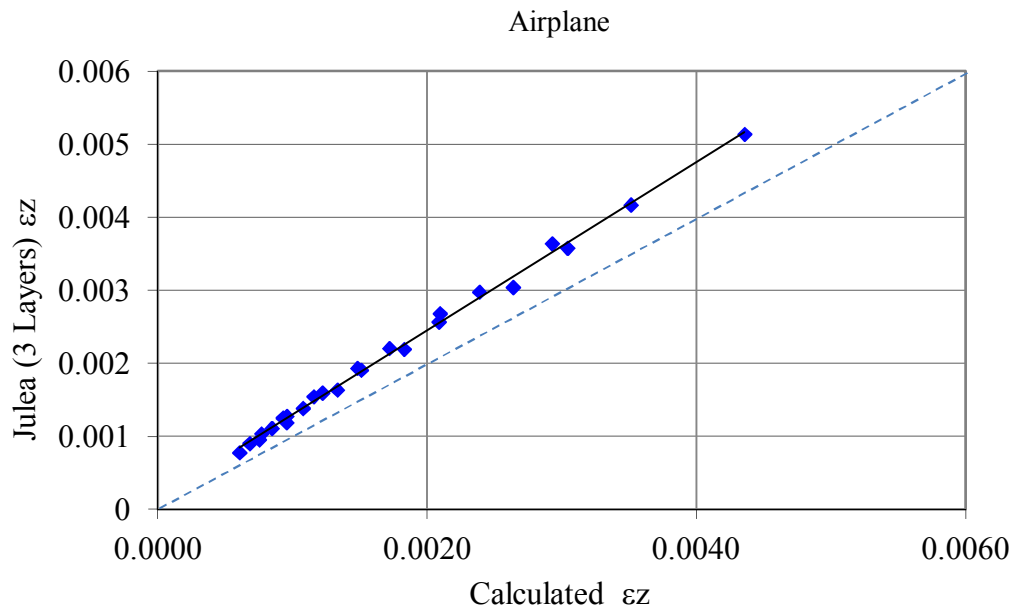


FIGURE 5-28 Calculated strain from JULEA (3 Layers) and ZAPRAM for heavy load.

Figures 5-29 through 5-34 are 3 sets of two figures that show the percentage errors associated with stress predictions and strain predictions as a function of CBR

(Figure 5-29 and 5-30) and AC layer Thickness (h_1) (Figure 5-31 and 5-31) and Base Thickness (h_2) Figures 5-33 and 5-34).

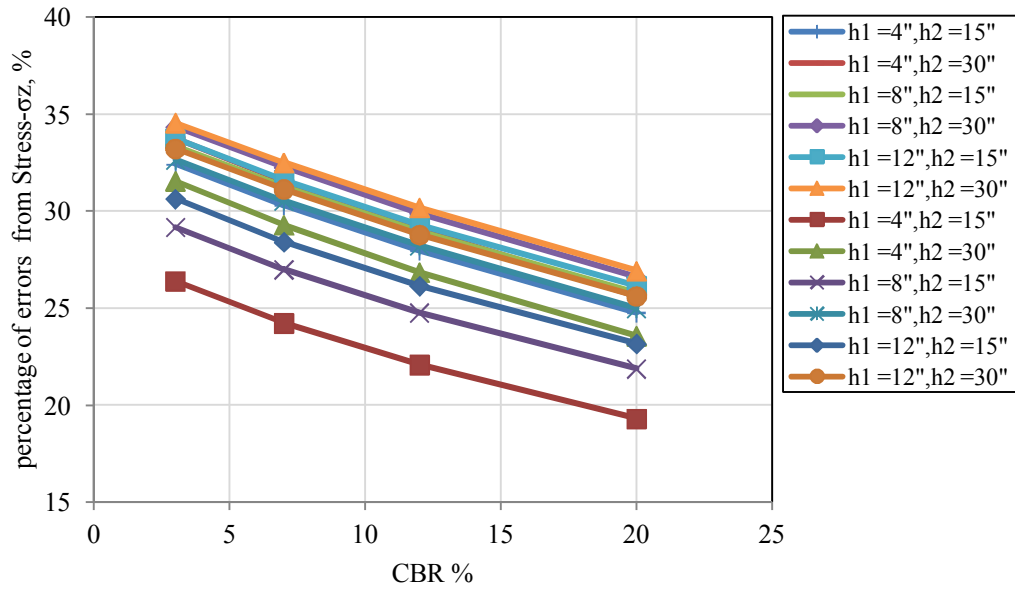


FIGURE 5-29 The effect of CBR on percent error (stress) – truck.

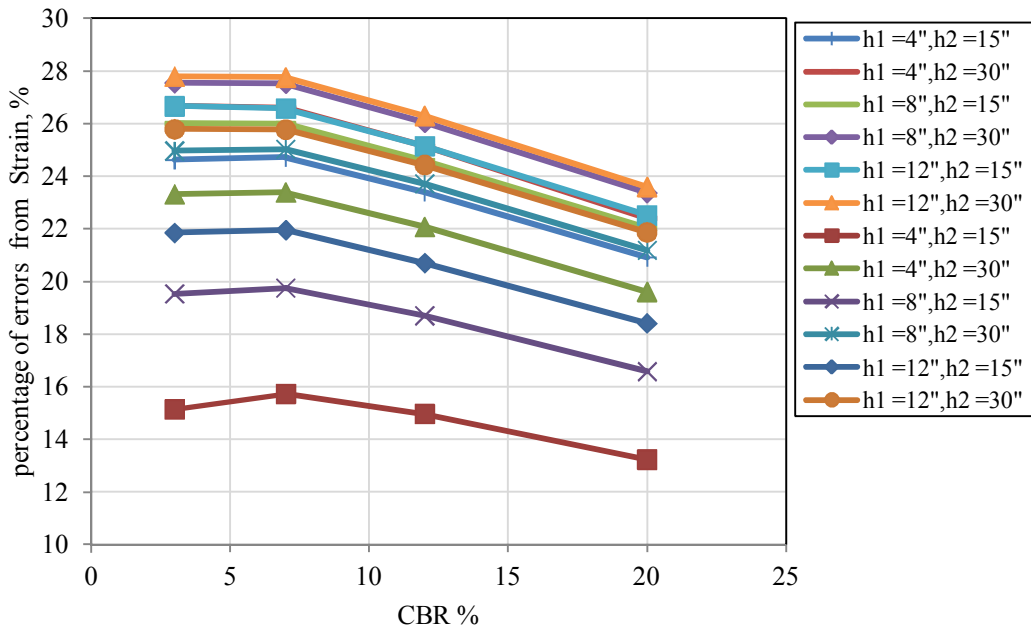


FIGURE 5-30 The effect of CBR on percent error (strain) – truck.

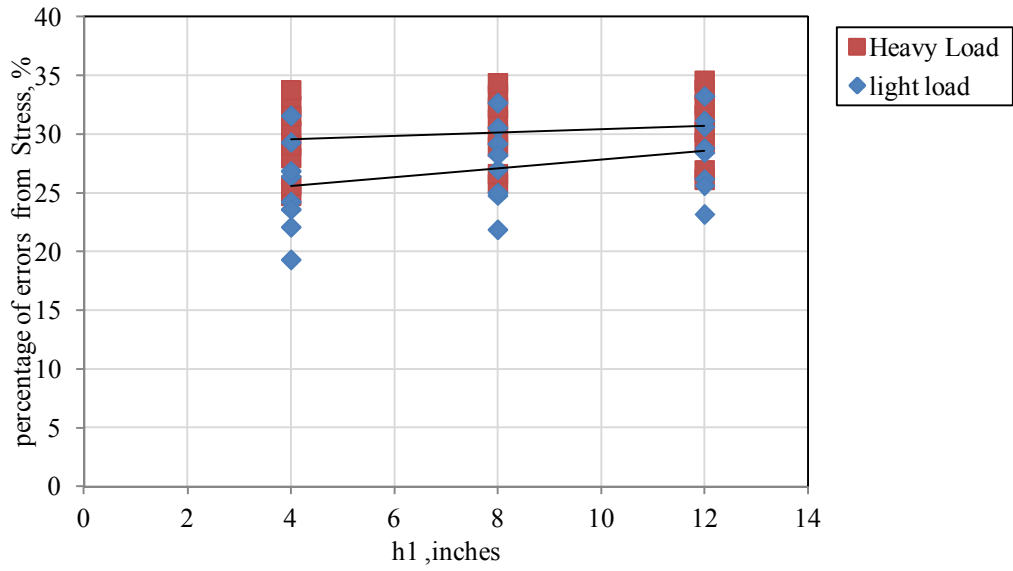


FIGURE 5-31 The effect of h_1 on percent error (stress).

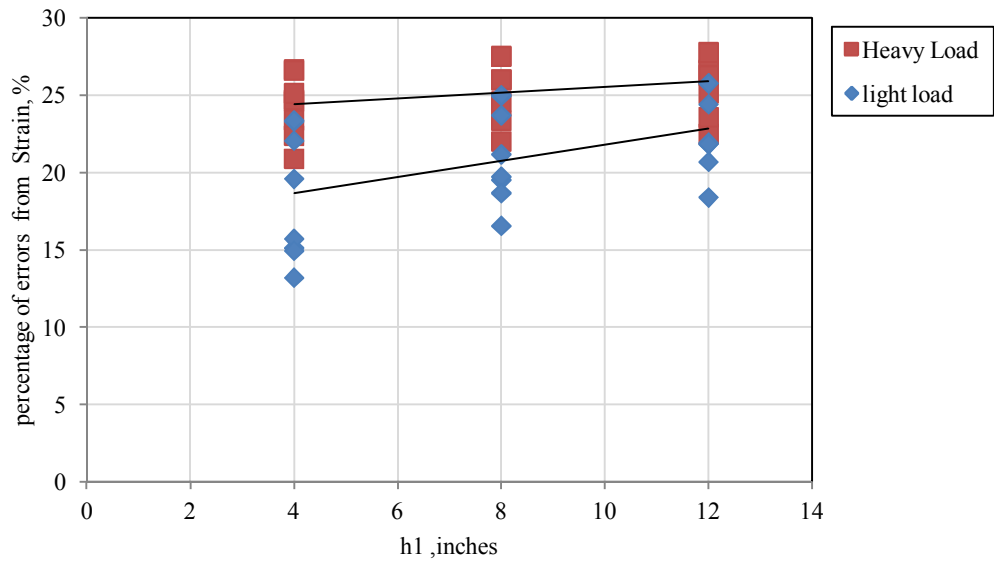


Figure 5-32 The effect of h_1 on percent error (strain).

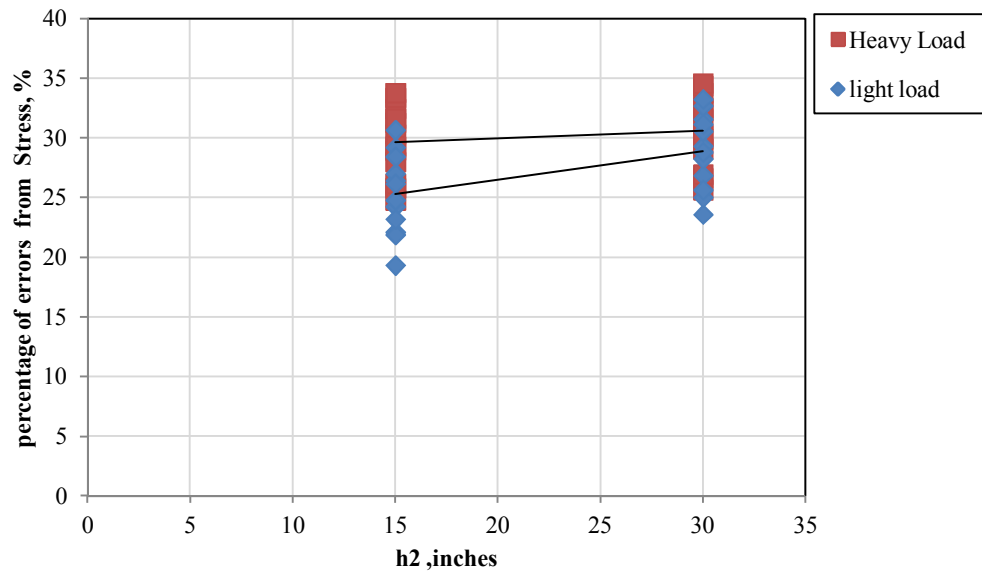


FIGURE 5-33 The effect of h_2 on percentage error (stress).

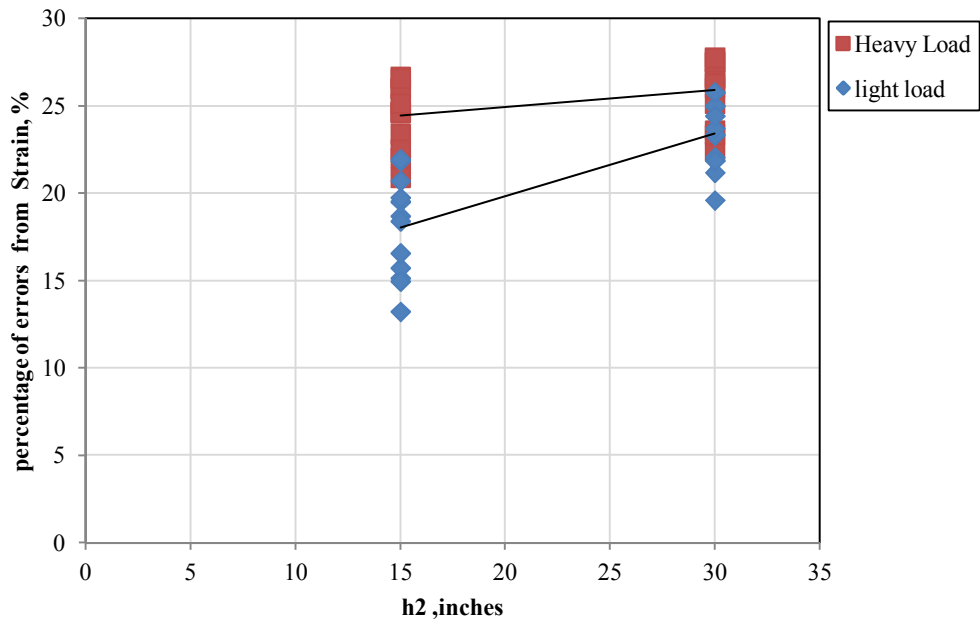


FIGURE 5-34 The effect of h_1 on percent error (strain).

Based upon a analysis of the previous six figures, in can be concluded that:

- For any given pavement structure, as the CBR of the subgrade is increased; the percent error decreases. This is typically true for either stress or strain prediction.
- For all factors being constant in the pavement structure; the percent error (Stress or Strain Predictions) increases as the load becomes heavier. However, this variable (load) appears to not be an overly significant or sensitive factor for such a large range in load types evaluated.
- The percent error was found to increase, for either stress or strain predictions, as either the thickness of the AC layer (h_1) is increased or the thickness of the base layer (h_2) is increased

5.3.6 The Back Calculation to Estimate f_2

The results of the previous study dealing with the percent error comparison between the 18KSALtruck and 100ktp single aircraft tire load lends itself to a similar analysis to back calculate the f_2 correction value that was accomplished for the two aircraft types (B-737 and A-310). Like the prior study, the value of f_1 (AC layer correction factor) was set at $f_1 = 1.0$.

Table 5-32 illustrates an example computation for both programs (for a given pavement structure) by varying the thickness of the first layer ($h_1 = 4.0$; 8.0 and 12.0 inches) while keeping all other characterizations for the three system constant.

TABLE 5-32 Strain and Stress Value from Both Programs with Changes of h_1

| Boeing B737-600 | | | JULEA(3 Layer) | | | ZAPRAM | | |
|-----------------|-------|--------|----------------|------------|--------------|--------|------------|--------------|
| h_1 | h_2 | CBR(%) | Z | σ_z | ϵ_z | Z | σ_z | ϵ_z |
| 4 | 15 | 3 | 19.00 | 3.4340 | 0.0006 | 42.61 | 2.3205 | 0.0004 |
| 8 | 15 | 3 | 23.00 | 2.2910 | 0.0004 | 52.70 | 1.5264 | 0.0003 |
| 12 | 15 | 3 | 27.00 | 1.6290 | 0.0003 | 62.82 | 1.0789 | 0.0002 |

Using this information Figure 5-37 can be developed to estimate the “true” equivalent thicknesses (and f_i) values that would yield the same stress and strain predictions as the JULEA MLET Program.

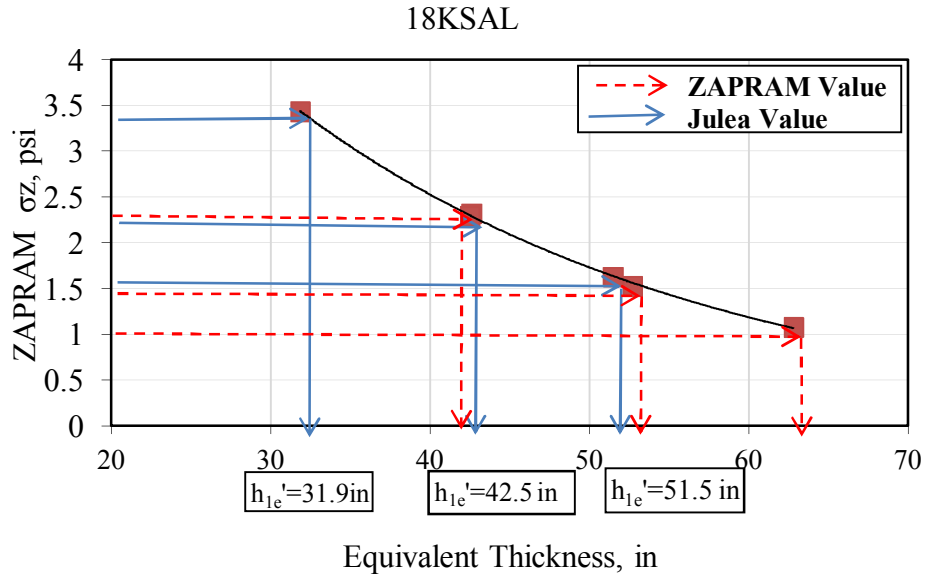


FIGURE 5-35 Estimate the equivalent depth that the stresses must be calculated.

By applying equation [5-9] below, the best correction factors can be estimated.

$$h_{eT} = h_{1e} + h_{2e} \quad (5-9)$$

$$h_{eT} = f_1 h_1^3 \sqrt{\frac{(E_1(1-\mu_3^2))}{(E_3(1-\mu_1^2))}} + f_2 h_2^3 \sqrt{\frac{(E_2(1-\mu_3^2))}{(E_3(1-\mu_2^2))}} \quad (5-10)$$

By applying the previous steps with the change of thickness of the first layer, it is possible to compute what the value of the correction factor (f_2) is. An example set of calculations, with the estimated f_2 values, are shown in Table 5-33, as an example.

TABLE 5-33 Steps of Best Correction Factor Calculation

| h1 | E1 | E2 | μ_1 | μ_2 | he | f_1 | f_2 | he ₁ | he ₂ | he | he ₁ ' | he' | he ₂ ' | f ₂ |
|----|--------|------|---------|---------|-----------------------|-------|-------|-----------------|-----------------|-------|-------------------|-------|-------------------|----------------|
| 4 | 100000 | 5639 | 0.35 | 0.45 | 10.10 | 1 | 1 | 10.10 | 32.51 | 42.61 | 10.10 | 31.87 | 21.76 | 0.67 |
| 15 | 60462 | 5639 | 0.4 | 0.45 | 32.51 | | | | | | | | | |
| | | | | | equivalent thickness= | 42.61 | | | | | | | | |
| h1 | E1 | E2 | μ_1 | μ_2 | he | f_1 | f_2 | he ₁ | he ₂ | he | he ₁ ' | he' | he ₂ ' | f ₂ |
| 8 | 100000 | 5639 | 0.35 | 0.45 | 20.21 | 1 | 1 | 20.21 | 32.51 | 52.72 | 20.21 | 42.52 | 22.31 | 0.69 |
| 15 | 60462 | 5639 | 0.4 | 0.45 | 32.51 | | | | | | | | | |
| | | | | | equivalent thickness= | 52.72 | | | | | | | | |
| h1 | E1 | E2 | μ_1 | μ_2 | he | f_1 | f_2 | he ₁ | he ₂ | he | he ₁ ' | he' | he ₂ ' | f ₂ |
| 12 | 100000 | 5639 | 0.35 | 0.45 | 30.31 | 1 | 1 | 30.31 | 32.51 | 62.82 | 30.31 | 51.49 | 21.18 | 0.65 |
| 15 | 60462 | 5639 | 0.4 | 0.45 | 32.51 | | | | | | | | | |
| | | | | | equivalent thickness= | 62.82 | | | | | | | | |

A total of 24 different pavement systems, for the 18KSAL load, were solved with the same steps. This allowed for 24 estimates of the f_2 for the vertical stress and vertical strain at the top of subgrade. As a result, 24 values for f_2 were estimated. The tabular summary of these results are shown in Table 5-34.

TABLE 5-34 All the f_2 Estimations from 24 Systems Due to Vertical Stress and Strain
(18KSAL)

| Pavement System | | | Back calculation σ_z | | Back calculation ϵ_z | |
|-----------------|-------|---------|-----------------------------|-------|-------------------------------|-------|
| h_1 | h_2 | CBR (%) | f_1 | f_2 | f_1 | f_2 |
| 4 | | | 1 | 0.67 | 1 | 0.77 |
| 8 | 15 | 3 | 1 | 0.69 | 1 | 0.78 |
| 12 | | | 1 | 0.65 | 1 | 0.75 |
| 4 | | | 1 | 0.70 | 1 | 0.77 |
| 8 | 15 | 7 | 1 | 0.72 | 1 | 0.78 |
| 12 | | | 1 | 0.69 | 1 | 0.74 |
| 4 | | | 1 | 0.73 | 1 | 0.79 |
| 8 | 15 | 12 | 1 | 0.75 | 1 | 0.80 |
| 12 | | | 1 | 0.72 | 1 | 0.77 |
| 4 | | | 1 | 0.75 | 1 | 0.79 |
| 8 | 15 | 20 | 1 | 0.77 | 1 | 0.80 |
| 12 | | | 1 | 0.74 | 1 | 0.77 |
| 4 | | | 1 | 0.74 | 1 | 0.82 |
| 8 | 30 | 3 | 1 | 0.75 | 1 | 0.83 |
| 12 | | | 1 | 0.74 | 1 | 0.82 |
| 4 | | | 1 | 0.75 | 1 | 0.84 |
| 8 | 30 | 7 | 1 | 0.75 | 1 | 0.84 |
| 12 | | | 1 | 0.74 | 1 | 0.83 |
| 4 | | | 1 | 0.78 | 1 | 0.84 |
| 8 | 30 | 12 | 1 | 0.79 | 1 | 0.85 |
| 12 | | | 1 | 0.78 | 1 | 0.84 |
| 4 | | | 1 | 0.80 | 1 | 0.81 |
| 8 | 30 | 20 | 1 | 0.80 | 1 | 0.81 |
| 12 | | | 1 | 0.79 | 1 | 0.80 |
| Avg. | | | | 0.74 | | 0.80 |

Similar to the 18KSAL (truck) analysis; the same approach was used with the results generated from the 100 kip single aircraft tire. The 48 predictions of the f_2 value (24 for each stress and strain prediction) are shown in Table 5-35.

TABLE 5-35 All the f_2 Estimations from 24 Systems Due to Vertical Stress and Strain
(100kip Tire)

| Pavement System | | | Back calculation σ_z | | Back calculation ϵ_z | |
|-----------------|-------|---------|-----------------------------|-------|-------------------------------|-------|
| h_1 | h_2 | CBR (%) | f_1 | f_2 | f_1 | f_2 |
| 4 | | | 1 | 0.72 | 1 | 0.86 |
| 8 | 15 | 3 | 1 | 0.71 | 1 | 0.84 |
| 12 | | | 1 | 0.66 | 1 | 0.79 |
| 4 | | | 1 | 0.75 | 1 | 0.85 |
| 8 | 15 | 7 | 1 | 0.74 | 1 | 0.84 |
| 12 | | | 1 | 0.70 | 1 | 0.79 |
| 4 | | | 1 | 0.78 | 1 | 0.84 |
| 8 | 15 | 12 | 1 | 0.78 | 1 | 0.82 |
| 12 | | | 1 | 0.74 | 1 | 0.77 |
| 4 | | | 1 | 0.79 | 1 | 0.85 |
| 8 | 15 | 20 | 1 | 0.79 | 1 | 0.84 |
| 12 | | | 1 | 0.75 | 1 | 0.79 |
| 4 | | | 1 | 0.75 | 1 | 0.83 |
| 8 | 30 | 3 | 1 | 0.75 | 1 | 0.82 |
| 12 | | | 1 | 0.74 | 1 | 0.81 |
| 4 | | | 1 | 0.75 | 1 | 0.83 |
| 8 | 30 | 7 | 1 | 0.74 | 1 | 0.83 |
| 12 | | | 1 | 0.73 | 1 | 0.82 |
| 4 | | | 1 | 0.78 | 1 | 0.84 |
| 8 | 30 | 12 | 1 | 0.77 | 1 | 0.84 |
| 12 | | | 1 | 0.75 | 1 | 0.83 |
| 4 | | | 1 | 0.81 | 1 | 0.84 |
| 8 | 30 | 20 | 1 | 0.81 | 1 | 0.84 |
| 12 | | | 1 | 0.79 | 1 | 0.82 |
| Avg. | | | | 0.75 | | 0.83 |

5.3.7 *The Factors of Equivalent Thickness Study for Three Layers System*

The Odemark Layer correction factor, f , has been shown to be a function of the number and properties of layers in the structure. The equation for the equivalent thickness that are used in this study and within ZAPRAM has the following form:

$$h_{eT} = h_{1e} + h_{2e} \quad (5-11)$$

$$h_{eT} = f_1 h_1 \sqrt[3]{\frac{(E_1(1-\mu_3^2))}{(E_3(1-\mu_1^2))}} + f_2 h_2 \sqrt[3]{\frac{(E_2(1-\mu_3^2))}{(E_3(1-\mu_2^2))}} \quad (5-12)$$

While this is the most common form of the equation for the equivalent thickness using correction factors directly applied to the layer thickness; a more generalized equation using up to six (6) factors can be written so that:

- i. f_1, f_2 assumed to be before the layer thickness h .
- ii. f_3, f_4 assumed to be instead of the cube on the root.
- iii. f_5, f_6 assumed to be before the subgrade modular ratios E_3 .

. The final form of this general equation becomes as follows

$$h_{eT} = f_1 h_1 \sqrt[f_3]{\frac{(E_1(1-\mu_3^2))}{(f_5 \times E_3 \times (1-\mu_1^2))}} + f_2 h_2 \sqrt[f_4]{\frac{(E_2(1-\mu_3^2))}{(f_6 \times E_3 \times (1-\mu_2^2))}} \quad (5-13)$$

As an example; if the Elastic Constants of each layer were used, so that:

$$E_1 = 100000 \text{ psi}, E_2 = 60462 \text{ psi}, \nu_1 = 0.35, \nu_2 = 0.40, \nu_3 = 0.45$$

For this example, the Transformed Thickness Equation would be as follows:

$$h_{eT} = f_1 h_1 \sqrt[f_3]{\frac{(100000 \times (1-(0.45)^2))}{(f_5 \times E_3 \times (1-(0.35)^2))}} + f_2 h_2 \sqrt[f_4]{\frac{(60462 \times (1-(0.45)^2))}{(f_6 \times E_3 \times (1-(0.40)^2))}} \quad (5-14)$$

$$h_{eT} = f_1 h_1 \sqrt[f_3]{\frac{(90883.19)}{f_5 \times (E_3)}} + f_2 h_2 \sqrt[f_4]{\frac{(57402.91)}{f_6 \times (E_3)}} \quad (5-15)$$

TABLE 5-36 illustrates all of the other variables (h_1, h_2, E_3) values and the equivalent thickness from the ZAPRAM calculation for all of the runs (sets) that were completed. The last column has the values of the equivalent thickness (h_{eT}) from JULEA.

TABLE 5-36 The Sets of Data Used to Determine the Correction Factors

| No | h ₁ (in) | h ₂ (in) | E ₃ (Psi) | h _{eT} (in) | |
|----|------------------------|------------------------|-------------------------|----------------------|-------|
| | | | | ZAPRAM | JULEA |
| 1 | 4 | 15 | 5639 | 42.61 | 31.87 |
| 2 | 4 | 15 | 9698 | 35.57 | 27.39 |
| 3 | 4 | 15 | 13693 | 31.70 | 25.15 |
| 4 | 4 | 15 | 18988 | 28.43 | 23.07 |
| 5 | 4 | 30 | 5639 | 75.12 | 58.52 |
| 6 | 4 | 30 | 9698 | 62.70 | 49.11 |
| 7 | 4 | 30 | 13693 | 55.89 | 45.40 |
| 8 | 4 | 30 | 18988 | 50.12 | 41.45 |
| 9 | 8 | 15 | 5639 | 52.72 | 42.52 |
| 10 | 8 | 15 | 9698 | 44.00 | 36.32 |
| 11 | 8 | 15 | 13693 | 39.22 | 33.15 |
| 12 | 8 | 15 | 18988 | 35.17 | 30.16 |
| 13 | 8 | 30 | 5639 | 85.23 | 69.03 |
| 14 | 8 | 30 | 9698 | 71.13 | 57.66 |
| 15 | 8 | 30 | 13693 | 63.41 | 53.08 |
| 16 | 8 | 30 | 18988 | 56.86 | 48.19 |
| 17 | 12 | 15 | 5639 | 62.82 | 51.49 |
| 18 | 12 | 15 | 9698 | 52.43 | 43.89 |
| 19 | 12 | 15 | 13693 | 46.74 | 39.94 |
| 20 | 12 | 15 | 18988 | 41.91 | 36.19 |
| 21 | 12 | 30 | 5639 | 95.33 | 78.59 |
| 22 | 12 | 30 | 9698 | 79.57 | 65.49 |
| 23 | 12 | 30 | 13693 | 70.92 | 60.11 |
| 24 | 12 | 30 | 18988 | 63.60 | 54.41 |
| 25 | 4 | 15 | 5639 | 42.61 | 35.15 |
| 26 | 4 | 15 | 9698 | 35.57 | 29.19 |
| 27 | 4 | 15 | 13693 | 31.70 | 26.58 |
| 28 | 4 | 15 | 18988 | 28.43 | 23.87 |
| 29 | 4 | 30 | 5639 | 75.12 | 63.55 |
| 30 | 4 | 30 | 9698 | 62.70 | 54.03 |
| 31 | 4 | 30 | 13693 | 55.89 | 48.26 |
| 32 | 4 | 30 | 18988 | 50.12 | 41.77 |
| 33 | 8 | 15 | 5639 | 52.72 | 45.65 |
| 34 | 8 | 15 | 9698 | 44.00 | 38.02 |
| 35 | 8 | 15 | 13693 | 39.22 | 34.50 |
| 36 | 8 | 15 | 18988 | 35.17 | 30.91 |
| 37 | 8 | 30 | 5639 | 85.23 | 73.93 |
| 38 | 8 | 30 | 9698 | 71.13 | 62.51 |
| 39 | 8 | 30 | 13693 | 63.41 | 55.92 |
| 40 | 8 | 30 | 18988 | 56.86 | 48.52 |
| 41 | 12 | 15 | 5639 | 62.82 | 54.53 |
| 42 | 12 | 15 | 9698 | 52.43 | 45.50 |
| 43 | 12 | 15 | 13693 | 46.74 | 41.21 |
| 44 | 12 | 15 | 18988 | 41.91 | 36.88 |
| 45 | 12 | 30 | 5639 | 95.33 | 83.47 |
| 46 | 12 | 30 | 9698 | 79.57 | 70.34 |
| 47 | 12 | 30 | 13693 | 70.92 | 62.97 |
| 48 | 12 | 30 | 18988 | 63.60 | 54.76 |
| 49 | 4 | 15 | 5639 | 42.61 | 33.52 |
| 50 | 4 | 15 | 9698 | 35.57 | 28.78 |
| 51 | 4 | 15 | 13693 | 31.70 | 26.38 |
| 52 | 4 | 15 | 18988 | 28.43 | 23.94 |
| 53 | 4 | 30 | 5639 | 75.12 | 58.92 |
| 54 | 4 | 30 | 9698 | 62.70 | 49.07 |
| 55 | 4 | 30 | 13693 | 55.89 | 45.04 |
| 56 | 4 | 30 | 18988 | 50.12 | 41.96 |
| 57 | 8 | 15 | 5639 | 52.72 | 43.34 |
| 58 | 8 | 15 | 9698 | 44.00 | 37.04 |
| 59 | 8 | 15 | 13693 | 39.22 | 33.80 |
| 60 | 8 | 15 | 18988 | 35.17 | 30.53 |
| 61 | 8 | 30 | 5639 | 85.23 | 68.96 |
| 62 | 8 | 30 | 9698 | 71.13 | 57.19 |
| 63 | 8 | 30 | 13693 | 63.41 | 52.28 |
| 64 | 8 | 30 | 18988 | 56.86 | 48.50 |
| 65 | 12 | 15 | 5639 | 62.82 | 51.89 |
| 66 | 12 | 15 | 9698 | 52.43 | 44.29 |
| 67 | 12 | 15 | 13693 | 46.74 | 40.36 |
| 68 | 12 | 15 | 18988 | 41.91 | 36.39 |
| 69 | 12 | 30 | 5639 | 95.33 | 78.18 |
| 70 | 12 | 30 | 9698 | 79.57 | 64.70 |
| 71 | 12 | 30 | 13693 | 70.92 | 59.05 |
| 72 | 12 | 30 | 18988 | 63.60 | 54.61 |
| 73 | 4 | 15 | 5639 | 42.61 | 38.04 |
| 74 | 4 | 15 | 9698 | 35.57 | 31.57 |
| 75 | 4 | 15 | 13693 | 31.70 | 27.77 |
| 76 | 4 | 15 | 18988 | 28.43 | 25.21 |
| 77 | 4 | 30 | 5639 | 75.12 | 63.88 |
| 78 | 4 | 30 | 9698 | 62.70 | 53.68 |
| 79 | 4 | 30 | 13693 | 55.89 | 48.31 |
| 80 | 4 | 30 | 18988 | 50.12 | 43.37 |
| 81 | 8 | 15 | 5639 | 52.72 | 47.61 |
| 82 | 8 | 15 | 9698 | 44.00 | 39.60 |
| 83 | 8 | 15 | 13693 | 39.22 | 34.83 |
| 84 | 8 | 15 | 18988 | 35.17 | 31.61 |
| 85 | 8 | 30 | 5639 | 85.23 | 73.65 |
| 86 | 8 | 30 | 9698 | 71.13 | 61.91 |
| 87 | 8 | 30 | 13693 | 63.41 | 55.66 |
| 88 | 8 | 30 | 18988 | 56.86 | 49.82 |
| 89 | 12 | 15 | 5639 | 62.82 | 56.10 |
| 90 | 12 | 15 | 9698 | 52.43 | 46.75 |
| 91 | 12 | 15 | 13693 | 46.74 | 41.16 |
| 92 | 12 | 15 | 18988 | 41.91 | 37.38 |
| 93 | 12 | 30 | 5639 | 95.33 | 82.73 |
| 94 | 12 | 30 | 9698 | 79.57 | 69.62 |
| 95 | 12 | 30 | 13693 | 70.92 | 62.56 |
| 96 | 12 | 30 | 18988 | 63.60 | 55.88 |

This table provides 96 values because each pavement set (analysis) was investigated for f_2 values due to both stress and strain.

By introducing the previous data as input in the statistics program (STATISTICA), estimates of the correction factors were obtained by the method of least square errors. The STATISTICA analysis was run for four cases for the equivalent thickness equation.

- Case I:

The first case, the equation has the following formula

$$h_{eT} = f_1 h_1^3 \sqrt{\frac{(90883.19)}{(E_3)}} + f_2 h_2^3 \sqrt{\frac{(57402.91)}{(E_3)}} \quad (5-16)$$

- Case II:

The second case, the equation is the following formula

$$h_{eT} = h_1^{f_1} \sqrt{\frac{(90883.19)}{(E_3)}} + h_2^{f_2} \sqrt{\frac{(57402.91)}{(E_3)}} \quad (5-17)$$

- Case III:

The third case, the formula equation could be clarified as follows

$$h_{eT} = h_1^3 \sqrt{\frac{(90883.19)}{f_1 \times (E_3)}} + h_2^3 \sqrt{\frac{(57402.91)}{f_2 \times (E_3)}} \quad (5-18)$$

- Case IV:

For the latter case, would impose the existence of all correction factors:

$$h_{eT} = f_1 h_1^{f_3} \sqrt{\frac{(90883.19)}{f_5 \times (E_3)}} + f_2 h_2^{f_4} \sqrt{\frac{(57402.91)}{f_6 \times (E_3)}} \quad (5-19)$$

For the previous models, the regression generated number value for f_1 , f_2 are listed in the TABLE 5-37. TABLE 5-37 illustrates the correction factors for the cases I, II

and III. The last column has the R^2 values which show these values work very well for the model.

TABLE 5-37 The Correction Factors for the Cases 1, 2 and 3

| Case | f_1 | f_2 | $R^2\%$ |
|------|-------|-------|---------|
| I | 0.93 | 0.81 | 99.27 |
| II | 3.37 | 4.45 | 98.79 |
| III | 1.26 | 1.85 | 99.27 |

The regression number value for $f_1, f_2, f_3, f_4, f_5, f_6$ with case IV differ due to the estimated initial value which is used in STATISTICA. For this reason, there are many options that will fit the model. Additionally the f_i values obtained are certainly a function of the initial “seed” values in the analysis. A trial and error method was used in the STATISTICA program until acceptable and stable values were achieved. TABLE 5-38 illustrates the correction factors for the case IV. The last column has the values R^2 which show these values work very well for the model. The last option was used for the model in case IV.

TABLE 5-38 The Correction Factors for the Case IV

| Trial Numbers | Start Value | f_1 | f_2 | f_3 | f_4 | f_5 | f_6 | R^2 |
|---------------|-------------|-------|-------|-------|-------|-------|-------|-------|
| 1 | 1 | 2.37 | 0.78 | 3.14 | 3.25 | 17.13 | 0.74 | 99.33 |
| 2 | 10 | 4.07 | 0.19 | 3.14 | 3.25 | 94.00 | 0.01 | 99.33 |
| 3 | 5 | 1.16 | 1.10 | 3.14 | 3.25 | 1.83 | 2.28 | 99.33 |
| 4 | 4 | 0.54 | 0.85 | 3.14 | 3.25 | 0.17 | 0.99 | 99.33 |
| 5 | 3 | 1.15 | 0.76 | 3.14 | 3.25 | 1.78 | 0.68 | 99.33 |
| 6 | 3.5 | 1.11 | 1.05 | 3.14 | 3.25 | 1.58 | 2.00 | 99.33 |
| 7 | 3.8 | 0.72 | 0.80 | 3.14 | 3.25 | 0.40 | 0.81 | 99.33 |
| 8 | 3.85 | 0.81 | 0.83 | 3.14 | 3.25 | 0.60 | 0.91 | 99.33 |
| 9 | 3.855 | 0.82 | 0.82 | 3.14 | 3.25 | 0.61 | 0.88 | 99.33 |
| 10 | 3.856 | 0.70 | 0.79 | 3.14 | 3.25 | 0.38 | 0.77 | 99.33 |
| 11 | 3.84 | 0.88 | 0.86 | 3.14 | 3.25 | 0.78 | 1.05 | 99.33 |
| 12 | 3.844 | 0.93 | 0.86 | 3.14 | 3.25 | 0.91 | 1.04 | 99.33 |
| 13 | 3.8447 | 0.95 | 0.86 | 3.14 | 3.25 | 0.96 | 1.04 | 99.33 |
| 14 | 3.84475 | 0.95 | 0.86 | 3.14 | 3.25 | 0.97 | 1.05 | 99.33 |

From the previous tables, the models for the four cases that were determined from the statistical analysis were as follows:

- Case I:

The first case, the equation has the following formula

$$h_{eT} = 0.93 * h_1 \sqrt[3]{\frac{(E_1(1-\mu_3^2))}{(E_3(1-\mu_1^2))}} + 0.81 * h_2 \sqrt[3]{\frac{(E_2(1-\mu_3^2))}{(E_3(1-\mu_2^2))}} \quad (5-20)$$

$$f_1 = 0.93; f_2 = 0.81$$

- Case II:

The second case, the equation is the following formula

$$h_{eT} = h_1 \sqrt[3.37]{\frac{(E_1(1-\mu_3^2))}{(E_3(1-\mu_1^2))}} + h_2 \sqrt[4.45]{\frac{(E_2(1-\mu_3^2))}{(E_3(1-\mu_2^2))}} \quad (5-21)$$

$$f_1 = 3.37; f_2 = 4.45$$

- Case III:

The third case, the formula equation could be clarified as follows

$$h_{eT} = h_1 \sqrt[3]{\frac{(E_1(1-\mu_3^2))}{(1.26 * E_3(1-\mu_1^2))}} + h_2 \sqrt[3]{\frac{(E_2(1-\mu_3^2))}{(1.85 * E_3(1-\mu_2^2))}} \quad (5-22)$$

$$f_1 = 1.26; f_2 = 1.85$$

- Case IV:

For the latter case, would impose the existence of all correction factors:

$$h_{eT} = 0.95 * h_1 \sqrt[3.14]{\frac{(E_1(1-\mu_3^2))}{(0.97 * E_3(1-\mu_1^2))}} + 0.86 * h_2 \sqrt[3.25]{\frac{(E_2(1-\mu_3^2))}{(1.05 * E_3(1-\mu_2^2))}} \quad (5-23)$$

$$f_1 = 0.95; f_2 = 0.86; f_3 = 3.14; f_4 = 3.25; f_5 = 0.97; f_6 = 1.05$$

TABLE 5-38 illustrates the h_{eT} measured and predicted value for each of the four cases; while Figures 5-38 through 5-41 show h_{eT} measured and predicted value for the four cases analyzed. It is noted from the R^2 values and plots that all the models work very well to estimate the equivalent thickness.

TABLE 5-39 h_{eT} Measured and predicted Value for Four Cases

| N _Q | h ₁ | h ₂ | E ₃ | h _{eT} JULEA | heT predicted -Case NO | | | |
|----------------|----------------|----------------|----------------|--------------------------|------------------------|-------|-------|-------|
| | | | | | 1 | 2 | 3 | 4 |
| 1 | 4 | 15 | 5639 | 31.87 | 35.73 | 34.39 | 35.84 | 35.25 |
| 2 | 4 | 15 | 9698 | 27.39 | 29.82 | 30.14 | 29.91 | 29.79 |
| 3 | 4 | 15 | 13693 | 25.15 | 26.58 | 27.71 | 26.66 | 26.76 |
| 4 | 4 | 15 | 18988 | 23.07 | 23.84 | 25.60 | 23.91 | 24.18 |
| 5 | 4 | 30 | 5639 | 58.52 | 62.06 | 59.66 | 62.32 | 61.20 |
| 6 | 4 | 30 | 9698 | 49.11 | 51.80 | 52.51 | 52.01 | 51.75 |
| 7 | 4 | 30 | 13693 | 45.40 | 46.17 | 48.41 | 46.36 | 46.51 |
| 8 | 4 | 30 | 18988 | 41.45 | 41.41 | 44.83 | 41.58 | 42.04 |
| 9 | 8 | 15 | 5639 | 42.52 | 45.13 | 43.52 | 45.19 | 44.55 |
| 10 | 8 | 15 | 9698 | 36.32 | 37.66 | 37.91 | 37.72 | 37.61 |
| 11 | 8 | 15 | 13693 | 33.15 | 33.57 | 34.73 | 33.62 | 33.77 |
| 12 | 8 | 15 | 18988 | 30.16 | 30.11 | 31.96 | 30.15 | 30.50 |
| 13 | 8 | 30 | 5639 | 69.03 | 71.46 | 68.79 | 71.67 | 70.50 |
| 14 | 8 | 30 | 9698 | 57.66 | 59.64 | 60.28 | 59.82 | 59.58 |
| 15 | 8 | 30 | 13693 | 53.08 | 53.16 | 55.43 | 53.32 | 53.52 |
| 16 | 8 | 30 | 18988 | 48.19 | 47.68 | 51.20 | 47.82 | 48.36 |
| 17 | 12 | 15 | 5639 | 51.49 | 54.52 | 52.65 | 54.55 | 53.85 |
| 18 | 12 | 15 | 9698 | 43.89 | 45.51 | 45.68 | 45.53 | 45.44 |
| 19 | 12 | 15 | 13693 | 39.94 | 40.56 | 41.74 | 40.58 | 40.78 |
| 20 | 12 | 15 | 18988 | 36.19 | 36.38 | 38.33 | 36.39 | 36.81 |
| 21 | 12 | 30 | 5639 | 78.59 | 80.86 | 77.91 | 81.03 | 79.80 |
| 22 | 12 | 30 | 9698 | 65.49 | 67.49 | 68.05 | 67.63 | 67.40 |
| 23 | 12 | 30 | 13693 | 60.11 | 60.16 | 62.44 | 60.28 | 60.54 |
| 24 | 12 | 30 | 18988 | 54.41 | 53.94 | 57.56 | 54.06 | 54.67 |
| 25 | 4 | 15 | 5639 | 35.15 | 35.73 | 34.39 | 35.84 | 35.25 |

| N _Q | h ₁ | h ₂ | E ₃ | h _{eT} JULEA | heT predicted -Case NO | | | |
|----------------|----------------|----------------|----------------|--------------------------|------------------------|-------|-------|-------|
| | | | | | 1 | 2 | 3 | 4 |
| 49 | 4 | 15 | 5639 | 33.52 | 35.73 | 34.39 | 35.84 | 35.25 |
| 50 | 4 | 15 | 9698 | 28.78 | 29.82 | 30.14 | 29.91 | 29.79 |
| 51 | 4 | 15 | 13693 | 26.38 | 26.58 | 27.71 | 26.66 | 26.76 |
| 52 | 4 | 15 | 18988 | 23.94 | 23.84 | 25.60 | 23.91 | 24.18 |
| 53 | 4 | 30 | 5639 | 58.92 | 62.06 | 59.66 | 62.32 | 61.20 |
| 54 | 4 | 30 | 9698 | 49.07 | 51.80 | 52.51 | 52.01 | 51.75 |
| 55 | 4 | 30 | 13693 | 45.04 | 46.17 | 48.41 | 46.36 | 46.51 |
| 56 | 4 | 30 | 18988 | 41.96 | 41.41 | 44.83 | 41.58 | 42.04 |
| 57 | 8 | 15 | 5639 | 43.34 | 45.13 | 43.52 | 45.19 | 44.55 |
| 58 | 8 | 15 | 9698 | 37.04 | 37.66 | 37.91 | 37.72 | 37.61 |
| 59 | 8 | 15 | 13693 | 33.80 | 33.57 | 34.73 | 33.62 | 33.77 |
| 60 | 8 | 15 | 18988 | 30.53 | 30.11 | 31.96 | 30.15 | 30.50 |
| 61 | 8 | 30 | 5639 | 68.96 | 71.46 | 68.79 | 71.67 | 70.50 |
| 62 | 8 | 30 | 9698 | 57.19 | 59.64 | 60.28 | 59.82 | 59.58 |
| 63 | 8 | 30 | 13693 | 52.28 | 53.16 | 55.43 | 53.32 | 53.52 |
| 64 | 8 | 30 | 18988 | 48.50 | 47.68 | 51.20 | 47.82 | 48.36 |
| 65 | 12 | 15 | 5639 | 51.89 | 54.52 | 52.65 | 54.55 | 53.85 |
| 66 | 12 | 15 | 9698 | 44.29 | 45.51 | 45.68 | 45.53 | 45.44 |
| 67 | 12 | 15 | 13693 | 40.36 | 40.56 | 41.74 | 40.58 | 40.78 |
| 68 | 12 | 15 | 18988 | 36.39 | 36.38 | 38.33 | 36.39 | 36.81 |
| 69 | 12 | 30 | 5639 | 78.18 | 80.86 | 77.91 | 81.03 | 79.80 |
| 70 | 12 | 30 | 9698 | 64.70 | 67.49 | 68.05 | 67.63 | 67.40 |
| 71 | 12 | 30 | 13693 | 59.05 | 60.16 | 62.44 | 60.28 | 60.54 |
| 72 | 12 | 30 | 18988 | 54.61 | 53.94 | 57.56 | 54.06 | 54.67 |
| 73 | 4 | 15 | 5639 | 38.04 | 35.73 | 34.39 | 35.84 | 35.25 |

| N _Q | h ₁ | h ₂ | E ₃ | h _{eT} JULEA | heT predicted -Case NQ | | | |
|----------------|----------------|----------------|----------------|--------------------------|------------------------|-------|-------|-------|
| | | | | | 1 | 2 | 3 | 4 |
| 26 | 4 | 15 | 9698 | 29.19 | 29.82 | 30.14 | 29.91 | 29.79 |
| 27 | 4 | 15 | 13693 | 26.58 | 26.58 | 27.71 | 26.66 | 26.76 |
| 28 | 4 | 15 | 18988 | 23.87 | 23.84 | 25.60 | 23.91 | 24.18 |
| 29 | 4 | 30 | 5639 | 63.55 | 62.06 | 59.66 | 62.32 | 61.20 |
| 30 | 4 | 30 | 9698 | 54.03 | 51.80 | 52.51 | 52.01 | 51.75 |
| 31 | 4 | 30 | 13693 | 48.26 | 46.17 | 48.41 | 46.36 | 46.51 |
| 32 | 4 | 30 | 18988 | 41.77 | 41.41 | 44.83 | 41.58 | 42.04 |
| 33 | 8 | 15 | 5639 | 45.65 | 45.13 | 43.52 | 45.19 | 44.55 |
| 34 | 8 | 15 | 9698 | 38.02 | 37.66 | 37.91 | 37.72 | 37.61 |
| 35 | 8 | 15 | 13693 | 34.50 | 33.57 | 34.73 | 33.62 | 33.77 |
| 36 | 8 | 15 | 18988 | 30.91 | 30.11 | 31.96 | 30.15 | 30.50 |
| 37 | 8 | 30 | 5639 | 73.93 | 71.46 | 68.79 | 71.67 | 70.50 |
| 38 | 8 | 30 | 9698 | 62.51 | 59.64 | 60.28 | 59.82 | 59.58 |
| 39 | 8 | 30 | 13693 | 55.92 | 53.16 | 55.43 | 53.32 | 53.52 |
| 40 | 8 | 30 | 18988 | 48.52 | 47.68 | 51.20 | 47.82 | 48.36 |
| 41 | 12 | 15 | 5639 | 54.53 | 54.52 | 52.65 | 54.55 | 53.85 |
| 42 | 12 | 15 | 9698 | 45.50 | 45.51 | 45.68 | 45.53 | 45.44 |
| 43 | 12 | 15 | 13693 | 41.21 | 40.56 | 41.74 | 40.58 | 40.78 |
| 44 | 12 | 15 | 18988 | 36.88 | 36.38 | 38.33 | 36.39 | 36.81 |
| 45 | 12 | 30 | 5639 | 83.47 | 80.86 | 77.91 | 81.03 | 79.80 |
| 46 | 12 | 30 | 9698 | 70.34 | 67.49 | 68.05 | 67.63 | 67.40 |
| 47 | 12 | 30 | 13693 | 62.97 | 60.16 | 62.44 | 60.28 | 60.54 |
| 48 | 12 | 30 | 18988 | 54.76 | 53.94 | 57.56 | 54.06 | 54.67 |

| N _Q | h ₁ | h ₂ | E ₃ | h _{eT} JULEA | heT predicted -Case NQ | | | |
|----------------|----------------|----------------|----------------|--------------------------|------------------------|-------|-------|-------|
| | | | | | 1 | 2 | 3 | 4 |
| 74 | 4 | 15 | 9698 | 31.57 | 29.82 | 30.14 | 29.91 | 29.79 |
| 75 | 4 | 15 | 13693 | 27.77 | 26.58 | 27.71 | 26.66 | 26.76 |
| 76 | 4 | 15 | 18988 | 25.21 | 23.84 | 25.60 | 23.91 | 24.18 |
| 77 | 4 | 30 | 5639 | 63.88 | 62.06 | 59.66 | 62.32 | 61.20 |
| 78 | 4 | 30 | 9698 | 53.68 | 51.80 | 52.51 | 52.01 | 51.75 |
| 79 | 4 | 30 | 13693 | 48.31 | 46.17 | 48.41 | 46.36 | 46.51 |
| 80 | 4 | 30 | 18988 | 43.37 | 41.41 | 44.83 | 41.58 | 42.04 |
| 81 | 8 | 15 | 5639 | 47.61 | 45.13 | 43.52 | 45.19 | 44.55 |
| 82 | 8 | 15 | 9698 | 39.60 | 37.66 | 37.91 | 37.72 | 37.61 |
| 83 | 8 | 15 | 13693 | 34.83 | 33.57 | 34.73 | 33.62 | 33.77 |
| 84 | 8 | 15 | 18988 | 31.61 | 30.11 | 31.96 | 30.15 | 30.50 |
| 85 | 8 | 30 | 5639 | 73.65 | 71.46 | 68.79 | 71.67 | 70.50 |
| 86 | 8 | 30 | 9698 | 61.91 | 59.64 | 60.28 | 59.82 | 59.58 |
| 87 | 8 | 30 | 13693 | 55.66 | 53.16 | 55.43 | 53.32 | 53.52 |
| 88 | 8 | 30 | 18988 | 49.82 | 47.68 | 51.20 | 47.82 | 48.36 |
| 89 | 12 | 15 | 5639 | 56.10 | 54.52 | 52.65 | 54.55 | 53.85 |
| 90 | 12 | 15 | 9698 | 46.75 | 45.51 | 45.68 | 45.53 | 45.44 |
| 91 | 12 | 15 | 13693 | 41.16 | 40.56 | 41.74 | 40.58 | 40.78 |
| 92 | 12 | 15 | 18988 | 37.38 | 36.38 | 38.33 | 36.39 | 36.81 |
| 93 | 12 | 30 | 5639 | 82.73 | 80.86 | 77.91 | 81.03 | 79.80 |
| 94 | 12 | 30 | 9698 | 69.62 | 67.49 | 68.05 | 67.63 | 67.40 |
| 95 | 12 | 30 | 13693 | 62.56 | 60.16 | 62.44 | 60.28 | 60.54 |
| 96 | 12 | 30 | 18988 | 55.88 | 53.94 | 57.56 | 54.06 | 54.67 |

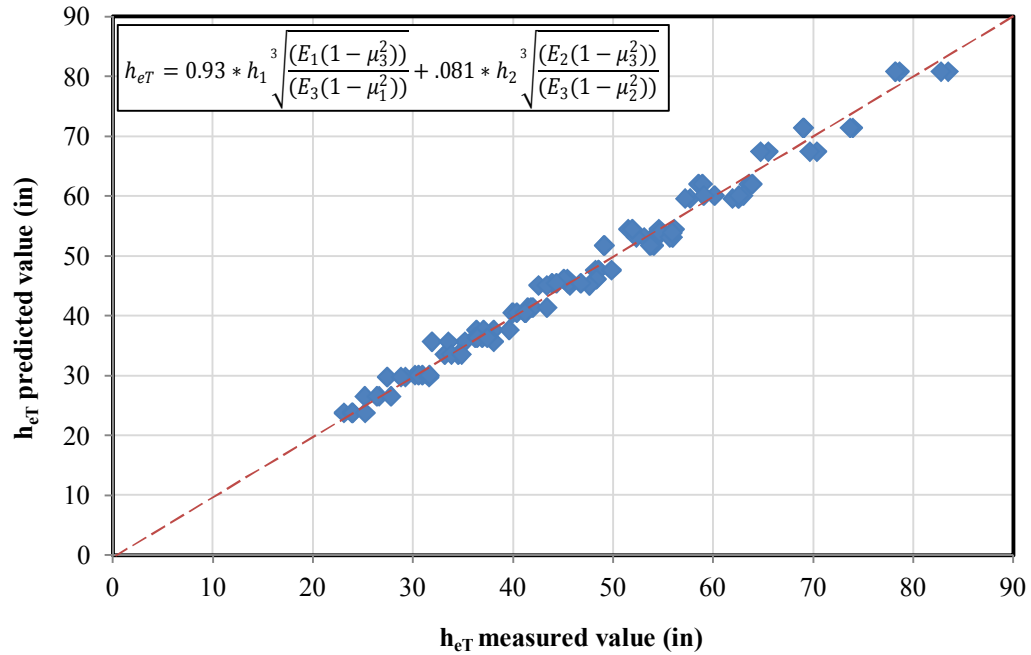


FIGURE 5-36 h_{eT} measured and predicted value for case I.

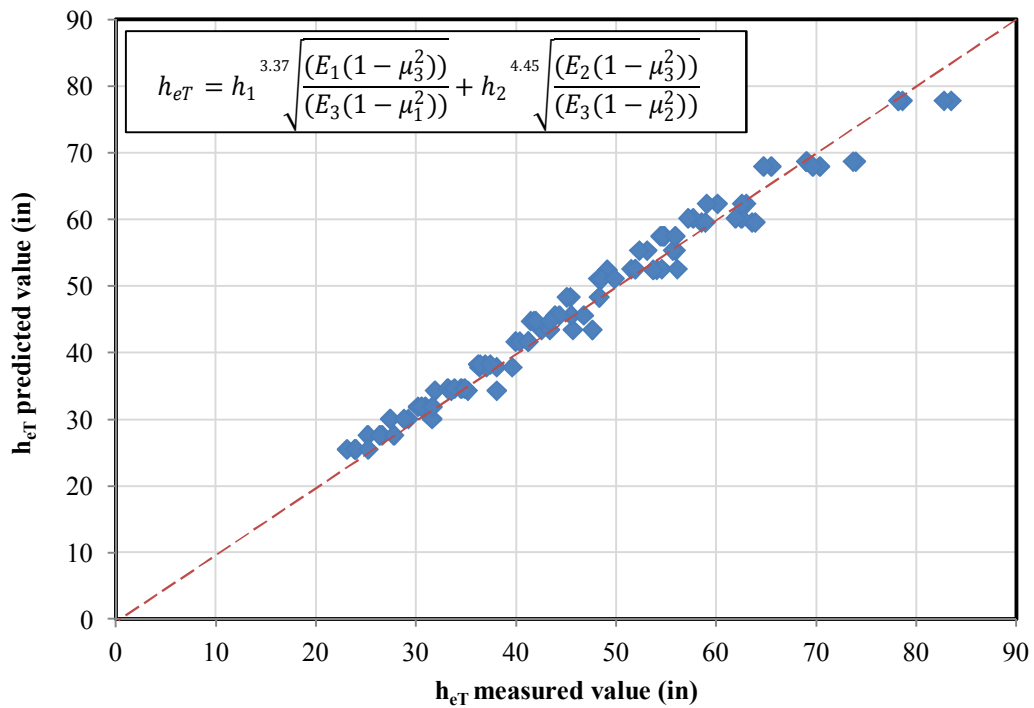


FIGURE 5-37 h_{eT} measured and predicted value for case II.

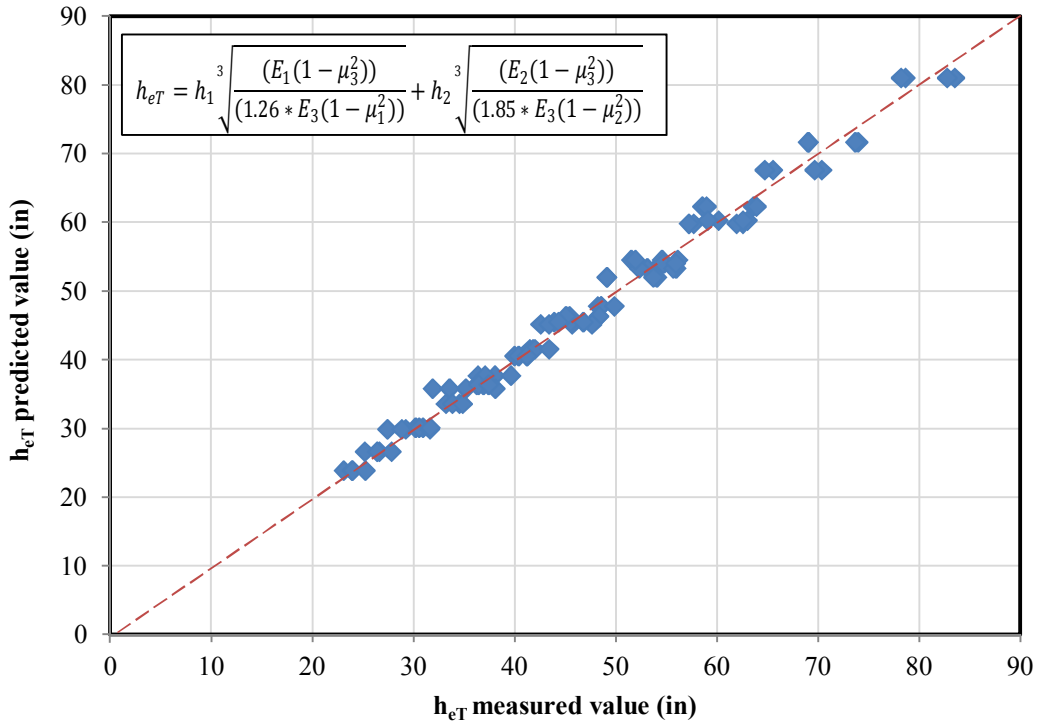


FIGURE 5-38 h_{eT} measured and predicted value for case III.

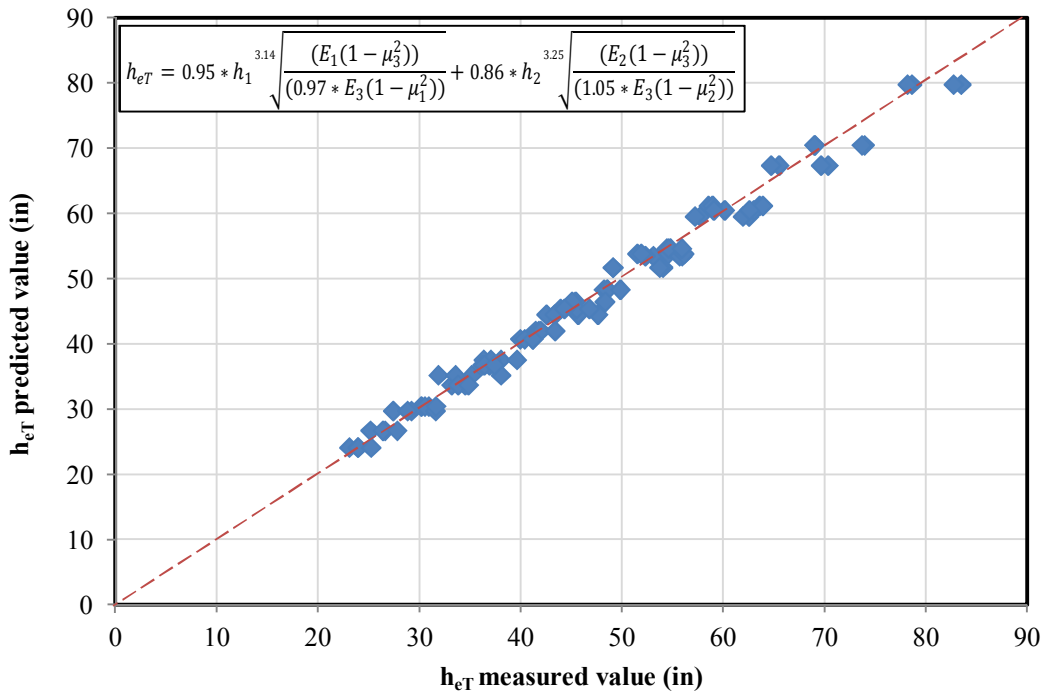


FIGURE 5-39 h_{eT} measured and predicted value for case IV.

5.4 Conclusion

This chapter has focused upon the question regarding the relative accuracy associated with the ZAPRAM stress and strain predictions compared to those obtained from the more precise MLET solutions. The study clearly showed that the Odemark Transformed Section Analysis in ZAPRAM provided stress and strain predictions that differed between MLET predictions. In general, differences in vertical stress prediction were low to moderate; differences in the vertical strain significant and differences in horizontal stress very different. It is apparent the reason for poor agreement in vertical strain is really heavily dependent upon difference generated in the σ_x and σ_y horizontal stresses.

An analysis clearly indicated that some type of empirical correction factor for each layer (f_1 , f_2) was necessary to enhance the relative agreement between the predicted stress and strains. A comprehensive set of studies involving a variety of wheel loads/types; (load-pressure); pavement structures (layer thickness, Moduli and Poisson's Ratio) along with a range of subgrade support values were conducted.

Using statistical least square error techniques (and other forms of analysis); it was concluded that the most optimum set of correction factors to be used with the equivalent thickness equation of Odemark were near average values of:

$$f_1 = 0.95 \text{ and } f_2 = 0.80$$

Accordingly, a set of correction factors of $f_1 = 0.95$ and $f_2 = 0.8$ have been used as the default set within ZAPRAM. It is also apparent that future work needs to be conducted to attempt to "fine tune" these values even more fully.

CHAPTER 6 COMPARISON OF AIRFIELD FLEXIBLE PAVEMENT DESIGN THICKNESS BASED UPON DIFFERING AGENCY LIMITING SUBGRADE STRAIN CRITERIA

6.1 Introduction

In this chapter, estimated design pavement life is assessed using three agency rutting failure criteria (based upon limiting subgrade strain criteria) for airfield design. The design criteria used were the Asphalt Institute, Shell Oil, and the revised USA Corps of Engineers rutting failure criteria. A study was conducted using the newly developed mechanistically based airfield HMA pavement design procedure described in this report. The performance of the pavement is calculated in terms of critical strains based on multilayer theory. A sub-base thickness is determined, using each design criterion, for all combination of pavements investigated to resist future traffic considering the total damage in the pavement from rutting. The main features of the analysis approach used include determination of design inputs, modeling of the pavement response, and establishment of the failure criteria.

6.2 Objective

The main objective of this investigation was to provide a comparison of flexible airfield pavement design thicknesses that are derived from three widely accepted design procedures used in practice today throughout the world. These three design procedures are: the Asphalt Institute, Shell Oil Co. and a new revised USACE-WES procedure. The focus of this chapter looks at the design thickness requirements for shear deformation (rutting distress) for an array of aircraft types, design traffic levels, and sub-grade types. This study is accomplished through the ZAPRAM computer code.

6.3 Experimental Factorial

As previously stated in the objectives of this study, a comparison between the three different permanent deformation criteria was performed upon a set of factorial variables in order to assess what, if any, final pavement thickness differences exists between these three major airfield pavement design agencies. The complete factorial of input parameters that were utilized for the analysis is as follows.

The total experimental factorial resulted in 162 computational runs. The variables used were:

- Three different permanent deformation (limiting sub-grade strain) criteria: Shell Oil, the Asphalt Institute and the Revised USACE- β approach.
- Three design levels of sub-grade modulus: A-4 (20,000 psi); A-6 (10,000 psi) and A-7-6 (5,000 psi).
- Three different design aircraft types: Boeing 737-600 (MGTOw = 145 kips); Airbus A300-C4 (MGTOw = 366 kips) and Boeing 747-400 (MGTOw = 856 kips).
- Three levels of design life number of aircraft passes: N_p (100,000; 1,000,000 and 10,000,000)
- Two levels of asphalt concrete thickness: $h_1=6"$ and $h_1=10"$
- One level of lateral aircraft traffic wander was used to simulate a taxiway condition (3.5 ft)

It should be recognized that the seasonal/annual environmental effects; upon unbound layers, are not considered within this study. Thus, moduli at equilibrium conditions for the unbound materials were assumed to be equal to the moduli at optimum

conditions. Also, no influence of the ground water table was considered. The influence of these environmental effects is described in the next chapter (Chapter 7).

TABLE 6-1 illustrates the range of input parameters used for the pavement structures evaluated. A very important fact in the design process is that the modulus of the surface AC layer is a specific function of the specific design agency criteria investigated. Thus, for example, if the Asphalt Institute criteria is used, an Effective Modulus of the AC layers equal to 100 psi must be used the Multilayer approach.

TABLE 6-1 Pavement Structure and Input Data

| Layer Number | 1 | 2 | 3 | 4 |
|-----------------------|---|------------|----------------|---------------------------|
| Material Type | Asphalt | Gran. Base | Gran. Sub-base | Sub-grade |
| Thickness (in) | 6 and 10 | 12 | Variable | Infinite |
| Poisson Ratio | 0.35 | 0.4 | 0.45 | 0.45 |
| Elastic Modulus (psi) | USACE: 300,000 Shell: 150,000 AI: 100,000 | 38,000 | 32,000 | 20,000 10,000 5,000 |
| AASHTO Class | -- | A-1-b | A-2-4 | A-4 A-6 A-7-6 |

In order to simplify the quantitative difference in both the design criteria and the varying factors upon the overall pavement design; either an increase or decrease of the sub-base thickness was used to define the agency differences. For purposes of simplicity, the thickness of the granular base was kept constant at 12", for each run. The surface AC layer thickness was evaluated at both 6 and 10 inches to assess its influence upon the overall design thickness. For each single simulation, the thickness of the granular sub-base was varied until a damage factor of 100% was achieved.

6.4 Results and Analysis

The final results of the 162 design simulations from ZAPRAM are summarized in TABLE 6-2. Also shown in this table are the population statistics (mean, standard deviation and coefficient of variation (CV%)) for each Combination ID. Thus the variability (standard deviation and CV%) parameters reflects the variability of the final pavement design thicknesses (sub-base designs) due to the three major design procedures investigated. A discussion of this variability is presented in the latter part of this chapter.

TABLE 6-2 Design Pavement Structure Required (Granular Base Thickness: 12 inches)

| ID | Aircraft | E _{SG} (psi) | N _f | Thickness of Sub-base (in) | | | | | | | | | | | | |
|----|----------------|--------------------------|-------------------|----------------------------|-----|-----------|-----|-----------|-----|---------|-----|-----------|-----|-----------|-----|---|
| | | | | Shell | | Asphalt | | USACE | | Average | | Standard | | Coeff. of | | |
| | | | | Oil | | Institute | | (Revised) | | | | Deviation | | Var. (%) | | |
| | | | | AC | AC | AC | AC | AC | AC | AC | AC | AC | AC | AC | AC | |
| | | | | 6" | 10" | 6" | 10" | 6" | 10" | 6" | 10" | 6" | 10" | 6" | 10" | |
| 1 | | | 1x10 ⁵ | 2 | 0 | 12 | 6 | 14 | 5 | 9 | 4 | 6 | 3 | 70 | 90 | |
| 2 | | 5 | 1x10 ⁶ | 12 | 5 | 14 | 7 | 18 | 8 | 15 | 7 | 3 | 2 | 20 | 20 | |
| 3 | | | 1x10 ⁷ | 26 | 18 | 15 | 9 | 21 | 11 | 21 | 13 | 6 | 5 | 30 | 40 | |
| 4 | Boeing 737 | | 1x10 ⁵ | 0 | 0 | 5 | 0 | 6 | 0 | 4 | 0 | 3 | 0 | 90 | - | |
| 5 | | 10 | 1x10 ⁶ | 5 | 0 | 6 | 0 | 8 | 0 | 6 | 0 | 2 | 0 | 20 | - | |
| 6 | | | 1x10 ⁷ | 15 | 8 | 7 | 0 | 11 | 1 | 11 | 3 | 4 | 4 | 40 | 15 | |
| 7 | | | 1x10 ⁵ | 0 | 0 | 0 | 0 | 0 | 0 | 0 | 0 | 0 | 0 | 0 | - | - |
| 8 | | 20 | 1x10 ⁶ | 0.5 | 0 | 0.5 | 0 | 1 | 0 | 1 | 0 | 0 | 0 | 40 | - | |
| 9 | | | 1x10 ⁷ | 7 | 1 | 2 | 0 | 3 | 0 | 4 | 0 | 3 | 1 | 70 | 17 | |
| 10 | | | 1x10 ⁵ | 12 | 5 | 28 | 21 | 38 | 28 | 26 | 18 | 13 | 12 | 50 | 70 | |
| 11 | | 5 | 1x10 ⁶ | 38 | 30 | 32 | 25 | 44 | 35 | 38 | 30 | 6 | 5 | 20 | 20 | |
| 12 | | | 1x10 ⁷ | 64 | 56 | 35 | 28 | 49 | 39 | 49 | 41 | 15 | 14 | 30 | 30 | |
| 13 | Airbus A300 | | 1x10 ⁵ | 1 | 0 | 8 | 2 | 12 | 3 | 7 | 2 | 6 | 2 | 80 | 90 | |
| 14 | | 10 | 1x10 ⁶ | 14 | 6 | 10 | 3 | 18 | 8 | 14 | 6 | 4 | 3 | 30 | 40 | |
| 15 | | | 1x10 ⁷ | 39 | 31 | 11 | 5 | 22 | 12 | 24 | 16 | 14 | 13 | 60 | 80 | |
| 16 | | | 1x10 ⁵ | 0 | 0 | 2 | 0 | 2 | 0 | 1 | 0 | 1 | 0 | 90 | - | |
| 17 | | 20 | 1x10 ⁶ | 4 | 0 | 4 | 0 | 5 | 0 | 4 | 0 | 1 | 0 | 10 | - | |
| 18 | | | 1x10 ⁷ | 13 | 7 | 5 | 0 | 7 | 0 | 8 | 2 | 4 | 4 | 50 | 17 | |

| ID | Aircraft | E _{SG} (psi) | N _f | Thickness of Sub-base (in) | | | | | | | | | | | |
|----|---------------|--------------------------|-------------------|----------------------------|-----|-------------------|-----|-----------------|-----|---------|-----|--------------------|-----|--------------------|-----|
| | | | | Shell Oil | | Asphalt Institute | | USACE (Revised) | | Average | | Standard Deviation | | Coeff. of Var. (%) | |
| | | | | AC | | AC | | AC | | AC | | AC | | AC | |
| | | | | 6" | 10" | 6" | 10" | 6" | 10" | 6" | 10" | 6" | 10" | 6" | 10" |
| 19 | | | 1x10 ⁵ | 20 | 12 | 35 | 28 | 46 | 36 | 34 | 25 | 13 | 12 | 40 | 50 |
| 20 | | 5 | 1x10 ⁶ | 49 | 42 | 39 | 32 | 53 | 43 | 47 | 39 | 7 | 6 | 20 | 20 |
| 21 | | | 1x10 ⁷ | 85 | 77 | 42 | 35 | 58 | 49 | 62 | 54 | 22 | 21 | 40 | 40 |
| 22 | Boeing 747 | | 1x10 ⁵ | 5 | 0 | 11 | 4 | 16 | 6 | 11 | 3 | 6 | 3 | 50 | 90 |
| 23 | | 10 | 1x10 ⁶ | 19 | 11 | 13 | 6 | 21 | 12 | 18 | 10 | 4 | 3 | 20 | 30 |
| 24 | | | 1x10 ⁷ | 53 | 45 | 14 | 7 | 29 | 19 | 32 | 24 | 20 | 19 | 60 | 80 |
| 25 | | | 1x10 ⁵ | 1 | 0 | 5 | 0 | 6 | 0 | 4 | 0 | 3 | 0 | 70 | - |
| 26 | | 20 | 1x10 ⁶ | 8 | 0.5 | 6 | 0 | 8 | 0 | 7 | 0 | 1 | 0 | 20 | 17 |
| 27 | | | 1x10 ⁷ | 21 | 13 | 7 | 0 | 10 | 0 | 13 | 4 | 7 | 8 | 60 | 17 |

In TABLE 6-2, every combination of factors for AC layer thicknesses of either 6 or 10 inches have a particular combination identification (ID) number. FIGURE 6-1 illustrates the results of the runs for the pavement structure with a surface AC layer thickness of 6 inches, while FIGURE 6-2 presents the results corresponding to the pavement structure with a surface AC thickness of 10 inches. It should be recalled that in all cases, a constant thickness of 12 inches of granular base has been used.

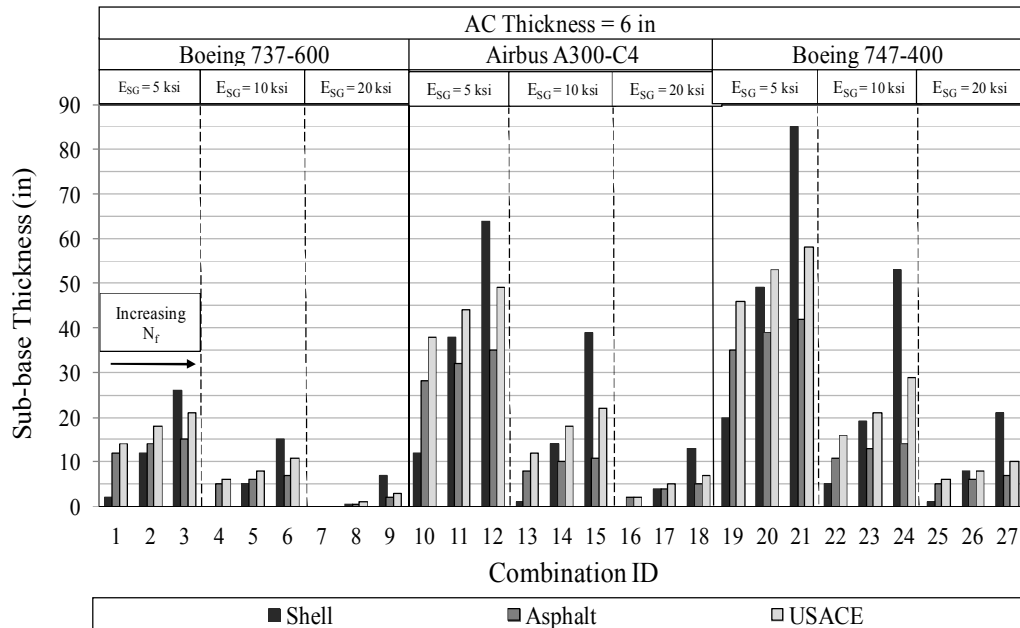


FIGURE 6-1 Design factors influence upon the sub-base thickness considering 6 inches of AC.

6.5 Influence of Design Factors

It should be noted that the number of passes to failure for every single subdivision within 3 combination ID numbers, increases from left to right. For instance in FIGURE 6-1, for an AC thickness of 6 inches, load corresponding to a Boeing 737, and a sub-grade modulus of 5 ksi; combination ID #1 is assigned to the results corresponding to the lowest number of passes to failure (100,000) as can also be seen in TABLE 6-2. On the other hand, combination ID #3 corresponds to the same combinations of factors except for the number of passes to failure. Here the design number of passes is for the maximum level (10,000,000). The same logic applies to every subdivision (with 3 combinations IDs) in all the figures presented for the analysis.

The results of the computer simulations reflect the *expected* influence of the design factors evaluated at different levels on this study. In both Figures FIGURE 6-1

and FIGURE 6-2, regardless of the permanent deformation criterion utilized, it can be seen that all parametric results are obviously correct. As can be observed, all design thicknesses increase with the heavier aircraft, increase with increasing design load repetitions, decrease with higher sub-grade design moduli and decrease as the AC thickness is increased from 6" to 10".

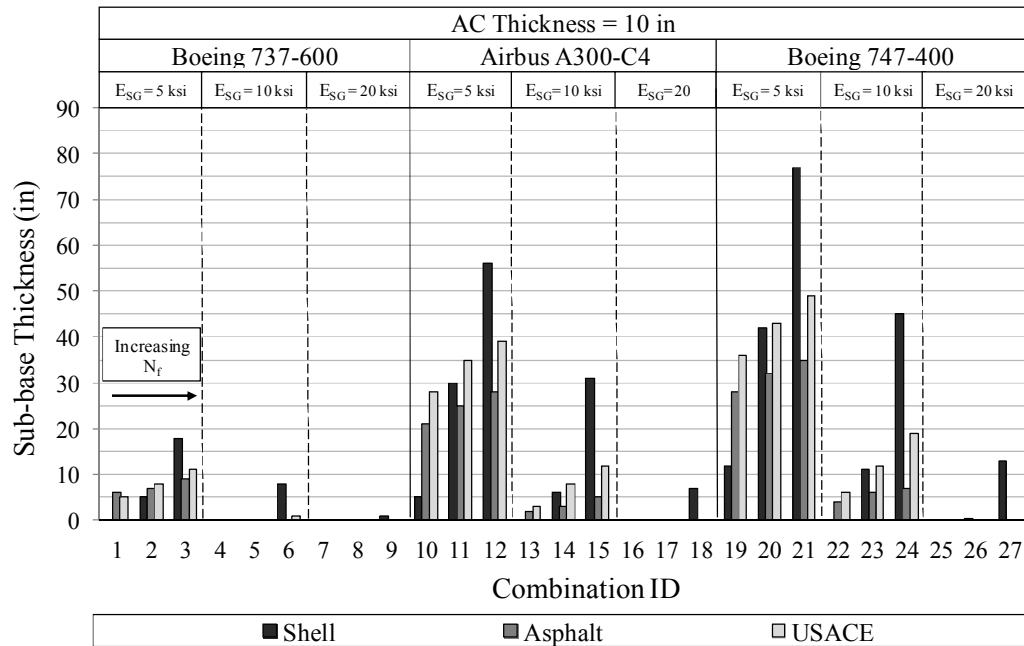


FIGURE 6-2 Design factors influence upon the sub-base thickness considering 10 inches of AC.

Overall, none of the results should be any different as they illustrate the extreme reasonableness of the ZAPRAM pavement design sensitivity solution. However, the most salient conclusions of this study deal with the extreme variability (difference) in pavement design generated for airfield pavement design methodologies currently available in the world today.

6.6 Comparison of Criteria

The three different pavement deformation criteria utilized in this study were compared using the AI criterion as the “reference” thickness. Please note that this assumption does not imply that the Asphalt Institute approach is the final typical design procedure to use or it is the “best” methodology available. In both Figures FIGURE 6-1 and FIGURE 6-2, it can be observed that by using the Shell Oil criterion, the required sub-base thicknesses are always less than the thickness required by the Asphalt Institute and USACE-WES criterion for low (100,000) number of passes to failure. On the other hand, for extremely high (10,000,000) passes to failure; the Shell Oil criterion yielded much larger thickness than the other two criteria. For traffic pass levels near 1,000,000 passes; it can be observed that the Shell Oil criteria yields thicknesses that are generally similar to the AI and USACE-WES criteria (refer to section ID No. 2, 5, 8, 11, 14, 17, 20, 23, 26) of both Figures FIGURE 6-1 and FIGURE 6-2. These conclusions are directly a result of the fact that the relative location of the vertical strain criteria for the Shell Oil approach (which is a linear function) passes through both of the non-linear strain criteria of the AI and USACE-WES criterion near the 1,000,000 repetition traffic level effect. (See FIGURE 3-17).

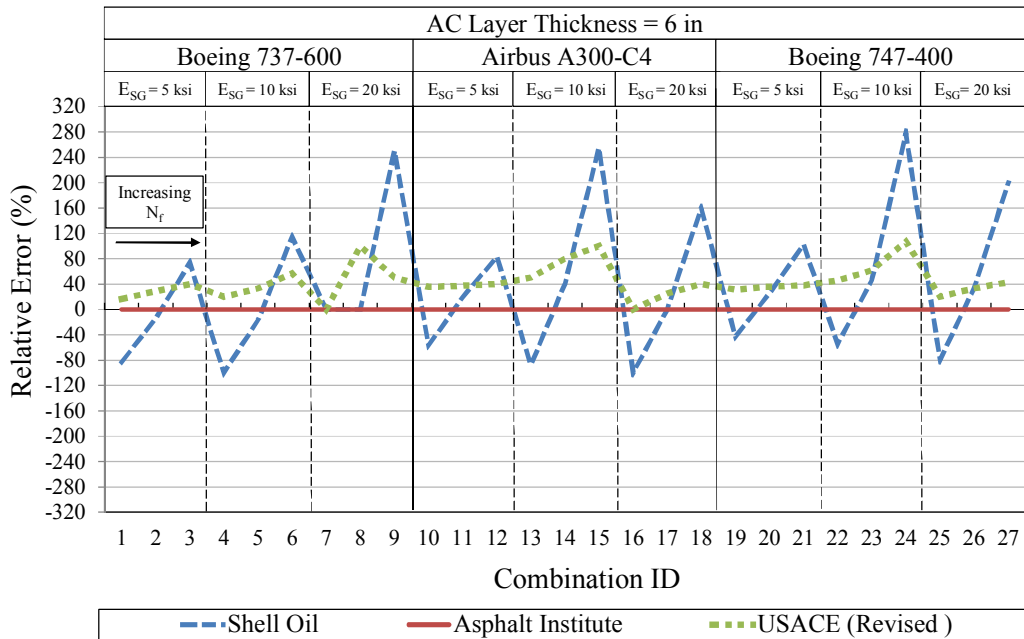


FIGURE 6-3 Difference in design thickness relative to the AI criterion (6 inches of AC).

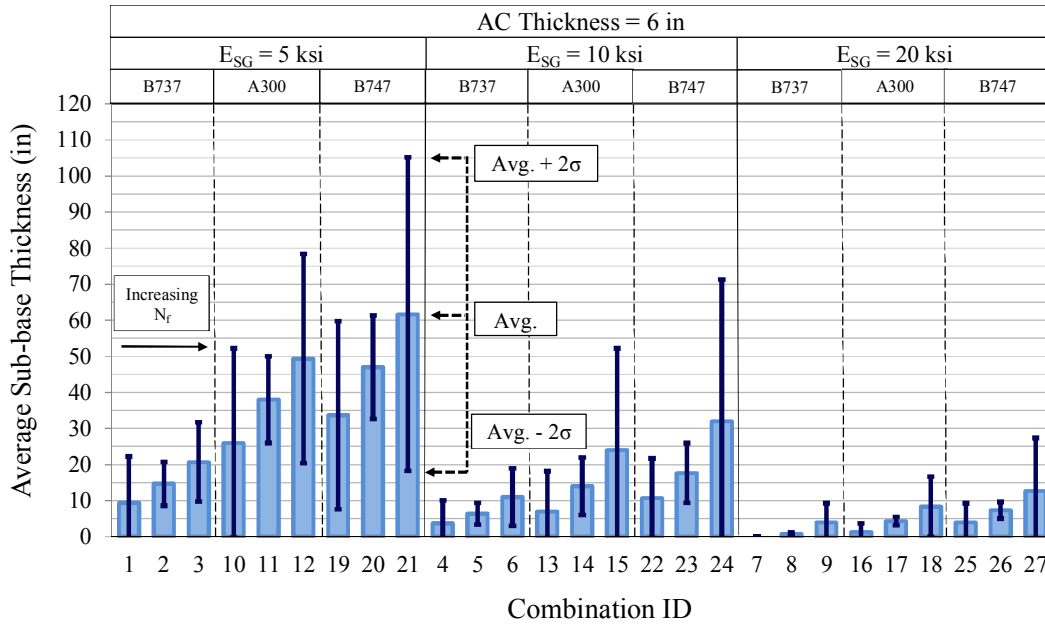
It can also be observed from FIGURE 6-1 and FIGURE 6-2 that the design thickness difference between the AI and USACE-WES approach are moderate across all variables investigated (aircraft type, design pass level, and sub-grade moduli). That this is true can also be explained by the relative proximity and shape of the limiting strain curves for these two criteria previously shown in FIGURE 3-17. Recalling that the USACE-WES limiting strain criterion has been developed in the 2006-2010 time period; it does truly offer general support to the limiting strain criteria developed by Witczak for the Asphalt Institute nearly 40 years before the latest USACE sub-grade strain criterion.

Finally, FIGURE 6-3 illustrates the same conclusions previously presented, except the plot illustrates the relative difference (%) of the Shell Oil and USACE-WES procedure relative to the AI “reference” criterion. This figure reinforces all of the prior conclusions that have been noted. In addition, the data illustrates that the range in relative

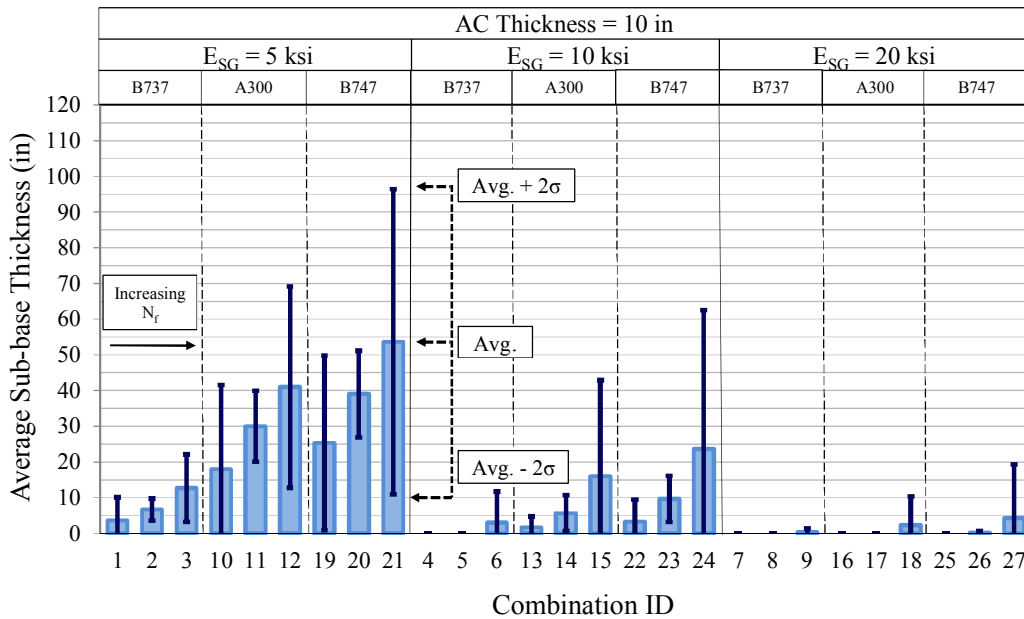
agency design thickness prediction may vary from a low of a -80% difference in thickness to a high difference value of +240% to 280% amongst these major pavement design agencies. This is considered to be a somewhat staggering and surprisingly large range and certainly indicate the lack of an accurate airfield pavement design methodology in the world.

6.7 Statistical Summary of Agency Pavement Design

For each combination ID number identified, the mean value and standard deviation of design thickness (sub-base), associated with the variability (differences) between Design Methods, were computed as a population of the three major design criterion studied in this chapter. These results were previously shown in TABLE 6-2 and are shown graphically in FIGURE 6-4. FIGURE 6-4a represents the plot for the case with a constant thickness of 6.0" of AC being used for the design; while FIGURE 6-4b represents the case when the AC thickness of 10" was kept constant. In these figures, the solid bars are representative of the mean sub-base thickness between all three design procedures and the black line covers a range of +/- 2 times the standard deviation. Thus, the range of the 4σ is approximately equivalent to a 90% Confidence Interval for the design Thickness (expressed by sub-base thickness). Stated in another fashion, if one viewed the sub-base design thickness for a B-747, for a very high traffic level, with a very poor sub-grade (ID #21); one would be 90% certain that the true design sub-base thickness would lie between 18" and 105". Again, this clearly shows the extreme discrepancy in final design thicknesses when varied between major agency design methodologies.



(a)



(b)

FIGURE 6-4 Statistical Summary of Agency Pavement Design (a) with 6 inches of AC, (b) with 10 inches of AC.

It is apparent that the differences associated between the design methods is very significant and certainly is indicative of the lack of having an accurate technological state

of the art for flexible airfield pavement design. These differences are maximized as the aircraft type becomes heavier, design traffic levels increase and the main foundation support is decreased.

Using the results of the variability shown in TABLE 6-2, “typical” +/- 2S limits, representative of the differences shown between the design methods investigated are shown in FIGURE 6-5. The plot illustrates the sensitivity of the two most significant considerations (Sub-grade Support and Aircraft Type). When applied to designs of B-737 type aircraft, the impact of the design method is not extremely significant. However, as the design sub-grade support decreases, the design thickness may approach +/- 10” of granular sub-base material. As observed, the sensitivity of the 366 kip A-300 is increased from the lighter 145 kip B-737. In general, as medium to low strength sub-grades are encountered; the +/- 2S thickness differences are observed to be in the order of magnitude of 12" to 24".

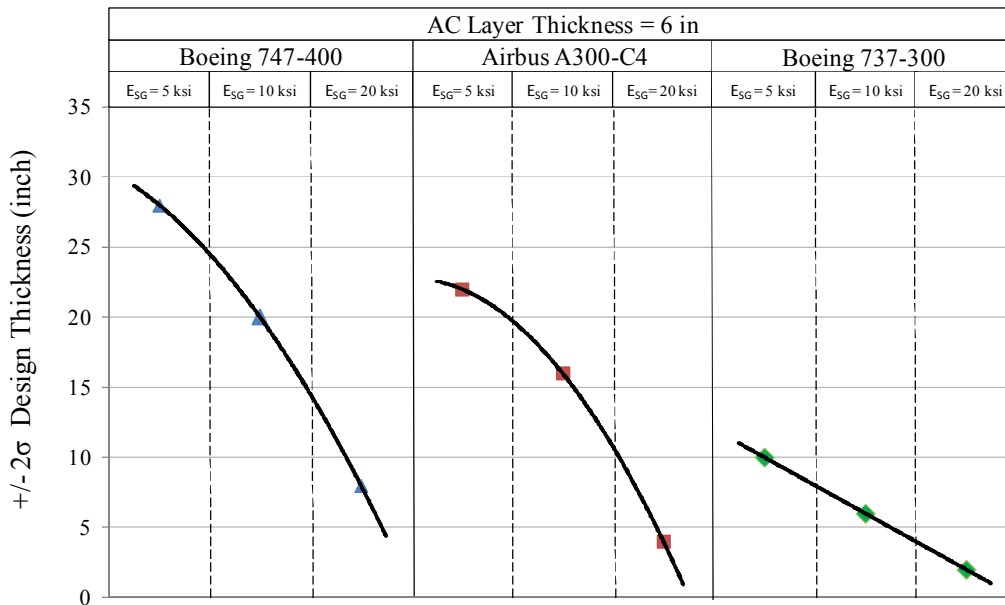


FIGURE 6-5 Typical design thickness $\pm 2 S$ error associated between design methods.

The impact of the design pavement thickness differences, by design method, take on a very significant impact as the operation of very heavy aircraft is considered. While the heavy aircraft considered in this study was the 856 kip B-747; it also needs to also be kept in perspective that the latest A-380 operational aircraft are in the order of magnitude of 1.2 million pounds. The +/- 2S values for the B-747, shown in FIGURE 6-5, are seen to approach values near 30" for weak sub-grades and 10" to 15" for relatively strong sub-grades. It is critically apparent that, even with several of the most widely used flexible pavement design procedures in practice today, there is a very large discrepancy in the final predicted design thicknesses determined from each of these approaches.

6.8 Conclusions

This chapter presents a new, but powerful theoretical pavement design computer code that is based upon mechanistic-empirical utilization of the concept of limiting strain criteria for the design of airfield flexible pavements. This program (ZAPRAM) was used to compare the flexible thickness design requirements for three widely acceptable airfield pavement design methodologies used in practice today: Shell Oil; The Asphalt Institute (MS-11) and the newly revised USACE-Beta procedure. The results of the comparative design study showed that there is a significant difference between the three widely used airfield pavement design procedures used in the study. Differences between the Asphalt Institute and the new USACE procedure were relatively moderate for all design situations. However, the greatest deviation was found between the Shell Oil approach and the other two criteria.

The comparison study, based upon a matrix of aircraft types/loads; sub-grade support values and design pass levels, leads to the clear conclusion that there is a significant difference in design thickness requirements between the different Design

Methods in use today. These design thickness differences are magnified as the gross aircraft weight is increased and the sub-grade support becomes weaker. Pavement design differences, between methods, (as denoted by the +/- 2S-90% variable) may be as large as 30" to 36" for heavy aircraft on weak sub-grades. Thus if a true design thickness requirement is 60", the "true" design thickness may range between 30" and 90". In contrast, if one is concerned with the influence for lighter (B-737) aircraft, this +/- 2S value may only be 5" or less for moderate to strong sub-grades.

The magnitude of these differences observed between design procedures is felt to be rather large, surprising and perhaps indicative of the lack of an advanced airfield pavement design technology in the airfield pavement design community. While pavement design procedures for the US highway industry have dramatically improved over the last two decades primarily due to a massive influx of research and development support; there has been no comparable increase of technological development on the airfield side. Finally, it should be called to the reader's attention that all three of the "Airfield Pavement Design Methods" that are utilized in this study represent the "latest" design technology available. However, it should be realized that all of these Design Procedures are based upon the "Limiting Strain Criteria" mechanistic technology that is well over 40 years old.

CHAPTER 7 IMPACT OF ENVIRONMENTAL SITE LOCATION AND GROUNDWATER TABLE DEPTH ON THE THICKNESS OF FLEXIBLE AIRFIELD PAVEMENTS

7.1 Introduction

Historically, the majority of structural designs for highway and airfield pavements have been developed on the simplifying assumption that sooner or later, in the pavement lifespan, all unbound material layers may be exposed to saturated conditions. In essence, the use of this assumption negates the real possibility that true saturation will never be the "norm" in a wide variety of environmental locations and groundwater table (GWT) conditions. This is true as hotter, arid locations are encountered with deep water tables. Another reason for the simplifying assumption is the fact that the area of unsaturated soil mechanics, coupled with the site environmental properties, is not yet well understood by most of the practicing community.

However, in the last decade, very significant advances in the area of unsaturated soil mechanics and the ability to model damage as a direct result of the environmental effects and groundwater table location have been made in the pavement design community. The first comprehensive subsystem to incorporate these environmental elements into the pavement design process were developed as a part of the new AASHTO Mechanistic Empirical Pavement Design Guide (MEPDG) developed under NCHRP projects 1-37A and 1-40D. These efforts were intended to predict/simulate the changes in behavior and material response in all unbound materials in conjunction with environmental conditions over years of operation.

Arizona State University (ASU) has played a significant role for the inclusions and implementation of the Enhanced Integrated Climatic Model (EICM) into the

MEPDG since 1999. From the 2006 period, a series of continuously enhanced, educational computer codes have been developed at ASU, under the overview of Dr. Claudia Zapata. The initial software, called ZAPMEDACA, incorporated unsaturated soil mechanics principles and environmental effects technology directly into structural pavement design software codes developed for flexible airfield pavements. The latest addition to the series of "ZAP" codes is called ZAPRAM and is the primary objectives of this research thesis. This code is an Excel-based software, that primarily focuses upon flexible airfield pavements and, most importantly, the incorporation of the real time effects of site environmental conditions and groundwater table depth upon airfield pavement performance. To the author's knowledge, this is the first program of its type that has been developed. The program is capable of running several different environmental scenarios to examine the sensitivity of these factors on the pavement response.

This chapter presents a comprehensive sensitivity study of the ZAPRAM computer code that incorporates the influence of environmental site factors and the groundwater table depth upon flexible airfield pavement design and performance. ZAPRAM program is a mechanistically based pavement model based upon Limiting Strain Criteria. The study, described in this paper, used the newly revised USACE failure criteria for subgrade shear deformation. The experimental factorial conducted was comprised of three different aircraft types; three different levels of as-compacted (optimum) subgrade support, two levels of design aircraft passes, an environmental combination of six groundwater table depths and five environmentally different city locations. The methodology used in this study utilized the same analytical methodology to achieve real time environmental effects upon unbound layer modulus, as the system used in the new AASHTO MEPDG.

7.2 Objective

The major objective of this investigation was to provide a quantitative assessment of the potential differences in pavement design thickness that may be caused by the specific environmental site properties (moisture -temperature) and the groundwater table depth. As previously noted, these factors are normally not considered at all in pavement design methodology. This study specifically focuses upon the prediction of pavement designs to guard against excessive shear deformations (rutting). While ZAPRAM is capable of analyzing performance for a wide variety of mechanistic design approaches, the study is based upon only performance predicted by the new revised USACE- β limiting strain criteria. The analysis is provided for a series of aircraft types, subgrade support values, a factorial matrix of geographic locations across the US, and a range of GWT depths.

7.3 Background of Environmental Effects

The concept of the environmental effects utilized in ZAPRAM has been based upon the fundamental concepts used in the MEPDG and developed under NCHRP 1-40D and NCHRP 1-37A. These technical reports define the fundamental methodology by which the Enhanced Integrated Climatic Model (EICM) module was developed by ASU researchers to predict real time variation in moisture content (degree of saturation) for all unbound pavement layers due to environmental conditions and soil properties.

A brief explanation of the most important steps and variables used to estimate the environmental effects for unsaturated soils has already been presented in Chapter 2. For a given in-situ condition and time, an environmental factor is computed and used to adjust the resilient modulus of the unbound material to real time conditions. The models, input and output parameters used in the EICM are presented below.

7.4 Experimental Matrix

In order to investigate the sensitivity of the matrix of environmental conditions upon the final design thickness of the airfield pavement; the ZAPRAM software program was run for five different climate conditions, three different soils, six groundwater table depths, two levels of design traffic, and three aircraft types. FIGURE 7-1 presents the experimental factorial of the study along with a U.S. map showing the environmental locations that were used in the study.

7.4.1 Design Loads

The design aircraft types selected for the study were the: Boeing 737-600 (145-kip MGTOW), the Airbus A300-C4 (366-kip MGTOW) and the Boeing 747-400 (856-kip MGTOW) aircraft. These aircraft have a wide range of gross weights, number and main gear types along with individual tire loads and tire contact pressures.

7.4.2 Number of Passes

The number of passes to failure at the end of the design life was selected to be 100,000 and 1,000,000 passes.

7.4.3 Subgrade Soil

A wide range of *initial* subgrade support properties was used in this study. Three levels of soil were introduced to the program to simulate a weak, medium and strong subgrade. Initial resilient modulus of 5, 10, and 20 ksi, corresponding to AASHTO classifications A-7-6, A-6 and A-4, respectively, were used in this study. The mean soil property values gathered from the National Resources Conservation Service database were selected for their characterization. It is extremely important to realize that these input Mr values only

represent the anticipated modulus at optimum field compaction conditions. With time and directly dependent upon the Environmental site properties and location of the GWT, these moduli are changed to reflect the long term equilibrium condition that would be reached at each environmental location and groundwater table condition.

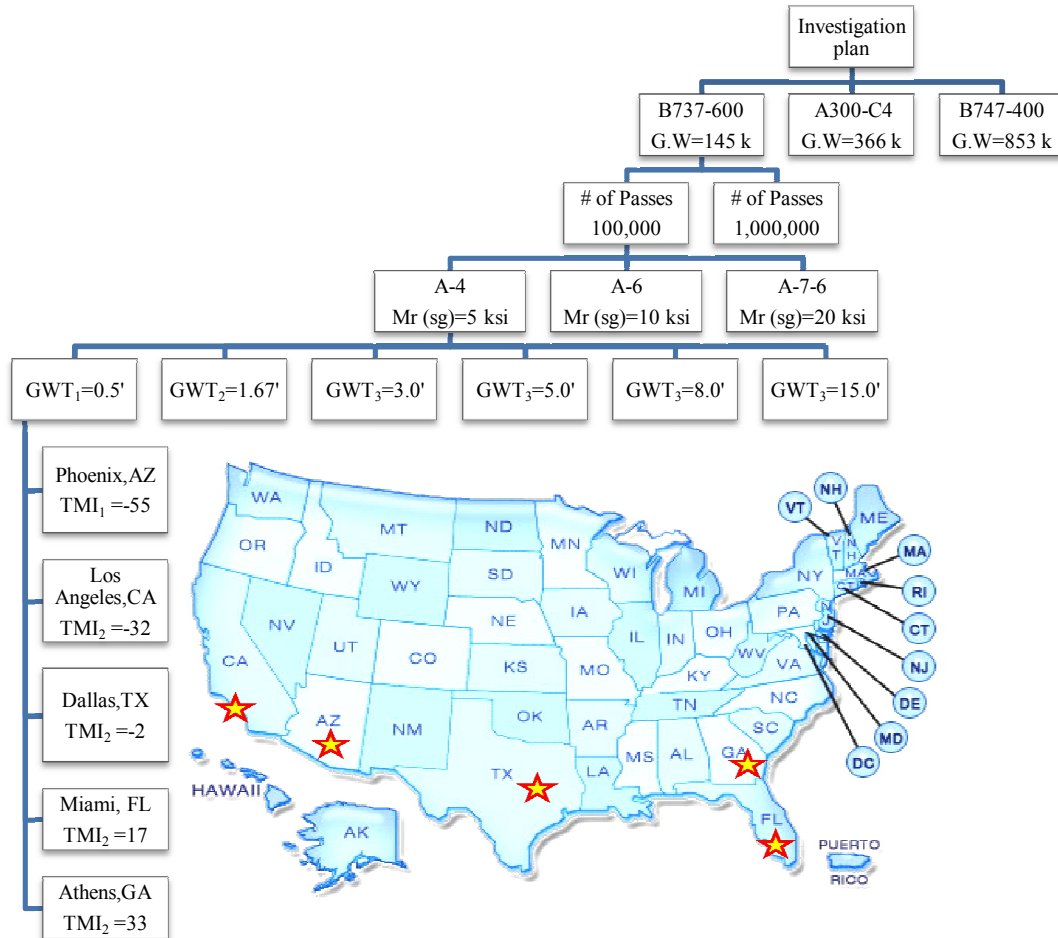


FIGURE 7-1 Investigation plan.

7.4.4 Groundwater Levels

Six different water level conditions were used for the research study. For the first water level condition, the water table was placed directly at the interface of the 6" thick AC

layer and granular base. Thus all unbound layers were considered fully saturated. For the second water level condition, the water level was at the base-subbase interface. This depth was taken to be 20 inches below the surface layer. The next three water level conditions were 3, 5, and 8 feet below the pavement surface. The groundwater table depth range used provided the capability to assess design conditions to reflect subgrade moduli both at unsaturated and saturated conditions. Finally, the last GWT depth used was 15 ft. This depth was an assumed boundary condition to reflect a structure that had no appreciable impact of the GWT upon the subgrade moduli. Thus, only the environmental effect of the site TMI environmental location would influence the final equilibrium modulus reached by the soil subgrade.

7.4.5 City Location

Five cities were selected in the no- frost region of the U.S. It should be noted that a range of TMI values was selected to simulate hot dry arid regions (negative TMI) to warm, humid areas that have high precipitation. The cities chosen were Phoenix, Los Angeles, Dallas, Miami, and Athens (Georgia).

TABLE 7-1 Input Parameters Used for the Pavement Structure

| Layer Number | 1 | 2 | 3 | 4 | | |
|---|---------|---------------|------------------|----------|--------|-------|
| Material Type | Asphalt | Granular Base | Granular Subbase | Subgrade | | |
| Thickness (in) | 6.0 | 14.0 | Variable | Infinite | | |
| Poisson Ratio, ν | 0.35 | 0.40 | 0.45 | 0.45 | | |
| Elastic Modulus (psi), | 300,000 | 38,000 | 32,000 | 20,000 | 10,000 | 5,000 |
| AASHTO Classification | -- | A-1-b | A-2-4 | A-4 | A-6 | A-7-6 |
| Passing #200, % | -- | 17 | 22 | 60 | 70 | 80 |
| Plasticity Index, PI | -- | 1.5 | 4 | 6 | 14 | 28 |
| Specific Gravity, G_s | -- | 2.65 | 2.68 | 2.68 | 2.69 | 2.68 |
| Optimum Moisture Content, w_{opt} % | -- | 8 | 14 | 12 | 15 | 20 |
| Maximum Dry Density, $\gamma_{d max}$ (pcf) | -- | 130 | 115 | 119 | 114 | 102 |

7.5 Pavement Structure

In this analysis; a four layer pavement system was used. The pavement layer parameters are shown in TABLE 7-1. The modulus of the surface AC layer used was the effective critical modulus, as defined by the specific limiting strain criteria used. For the USACE criteria, an effective modulus of 300,000 psi must be used according to the requirements of the permanent deformation criteria considered for this study. Also, it should be noted that the elastic modulus of the sub-grade related to 3 different soil types shown in Table 7-1.

The influence of the GWT and the geographic location upon the overall geometric design was captured by either an increase or decrease of the sub-base thickness. In this study, the thickness of the granular base and surface AC layer were kept constant for every run. For every single simulation, the thickness of the granular subbase was varied until the cumulative damage at the end of the design life was equal to 100%.

7.6 Subgrade Soil Modulus Variations

The impact of the environmental location, through the TMI , suction, soil water characteristic curve and degree of saturation directly leads to the expected equilibrium in-situ value of the partly saturated subgrade moduli (above the groundwater table). All subgrade materials below the groundwater table are obviously modeled as saturated. In the environmental analysis using the EICM - TMI approach; TABLE 7-2 is a summary of the in-situ subgrade moduli that were generated for the conditions of the analysis used in the study. The first column displays the initial optimum in-situ compacted modulus for each of the three subgrades investigated. Using the environmental analysis developed in ZAPRAM, the estimated fully saturated (soaked) M_R value is shown in the second column. These values represent the M_R values that would exist below the GWT for each

of the three subgrades investigated. The remaining columns identify the equilibrium condition of the partly saturated subgrade modulus that would be reached for each of the 5 cities (TMI value). Also shown is the equilibrium degree of saturation that would be expected in the design life of the pavement. For example, if one would consider the Phoenix location for an A-7-6 material subgrade; an existing as compacted modulus value would be in the 5000 (5161 psi) range. If this material were to ever become saturated, it is estimated that the M_R would decline to a value of 2073 psi. However, in a climatic location such as Phoenix, the hot, arid climate would probably result in long term equilibrium of over 16,000 psi. In contrast, the exact same soil would have as an estimate of the equilibrium moduli in a very warm, humid and rainy environmental condition such as Athens (GA), of 2400 psi. It should be noticed that the soil is approaching a near saturated condition in this instance.

Finally, FIGURE 7-2 is a representative plot of the various subgrade moduli that were used in this study. Clearly, it can be observed from either the table and/or figure that the impact of the environmental conditions at the site is critically important in selecting the eventual subgrade M_R that will be used in the study.

TABLE 7-2 Environmental Stages of the Subgrade M_R Values

| M_R opt (psi) | M_R Sat (psi) | M_R for Unsaturated Soil Conditions | | | | | | | | | |
|-----------------------|-----------------------|---------------------------------------|----------------|--------------|----------------|--------------|----------------|--------------|----------------|--------------|----------------|
| | | Athens | | Miami | | Dallas | | L.A. | | Phoenix | |
| | | S_f (%) | M_R (psi) | S_f (%) | M_R (psi) | S_f (%) | M_R (psi) | S_f (%) | M_R (psi) | S_f (%) | M_R (psi) |
| 5161 | 2073 | 97.2 | 2424 | 96.2 | 2575 | 93.6 | 2984 | 82.4 | 5593 | 60.4 | 16261 |
| 10046 | 4788 | 96.4 | 5834 | 95.5 | 6111 | 93.6 | 6763 | 86.1 | 10046 | 69.4 | 22174 |
| 20048 | 7384 | 96.4 | 8799 | 95.6 | 9158 | 93.8 | 10020 | 86.1 | 14544 | 69.0 | 31637 |

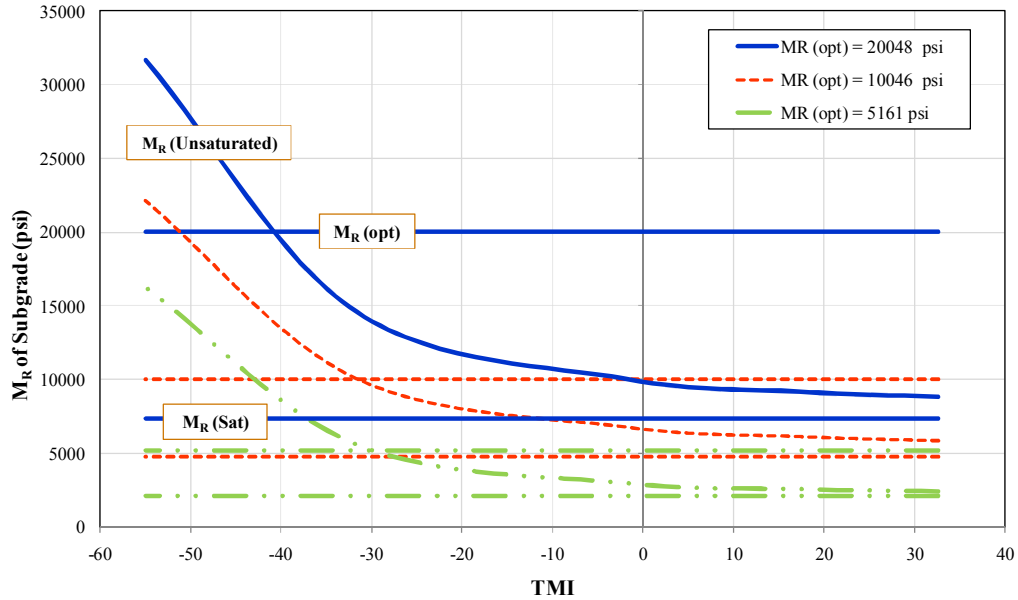


FIGURE 7-2 Subgrade soil modulus variations.

7.7 Results and Analysis

With this background, the full set of ZAPRAM runs was developed to establish the appropriate pavement design thickness requirements for the study. Since a constant AC and Base thickness were used for each combination (done for simplicity in the analysis), the total number of runs were $3*2*3*6*5=540$ runs. However, it should be recalled that several trial and error runs, per simulation, were required to converge to a damage of 100%; the total number of estimated runs for the entire study approached 2000. The experimental factorial results for the total of 540 simulations are summarized TABLE 7-3.

One extremely important point of the analysis must be pointed out and understood by the reader. When modeling the layered system for GWT conditions that result in a partly saturated subgrade below the subbase and above the saturated subgrade sublayer; the limiting strain analysis was always modeled to predict the design subbase thickness for:

Case (a): at the top of the partly saturated subgrade

Case (b): at the top of the saturated subgrade (top of the GWT)

Obviously the thickness of the partly saturated layer will vary directly upon the depth of the GWT within the subgrade layer. This results in the need to have two differing Odemark transformed sections to be analyzed. Case (a) requires the use of the effective transformed section thickness of all layers above the partly saturated subgrade and case (b) uses the transformed section based upon the transformation of all layers above the saturated subgrade.

The final thickness shown in TABLE 7-3 reflects the fact that the largest subbase thickness found between case (a) and case (b) is the final controlling design thickness.

TABLE 7-3 Thickness of Subbase (in) for the Selected Aircraft

| Number of Passes | M _R of Subgrade (psi) | GWT (ft) | Thickness of subbase (in) | | | | | | | | | | | | | | |
|------------------|----------------------------------|----------|---------------------------|-------|--------|------|---------|--------------------------|-------|--------|------|---------|-----------------|-------|--------|------|---------|
| | | | Boeing B737-600 | | | | | AIRBUS INDUSTRIE A300-C4 | | | | | BOEING B747-400 | | | | |
| | | | Athens | Miami | Dallas | L.A. | Phoenix | Athens | Miami | Dallas | L.A. | Phoenix | Athens | Miami | Dallas | L.A. | Phoenix |
| 100,000 | 5 | 0.50 | 29 | 29 | 29 | 29 | 29 | 68 | 68 | 68 | 68 | 68 | 95 | 95 | 95 | 95 | 95 |
| | | 1.67 | 27 | 27 | 26 | 26 | 26 | 66 | 66 | 65 | 65 | 65 | 93 | 93 | 93 | 92 | 92 |
| | | 3.00 | 20 | 19 | 19 | 18 | 17 | 59 | 58 | 58 | 57 | 56 | 86 | 86 | 85 | 84 | 84 |
| | | 5.00 | 17 | 16 | 14 | 8 | 0 | 49 | 48 | 47 | 45 | 43 | 76 | 75 | 74 | 72 | 71 |
| | | 8.00 | 17 | 16 | 14 | 8 | 0 | 43 | 42 | 38 | 24 | 1 | 60 | 58 | 56 | 51 | 36 |
| | 15.00 | 17 | 16 | 14 | 8 | 0 | 43 | 42 | 38 | 24 | 1 | 58 | 54 | 48 | 30 | 4 | |
| | 10 | 0.50 | 16 | 16 | 16 | 16 | 16 | 44 | 44 | 44 | 44 | 44 | 54 | 54 | 54 | 54 | 54 |
| | | 1.67 | 14 | 14 | 14 | 13 | 13 | 43 | 42 | 42 | 42 | 41 | 52 | 52 | 52 | 51 | 51 |
| | | 3.00 | 8 | 7 | 6 | 2 | 1 | 36 | 35 | 35 | 34 | 33 | 45 | 45 | 44 | 43 | 42 |
| | | 5.00 | 8 | 7 | 6 | 2 | 0 | 25 | 23 | 19 | 14 | 1 | 33 | 32 | 29 | 27 | 19 |
| | | 8.00 | 8 | 7 | 6 | 2 | 0 | 25 | 23 | 19 | 7 | 0 | 31 | 29 | 25 | 10 | 1 |
| | | 15.00 | 8 | 7 | 6 | 2 | 0 | 25 | 23 | 19 | 7 | 0 | 31 | 29 | 25 | 10 | 1 |
| | | 0.50 | 10 | 10 | 10 | 10 | 10 | 25 | 25 | 25 | 25 | 25 | 35 | 35 | 35 | 35 | 35 |
| | | 1.67 | 8 | 8 | 7 | 7 | 7 | 23 | 23 | 23 | 22 | 22 | 33 | 32 | 32 | 32 | 31 |
| | | 3.00 | 4 | 3 | 2 | 0 | 0 | 17 | 16 | 15 | 13 | 9 | 26 | 25 | 25 | 24 | 23 |
| 5.00 | | 4 | 3 | 2 | 0 | 0 | 11 | 10 | 8 | 2 | 0 | 14 | 13 | 10 | 5 | 0 | |
| 8.00 | 4 | 3 | 2 | 0 | 0 | 11 | 10 | 8 | 2 | 0 | 14 | 13 | 10 | 5 | 0 | | |
| 15.00 | 4 | 3 | 2 | 0 | 0 | 11 | 10 | 8 | 2 | 0 | 14 | 13 | 10 | 5 | 0 | | |
| 1,000,000 | 5 | 0.50 | 33 | 33 | 33 | 33 | 33 | 74 | 74 | 74 | 74 | 74 | 107 | 107 | 107 | 107 | 107 |
| | | 1.67 | 31 | 31 | 31 | 31 | 30 | 73 | 72 | 72 | 72 | 71 | 105 | 105 | 105 | 104 | 104 |
| | | 3.00 | 24 | 24 | 23 | 23 | 22 | 66 | 65 | 65 | 64 | 63 | 98 | 98 | 97 | 96 | 96 |
| | | 5.00 | 20 | 19 | 17 | 10 | 0 | 55 | 54 | 53 | 52 | 50 | 88 | 87 | 86 | 84 | 83 |
| | | 8.00 | 20 | 19 | 17 | 10 | 0 | 48 | 46 | 43 | 29 | 5 | 72 | 71 | 69 | 65 | 56 |
| | 15.00 | 20 | 19 | 17 | 10 | 0 | 48 | 46 | 43 | 29 | 5 | 65 | 62 | 54 | 35 | 6 | |
| | 10 | 0.50 | 20 | 20 | 20 | 20 | 20 | 51 | 51 | 51 | 51 | 51 | 62 | 62 | 62 | 62 | 62 |
| | | 1.67 | 18 | 18 | 18 | 18 | 17 | 50 | 49 | 49 | 49 | 48 | 60 | 59 | 59 | 59 | 58 |
| | | 3.00 | 11 | 10 | 9 | 7 | 2 | 43 | 42 | 42 | 41 | 40 | 53 | 52 | 52 | 51 | 50 |
| | | 5.00 | 11 | 10 | 9 | 4 | 0 | 30 | 29 | 28 | 24 | 15 | 43 | 42 | 41 | 38 | 35 |
| | | 8.00 | 11 | 10 | 9 | 4 | 0 | 30 | 28 | 25 | 11 | 1 | 36 | 34 | 31 | 14 | 3 |
| | | 15.00 | 11 | 10 | 9 | 4 | 0 | 30 | 28 | 25 | 11 | 1 | 36 | 34 | 31 | 14 | 3 |
| | | 0.50 | 13 | 13 | 13 | 13 | 13 | 34 | 34 | 34 | 34 | 34 | 43 | 43 | 43 | 43 | 43 |
| | | 1.67 | 11 | 11 | 11 | 11 | 10 | 32 | 32 | 32 | 31 | 31 | 42 | 41 | 41 | 41 | 40 |
| | | 3.00 | 7 | 6 | 5 | 1 | 0 | 25 | 25 | 24 | 23 | 23 | 35 | 34 | 34 | 33 | 32 |
| 5.00 | | 7 | 6 | 5 | 1 | 0 | 16 | 14 | 12 | 3 | 0 | 22 | 19 | 15 | 7 | 0 | |
| 8.00 | 7 | 6 | 5 | 1 | 0 | 16 | 14 | 12 | 3 | 0 | 22 | 19 | 15 | 7 | 0 | | |
| 15.00 | 7 | 6 | 5 | 1 | 0 | 16 | 14 | 12 | 3 | 0 | 22 | 19 | 15 | 7 | 0 | | |

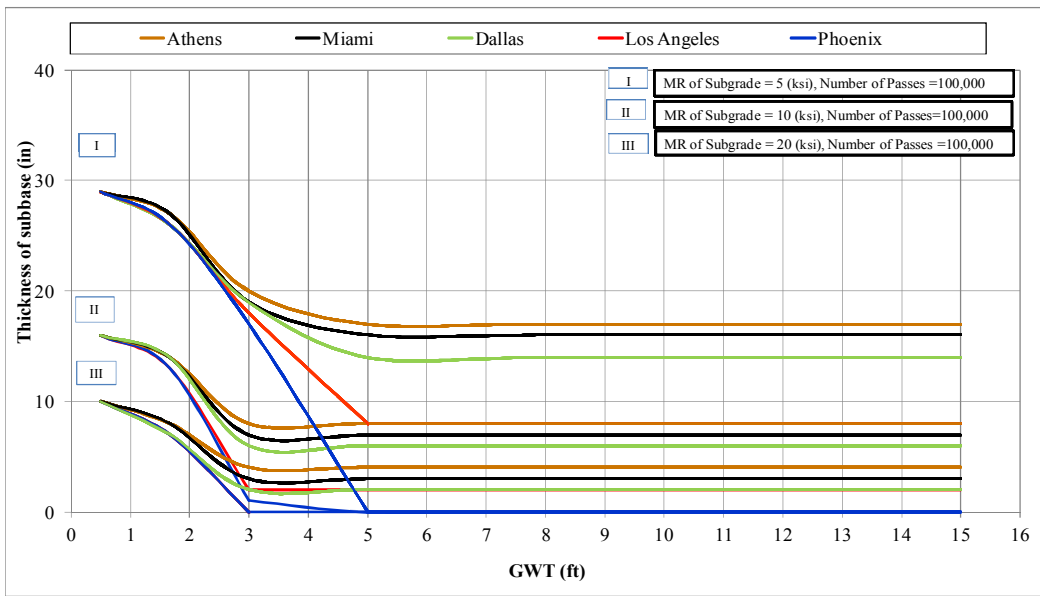
7.8 Discussion of Results

The results shown in TABLE 7-3 are plotted in FIGURE 7-3 to FIGURE 7-5. Each figure presents the results obtained for a particular aircraft type (B-737, A-300 and B-747, respectively). Each figure distinguishes between thickness requirements for 100,000 passes (a) and those for 1,000,000 passes (b). The plots represent the required design thickness of subbase (in reality total pavement thickness), for each of the three initial M_R at optimum compaction condition, as a function of the depth of the GWT from the surface of the pavement surface. As shown in the plot, each line distinguishes the design thickness versus the GWT depth, as a function of the environmental location (TMI Climatic Index) for the 5 cities that have been investigated.

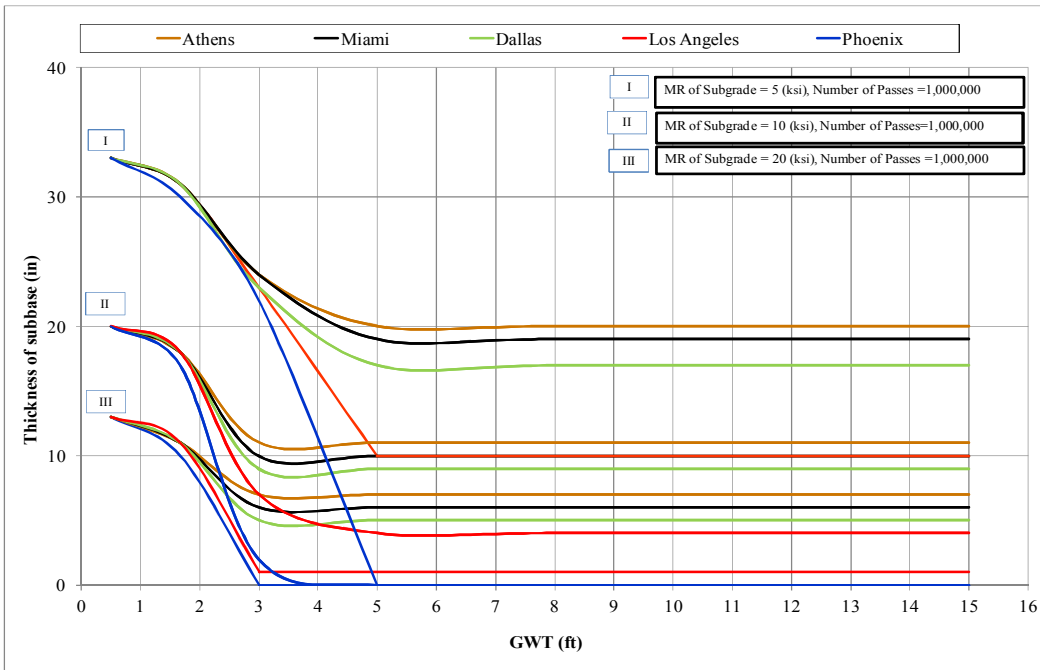
The results shown in these figures provide an initial but powerful look into the significant quantitative impact of the site environmental regime upon pavement thickness and performance. First of all, the figures clearly show the impact of the environmental factors upon the magnitude of the aircraft load (types) and design passes. Nonetheless, it is obvious that the combined effects of the environmental location (as noted by the TMI index and the GWT depth) play a *very significant* influence upon the final design thickness that is generated. As a general observation, for GWT near the pavement surface, the influence of the environmental location is not significant as the in-situ moisture effect is controlled by the higher degree of saturation in the layers caused by the presence of the high GWT. The depths where the GWT overpowers the environmental site TMI factors are generally less than about 1-3 feet for the B-737; 3-5 feet for the A-300 and 4-6 feet for the B-747.

For each figure (aircraft type), it can be observed that the influence of the environmental location plays a very significant influence upon the recommended

pavement thickness, once the GWT becomes deeper in the pavement. Additionally, as one would anticipate, the impact (difference in design thickness) due to the TMI (environmental effect) is greatest for the most plastic materials (A-7-6) and decreases (but is still significant) as the subgrade support becomes stronger.

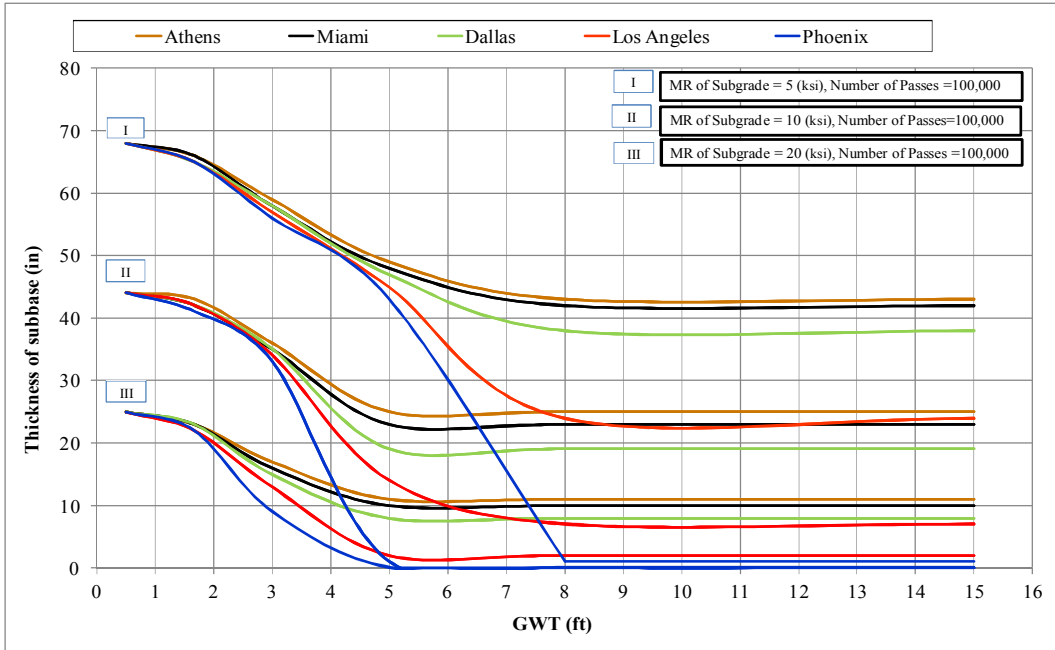


(a)

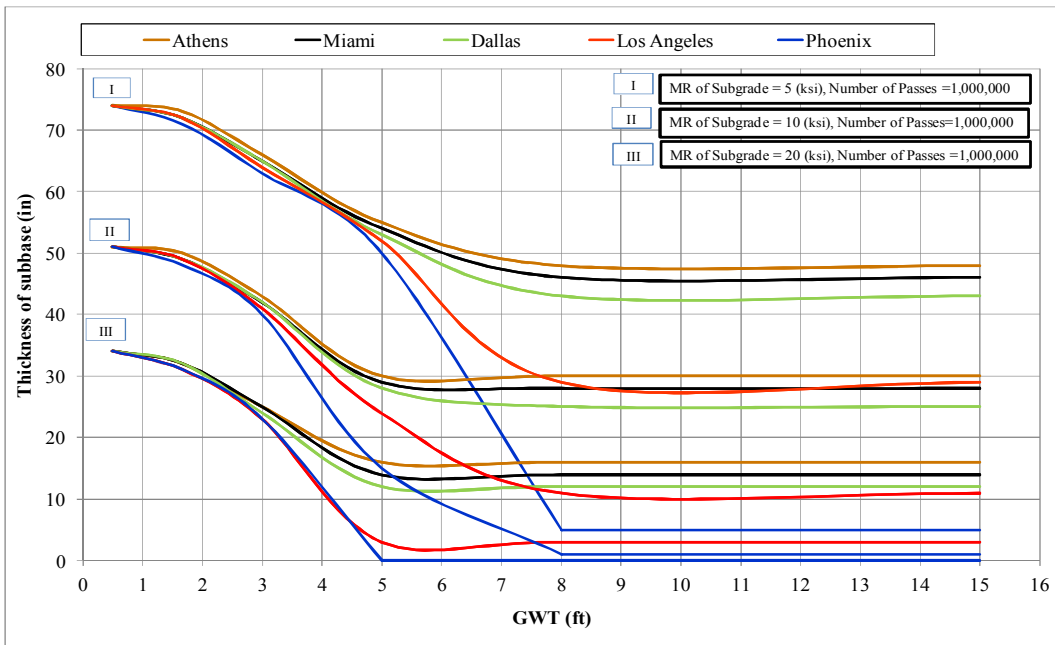


(b)

FIGURE 7-3 Required subbase thickness (in) for Boeing B737-600.

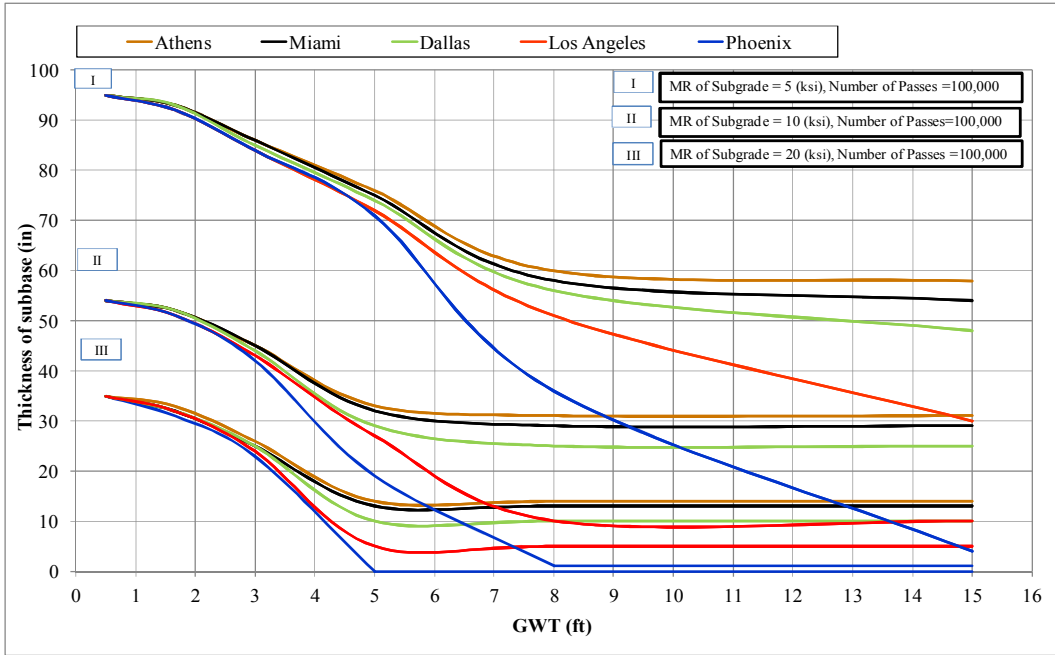


(a)

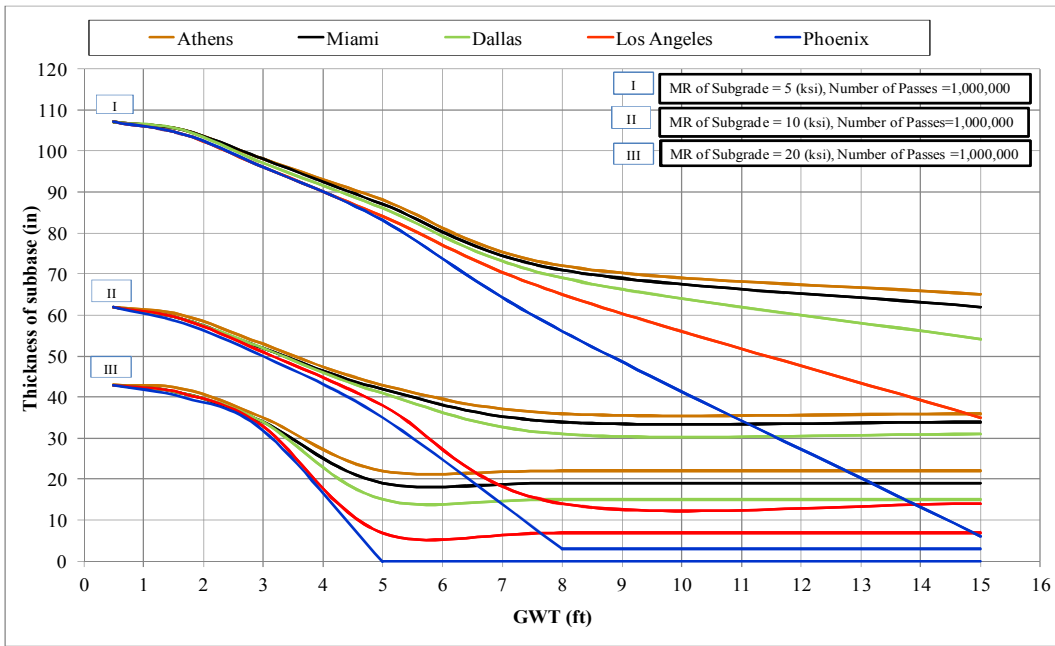


(b)

FIGURE 7-4 Required subbase thickness (in) for airbus INDUSTRIE A300-C4.



(a)



(b)

FIGURE 7-5 Required subbase thickness (in) for Boeing B747-400.

If one examines TABLE 7-3 and computes the associated reduction (savings) in subbase thickness that one obtains to the commonly used thickness generated from saturated design thicknesses (considered as the norm); the savings can be enormous, provided the GWT depth, is greater than 5 to 8 feet below the pavement surface. For the B-737, cost savings equivalent to about 0.5 to 1.0 feet of granular subbase occurs within warm, humid and rainy areas. In the warmer, dry desert areas, the savings in thickness may reach as much as 1 to 2.5 feet of granular subbase material.

Obviously, the potential savings in cost and material is significantly higher for the heavier B-747 aircraft. In the warm, humid and rainy sites; the cost savings can be as large as 2 to 3 feet. In contrast, desert type environments (such a Phoenix); may result in savings of up to 7 to 8 feet in granular subbase.

7.9 Summary and Conclusions

The results of this effort study analysis have shown (it is believed for the first time), the significant quantitative impact of the effects of the climatic conditions at the design site, coupled with the importance of the depth of the groundwater table, on the predicted design thicknesses. Significant cost savings appear to be quite reasonable by introducing and utilizing principles of unsaturated soil mechanics into pavement design practice. This has been clearly demonstrated by the results of the new airfield pavement design procedure found in program ZAPRAM. Also, the results of this study have clearly demonstrated ZAPRAM is a powerful analytical tool that can be effectively utilized to assess the importance of the environment site location (as reflected by its moisture-temperature regime) and the location of the groundwater table within a flexible airfield pavement structure.

The results of this investigation have quantified the very significant effect upon the final design thickness caused by the total environment regime. For GWT locations close to the proximity of the pavement surface; the influence of the in-situ moisture regime of the unbound layers is primarily controlled by the presence of the GWT depth and the influence of the external environment plays little to no effect upon radically changing the degree of saturation in the unbound layers. Typical GWT depths where this phenomenon may occur for B-737 type aircraft are typically 1 to 3 feet from the pavement surface, depending upon the type of subgrade material that may be present. The significant zone of the GWT for heavier aircraft, such as the B-747, may be 4 to 6 feet deep.

However, as the depth of the GWT becomes greater than about 5 to 8 feet from the pavement surface; the effect of the external environment, as measured by the Thornthwaite Moisture Index (TMI) completely takes over the impact of the soil suction and its importance to defining the in-situ partially saturated resilient modulus that may be obtained in-situ. These suctions may significantly increase the resilient modulus of the partially saturated soil (particularly plastic clays) in hot, arid areas having high TMI values approaching -55. This actual subgrade support equilibrium modulus may cause potential savings in equivalent subbase material of up to 2.5 feet for lighter B-737 aircraft to as much as 3 to 8 feet for heavier B-747 aircraft, when design thicknesses are compared to the classical assumption used in most pavement design methods that rely upon fully saturated evaluation of all unbound material layers. It is clear that the time has come to start integrating the principles of unsaturated soil mechanics into airfield pavement design procedures.

CHAPTER 8 SUMMARY AND CONCLUSIONS

8.1 Summary

The structural design of pavements in both highways and airfields is in reality, one of the most complex engineering structures to design. This is, in part, due to the complexities associated with the environmental effect and the ground water table variation. Nonetheless, environmental effects are now a major fundamental component of the new AASHTO Mechanistic-Empirical Pavement Design Guide (MEPDG) developed under the NCHRP Project 1-37A and 1-40D projects. These effects are intended to predict or simulate the changes in behavior and characteristics of pavement and unbound materials in conjunction with environmental conditions over years of operation.

The newly developed code, presented in this report, is called ZAPRAM and is a mechanistically based pavement model based upon Limiting Strain Criteria for airfield HMA pavement design procedures. The program has been implemented in an event-driven, user-friendly educational computer program, which runs in the Excel 2007 environment coupled with visual basic programming. One very important attribute of this new code is that it can be used to analyze airfield designs for partly saturated design locations. As a result, a much better understanding of the environmental effects on the entire pavement structure can be achieved. This program is an important tool that incorporates environmental effects in airfield design for the first time. Also, it helps in the assessment of airfield location by taking into account the regional GWT depth. Furthermore, the program is a great tool to perform sensitivity analysis of the different parameters required for airfield design.

This thesis has evaluated several very important ramifications of the new computer code and its analysis of several significant studies dealing with airfield

pavement design. One of these research tasks focused on the evaluation of the optimal differential areas used in the resolution of vertical stresses and strain calculations used in the numerical integration approach within ZAPRAM. Two different tire imprint shapes may be used in ZAPRAM; circular and elliptical tire imprint shapes. The major objective of this study was to provide some guidance to the user regarding the recommended size and number of the differential point loads to be used to compute stresses/strains. In addition, the minimum threshold number of computational points for the user to use at a specific depth within the pavement system has also been developed.

Another investigation has been completed to establish the most accurate set of correction factors for the Odemark transformed thickness equation. In the Pavement Structure module, the program also allows the user to input a correction factor for the transformed thickness equation. Default correction factors are included in the code and have been determined from a comprehensive comparative study between Odemark's Transformed Section analysis (coupled with the numerical integration of Boussinesq stress/strain equations) to the most accurate codes used in MLET (Multi Layered Elastic Theory).

As part of this thesis, a study was also conducted to provide a comparison of flexible airfield pavement design thicknesses that were derived from three widely accepted subgrade shear (rutting) design procedures used in practice today throughout the world. The study utilized the Asphalt Institute, Shell Oil, and the revised Corps of Engineering rutting failure criteria to calculate the thickness requirements necessary for a range of design input variables. The results of the comparative design study showed that there is a significant difference between the three widely used airfield pavement design procedures used in the study. Differences between the Asphalt Institute and the new USACE procedure were relatively moderate for all design situations. However, the

greatest deviation was found between the Shell Oil approach and the other two criteria. It is recommended that a major effort be initiated to enhance the state of the art for airfield pavement design models.

This report also presents a comprehensive sensitivity study of ZAPRAM concerning the influence of environmental site factors and the groundwater table depth upon flexible airfield pavement design and performance. The completed study used the newly revised USACE failure criteria for subgrade shear deformation. The experimental factorial conducted was comprised of three different aircraft types; three different levels of as-compacted (optimum) subgrade support, two levels of design aircraft passes, an environmental combination of six groundwater table depths and five environmentally different city locations. The methodology used in this study utilized the same analytical methodology to achieve real time environmental effects upon unbound layer modulus, used in the new AASHTO MEPDG. The results of this effort showed, for the first time, the quantitative impact of the significant effects of the climatic conditions at the design site, coupled with the importance of the depth of the groundwater table, on the predicted design thicknesses. Significant cost savings appear to be quite reasonable by utilizing principles of unsaturated soil mechanics into the new airfield pavement design procedure found in program ZAPRAM.

8.2 Conclusions

Based upon this study, the following specific conclusions have been found:

8.2.1 *Evaluation of Optimal Differential Areas in Numerical Integration Process*

- The larger the number of computational dA values selected for the pavement response predictions; the time required to run the program will be increased in direct proportion to the elements used.
- After a certain number of dA values; the pavement response value becomes stable. At this point, further increases in the number of areas (dA) in the segment will not improve the precision.
- For both stress and strain calculations, the accuracy of the program increases as the number of computational points increases, at any depth.
- For both stress and strain calculations, the percentage difference between the target and calculated stress/strain values decreases as the desired computational depth selected depth increases. This is highly logical and allows one to conclude that the greatest number of dA used should occur closer to the pavement surface where the external loads are applied. As deeper depths are used, the prediction of stress/strain can be approximated, more accurately, by a single point surface load for each tire. As a result, the appropriate number of computational points decreases as the selected depth is increased.
- For circular tire shapes at a deep depth, the range of # dA combinations (100-150) is a general optimal number of dA that should be used for time concern and precision of the strain and stress values.
- The range of $dr = (3-5)$, and $d\phi = (10-12)$ appears to be an accurate number to use for circular tire shape calculation with deep depth.
- For an elliptical tire shape at a deep depth, the range of # dA combinations (50-100) appears to be an optimal number that should be used for a compromise between time issues and accuracy in the strain and stress values.

- When an elliptical tire shape is used; the $d\phi$ selected must be an odd integer; and $360/d\phi$ should be an even integer.
- For a circular tire shape at mid depth, the range of the optimum number of dA combinations appears to be in the 150-250 range. This will insure the most accurate predictions of stress/strain at the minimum amount of computational time.
- For elliptical tire shapes at mid depth, the range of the number of dA combinations appears to be in the 100-200 range. This will insure the most accurate prediction of stress/strains at the minimum account of computational time.
- For a circular tire shape at shallow depths, the range of the number of dA combinations is recommended to be 200-300.

8.2.2 *Stress And Strain Analysis in ZAPRAM:*

- This chapter focused on the comparative accuracy of stresses/strains predicted by ZAPRAM and those computed by the precise MLET pavement response computer codes.
- It was concluded, after an intensive number of comparisons that the ZAPRAM code, using a correction factor, $f_i = 1.0$ in the Odemark Transformed Section analysis, gave higher predictions than the MLET Code JULEA.

8.2.2.1 *The Transformed Section Correction Factor for Three Layer Systems “f”:*

- The correction factor used in the Odemark equation, f_1 and f_2 , are function of several variables (layer thickness, modular ratios, Poisson’s ratios and the number of layers in the structure).
- The least square errors calculated for strain predictions are much higher than those calculated for stress predictions.

- In contrast, the differences in vertical stress between the two approaches (ZAPRAM and JULEA) are not as large.
- The predicted strain value depends on the vertical and horizontal stresses. It was found that there are significant differences in horizontal stress between two programs. This explains the relatively big differences and the wide range in the values of the least square error calculated for the strain production based upon Transformed Section analysis.

8.2.2.2 *The Back Calculation to Estimate f_2*

- When all pavement structure properties, except the thickness of the first layer, are held constant; it was noted that the larger the thickness, the smaller the correction factor would be.
- In general, the range of the correction factor (f_2) for back calculation of stresses is smaller than the range of the correction factor (f_2) from the strain back calculation approach. Two reasons for this are postulated:
 - i. The percentage difference for the strain value is larger than the percentage difference for the stress value.
 - ii. In general, the difference in vertical stress between the two programs is not large. From the strain equation, it is known that its value depends on the vertical and horizontal stresses. Since there is a significant difference in a horizontal stress between two programs; this logically explains the difference and wide range in the values of the correction factor f_2 that is calculated from strains

8.2.2.3 The Factors of Equivalent Thickness Study for Three Layer System

- As a result of these comparative studies, a correction factor of 0.95 for the asphalt layer and a correction factor of 0.80 for any unbound layers were found to typically provide the most accurate stress/strain prediction models. The correction factor icon was created in Pavement Structure Model. Using this set of values as the default values within the ZAPRAM program.

8.2.3 Comparison Of Airfield Flexible Pavement Design Thickness Based Upon Differing Agency Limiting Subgrade Strain Criteria

- This chapter provided an analysis using the new ZAPRAM code based upon the mechanistic-empirical utilization of limiting strain criteria for the design of airfield flexible pavements against shear failure.
- Program ZAPRAM was used to compare the flexible thickness design requirements for three widely acceptable airfield pavement design methodologies used in practice today: Shell Oil; The Asphalt Institute (MS-11) and the newly revised USACE-Beta procedure.
- The results of the comparative design study showed that there is a significant difference between the three widely used airfield pavement design procedures used in the study. Differences between the Asphalt Institute and the new USACE procedure were relatively moderate for all design situations. However, the greatest deviation was found between the Shell Oil approach and the other two criteria.
- The comparison study, based upon a matrix of aircraft types/loads; sub-grade support values and design pass levels, leads to the clear conclusion that there is a

significant difference in design thickness requirements between the different Design Methods in use today.

- These design thickness differences are magnified as the gross aircraft weight is increased and the sub-grade support becomes weaker. Pavement design differences, between methods, (as denoted by the +/- 2S-90% variable) may be as large as 30” to 36” for heavy aircraft on weak sub-grades. Thus if a true design thickness requirement is 60”, the “true” design thickness may range between 30” and 90”. In contrast, if one is concerned with the influence for lighter (B-737) aircraft, this +/- 2S value may only be 5” or less for moderate to strong sub-grades.
- The magnitude of these differences observed between design procedures is felt to be rather large, surprising and perhaps indicative of the lack of an advanced airfield pavement design technology in the airfield pavement design community.
- While pavement design procedures for the US highway industry have dramatically improved over the last two decades, primarily due to a massive influx of research and development support; there has been no comparable increase on the airfield side.
- Finally, it should be called to the reader’s attention that all three of the “Airfield Pavement Design Methods” that are utilized in this study represent the “latest” design technology available. However, it should be realized that all of these Design Procedures are based upon a “Limiting Strain Criteria” mechanistic technology that is well over 40 years old.

8.2.4 Impact Of Environmental Site Location And Groundwater Table Depth On The Thickness Of Flexible Airfield Pavements

- The results of this effort, with the ZAPRAM code, showed, for the first time, the quantitative impact of the significant effects of site climatic conditions, coupled with the importance of the depth of the groundwater table, on the predicted design thicknesses. The approach embedded in ZAPRAM is the same identical environmental technology that has been used as a subsystem within the new AASHTO MEPDG design procedure.
- Significant cost savings appear to be quite reasonable by utilizing principles of unsaturated soil mechanics into the new airfield pavement design procedure found in program ZAPRAM.
- The results of this study have clearly concluded that ZAPRAM is a powerful analytical tool that can be effectively utilized to assess the importance of the environment site location (as reflected by its moisture-temperature regime) and the location of the groundwater table within a flexible airfield pavement structure.
- The results of this investigation have quantified the very significant effect upon the final design thickness caused by the total environment regime.
- For GWT locations close to the proximity of the pavement surface; the influence of the in-situ moisture regime of the unbound layers is primarily controlled by the presence of the GWT depth and the influence of the external environment plays little to no effect upon radically changing the degree of saturation in the unbound layers. Typical GWT depths where this phenomena may occur for B-737 type aircraft is typically 1 to 3 feet from the pavement surface, depending

upon the type of subgrade material that may be present. The significant zone of the GWT for heavier aircraft, such as the B-747, may be 4 to 6 feet deep.

- As the depth of the GWT becomes greater than about 5 to 8 feet from the pavement surface; the effect of the external environment, as measured by the Thornthwaite Moisture Index (TMI) completely takes over the impact of the soil suction and its importance to defining the in-situ partially saturated resilient modulus that may be obtained in-situ.
- These suctions will significantly increase the resilient modulus of the partially saturated soil (particularly plastic clays) in hot, arid areas having high TMI values approaching -55.
- The actual subgrade support equilibrium modulus was found to lead to potential savings in the equivalent subbase material of up to 2.5 feet for lighter B-737 aircraft to as much as 3 to 8 feet for heavier B-747 aircraft, when design thicknesses are compared to the classical assumption used in most pavement design methods that rely upon fully saturated evaluation of all unbound material layers.
- It is clear that the time has come to start integrating the principles of unsaturated soil mechanics into airfield pavement design procedures.

CHAPTER 9 RECOMMENDATIONS AND FUTURE STUDIES

Based upon the results of this study; the following future research recommendations to continuously enhance the ZAPRAM code are made. While the current ZAPRAM code is a very enhanced pavement analysis code for flexible airfield pavement; it should be recognized that there are still a multitude of additional studies and enhancements to the current ZAPRAM code that needs to be made before it is even recognized as a fully comprehensive pavement analysis code. The following list provides a comprehensive list of recommended studies and enhancements that should be completed to evolve ZAPRAM into the most powerful flexible airfield pavement analysis program available in the world:

- It is strongly recommended that the entire US airfield pavement design community and those agencies directly responsible for their operation; carefully re-evaluate the current state of the art that now exists in the industry. US controlled commercial, as well as military airfields around the world constitute an enormous infrastructure system for the US. It appears that the pavement design technology for the design, rehabilitation and preservation of this airside infrastructure investment needs to be significantly enhanced.
- It is highly recommended that several major additions and enhancements be made to upgrade ZAPRAM to consider a wider range of computational enhancements to more accurately model real time environmental changes in unbound layers for the design of flexible airfield pavement systems.
- Enhancements related to the incorporation of monthly variation in environmental characteristics, expansion of the aircraft and environment TMI libraries, inclusion of a strain based distress criteria of the fatigue of AC layer and the addition of analyzing mixed aircraft traffic effects would certainly improve the

analytical power of this program for analyzing the performance of flexible airfield pavements.

- Another important recommendation from this study is to initiate studies that are aimed at including the use of unsaturated soil mechanics into pavement design and performance prediction. In the opinion of the author, the topic of incorporating soil suction and real time environmental changes upon layer properties and response is truly the last major frontier to be integrated into advanced pavement design practice today. Results generated from this study showed some quantitative evidence of the significant savings that may be accrued in the design, construction and rehabilitation of airfield pavements by using unsaturated soil mechanics principles in the design methodologies.
- Further comparison of MLET Vertical Strain Criteria should be a future enhancement study of ZAPRAM. While an initial study on this topic has been addressed in this report: this comparison focused upon only four vertical strain criteria. Currently the program has the Shell Oil, TAI MS-11, and the 2 USACE criteria. It is considered important that one more criteria should be added to the program which is based on subgrade strain criteria. The latest FAA criterion (FAARFIELD) needs to be incorporated into the ZAPRAM program. After this is completed, a study similar to the investigation presented in the chapter six and seven should be expanded to include the FAA criteria.
- The prediction of typical Aircraft Damage Factors (F_{jh}) for subgrade strain criteria (rutting) should be studied to more easily incorporate the influence of a traffic mix, rather than a single critical aircraft:
- ZAPRAM could be easily used to estimate the theoretical F_{jh} damage factor (as a function of z depth to subgrade) for a wide range of aircraft type. This would be a

very practical study similar to the approach used in the Asphalt Institute (MS-11) to compute $F_{jh} = f(E_{vsg})$, for a variety of rutting criteria. This would be a very practical benefit in pavement design by separating complex aircraft traffic mixtures into a standard level of design repetitions for a standard aircraft.

- It is strongly suggested that a study attempting to assess the significance of the lateral wander standard deviation (σ_{wj}) of the specific aircraft type upon life performance be conducted, for a variety of pavement structures (taxiways, runways, ladder and high speed taxiway system):
- The involving the study solution of appropriate f_i correction factors to be used in the Odemark Transformed Section analysis for computing stresses and strain in ZAPRAM, provided a significant increase to the accuracy of the ZAPRAM program. It is highly recommended that future research be undertaken to improve the prediction accuracy of the ZAPRAM stresses/strain state by attempting to develop regression models of the f_i coefficient as a function of key independent variables, such as layer E_i (moduli), h_i (thickness), P (load) etc..
- One enhancement that can be directly made to the existing code is to expand the list aircraft types within the “Aircraft library”. In fact a wide range of other heavy vehicle gear configuration, such as used in Ports; Mine Haul Roads etc. can immediately be added. This actually would be a big enhancement to have a large number of vehicles and their pavement characteristics automatically obtained from the vehicle library.
- One of the significant limitations of the current version of ZAPRAM is that it is limited to the pavement design analysis for a single critical aircraft. The computational damage procedure of ZAPRAM should be eventually based upon a mixture (variety) of different aircraft that incorporate their specified (X_j) –

distance from center line of fuselage to geometric center of gear and σ_w – standard deviation of their lateral wander along the pavement. Damage needs to be computed for a user defined input of design life operation (passes) for each aircraft type in the mixture.

- After the study to compute the cumulative damage associated with mixture of aircraft traffic is completed; an excellent practical study would involve conducting simulation studies, for differing real airfield traffic mixtures to estimate what the “Nes – Equivalent Standard design repetitions” as a sample percentage of “the total Number of Aircraft Passes” would be. Several major publications emanating from these studies could be produced. This would allow simple and practical ways of incorporating aircraft traffic mixture damage estimates for use in the design program.
- One of the major current limitations of ZAPRAM is the fact that it only analyzes subgrade shear (rutting) behaviour of flexible pavement system. As this is one of two major load associated distresses for airfield pavement; the subsystem to incorporate AC fatigue cracking into ZAPRAM must be developed to make ZAPRAM a complete program.
- Once the fatigue criterion is introduced into ZAPRAM, several possible research studies can be conducted. These studies can range from computation studies of several fatigue criterion; calibration of the cracking subsystem by airfield PCI condition survey etc. Another example that is both actual and economic importance is to develop a procedure to determine what is the minimum AC thickness required for different airfield types. Because of the very high cost of AC, several agencies (such as the USAF) have taken the position to use only the minimum required in airfield pavement design.

- Another significant pavement enhancement to ZAPRAM is to take into account the nonlinear behaviour of base / subbase material (unbound). This would be a very difficult challenge to accomplish, within a very accurate methodology, because the most precise solution would be to use 3D finite element models. However as a quick example of an expanded solution; the use of a “Pseudo elastic layered” approach could be developed for the vertical axis under the gears where the maximum damage (either fatigue or shear) is expected. This solution would save very significant amount of computational time of the pavement analysis / design code.

REFERENCES

1. N. Odemark, Undersökning av elasticitetegenskaperna hos olika jordarter samt teori för beräkning av belagningar enligt elasticitetsteorin, statens väg-institut, meddelande 77, (in Swedish), 1949.
2. Boussinesq, J. "Application des Potentials à l'Étude de l'Équilibre et du Mouvement des Solides Élastiques", Gauthiers Villars, Paris, France, 1985.
3. Huang, Yang H., "Pavement Analysis and Design," Prentice-Hall, New Jersey, 2004
4. Witczak, M.W., W.N. Houston, C.E. Zapata, C. Richter, G. Larson, and K. Walsh. Improvement of the Integrated Climatic Model for Moisture Content Predictions. Development of the 2002 Guide for the Development of New and Rehabilitated Pavement Structures, NCHRP 1-37 A, Inter Team Technical Report (Seasonal 4), Tempe, AZ, 2000.
5. Witczak, M.W., D. Andrei, and W.N. Houston. Resilient Modulus as Function of Soil Moisture – Summary of Predictive Models. Development of the 2002 Guide for the Development of New and Rehabilitated Pavement Structures, NCHRP 1-37 A, Inter Team Technical Report (Seasonal 1), Tempe, AZ, 2000.
6. Witczak, M.W., W.N. Houston and D. Andrei. Resilient Modulus as Function of Soil Moisture – A Study of the Expected Changes in Resilient Modulus of the Unbound Layers with Changes in Moisture for 10 LTPP Sites. Development of the 2002 Guide for the Development of New and Rehabilitated Pavement Structures, NCHRP 1-37 A, Inter Team Technical Report (Seasonal 2), Tempe, AZ, 2000.
7. Witczak, M. W., C. E. Zapata, and W. N. Houston. Models Incorporated into the Current Enhanced Integrated Climatic Model: NCHRP 9-23 Project Findings and Additional.
8. Zapata, C.E., Y.Y. Perera, and W.N. Houston. Matric Suction Prediction Model in New AASHTO Mechanistic-Empirical Pavement Design Guide. Transportation Research Record: Journal of the Transportation Research Board, No. 2101, Geology and Properties of Earth Materials. 2009. pp. 53-62.
9. McKeen, R.G. and L.D. Johnson. Climate-Controlled Soil Design Parameters for Mat Foundations. Journal of Geotechnical Engineering, Vol. 116, No. 7, July 1990, pp 1073-1094.
10. Russam, K. The Prediction of Subgrade Moisture Conditions for Design Purposes. Moisture Equilibria and Moisture Changes in Soils Beneath Covered Areas, A symposium in Print, Australia Butterworths, 1965, pp. 233 to 236.

11. Russam, K. and J. D. Coleman. The Effect of Climatic factors on Subgrad Moisture Conditions. *Geotechnique*, Volume XI, No. 1, March 1961, pp 22 to 28.
12. Perera Y. Y. Moisture Equilibria beneath Paved Areas. PhD Dissertation, Arizona State University, Arizona, USA, May 2003.
13. Fredlund, D. G. and A. Xing. Equations for the Soil-Water Characteristic Curve. *Canadian Geotechnical Journal*, Vol. 31, No. 4, 1994. pp. 521 - 532.
14. Perera, Y.Y., C.E. Zapata, W.N. Houston and S.L. Houston. Prediction of the Soil-Water Characteristic Curve Based on Grain-Size Distribution and Index Properties. In E.M. Rathje (ed.), *Geotechnical Special Publications 130-142 & GRI-18; Proceedings of the Geo-Frontiers 2005 Congress*, Jan. 24-26, Austin, Texas; ASCE Geo-Institute and Geosynthetic Materials Association of the Industrial Fabrics Association International Geosynthetic Institute. CD-ROM. 2005.
15. Cary, C.E. and C.E. Zapata. Enhanced Model for Resilient Response of Soils Resulting from Seasonal Changes as Implemented in "Mechanistic-Empirical Pavement Design Guide". *Transportation Research Record: Journal of the Transportation Research Board of the National Academies*, No 2170, Geology and Properties of Earth Materials, 2010. pp. 36-44.
16. Zapata, C.E. Research Results Digest 347: A National Catalog of Subgrade Soil-Water Characteristic Curves and Selected Soil Properties for Use with the MEPDG. National Cooperative Highway Research Program, Transportation Research Board, of the National Academies. ISSN 0077-5614. ISBN: 978-0-309-09929-5. Library of Congress Control Number 2008924251. pp. 23. 2010.
17. N. N. Som, S. C. Das, "Theory and Practice of Foundation Design" Prentice-Hall, 2004.
18. Ullidtz, P.1987 .Pavement Analysis. Instisute of Roads, Transport and Town Planning, The Technical University of Denmark, Lyngby, Denmark.
19. M. W. Witzcak and Zapata, C. E., NCHRP 1-40D Final Report Models Incorporated into the Current Enhanced integrated Climatic Model, Ira A. Fulton School of Engineering ,Department of Civil and Environmental Engineering ,Tempe, AZ 85287-5306, December 2006.
20. E. J. Yoder and M. W. Witzcak, *Principles of Pavement Design*, Second Edition, John Wiley & Sons, 1975.
21. Yang HH. Asphalt Pavement Design – The Shell Method. *Proceedings, 4th International Conference on Structural Design of Asphalt Pavements*, 1973.
22. The Asphalt Institute, "Design of Full Depth Asphalt Airfield Pavements", Manual Series No 11, (MS-11), The Asphalt Institute, College Park, Maryland, 1972.

23. Department of the Army and the Air Force Technical Manual. Flexible Pavement Design for Airfields (Elastic Layer Method). Army TM 5-825-2-1 and Air Force AFM 88-6, Chap2, Section A, November 1989
24. W. Barker and C. Gonzalez, Renovation of the CBR Design Procedure, (Report 1- Understanding, Scrutinizing and Revamping the CBR Thickness Design Methodology), US Army Corps Of Engineers- Waterways Experiment Station, (Vicksburg Mississippi, USA), May 2006.
25. W. Barker and C. Gonzalez, Renovation of the CBR Design Procedure, 2nd international Airports Conference: Planning Infrastructure and Environment, Sao Paulo, Brazil, August 2006.
26. M. W. Witzak. Design of Full-Depth Asphalt Airfield Pavements. Third International Conference on the Structural Design of Asphalt Pavements, Volume I, London, England, September, 1972.

APPENDIX A
USER'S OPERATIONAL GUIDE

A.1 Introduction

The user's guide is a technical communication document intended to give assistance to people using the program. In this chapter, the step by step procedure on how to run the program will be clearly explained. Wherever possible, all of the instructions are illustrated with a copy of the screens to help the user better understand the instructions.

A.1.1 Steps for the ZAPRAM Flow for Stress and Strain Calculations

1. Open the excel spreadsheet and then go to the user welcome sheet (Main menu).
2. To enable the macro, Click on the button Options that is located above the Main menu. Choose the second option (Enable this content) and press OK. (As shown in FIGURE A. 1).

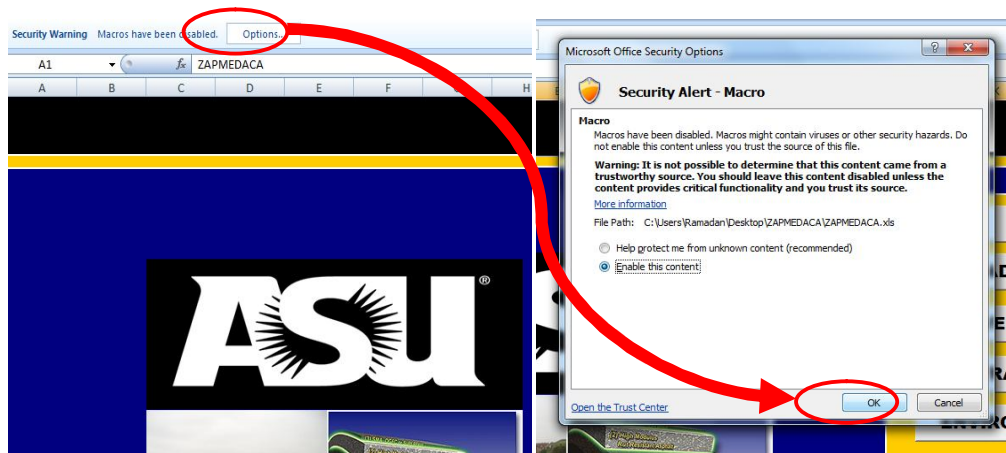


FIGURE A. 1 Enable the macro.

The next three steps *must be* followed when using the program for the first time:

3. Click on the 6th Icon from the list “STRESS ANALYSIS” to direct the user to the stress sheet.

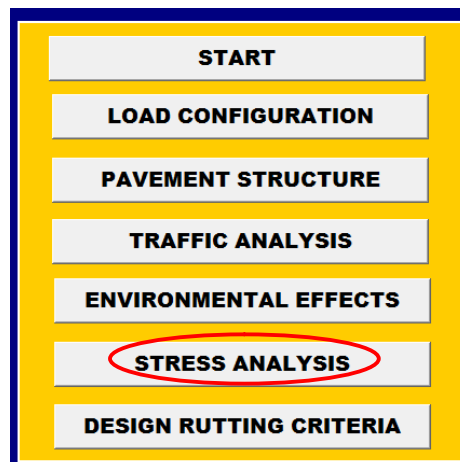


FIGURE A. 2 List of the icon in the main menu.

- In the stress sheet, Specify the location of the ZAPMEDACA file folder in the white box. Follow the example shown in FIGURE A. 3. The file location must include the "\" at the end, or the program will not work.

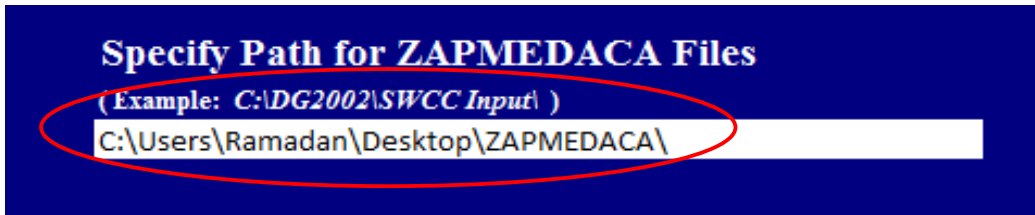


FIGURE A. 3 The white box that the user should specify the location of the ZAPMEDACA file folder in.

- Click on the Main Menu Icon to start the program from the beginning.

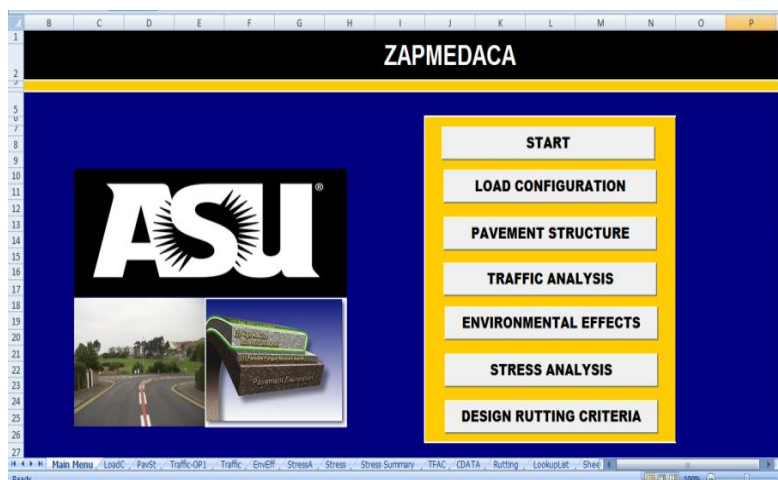
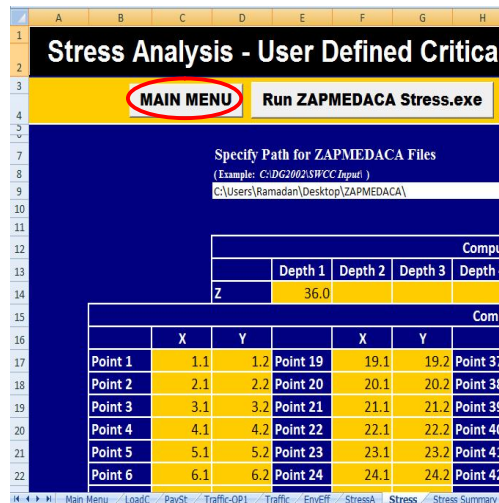


FIGURE A. 4 Start the program from the beginning.

A.2 Main Screen:

1. The main screen of the software illustrates the name of the software; ZAPRAM and list of buttons which link it to different modules.

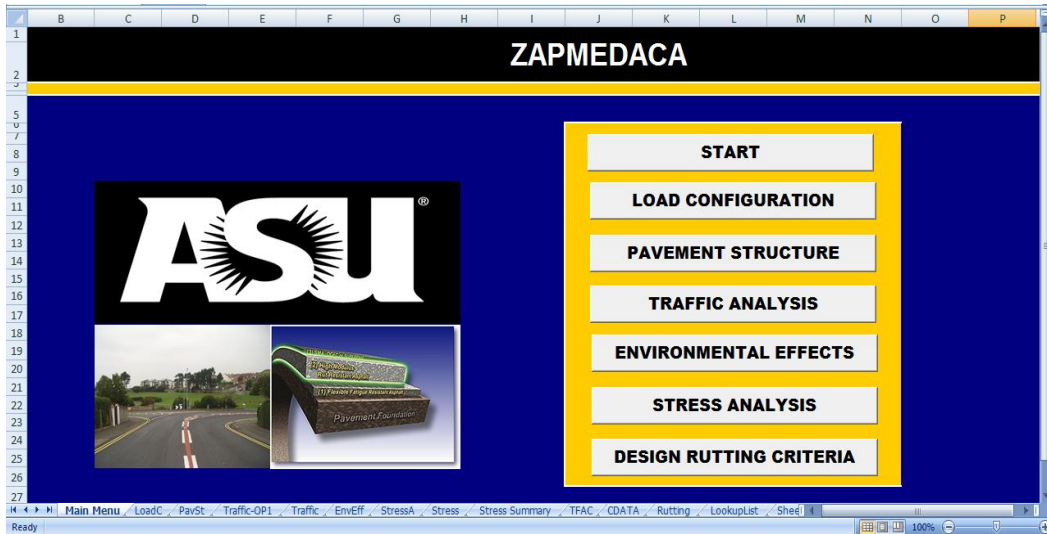


FIGURE A. 5 Main screen of the program.

2. The first button in the list is START. Clicking on this button, the user will be asked to select one of the following design types:
 - Type A: 18KSAL Highway Approach.
 - Type B: User Defined Critical Vehicle Gear.
 - Type C: USACE Airfield Design (Revised).

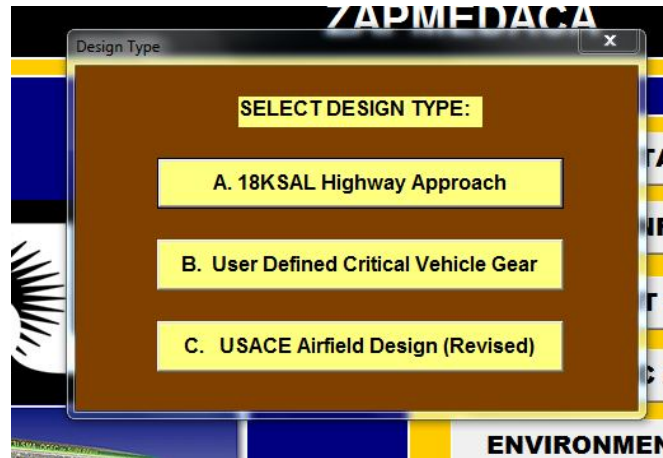


FIGURE A. 6 List of the design types that show by clicking on start button.

3. After the user selected one of the design types, he/she should start entering all data needed for the program to start the pavement analysis procedure. The user needs to click on the first module which is load configuration (second Icon in the list), and then the user will be directed to the following module once he/she completes each module.

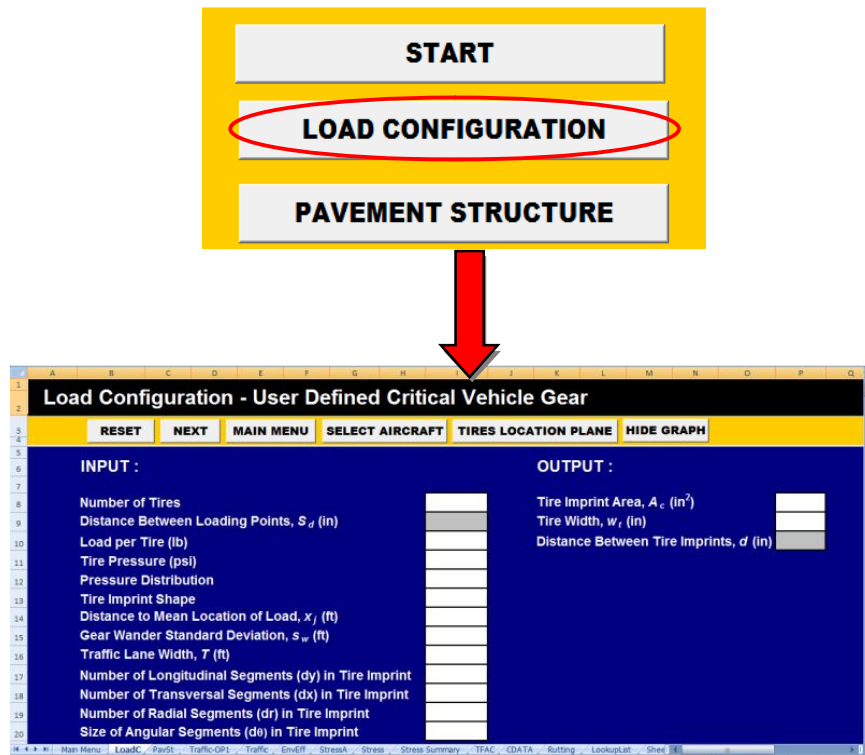


FIGURE A. 7 Clicking on the first module which is load configuration (second icon in the list).

A.3 Load Configuration Module:

1. This spreadsheet (shown in FIGURE A. 8) has three strips that differ by color (Black, Orange, Dark blue).

1.1. The black area has the name of the active sheet with the selected design type.

1.2. The orange one has six gray buttons.

1.2.1. **Reset Icon:** to allow the user to delete all the previous inputs in the sheet.

1.2.2. **Next Icon:** to allow the user to go ahead to the next sheet.

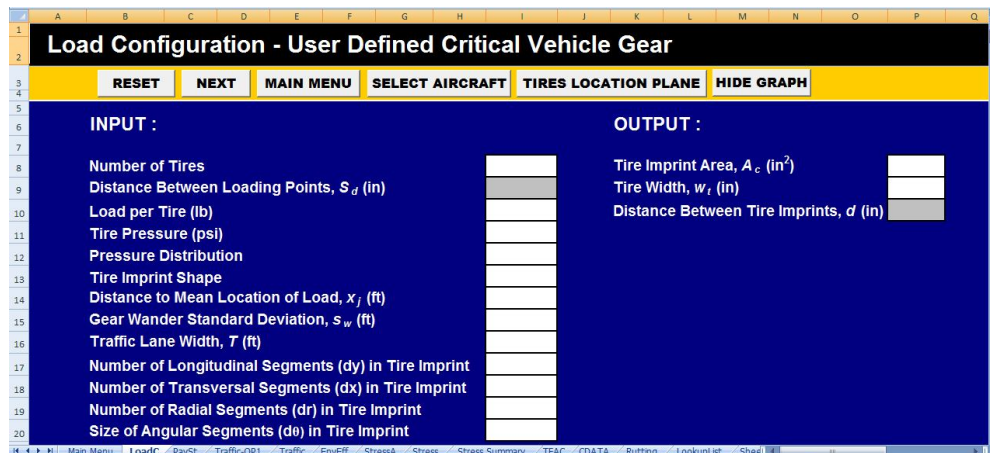


FIGURE A. 8 Spreadsheet “load configuration”.

- 1.2.3. **Main Menu Icon:** to allow the user to go back to the main menu.
- 1.2.4. **Select Aircraft Icon:** This Icon has a large library from current aircraft that contains all of the necessary input information concerning the load-gear that are required to conduct the stress-strain analysis. The user will use this icon only when he/she is in the Airfield design type model and desire to enter stored input already in the library of aircraft. By clicking it, the “Aircraft Company/Model” Multipage will appear as shown in the FIGURE A. 9.



FIGURE A. 9 The “aircraft company/model” multipage.

- 1.2.5. **Tires location Plane Icon:** As shown in FIGURE A. 8, this icon is located as the 5th icon at the top black row in this sheet. By clicking on this button, the program will automatically draw The Tires location Curve. FIGURE A. 10 shows the example when the user selects the Airbus A-380 and needs to see the tire location plane.

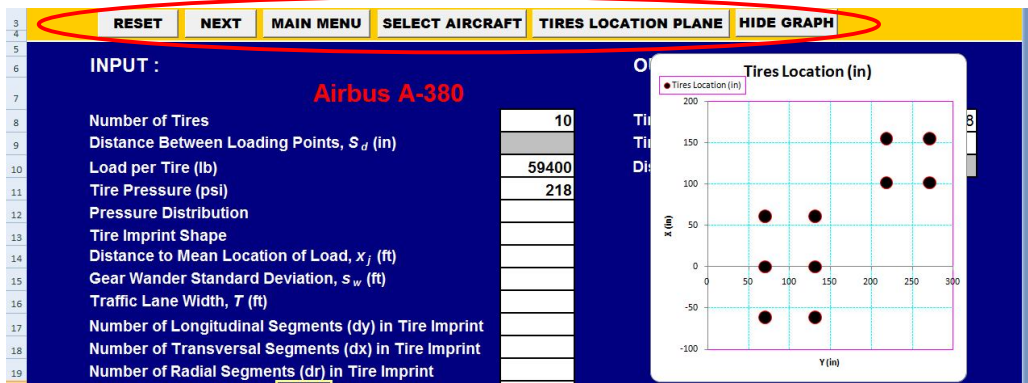


FIGURE A. 10 Tires location plane.

1.2.6. **Hide Graph Icon:** As shown in the FIGURE A. 8, the last icon at the end of the black strip in this sheet is the “Hide Graph Icon”. By clicking on this button, the program will automatically hide the created graph in the previous step.

1.3. The dark blue area has a list of variable inputs that the user should enter to run the program. The following required input parameters in the load configuration module are shown in FIGURE A. 11.



FIGURE A. 11 Required input parameters on load configuration module.

1.3.1. **Number of tires:** The user has to specify how many tires will be used in the analysis. It is noted that the number of tires will be entered automatically as two if the user selected type a design approach which refers to an 18 KSAL Highway approach. As was explained from the previous steps, the user has the possibility of select from the vehicle library or entering the number of tires manually as shown in FIGURE A. 12.

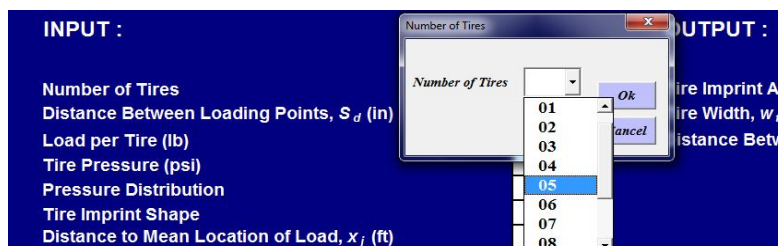


FIGURE A. 12 Select number of tires manually.

1.3.2. **Loading Points Cartesian Coordinates:** if the user selected the type A analysis from the main menu, two point loads will be used as a default value and the distance between the centers of these two points will be the S_d value entered earlier in this module (input number 2). Otherwise, the user has to specify the Cartesian coordinates of each single loading point. The maximum number of the tire load points that the user can input is 12. This input will be automatically filled if the user selected any aircraft from the vehicle library. FIGURE A. 13 illustrates the tabular input file to be used. In general, the x-y axis can be user specified. However it is recommended to constantly treat the “y axis” as being parallel with the axis generated by the aircraft fuselage centerline. This will cause all X_i values to be perpendicular (transverse) distance from the y axis.

| Loading Points Cartesian Coordinates (in) | | | | | | | | | | | | |
|---|---|---|---|---|---|---|---|---|---|----|----|----|
| | 1 | 2 | 3 | 4 | 5 | 6 | 7 | 8 | 9 | 10 | 11 | 12 |
| X | | | | | | | | | | | | |
| Y | | | | | | | | | | | | |

FIGURE A. 13 Loading points cartesian coordinates table.

1.3.3. **Distance to Mean Location of Load, x_j (ft):** If the user selected the type B or C of analysis from the main menu, he/she will be asked to input the distance between the mean location of the gears load to the center line of the air craft. It is to be noted that some aircraft may have more than one main gear on each side of the aircraft. As a result, the user may have to input two specific x_j s. This input will be automatically filled if the user selected any aircraft from the library. Please note that the X_j aircraft distance represents the transverse distance (x) from the geometric centerline of each gear location to the centerline of the aircraft fuselage.

| | |
|---|-------|
| Distance to Mean Location of Load for main Gear1 , x_{j1} | 20.40 |
| Distance to Mean Location of Load for main Gear2 , x_{j2} | 8.40 |

FIGURE A. 14 Distance to mean location of load, x_j (ft).

1.3.4. **Distance between the loading points, S_d (in):** The user will be asked to input the distance between the loading points if and only if he/she selects the type A design approach (18 KSAL Highway approach). It will not be required for the other two approaches.

1.3.5. **Load per tire (lb):** The user will be asked to input the magnitude of load that each tire will have. If the user selects the type A design approach (18 KSAL Highway approach), the load per tire will be a default value of 4500 lb. This input will be automatically filled in the table if the user selects any aircraft from the existing library.

1.3.6. **Tire pressure (psi):** The user will be asked to input the value of the contact pressure (psi) that each tire will have. For the type B or C analysis, this input is automatically filled in the table if the user selects any aircraft from the library.

1.3.7. **Pressure distribution:** The user will be asked to select the type of tire pressure distribution derived in the analysis. There are two options available; uniform and non uniform pressure distribution. By selecting the uniform distribution, the analysis is based upon the use of a constant pressure applied on the entire imprint of the tire. The use of a non uniform pressure will indicate that the pressure varies beneath the tire depending on

the coordinate of the point of interest. Accordingly, the user will be asked to input a wall stiffening ratio. The non uniform pressure is only applicable for the analysis assuming that tire imprint contact shape is elliptical rather than circular.

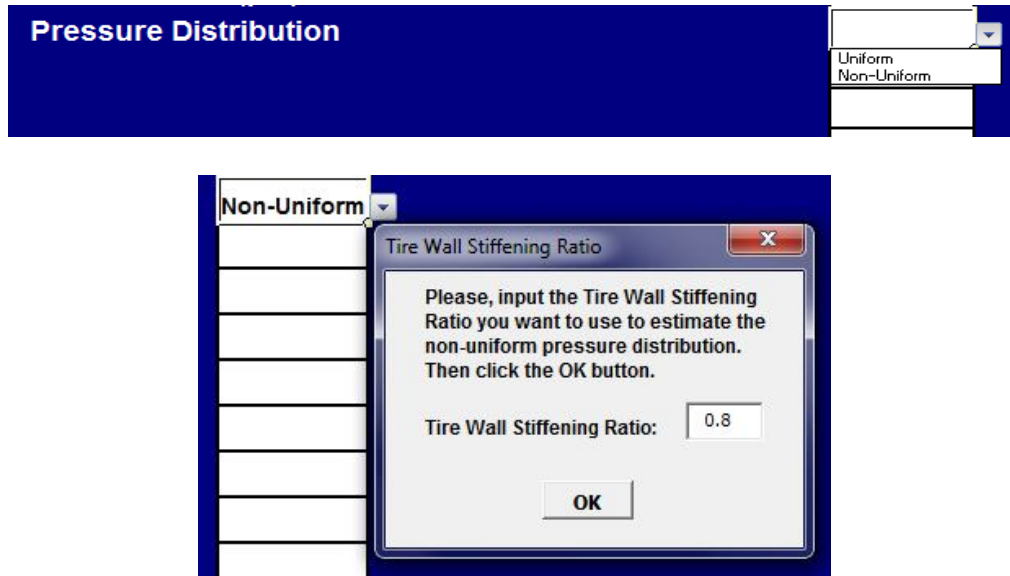


FIGURE A. 15 Pressure distribution input.

1.3.8. **Tire imprint shape:** The user has three tire imprint shapes that he can select from; circular, rectangular, and elliptical.



FIGURE A. 16 Tire imprint shape input.

1.3.9. **Number of the Main Gear for Each Side:** If the user selected the type B or C analysis from the main menu, he/she will be asked to input the number of the main gears for each side of the air craft. This will vary depending upon the aircraft type. This input will be automatically created if the user selects any aircraft from the vehicle library.

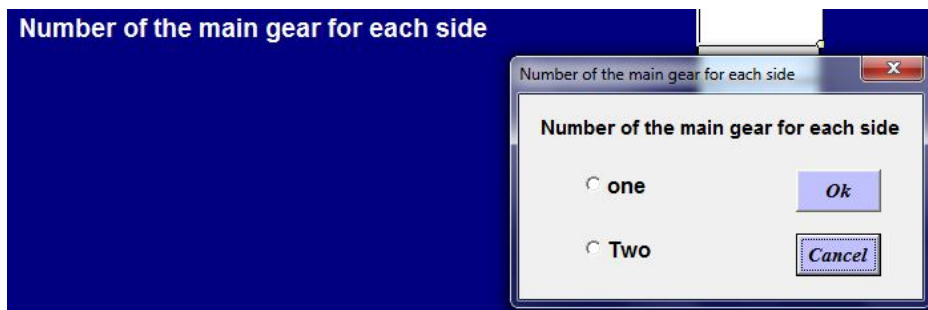


FIGURE A. 17 Number of the main gear input.

1.3.10. **Gear Wander Standard Deviation, s_w (ft):** The user will be asked to input what the design vehicle wander standard deviation will be. This is also one of the inputs which are applicable for type B and C analysis only. A message will pop up to ask the user to specify whether to design for a runway or a taxiway. The second message that will pop up will be in order to ask the user if he/she has a certain value of the gear wander standard deviation or not. If not, a default value will be used. The default gear wander standard deviation for a runway is equal to 16.3 ft, while for a taxiway it is set equal to 3.26 ft. These variations are shown in FIGURE A. 18.

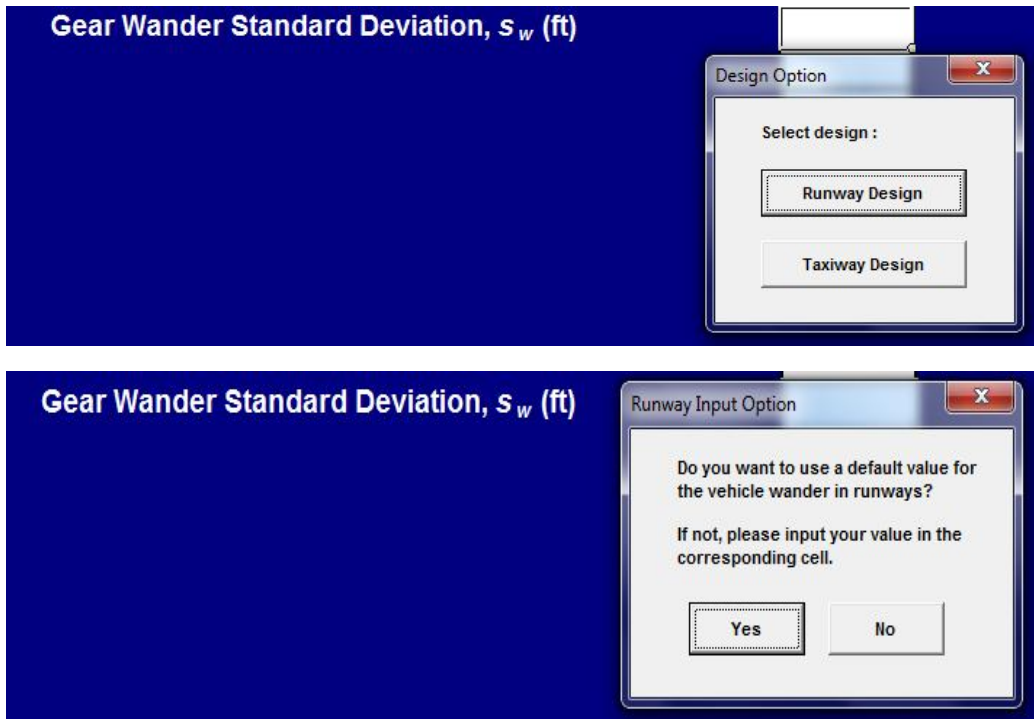


FIGURE A. 18 Gear wander standard deviation input, (ft).

1.3.11. **Traffic Lane Width (ft):** the user will be asked to input what the traffic lane width is if the design analysis is to be conducted using the classical USACE Operation to coverage factor and the use of a "Traffic Lane Width" . This is also one of the inputs which are applicable for Type B and C analysis only. A message will pop up to ask the user to specify whether to design for a runway or a taxiway. The second message that will pop up in order to ask the user if he/she has a certain value of the traffic lane width or not. If not, a default value will be used. The default traffic lane width for a runway is equal to 37.5 ft, while for a taxiway is equal to 7.5 ft. This is convenient with older, historic USA Corps of Engineers pavement design methodologies.

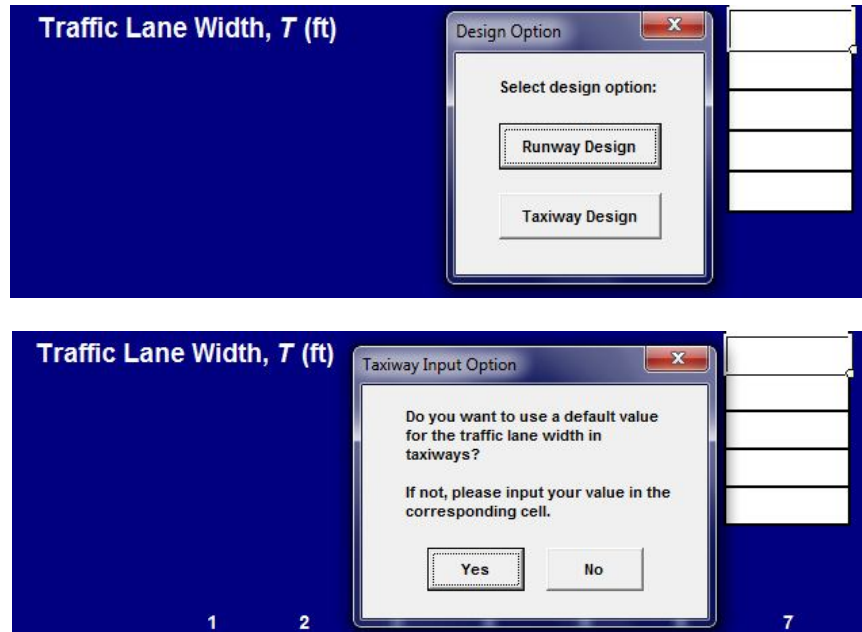


FIGURE A. 19 Traffic lane width input (ft).

1.3.12. **Number of Longitudinal Segments in Tire Imprint:** If a rectangular or elliptical tire imprint is selected, the user has to specify the accuracy of the stress/strain analysis calculations which will be based on the number of segments that he/she wants to subdivide each tire into, for the numerical integration. The number of segments per tire will be calculated based on the number of longitudinal and transverse segments in the tire imprint.

1.3.13. **Number of Transverse Segments in Tire Imprint.** This is similar to 1.3.12.

1.3.14. **Number of Radial Segments in Tire Imprint:** If a circular tire imprint is selected, the user must specify the number of angular/radial segments to be used in the stress/strain analysis. The number of segments per tire will be calculated based on number of radial and angular segments in the tire imprint. For the elliptical tire imprint, is recommended to use similar number of radial and longitudinal segments and similar number of angular and transverse segments.

1.3.15. **Number of Angular Segments in Tire Imprint.** This is similar to 1.3.14.

1.3.16. **Tire Imprint Area, A_c (in²):** the tire imprint area calculated by the quotient of the tire load and tire pressure, regardless of the shape of the tire imprint.

1.3.17. **Tire Width, w_t (in):** the tire imprint width is calculated as a direct function of the shape of the tire imprint. For circular imprints, the tire width is mostly the circle diameter while for an elliptical imprint; a width of $0.6L$ is used.

1.3.18. **Distance between Tire Imprints, d (in):** the distance between tire imprints is calculated for the type A analysis only to check that there is no overlap between the two tires. If this occurs, a message will indicate that the distance between the tires is sufficient or not. Distance between tire imprints can be calculated using the following equation: $d = S_d - 2a_c$. Figure A. 20 shows the tire width ($2a_c$) as well as the final computed “ d ” value.

OUTPUT :

| | |
|---|----------|
| Tire Imprint Area, A_c (in ²) | 45 |
| Tire Width, w_t (in) | 7.6 |
| Distance Between Tire Imprints, d (in) | 2.4 OK!! |

FIGURE A. 20 Output results from the load configuration module.

A.4 Pavement Structure Module

1. This spreadsheet (shown in FIGURE A. 21) has three strips differing by color (Black, Orange, Dark blue).

1.1. The black area has the name of the active sheet with the selected design type.

1.2. The orange has two gray buttons.

1.2.1. **Next Icon:** to allow the user to go ahead to the next sheet.

1.2.2. **Main Menu Icon:** to allow the user to go back to the main menu.

Pavement Structure and Material Properties- User Defined Critical Vehicle Gear

INPUT :

Number of Layers Ground Water Table Depth, (ft)

| Layer Number | 1 | 2 | 3 | 4 |
|---|---------|------------|----------------|----------|
| Material Type | Asphalt | Gran. Base | Gran. Sub-base | Subgrade |
| Thickness (in) | 8.00 | 12.0 | 20.0 | |
| Poison Ratio, u | 0.35 | 0.40 | 0.45 | 0.45 |
| E^* or E at Optimum Conditions, (psi) | 300,000 | 38,000 | 24,000 | 8,877 |
| CBR (%) | | | | 7 |
| R value | | | | |
| AASHTO Layer Coefficient, a_i | | | | |
| Soil Classification (AASHTO or SUCS) | | A-1-b | A-2-7 | |
| Percentage Passing Sieve #200, P_{200} | | 17 | 28 | 65 |
| Plasticity Index, PI | | 14 | 24 | 30 |
| Specific Gravity of Solids, G_s | | 2.65 | 2.75 | 2.7 |
| Optimum Moisture Content, w_{opt} % | | 8 | 12 | 16 |
| Maximum Dry Density, $\gamma_{d max}$ (pcf) | | 130 | 112 | 110 |

CORRECTION FACTOR FOR TRANSFORMED SYSTEM

| Correction Factor (f) | 1 | 2 | 3 |
|-------------------------|------|------|------|
| | 0.95 | 0.80 | 0.80 |

FIGURE A. 21 Spreadsheet “pavement structure”.

1.3. The dark blue area has a list of variable inputs that the user must enter to run the program. The following are the required input parameters for the pavement structure module:

1.3.1. **Number of Layers:** the user has to input the total number of layers in the pavement structure. The maximum number of layers that can be entered is ten.

1.3.2. **Ground Water Table Depth, (ft):** the user has to input the ground water table depth. This depth is measured from the top of the pavement surface. If the layer is above the water table depth, partial saturation will be applied. For all layers (sub-layers) which are beneath the ground water table depth; these materials will be assumed to be fully saturated. This will affect the calculation of the resilient modulus of each layer.

INPUT :

Number of Layers Ground Water Table Depth, (ft)

FIGURE A. 22 Number of layers and ground water table depth, (ft)

1.3.3. **Material Type:** the user has to indicate the material type for each layer. The user will have a drop menu that will allow him/her to select from. The available material options are asphalt, granular base, granular sub-base, sub-grade, or bedrock. If the user selected a subgrade layer, a pop up message will ask him/her to indicate whether this layer is a compacted or natural subgrade layer.

FIGURE A. 23 Material type input.

1.3.4. **Thickness (in):** the user is asked to input the total thickness of each layer.

1.3.5. **Poisson Ratio, ν :** the user is asked to input the Poisson Ratio of each layer.

1.3.6. **Modulus at Optimum Conditions, E (psi):** the user has to input the modulus value for the asphalt layer. Recall that if limiting strain criteria are used; the asphalt E^* must reflect the effective modules recommended by the agency to conduct limiting strain analysis. For the remaining unbound layers, the user can input a user defined value or he/she can select one of the following methods to estimate the modulus at optimum conditions:

- **CBR (%)**
- **R value**
- **AASHTO Layer Coefficient, a_i**
- **Soil Classification (AASHTO or USCS)**

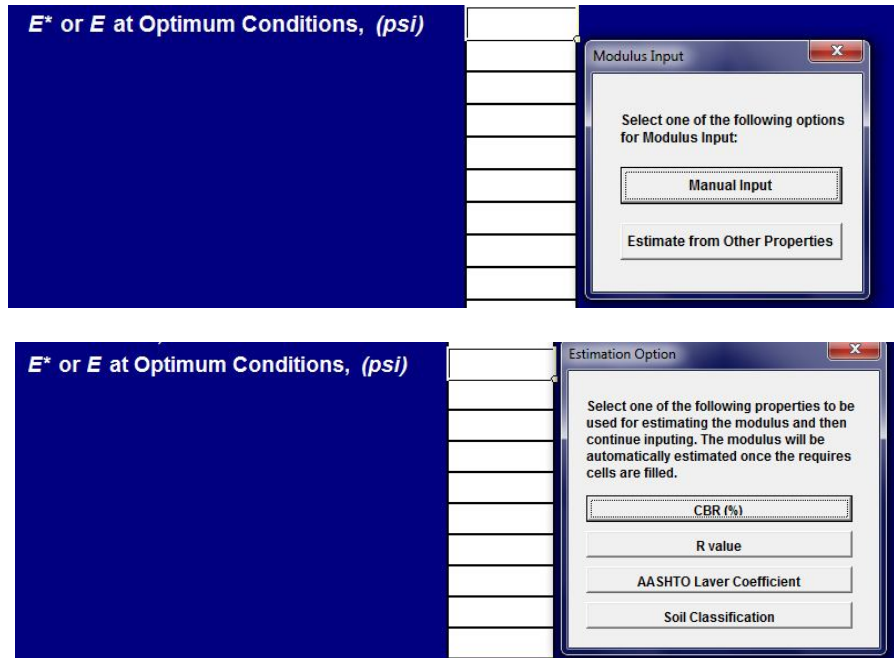


FIGURE A. 24 Modulus at optimum conditions, E (psi).

- 1.3.7. **Passing Sieve #200 in decimal, P200**
- 1.3.8. **Plasticity Index , PI**
- 1.3.9. **Specific Gravity of Solids, G_s**
- 1.3.10. **Optimum Moisture Content, w_{opt} %**
- 1.3.11. **Maximum Dry Density, γ_d max (pcf)**

1.3.12. **Correction Factor Icon (f)**: As shown in the FIGURE A. 25, the derived correction factors to be used in the Odemark Transformed Section analysis are located at the end of the blue area in this sheet. By clicking on this button, the program will automatically show the correction factor for transformed system with default value. (These are the final recommended values from the study described in chapter 5. However, the user can override any of this default values.

| CORRECTION FACTOR FOR TRANSFORMED SYSTEM | | 1 | 2 | 3 |
|--|--|------|------|------|
| Correction Factor (f) | | 0.95 | 0.80 | 0.80 |

FIGURE A. 25 Correction factor for transformed system.

A.5 Traffic Analysis

This module has two different menus that are dependent on user selected analysis from the main menu. FIGURE A. 26 shows both lists of options that the user will deal with. If the user selects type A analysis from the main menu, he or she will deal with the 18ESAL approach shown in FIGURE A. 26. If the user selects type B or C of analysis from the main menu, the user will work with user Defined Critical Vehicle gear.

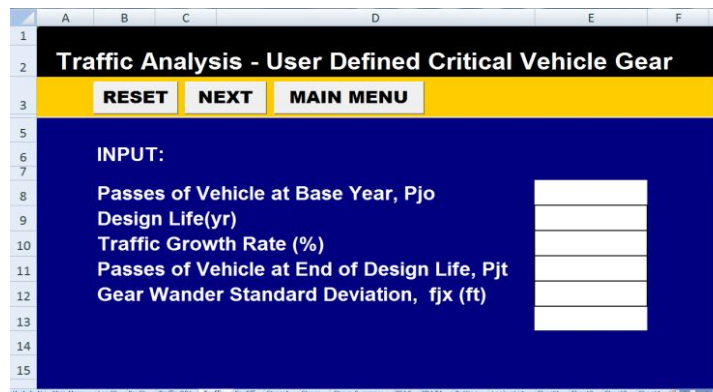
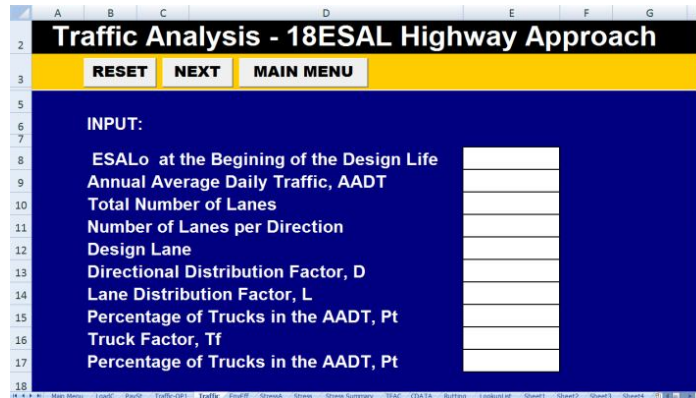


FIGURE A. 26 Spreadsheet “traffic analysis”.

The following are the required input parameters for the traffic analysis module:

1. This spreadsheet (shown in FIGURE A. 26) has three strips differing by color (Black, Orange, Dark blue).
 - 1.1. The black area has the name of the active sheet with the selected design type.
 - 1.2. The orange one has three gray buttons.
 - 1.2.1. **Reset Icon**: to allow the user to delete all the previous inputs in the sheet.
 - 1.2.2. **Next Icon**: to allow the user to go ahead to the next sheet.
 - 1.2.3. **Main Menu Icon**: to allow the user to go back to the main menu.
 - 1.3. The dark blue area has the list of all variable inputs that the user must enter to run the program. The following are the required input parameters for the traffic analysis module with the selected design type A:
 - 1.3.1. **ESALo at the Beginning of the Design Life**: the user will be asked to input the expected ESAL at the base year, if the user does not know this value, he will be directed to input other traffic inputs in order to obtain a reasonable ESALo.

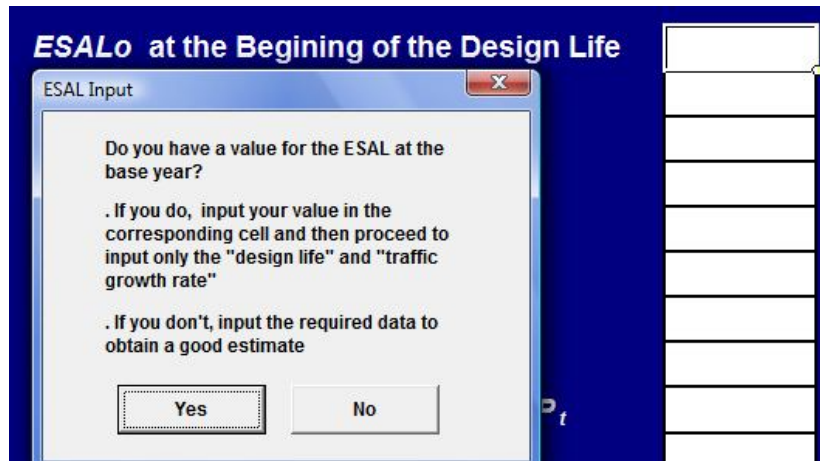


FIGURE A. 27 ESALo at the beginning of the design life.

1.3.2. **Annual Average Daily Traffic, AADT:** this input will be required only if the user does not have an estimated ESALo.

1.3.3. **Total Number of Lanes:** the user will be asked to input the total number of lanes that exist on a certain highway. The user will have to select one option from the drop down menu: 2, 4, or 6+ lanes.



FIGURE A. 28 Total number of lanes.

1.3.4. **Number of Lanes per Direction:** the user needs to select the number of lanes per direction. the user has to select one of the following numbers from the drop down menu: 1, 2, 3, or 4.

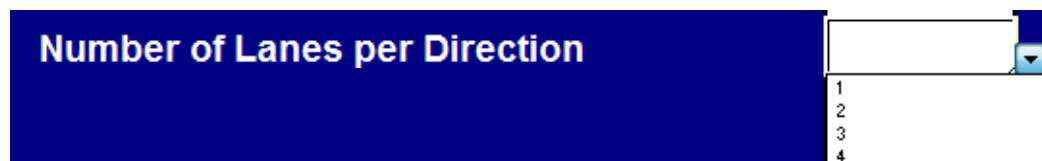


FIGURE A. 29 Number of lanes per direction.

1.3.5. **Design Lane:** the user needs to select the location of the design lane. The user has to select one of the following options from the drop down menu: inner, center, or outer lane.



FIGURE A. 30 Design lane.

1.3.6. **Directional Distribution Factor, D:** the user will see a pop up message asking him/her to input the directional distribution factor, if there is no data available the user can select “use default value” option. The default value of $D = 0.5$ (Equal traffic volume in both directions)

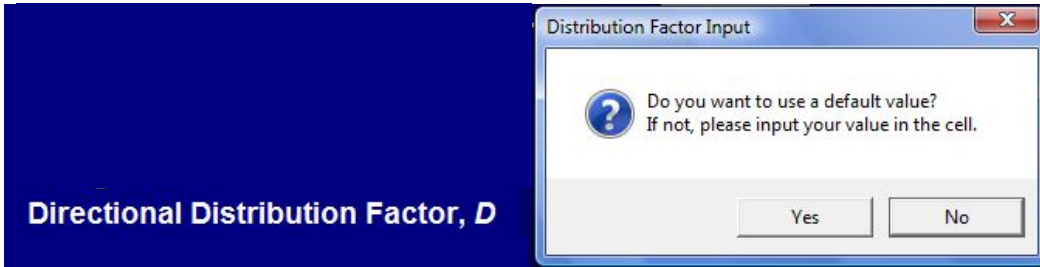


FIGURE A. 31 Directional distribution factor, D.

1.3.7. **Lane Distribution Factor, L:** the user has to input the lane distribution factor, L. The user will have two options from the pop up message: user defined or default value.



FIGURE A. 32 Lane distribution factor, L.

1.3.8. **Percentage of Trucks in the AADT, Pt:** the user will need to enter the percentage of trucks in the AADT. Four options are available to the user to select from: 0.15, 0.25, 0.35 or a user defined value. Note that a number such as 0.15 is 15%

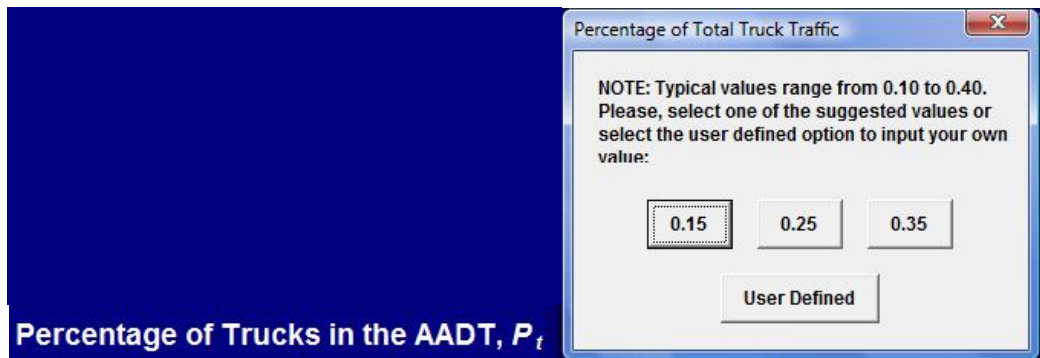


FIGURE A. 33 Percentage of trucks in the AADT, P_t.

1.3.9. **Truck Factor, T_f:** the user will be asked to input the truck factor, T_f. The user has three options to estimate the T_f: default value, compute from user input, user defined.

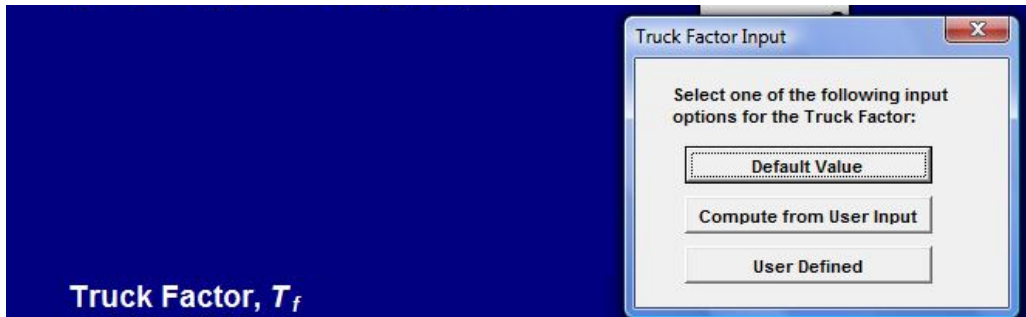


FIGURE A. 34 Truck factor, T_f .

1.4. . The following are the required input parameters for the traffic analysis module with the selected design type B or C (shown in FIGURE A. 35) :

1.4.1. **Passes of Vehicle at Base Year, P_{jo}** : if Type B or C analyses were selected, the user will be asked to input the number of passes of the vehicle at base year. The user will see a pop up message asking him/her “Do you have the number of vehicle passes for the design life? If you do, please input your value in the corresponding cell. If you don't, please input the information required by the program to obtain a good estimate” (shown in FIGURE A. 36).

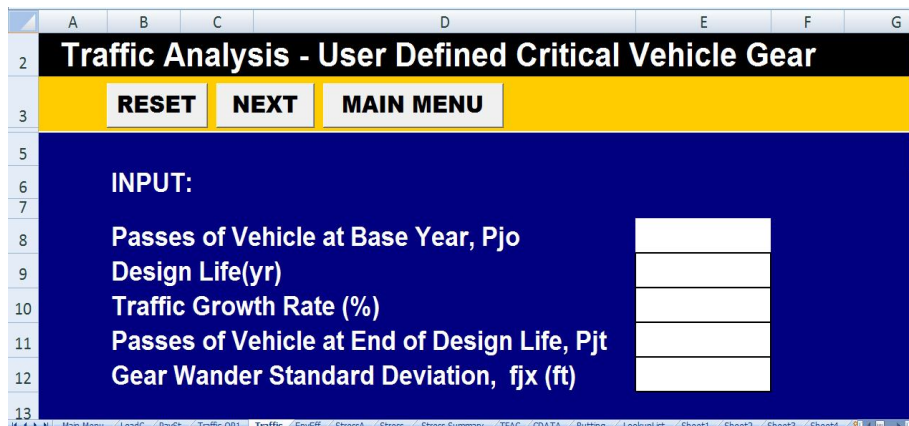


FIGURE A. 35 The traffic analysis module with the selected design type B or C.

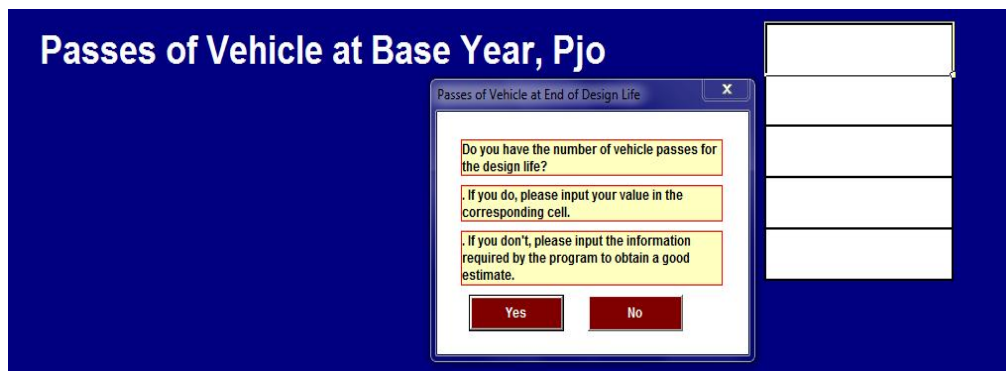


FIGURE A. 36 Passes of vehicle at base year, p_{jo} .

- 1.4.2. **Design Life, years:** the user has to input the required design life in years.
- 1.4.3. **Traffic Growth Rate (%):** the user will be asked to input the traffic growth rate as a percentage value.
- 1.4.4. **Passes of Vehicle at End of Design Life, Pjt:** the user has to input the number of passes of vehicle at the end of the design life, Pjt. This input will be required if the user selected type B or C analysis.
- 1.4.5. **Gear Wander Standard Deviation, S_w (ft):** The user has to input the wander effect f_{jx} . The user will be advised by a pop up message that selects the design option for either a runway design or taxiway design. After that, there is another pop up form to ask the user: Do you want to use a default value for the Pavement Width Analyzed in runways? . (Shown in FIGURE A. 37).

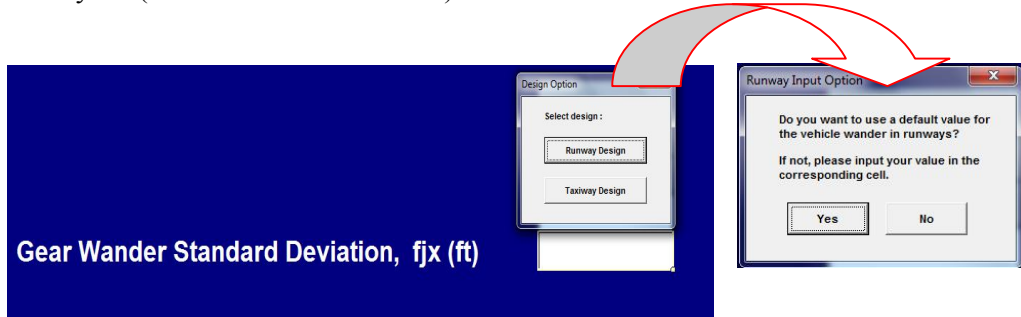


FIGURE A. 37 Gear wander standard deviation, f_{jx} (ft).

A.6 Environmental Effects Module

- 1. This spreadsheet (shown in FIGURE A. 38) has three strips differing by color (Black, Orange, Dark blue).

| Layer | Suction, ψ (psi) | SWCC Constants | | | | Degree of Saturation, S% | S% at Optimum | Environmental Factor, F_u | Resilient Modulus, M_R (psi) |
|-----------------------|-----------------------|----------------|-------|-------|----------|--------------------------|---------------|-----------------------------|--------------------------------|
| | | a_r | b_r | c_r | h_{r1} | | | | |
| Above GWT: Asphalt | | | | | | | | | |
| Above GWT: Gran. Base | 55 | 61.2 | 1.08 | 0.53 | 500 | 86.4 | 52.4 | 0.248 | 4,973 |
| Below GWT: Subgrade | 0 | | | | | 100.0 | 47.3 | 0.232 | 1,809 |

FIGURE A. 38 Spreadsheet “load configuration”.

- 1.1. The black area has the name of the active sheet with the selected design type.
- 1.2. The orange has four gray buttons.
 - 1.2.1. **Reset Icon:** to allow the user to delete all the previous inputs in the sheet.
 - 1.2.2. **Next Icon:** to allow the user to go ahead to the next sheet.
 - 1.2.3. **Main Menu Icon:** to allow the user to go back to the main menu.
 - 1.2.4. **Select City:** clicking on this icon will lead the user to a library list of cities to choose from that are presently created in ZAPRAM. The following environmental data are shown in the library: (TMI, Longitude in decimal, and Latitude in decimal) will fill out for the selected city.

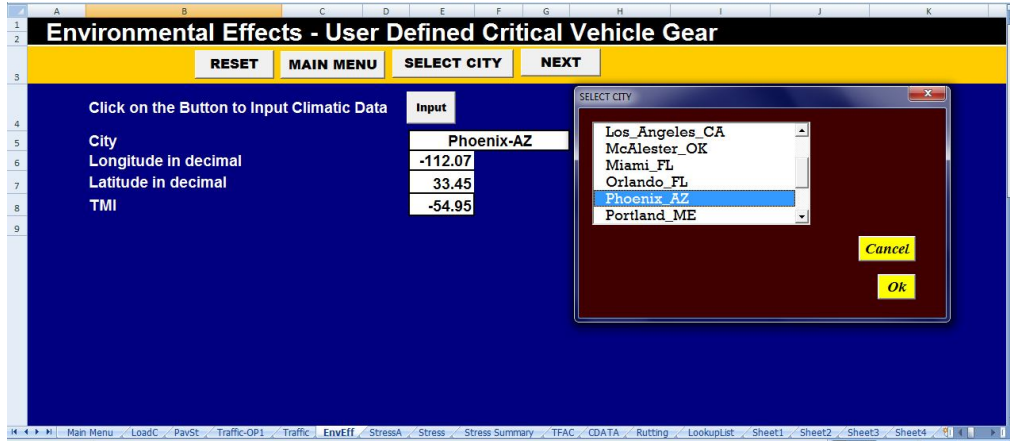


FIGURE A. 39 Select city.

1.3. The dark blue area has variable inputs that the user must enter to run the program. The following are the required input parameters in the environmental effects module:

1.3.1. **Click on the Button to Input Climatic Data:** If the user did not have the TMI for the location, he/she must click this button and input all of the information shown in the table (FIGURE A. 40):

1.3.2. **Average Monthly Temperature (°C):** the user will be asked to input the average monthly air temperature at the design site. This will be used in conjunction with the average monthly precipitation and latitude in order to calculate the TMI.

1.3.3. **Average Monthly Precipitation (mm)** similar to 1.3.2.

1.3.4. **Latitude:** the user has to input the geographical latitude of the pavement structure location, this is correlated to the amount of sunshine.

| Year | Month | t ₁ (°C) | P ₁ (cm) | P (cm) | h ₁ | H _y | a | PE ₁ * (cm) | D _i | PE* (cm) | PE (cm) | TMI Monthly | TMI Yearly | TMI Average | |
|------|-------|------------------------|------------------------|-----------|----------------|----------------|-----|---------------------------|----------------|-------------|------------|----------------|---------------|----------------|--|
| 1 | 1 | 35.3 | 2.6 | 10.8 | 19.3 | 132.9 | 3.1 | 3.29E+01 | 1.22 | 41.49288 | 184.424 | -55.0 | -55.0 | -55.0 | |
| | 2 | 34.5 | 0.9 | 8.6 | 18.6 | 132.4 | 3.1 | 3.06E+01 | 1.16 | 3.67E+01 | 182.091 | -55.0 | -55.0 | -55.0 | |
| | 3 | 28.9 | 1.4 | 11.3 | 14.3 | 131.8 | 3.1 | 1.78E+01 | 1.03 | 1.89E+01 | 179.257 | -55.0 | -55.0 | -55.0 | |
| | 4 | 23.7 | 0.9 | 11.1 | 10.6 | 134.3 | 3.1 | 9.55E+00 | 0.97 | 9.576447 | 187.07 | -55.0 | -55.0 | -55.0 | |
| | 5 | | | | | | | | | | | | | | |
| | 6 | | | | | | | | | | | | | | |
| | 7 | | | | | | | | | | | | | | |
| | 8 | | | | | | | | | | | | | | |
| | 9 | | | | | | | | | | | | | | |
| | 10 | | | | | | | | | | | | | | |

FIGURE A. 40 Input climatic data.

Output results from the environmental effects module (as shown in FIGURE A. 38):

- 1- TMI
- 2- Suction, ψ (psi)
- 3- SWCC constants
- 4- Degree of Saturation, S%
- 5- Degree of Saturation, S% at Optimum
- 6- Environmental Factor, FU
- 7- Resilient Modulus, M_R (psi)

A.7 Stress Analysis Module

This spreadsheet (shown in FIGURE A. 41) has three strips differing by color (Black, Orange, Dark blue).

| No | Layer | Thickness (in) | Poisson Ratio (u) | Suction (psi) | M _R (psi) | Number of Sub-Layers |
|----|-----------------------|----------------|-------------------|---------------|----------------------|----------------------|
| 1 | Above GWT: Asphalt | 12.0 | 0.35 | NA | 300,000 | |
| 2 | Above GWT: Gran. Base | 24.0 | 0.40 | 55.33 | 4,973 | |
| 3 | Below GWT: Subgrade | | 0.40 | 0.00 | 1,809 | |
| | | | | NA | | |

Follow the next steps:

1. Choose Solution type.
2. Click on the "Update Data" button to retrieve the summary of results obtained in the Environmental Effects Module and then define the number of sub-layers per layer you want to consider for the Stress Analysis.
3. Click on the "Subdivide" button to obtain the pavement profile to be analyzed.
4. Select the location within every sublayer for stress and strain computations, then click on the "Get Depths" button to obtain the corresponding effective depths.

FIGURE A. 41 Spreadsheet "stress analysis module".

- 1.1. The black area has the name of the active sheet with the selected design type.
- 1.2. The dark blue area has some tables that have the calculations and the output
- 1.3. The orange one has five gray buttons.
 - 1.3.1. **Solution Type:** to choose a solution type. The choices are either Boussinesq solution or multi-layer (Transformed Section) solution.
 - 1.3.2. **Update Data:** Click on the "Update Data" button to retrieve the summary of results obtained in the Environmental Effects Module and then define the number of sub-layers per layer you want to consider for the Stress Analysis. He/she needs to click on the "Subdivide" button to obtain the pavement profile to be analyzed the maximum allowable number of sublayers is two.

| No | Layer | Thickness (in) | Pison Ratio (u) | Suction (psi) | M _R (psi) | Number of Sub-Layers |
|----|---------------------------|----------------|-----------------|---------------|----------------------|----------------------|
| 1 | Above GWT: Asphalt | 6.0 | 0.50 | NA | 500,000 | 1 |
| 2 | Above GWT: Gran. Base | 11.0 | 0.40 | 0.94 | 50,286 | 2 |
| 3 | Above GWT: Gran. Sub-base | 12.0 | 0.45 | 0.94 | 61,164 | 2 |
| 4 | Above GWT: Subgrade | 7.0 | 0.35 | 2.13 | 44,984 | 1 |
| 5 | Below GWT: Subgrade | 4.5 | 0.35 | 0.00 | 9,475 | 2 |
| 6 | Below GWT: Subarade | | 0.30 | 0.00 | 1.281 | |

FIGURE A. 42 Click on update data.

- 1.3.3. **Subdivide Icon:** Click on the "Subdivide" button to obtain the pavement profile to be analyzed. Then Select the location within every sublayer for stress and strain computations. The user has three choices regarding the location of interest: top, bottom, or top and bottom. This is shown in FIGURE A. 43.
- 1.3.4. **Get Depths Icon:** the user has to click on the "Get Depths" button to obtain the corresponding effective depths.
- 1.3.5. **Main Menu Icon:** to allow the user to go back to the main menu.

| No | Layer | Thickness (in) | Pison Ratio (u) | Suction (psi) | M _R (psi) | Equivalent Thickness (in) | Point Location | Equivalent Depths (in) | |
|-----|---------------------------|----------------|-----------------|---------------|----------------------|---------------------------|----------------|------------------------|--------|
| | | | | | | | | Top | Middle |
| 1 | Above GWT: Asphalt | 6.0 | 0.5 | NA | 500,000 | 24.1 | Middle | | 12.1 |
| 2-A | Above GWT: Gran. Base | 5.5 | 0.4 | 0.94 | 50,286 | 22.1 | Top & Middle | 24.1 | 35.2 |
| 2-B | Above GWT: Gran. Base | 5.5 | 0.4 | 0.94 | 50,286 | 22.1 | Top | 46.2 | |
| 3-A | Above GWT: Gran. Sub-base | 6.0 | 0.45 | 0.94 | 61,164 | 24.1 | Middle | | 80.4 |
| 3-B | Above GWT: Gran. Sub-base | 6.0 | 0.45 | 0.94 | 61,164 | 24.1 | Top & Middle | 92.4 | 104.5 |
| 4 | Above GWT: Subgrade | 7.0 | 0.35 | 2.13 | 44,984 | 28.1 | Top & Middle | 116.5 | 130.6 |
| 5-A | Below GWT: Subgrade | 2.3 | 0.35 | 0.00 | 9,475 | 9.0 | Top | 144.6 | |
| 5-B | Below GWT: Subgrade | 2.3 | 0.35 | 0.00 | 9,475 | 9.0 | | | |
| 6 | Below GWT: Subgrade | | 0.3 | 0.00 | 1,281 | | | | |

FIGURE A. 43 Subdivide icon.

1.3.6. **Select Points Icon:** the user has to click on the “Select Points” button which will refer him/her to input the X and Y coordinates of the computational points of interest. The maximum number of the X and Y points of interest is 88 points for each depth (z). It is noted that the depth of interest is already entered from the previous step. This input will be automatically filled if the user selected any aircraft from the vehicle library.

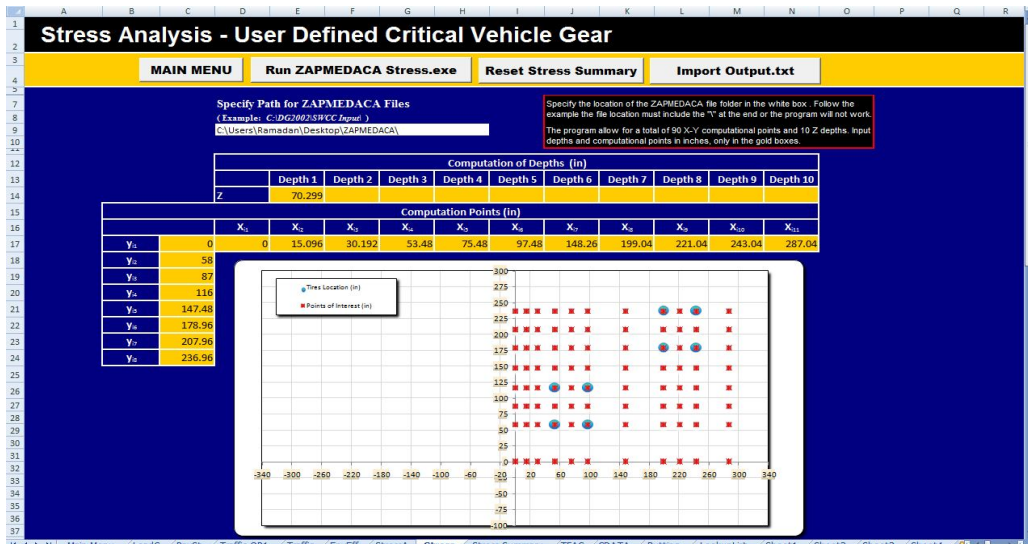


FIGURE A. 44 The X and Y points of interest.

1.3.7. **Run ZAPMEDACA Stress.exe Icon:** The user has to click “Run ZAPMEDACA Stress.exe” button to run the stress analysis procedure. A pop up message (See FIGURE A. 45) will notify the user that the analysis is completed and the user has to click the Enter button.

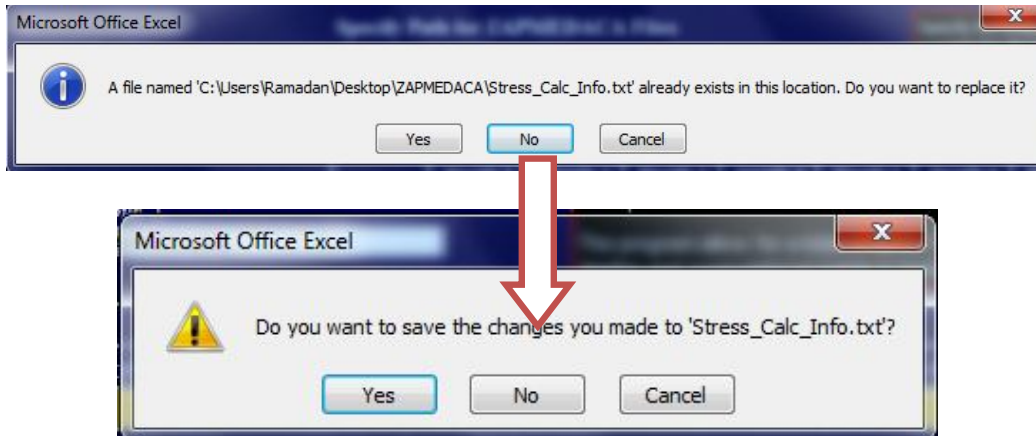


FIGURE A. 45 A pop message come up when the analysis is completed.

1.3.8. **Reset Stress Summary Icon:** to allow the user to delete all the previous outputs in the stress summary sheet.

1.3.9. **Import Output.txt Icon:** The user needs to click “import Output.txt” button to get the finalized format of the stress analysis results.

Output results from the stress analysis module:

- 1- Normal stress in the x direction, σ_x
- 2- Normal stress in the y direction, σ_y
- 3- Normal stress in the z direction, σ_z
- 4- Shear stress in the xz plane, τ_{xz}
- 5- Shear stress in the yz plane, τ_{yz}
- 6- Shear stress in the xy plane, τ_{xy}
- 7- Strain in the x direction, ϵ_x
- 8- Strain in the y direction, ϵ_y
- 9- Strain in the z direction, ϵ_z

| Stress Analysis - User Defined Critical Vehicle Gear | | | | | | | | | | | | | | | | | |
|--|---------------|------------------------|------------------------|------------|-------------|-------------|-------------|--------------|--------------|--------------|--------------|------------|------------|------------|------------|------------|--|
| | | MAIN MENU RUTTING | | | | | | | | | | | | | | | |
| | | Computation of Point = | | | | Point 1 | | | x = | | | 0.00 | | y = | | 0.00 | |
| | | σ_x | σ_y | σ_z | τ_{xz} | τ_{yz} | τ_{xy} | ϵ_x | ϵ_y | ϵ_z | δ_x | δ_y | δ_z | δ_x | δ_y | | |
| 7 | Depth 1 (in) | 221.73 | 1.20E+00 | 2.04E-01 | 2.22E-01 | -5.17E-01 | -4.86E-01 | 2.32E-01 | 5.69E-04 | -2.01E-04 | -1.88E-04 | 5.27E-06 | -1.87E-06 | -1.74E-06 | | | |
| 8 | Depth 2 (in) | 230.00 | 1.17E+00 | 1.90E-01 | 2.05E-01 | -4.92E-01 | -4.63E-01 | 2.17E-01 | 5.58E-04 | -1.99E-04 | -1.87E-04 | 5.17E-06 | -1.84E-06 | -1.73E-06 | | | |
| 9 | Depth 3 (in) | 250.00 | 1.09E+00 | 1.60E-01 | 1.71E-01 | -4.38E-01 | -4.13E-01 | 1.87E-01 | 5.31E-04 | -1.91E-04 | -1.83E-04 | 4.92E-06 | -1.77E-06 | -1.69E-06 | | | |
| 10 | Depth 4 (in) | 270.00 | 1.02E+00 | 1.36E-01 | 1.43E-01 | -3.90E-01 | -3.70E-01 | 1.61E-01 | 5.04E-04 | -1.83E-04 | -1.77E-04 | 4.66E-06 | -1.69E-06 | -1.64E-06 | | | |
| 11 | Depth 5 (in) | 290.00 | 9.57E-01 | 1.16E-01 | 1.20E-01 | -3.50E-01 | -3.33E-01 | 1.40E-01 | 4.77E-04 | -1.74E-04 | -1.71E-04 | 4.42E-06 | -1.61E-06 | -1.58E-06 | | | |
| 12 | Depth 6 (in) | 310.00 | 8.98E-01 | 9.85E-02 | 1.01E-01 | -3.14E-01 | -3.01E-01 | 1.22E-01 | 4.51E-04 | -1.66E-04 | -1.64E-04 | 4.18E-06 | -1.54E-06 | -1.52E-06 | | | |
| 13 | Depth 7 (in) | 330.00 | 8.40E-01 | 8.41E-02 | 8.55E-02 | -2.83E-01 | -2.72E-01 | 1.07E-01 | 4.27E-04 | -1.58E-04 | -1.57E-04 | 3.95E-06 | -1.46E-06 | -1.45E-06 | | | |
| 14 | Depth 8 (in) | 350.00 | 7.88E-01 | 7.19E-02 | 7.24E-02 | -2.56E-01 | -2.47E-01 | 9.35E-02 | 4.04E-04 | -1.50E-04 | -1.50E-04 | 3.74E-06 | -1.39E-06 | -1.39E-06 | | | |
| 15 | Depth 9 (in) | 370.00 | 7.40E-01 | 6.16E-02 | 6.14E-02 | -2.32E-01 | -2.24E-01 | 8.21E-02 | 3.82E-04 | -1.43E-04 | -1.43E-04 | 3.54E-06 | -1.33E-06 | -1.33E-06 | | | |
| 16 | Depth 10 (in) | 390.00 | 6.96E-01 | 5.27E-02 | 5.22E-02 | -2.11E-01 | -2.04E-01 | 7.23E-02 | 3.62E-04 | -1.36E-04 | -1.37E-04 | 3.35E-06 | -1.26E-06 | -1.27E-06 | | | |
| 18 | | | Computation of Point = | | | | Point 2 | | | x = | | | 0.00 | | 58.00 | | |
| 19 | | | σ_x | σ_y | σ_z | τ_{xz} | τ_{yz} | τ_{xy} | ϵ_x | ϵ_y | ϵ_z | δ_x | δ_y | δ_z | δ_x | δ_y | |
| 20 | Depth 1 (in) | 221.73 | 1.58E+00 | 2.85E-01 | 7.71E-02 | -3.04E-01 | -6.52E-01 | 1.72E-01 | 7.93E-04 | -2.09E-04 | -3.69E-04 | 7.34E-06 | -1.93E-06 | -3.42E-06 | | | |
| 21 | Depth 2 (in) | 230.00 | 1.52E+00 | 2.63E-01 | 7.09E-02 | -2.90E-01 | -6.15E-01 | 1.62E-01 | 7.65E-04 | -2.06E-04 | -3.54E-04 | 7.09E-06 | -1.91E-06 | -3.28E-06 | | | |
| 22 | Depth 3 (in) | 250.00 | 1.38E+00 | 2.18E-01 | 5.80E-02 | -2.60E-01 | -5.37E-01 | 1.41E-01 | 7.04E-04 | -1.99E-04 | -3.22E-04 | 6.52E-06 | -1.84E-06 | -2.98E-06 | | | |
| 23 | Depth 4 (in) | 270.00 | 1.27E+00 | 1.81E-01 | 4.75E-02 | -2.34E-01 | -4.72E-01 | 1.22E-01 | 6.49E-04 | -1.90E-04 | -2.94E-04 | 6.01E-06 | -1.76E-06 | -2.72E-06 | | | |
| 24 | Depth 5 (in) | 290.00 | 1.16E+00 | 1.52E-01 | 3.87E-02 | -2.12E-01 | -4.17E-01 | 1.06E-01 | 6.01E-04 | -1.82E-04 | -2.69E-04 | 5.56E-06 | -1.68E-06 | -2.49E-06 | | | |
| 25 | Depth 6 (in) | 310.00 | 1.07E+00 | 1.28E-01 | 3.14E-02 | -1.92E-01 | -3.71E-01 | 9.29E-02 | 5.57E-04 | -1.73E-04 | -2.48E-04 | 5.16E-06 | -1.61E-06 | -2.30E-06 | | | |
| 26 | Depth 7 (in) | 330.00 | 9.91E-01 | 1.08E-01 | 2.52E-02 | -1.74E-01 | -3.31E-01 | 8.11E-02 | 5.19E-04 | -1.65E-04 | -2.29E-04 | 4.80E-06 | -1.53E-06 | -2.12E-06 | | | |
| 27 | Depth 8 (in) | 350.00 | 9.19E-01 | 9.11E-02 | 2.01E-02 | -1.58E-01 | -2.97E-01 | 7.10E-02 | 4.84E-04 | -1.57E-04 | -2.12E-04 | 4.48E-06 | -1.46E-06 | -1.97E-06 | | | |
| 28 | Depth 9 (in) | 370.00 | 8.55E-01 | 7.71E-02 | 1.58E-02 | -1.44E-01 | -2.67E-01 | 6.22E-02 | 4.52E-04 | -1.50E-04 | -1.97E-04 | 4.18E-06 | -1.39E-06 | -1.83E-06 | | | |
| 29 | Depth 10 (in) | 390.00 | 7.96E-01 | 6.53E-02 | 1.22E-02 | -1.31E-01 | -2.41E-01 | 5.46E-02 | 4.23E-04 | -1.43E-04 | -1.84E-04 | 3.92E-06 | -1.32E-06 | -1.70E-06 | | | |

FIGURE A. 46 Output results from the stress analysis module.

1.3.10. **Rutting Icon:** The user needs to click the “Rutting” button to proceed to the rutting calculation for the airfield design analysis problem.

A.8 Design Rutting Criteria

1. This spreadsheet (shown in FIGURE A. 47) has three strips that differ by color (Black, Orange, Dark blue).

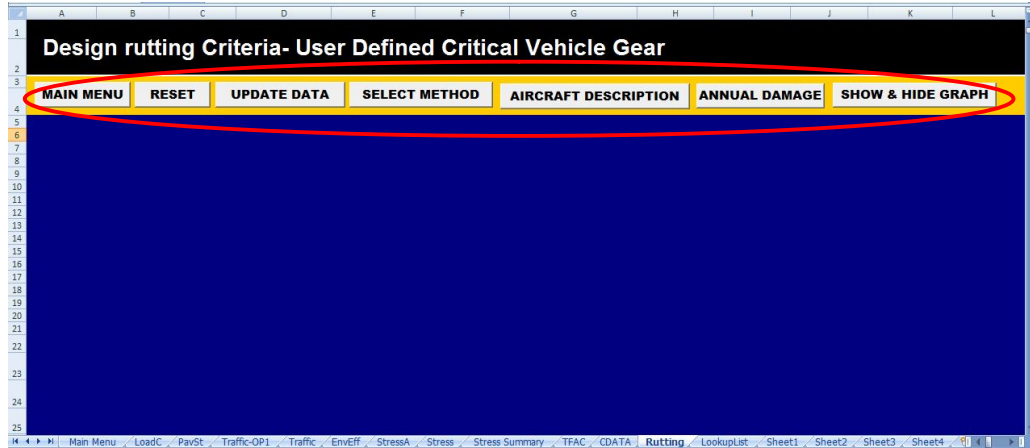


FIGURE A. 47 Spreadsheet “design rutting criteria”.

- 1.1. The black area has the name of the active sheet with the selected design type.
- 1.2. The orange has seven gray buttons.
 - 1.2.1. **Reset Icon:** to allow the user to delete all the previous inputs in this sheet.
 - 1.2.2. **Main Menu Icon:** to allow the user to go back to the main menu.
 - 1.2.3. **Update Data:** Click on the "Update Data" button to retrieve the summary of results obtained from the Stress Analysis Module. The result will be set in a table as shown in FIGURE A. 48. The table has the X, Y, and Z coordinates in inches of the points of interest for the maximum vertical strain at the top of subgrade layer. The fourth row has the maximum vertical strain at the top of the layer associated with the derived computation point (in/in).

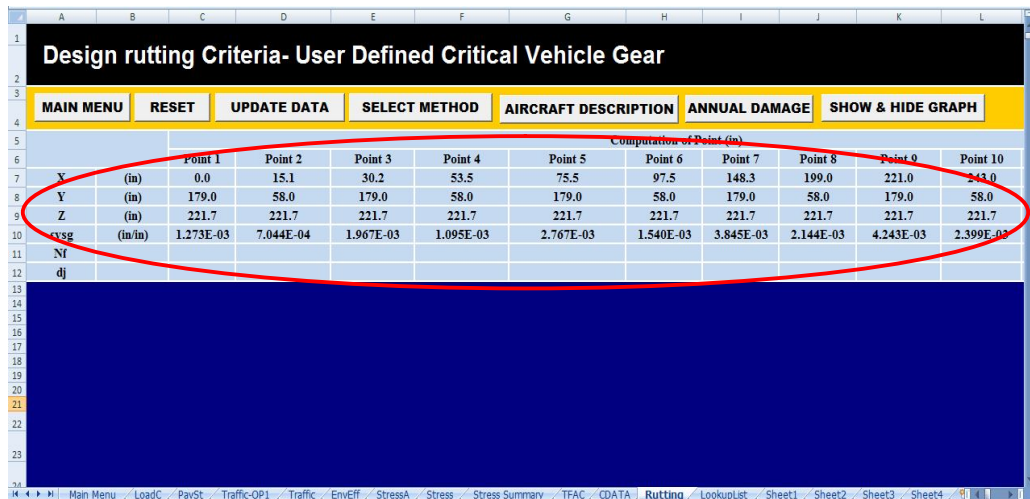


FIGURE A. 48 Click on the "update data" button.

1.2.4. **Select Method Icon:** This Icon has four methods to calculate the allowable number of repetitions as a function of the vertical strain at the top of the subgrade. This analysis is linked to the expected permanent deformation (rutting). Also this will calculate the unit damage of all computation points. The four different criteria that can be reflected for the rutting analysis are shown in FIGURE A. 49.

1. Shell Oil Criteria (Airfields).
2. MS-11 the Asphalt Institute (Airfields).
3. USACE. WES (U.S. Army Corps of Engineers) ... (Original MLET).
4. USACE. WES (U.S. Army Corps of Engineers) ... (Revised β Approach).

FIGURE A. 49 Vertical subgrade strain criteria user form.

1.2.5. **How to Use Vertical Subgrade Strain Criteria User form:**

1.2.5.1. **Select the Criteria:** The user has to choose the criteria by clicking on the criteria name on the top of the user form. The criterion in progress is the one that its title differs by color (Dark gray).

1.2.5.2. **Update Data Icon:** Click on the "Update Data" button to retrieve the maximum vertical strain at the top of subgrade layer (in/in) which were calculated in the rutting sheet (as shown in FIGURE A. 50).

FIGURE A. 50 Clicking update data icon.

1.2.5.3. **Calculate Icon:** Click on the "Calculate Icon" button to compute the allowable number of repetitions as a function of the vertical strain at the top of the subgrade. Also this will calculate the unit damage of all computation points (as shown in FIGURE A. 51).

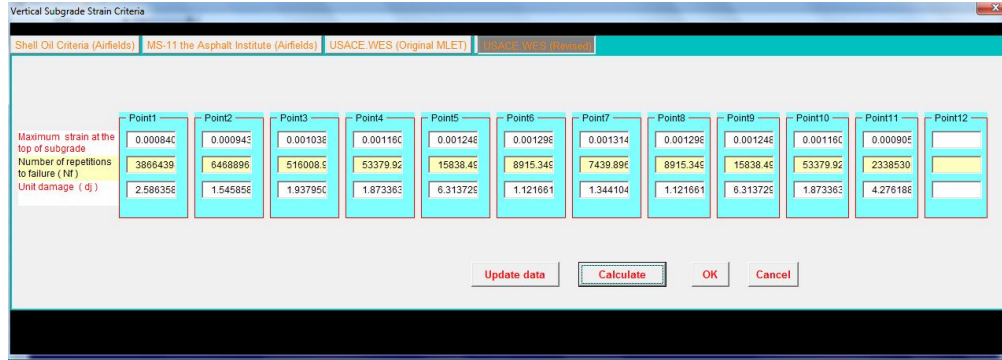


FIGURE A. 51 Clicking calculate icon.

1.2.5.4. **Ok Icon:** Click on the “Ok Icon” button to copy the results down on the sheet (the allowable number of repetitions and the unit damage of all computation points as shown in FIGURE A. 52).

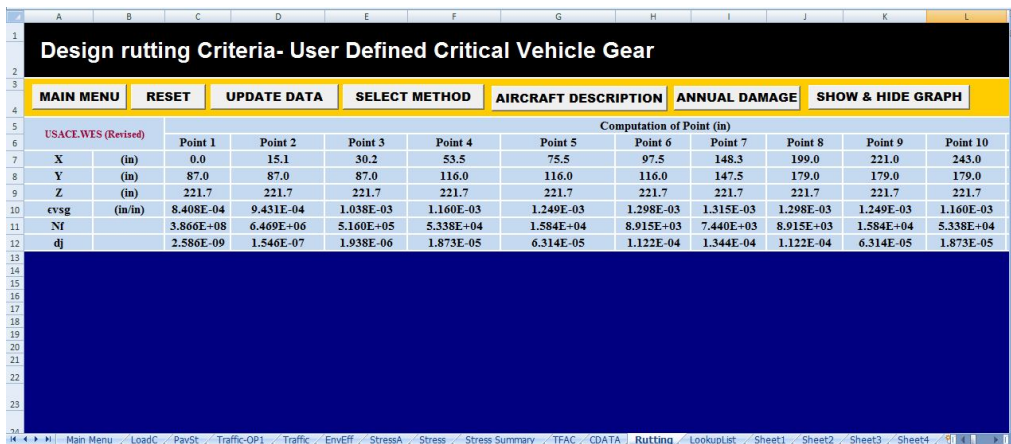


FIGURE A. 52 Clicking ok icon.

1.2.5.5. **Cancel Icon:** Click on the “Cancel Icon” button to hide the user form and cancel all calculations.

1.2.6. **Aircraft Description Icon:** Clicking on this Icon will cause a multi-user form to determine the actual design deflection repetitions (Coverage) that would be used to design the Taxiway and Runway, based upon a normal distribution approach. The user form has three options upon aircraft type:

One Main Gear.

Two Main Gears in one path.

Two Main Gears in Two paths.

These 3 possibilities are shown in FIGURE A. 53.

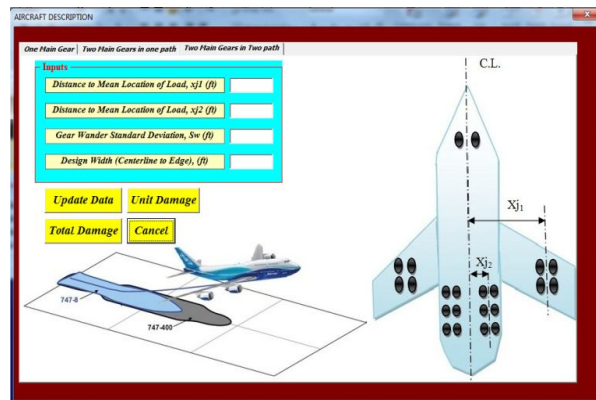
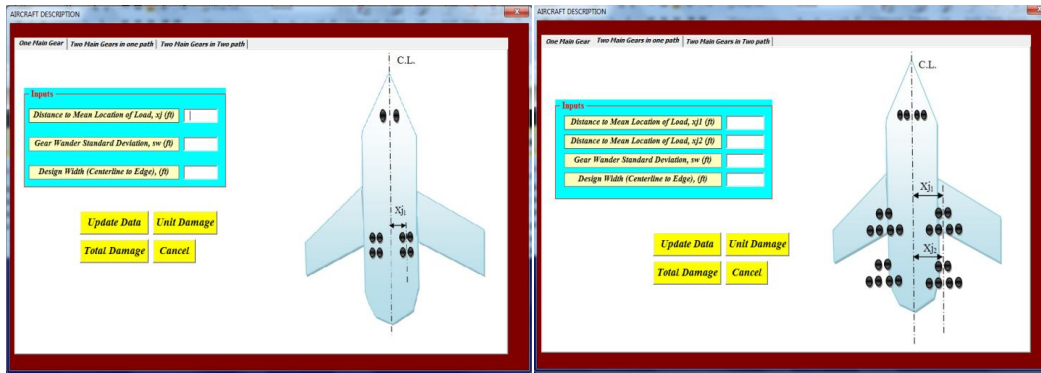


FIGURE A. 53 Clicking aircraft description icon.

1.2.6.1. **Update Data Icon:** Click on the "Update Data" button to retrieve the Distance to the Mean Location of Load, x_{j1} (ft), Distance to Mean Location of Load, x_{j2} (ft), Gear Wander Standard Deviation, S_w (ft), Design Width (Centerline to Edge), (ft), and the name of the selected aircraft. These variable have been entered in previous sheets (as shown in FIGURE A. 54). The user has the ability to change the value of these input from the original user form.

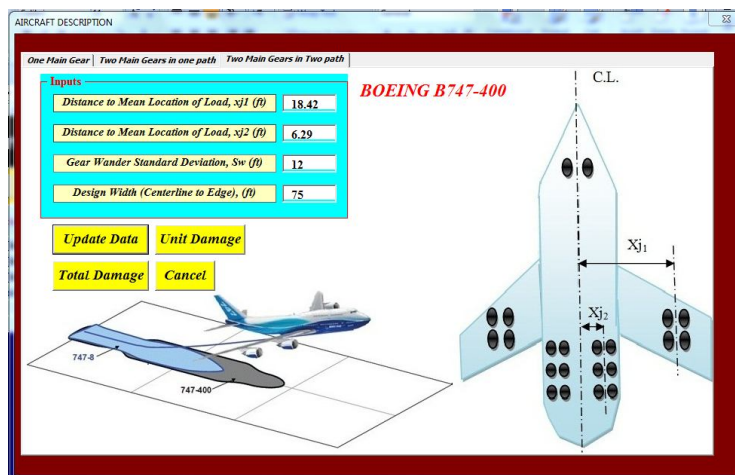


FIGURE A. 54 Clicking update data icon.

- 1.2.6.2. **Unit Damage Icon:** Clicking on this button estimates the unit damage(damage on one pass) as shown in FIGURE A. 55.
- 1.2.6.3. **Total Damage Icon:** Clicking on this button will estimate the damage associated with proportional standard deviation of wander according to the normal distribution approach (as shown in FIGURE A. 55).
- 1.2.6.4. **Cancel Icon:** Click on the "Cancel Icon" button to hide the user form and cancel all the calculation.

| Design rutting Criteria- User Defined Critical Vehicle Gear | | | | | | | | | | | |
|---|---------|---------------------------|-------------|---------------|----------------------|---------------|-------------------|-----------|-----------|-----------|-----------|
| MAIN MENU | | RESET | UPDATE DATA | SELECT METHOD | AIRCRAFT DESCRIPTION | ANNUAL DAMAGE | SHOW & HIDE GRAPH | | | | |
| USACE.WES (Revised) | | Computation of Point (in) | | | | | | | | | |
| | | Point 1 | Point 2 | Point 3 | Point 4 | Point 5 | Point 6 | Point 7 | Point 8 | Point 9 | Point 10 |
| X | (in) | 0.0 | 15.1 | 30.2 | 55.5 | 75.5 | 97.5 | 148.3 | 199.0 | 221.0 | 243.0 |
| V | (in) | 87.0 | 87.0 | 87.0 | 116.0 | 116.0 | 116.0 | 147.5 | 179.0 | 179.0 | 179.0 |
| Z | (in) | 221.7 | 221.7 | 221.7 | 221.7 | 221.7 | 221.7 | 221.7 | 221.7 | 221.7 | 221.7 |
| cvsg | (in/in) | 8.408E-04 | 9.431E-04 | 1.038E-03 | 1.160E-03 | 1.249E-03 | 1.298E-03 | 1.315E-03 | 1.298E-03 | 1.249E-03 | 1.160E-03 |
| NI | | 3.866E+08 | 6.469E+06 | 5.160E+05 | 5.338E+04 | 1.584E+04 | 8.915E+03 | 7.440E+03 | 8.915E+03 | 1.584E+04 | 5.338E+04 |
| dj | | 2.586E-09 | 1.546E-07 | 1.938E-06 | 1.873E-05 | 6.314E-05 | 1.122E-04 | 1.344E-04 | 1.122E-04 | 6.314E-05 | 1.873E-05 |
| X | (ft) | -75.0 | -74.0 | -73.0 | -72.0 | -71.0 | -70.0 | -69.0 | -68.0 | -67.0 | -66.0 |
| U.D.T | | 0.000E+00 | 0.000E+00 | 0.000E+00 | 0.000E+00 | 0.000E+00 | 0.000E+00 | 0.000E+00 | 0.000E+00 | 0.000E+00 | 0.000E+00 |
| X | (ft) | -74.5 | -73.5 | -72.5 | -71.5 | -70.5 | -69.5 | -68.5 | -67.5 | -66.5 | -65.5 |
| F(x) | | 1.435E-10 | 2.398E-10 | 3.980E-10 | 6.561E-10 | 1.074E-09 | 1.746E-09 | 2.818E-09 | 4.517E-09 | 7.192E-09 | 1.137E-08 |
| Dj by One Pass | | 2.815E-10 | 4.153E-10 | 6.089E-10 | 8.869E-10 | 1.283E-09 | 1.845E-09 | 2.636E-09 | 3.742E-09 | 5.277E-09 | 7.394E-09 |
| T.D.D.L. | | 0.000 | 0.000 | 0.000 | 0.000 | 0.000 | 0.000 | 0.000 | 0.000 | 0.001 | 0.001 |

| | |
|--|-------|
| Gear Wander Standard Deviation, Sw (ft) | 12.00 |
| Location of the Max Damage, Xj- max (ft) | 0.50 |

FIGURE A. 55 Clicking unit damage and total damage icon.

- 1.2.7. **Annual Damage Icon:** Clicking on this Icon opens a user form to determine the Annual Traffic (Pass), Annual Max Damage (%), Cumulative Traffic (Pass), Cumulative Max Damage (%), and Interval of the Max Damage, Xj- max (ft).The user form has three Icons that are used to input the above noted variables:

FIGURE A. 56 Clicking on annual damage icon.

- 1.2.7.1. **Update Data Icon:** Click on the "Update Data" button to retrieve the Passes of Vehicle at Base Year, Pjo, Traffic Growth Rate (%), and Design Life (Years).These variable were entered in previous sheets (as shown in FIGURE A. 57).The user has the ability to change the value of these input from the user form.



FIGURE A. 57 Clicking on update data icon.

1.2.7.2. **OK Icon:** Click on the “Ok Icon” button to calculate and copy the results (Traffic Growth Rate Assumed, rg (%), the Annual Traffic (Pass), Annual Max Damage (%), Cumulative Traffic (Pass), Cumulative Max Damage (%), and Interval of the Max Damage, X_j - max (ft). A tabular format as shown in FIGURE A. 58).

| Gear Wander Standard Deviation, S_w (ft) | | 12.00 | | | |
|--|-----------------------|-----------------------|---------------------------|---------------------------|-----------------------------|
| Location of the Max Damage, X_j - max (ft) | | 0.50 | | | |
| Traffic Growth Rate Assumed, rg (%) | | 2.00 | | | |
| Year | Annual Traffic (Pass) | Annual Max Damage (%) | Cumulative Traffic (Pass) | Cumulative Max Damage (%) | Interval of the Max Damage, |
| 1 | 4040 | 24.74 | 4040 | 24.74 | ± 0.5 |
| 2 | 4121 | 25.24 | 8161 | 49.98 | ± 0.5 |
| 3 | 4203 | 25.74 | 12364 | 75.72 | ± 0.5 |
| 4 | 4287 | 26.26 | 16651 | 101.98 | ± 0.5 |
| 5 | 4373 | 26.78 | 21024 | 128.76 | ± 0.5 |
| 6 | 4460 | 27.32 | 25484 | 156.08 | ± 0.5 |
| 7 | 4550 | 27.86 | 30034 | 183.94 | ± 0.5 |
| 8 | 4641 | 28.42 | 34674 | 212.37 | ± 0.5 |
| 9 | 4733 | 28.99 | 39407 | 241.36 | ± 0.5 |
| 10 | 4828 | 29.57 | 44235 | 270.93 | ± 0.5 |
| 11 | 4925 | 30.16 | 49160 | 301.09 | ± 0.5 |
| 12 | 5023 | 30.76 | 54183 | 331.85 | ± 0.5 |
| 13 | 5124 | 31.38 | 59307 | 363.23 | ± 0.5 |
| 14 | 5226 | 32.01 | 64533 | 395.24 | ± 0.5 |
| 15 | 5331 | 32.65 | 69863 | 427.89 | ± 0.5 |
| 16 | 5437 | 33.30 | 75300 | 461.19 | ± 0.5 |
| 17 | 5546 | 33.97 | 80846 | 495.15 | ± 0.5 |
| 18 | 5657 | 34.65 | 86503 | 529.80 | ± 0.5 |
| 19 | 5770 | 35.34 | 92273 | 565.14 | ± 0.5 |
| 20 | 5885 | 36.05 | 98158 | 601.18 | ± 0.5 |

FIGURE A. 58 Clicking ok icon.

1.2.7.3. **Cancel Icon:** Click on the “Cancel Icon” button to hide the user form and cancel all calculation.

1.2.8. **Show & Hide Graph Icon:** Clicking on this Icon will pop up a “show graph” user form. This user form has a list of graph that the user may choose to select as shown in FIGURE A. 59:

- STRAIN PROFILE
- UNIT DAMAGE-T
- DAMAGE PROFILE BY ONE PASS
- DAMAGE PROFILE AT THE END OF DESIGN LIFE
- DAMAGE VERSUS TIME
- ANNUAL AND CUMULATIVE TRAFFIC

Moreover, the user form has four buttons:

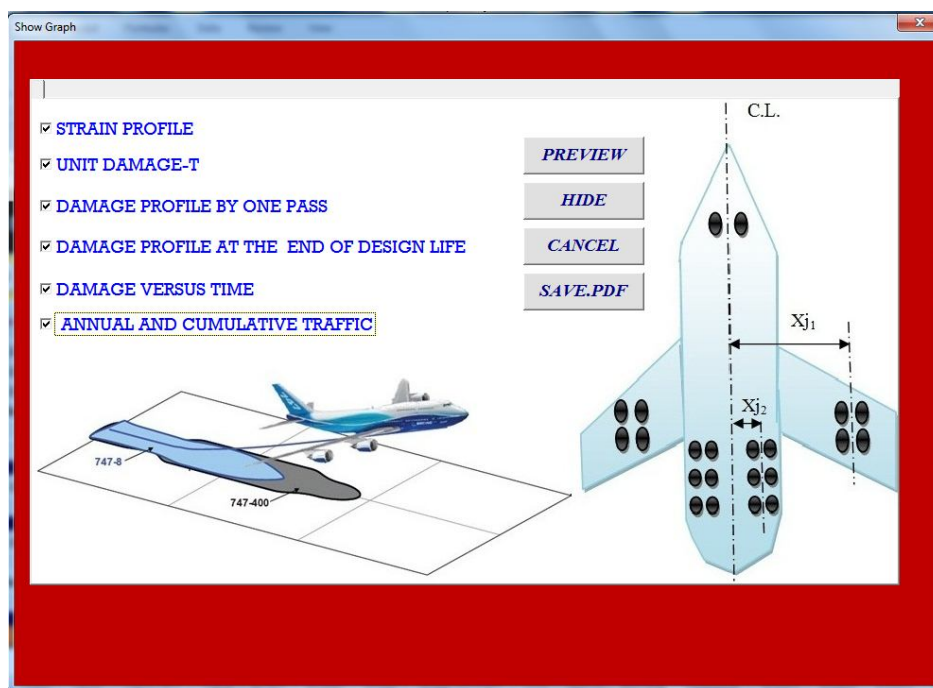


FIGURE A. 59 “show graph” user form.

1.2.8.1. **Preview Icon:** Check any of the options on the list and click “Preview Icon”. The program will show the selected graph in the same sheet as shown in FIGURE A. 60:

1.2.8.2. **Hide Icon:** Click on the “Hide Icon” button to delete any graph that sheet has.

1.2.8.3. **Cancel Icon:** Click on the “Cancel Icon” button to hide the user form and cancel all selected options.

1.2.8.4. **Save PDF Icon:** Check any of the options on the list and click “Preview Icon”, the program will show the selected graph in the same sheet. After that, if the user needs to save any graph as a PDF file, just click any of them and click “Save PDF” Icon to save (It should be noted that the selected graph must be shown in the sheet in this way in order for the user to save it).

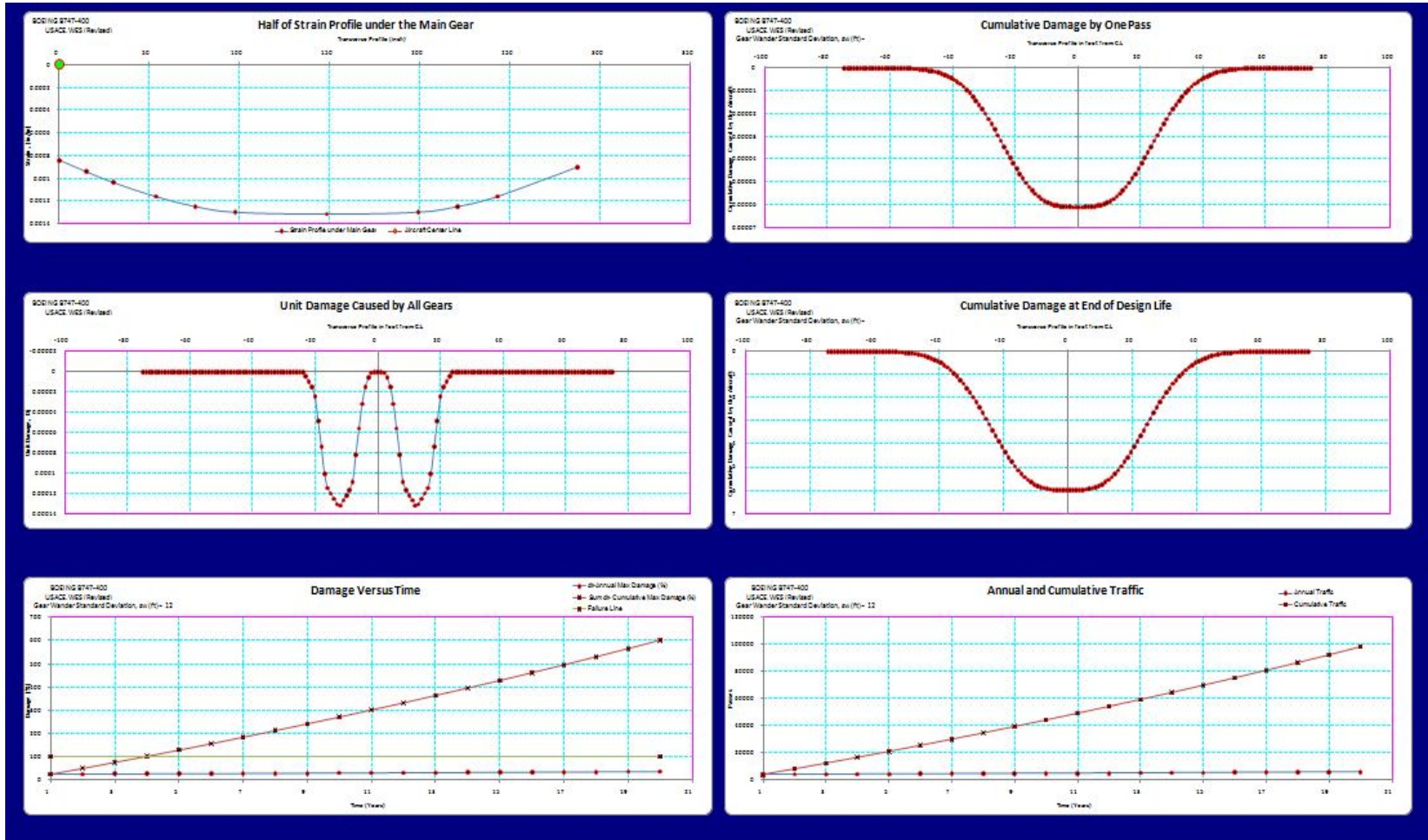


FIGURE A. 60 The selected graph on the sheet.